AD-A094 011 STANFORD UNIV CALIF THERMOSCIENCES DIV F/G 20/4
THE THERMAL AND HYDRODYNAMIC BEHAVIOR OF THICK, ROUGH-WALL, TUR--ETC(U)
AUG 79 P M LIGRANI, R J MOFFAT, W M KAYS N00014-67-A-0112-0072
UNCLASSIFIED HMT-29 NL

1 OF 3
AD A
094011

STANFORD UNIVERSITY
COMPLIMENTS OF
THE THERMOSCIENCES AFFILIATES PROGRAM
DEPARTMENT OF MECHANICAL ENGINEERING

THE THERMAL AND HYDRODYNAMIC BEHAVIOR OF THICK, ROUGH-WALL, TURBULENT BOUNDARY LAYERS

LEVEL

by

P. M. Ligrani, W. M. Kays and R. J. Moffat

AD A094011

Report No. HMT-29

The Ruth H. Hooker Technical Library
MAY 21 1980
Naval Research Laboratory

Prepared in part with support from
The Office of Naval Research
N00014-67-A-0112-0072
and
N00014-76-C-0532

APPROVED FOR PUBLIC RELEASE
DISTRIBUTION UNLIMITED

Thermosciences Division
Department of Mechanical Engineering
Stanford University
Stanford, California

August 1979

DDC FILE COPY

81 1 22 011

THE THERMAL AND HYDRODYNAMIC BEHAVIOR OF THICK, ROUGH-WALL, TURBULENT BOUNDARY LAYERS

by

P. M. Ligrani, R. J. Moffat, and W. M. Kays

Report No. HMT-29

Prepared in part with support from
The Office of Naval Research
N00014-67-A-0112-0072
and
N00014-76-C-0532

APPROVED FOR PUBLIC RELEASE
DISTRIBUTION UNLIMITED

Thermosciences Division
Department of Mechanical Engineering
Stanford University
Stanford, California

August 1979

ACKNOWLEDGMENTS

The initial phases of this research were made possible by support from the Office of Naval Research, Contracts N00014-67-A-0112-0072 and N00014-76-C-0532. The experimental apparatus was constructed during an earlier contract from the Department of the Navy, Contract N00123-71-0-0372. The authors thank Mr. James Patton for his support.

The authors also thank Professor James P. Johnston for his many helpful comments and suggestions with regard to this research effort. In addition, this project would not have been possible without the expert craftsmanship of Tots Ikebe, George Yoshida, and especially Robin Birch, who handled the probes for this study. We also thank Ruth Korb, who handled the final forms of the manuscript and did an excellent typing job.

Technical contributions to this project were made by H. W. Coleman, E. J. Kerschen, D. J. Vitanye, and K. W. Randall. The authors thank these individuals and other members of the Department of Mechanical Engineering who contributed ideas and support leading to the success of this project.

A

ABSTRACT

Thick, fully rough, and transitionally rough turbulent boundary layers were studied in order to investigate the differences between fully rough and transitionally rough behavior and to observe how downstream development affects these flows as the boundary layers become very thick. Measurements included Stanton numbers, skin friction coefficients, mean temperature and velocity profiles, Reynolds stress tensor component profiles, and spectra of the longitudinal velocity fluctuations. Predictions of wall heat transfer, wall shear, and mean profiles were made using a mixing-length and turbulent Prandtl number closure scheme which accounted for the effects of wall roughness in the boundary layer equations.

The turbulent boundary layers were artificially thickened using an array of solid obstacles which produced a two-dimensional equilibrium flow field with properties representative of natural bounday layers, at least up to the level of the turbulent correlations on a smooth wall, and to the level of the spectra of longitudinal velocity fluctuations on a rough wall. A rough-wall boundary layer environment was provided in which all measurements of lower order than the turbulence correlations could be discussed regarding the influence of roughness, and considered to have properties representative of natural behavior.

The change from smooth to fully rough behavior in boundary layers over uniform-spheres roughness occurs over a smaller range of roughness Reynolds numbers than boundary layer flows over sandgrain roughness. A correlation for the velocity distribution constant, B, as a function of Re_k for uniform-spheres roughness can be used in conjunction with the law of the wake and the law of the wall equations to predict the dependence on Re_k of viscous sublayer thickness, velocity profile shifts, and skin friction coefficients in transitionally rough flows. Transitionally rough skin friction coefficient data usually show qualitative trends which could be interpreted as being consistent with the Prandtl-Schlichting hypothesis that fully rough flows will eventually become transitionally rough and then smooth if allowed to develop far enough downstream.

The Stanton number data in the thickened boundary layers show characteristics of flows having an unheated starting length for transitionally

rough and fully rough cases, since the flows effectively develop from a point far upstram from the origin of the thermal boundary layer. Temperature profiles in these flows do not show the typical wake-like behavior characteristic of thermal boundary layers without an unheated starting length.

The non-dimensionalized distribution of the longitudinal component of turbulence intensity in transitionally rough flows has a continuously varying distribution from fully rough to smooth behavior which is strongly characterized by the freestream velocity of the flow. As the freestream velocity is lowered and the flow moves from fully rough to transitionally rough behavior, a near-wall peak in turbulence intensity increases in magnitude, and a large hump of turbulence, which is characteristic of fully rough conditions, flattens out. The most appropriate velocity scale for longitudinal turbulence and turbulence kinetic energy is the friction velocity, whereas the freestream velocity is more appropriate in scaling the transverse and normal components of turbulence.

Predictions of rough-wall skin friction coefficients, Stanton numbers, and mean profiles are made using two different mixing-length schemes and a smooth-wall turbulent Prandtl number distribution, in conjunction with a wall temperature step representing a conduction sublayer. Predictions are made of pipe flows with different values of the molecular Prandtl numbers over surfaces having different roughness heights, and boundary layers developing over uniform-spheres roughness at one value of the molecular Prandtl number.

Table of Contents

	Page
Acknowledgments	iii
Abstract	iv
List of Tables	ix
List of Figures	x
Nomenclature	xv
Chapter	
1 INTRODUCTION	1
1.1 Background	1
1.2 Objectives	3
1.3 The Experiment	4
1.3.1 Cases Studied	5
1.3.2 Apparatus and Measurement Techniques	6
1.3.2a Smooth Surface	6
1.3.2b Rough Surface	7
1.4 Predictions	8
1.5 Organization	8
2 ARTIFICIALLY THICKENED TURBULENT BOUNDARY LAYERS	11
2.1 Introduction	11
2.1.1 Classification of Techniques	11
2.1.2 Prior Work	12
2.1.3 Present Approach	15
2.1.3a Coordinate System	15
2.1.3b Equilibrium	16
2.1.3c Information Hierarchy	18
2.2 Smooth-Surface, Artificially Thickened Boundary Layers	18
2.2.1 Objective	18
2.2.2 Apparatus	19
2.2.2a Final Design	19
2.2.2b Component Effects	19
2.2.2c Design Development	22
2.2.3 Boundary Layer Characteristics	23
2.2.3a Hydrodynamic Results	23
2.2.3b Heat Transfer Results	26
2.2.3c Conclusions	28
2.3 Rough-Surface, Artificially Thickened Boundary Layers	29
2.3.1 Objectives	29
2.3.2 Apparatus	30
2.3.2a Final Design	30
2.3.2b Component Effects	31
2.3.2c Design Development	32
2.3.3 Boundary Layer Characteristics	32
2.3.3a Growth	33
2.3.3b Two-dimensionality	34
2.3.3c Structural Similarity	35
2.3.3d Structural Equilibrium	40
2.3.3e Conclusions	40

Chapter Page

3 EXPERIMENTAL RESULTS: FULLY ROUGH AND TRANSITIONALLY ROUGH TURBULENT BOUNDARY LAYERS 69

3.1 Hydrodynamic Scalar Properties and Mean Velocity Profiles 69
3.1.1 Introduction 69
3.1.2 Prior Work 70
3.1.3 Experimental Background 70
3.1.4 B versus Re_k 72
3.1.5 Skin Friction 73
3.1.6 Viscous Sublayer 76
3.1.7 Mean Velocity Profiles - U/U_∞ versus y/δ_2 Coordinates 78
3.1.8 Mean Velocity Profiles - Smooth-Wall Coordinates 79
3.1.9 Mean Velocity Profiles - Fully Rough Coordinates 80

3.2 Thermal Scalar Properties and Mean Temperature Profiles 81
3.2.1 Introduction 81
3.2.2 Prior Work 81
3.2.3 Fully Rough, Transitionally Rough, and Smooth Behavior of Thermal Boundary Layers 82
3.2.4 Effect of Unheated Starting Length on Rough-Wall Thermal Boundary Layers 83
3.2.5 Effect of Freestream Velocity on Thermal Boundary Layers with an Unheated Starting Length . . 85
3.2.6 The Behavior of Thick, Rough-Wall, Thermal Boundary Layers Without an Unheated Starting Length 86

3.3 Turbulence Structure 88
3.3.1 Introduction 88
3.3.2 Prior Work 89
3.3.3 Summary of Results 90
3.3.4 Effect of Freestream Velocity on the Normal Reynolds Stress Tensor Components 91
3.3.4a Qualitative data trends 91
3.3.4b Normalizing parameters 93
3.3.5 Downstream Development of the Normal Reynolds Stress Tensor Components 94
3.3.5a Qualitative data trends 94
3.3.5b Normalizing parameters 95
3.3.6 Turbulence Kinetic Energy 96

3.4 Spectra of the Longitudinal Velocity Fluctuations . . 97
3.4.1 Introduction 97
3.4.2 Prior Work 97
3.4.3 Experimental Background 98
3.4.4 Effects of Roughness 100

Chapter Page

4 ROUGH-WALL BOUNDARY LAYER PREDICTIONS 129

4.1 Introduction 129
4.2 Prior Work 129
4.3 Prediction Program 133
4.4 Rough-Wall Transport Properties - Outer Regions of the Boundary Layer 134
4.5 Rough-Wall Transport Properties - Inner Regions of the Boundary Layer 135
4.5.1 Hydrodynamic Transport 135
4.5.1a Mixing-length offset scheme 136
4.5.1b Slip velocity scheme 139
4.5.2 Thermal Transport 140
4.5.2a Thermal transport in smooth, transitionally rough, and fully rough boundary layers 140
4.5.2b Fully rough temperature profile 141
4.5.2c Fully rough conduction sublayer thickness 142
4.5.2d Fully rough conduction sublayer Stanton number 143
4.5.2e Thermal, fully rough law of the wall . 144
4.6 Prediction Model 144
4.7 Prediction Results 148

5 CONCLUSIONS 161

REFERENCES 165

Appendix

I WIND TUNNEL MODIFICATIONS 173

II MEASUREMENT TECHNIQUES 175

II.1 Stanton Numbers 175
II.2 Mean Temperatures 176
II.3 Skin Friction 176
II.4 Mean Velocity 177
II.5 Reynolds Stress Tensor Components 177
II.6 Spectra of the Longitudinal Velocity Fluctuations . . 181

III THE EFFECT OF SENSOR LENGTH OF HOT-WIRE ANEMOMETRY PROBES ON THE MEASUREMENT OF TURBULENCE INTENSITY IN A FULLY ROUGH TURBULENT BOUNDARY LAYER 183

III.1 Introduction and Prior Work 183
III.2 Present Experiment 184
III.3 Experimental Results 184

IV TABULATION OF EXPERIMENTAL DATA 189

List of Tables

Table		Page
1-1	Artificially Thickened Boundary Layer Cases Studied	5
1-2	Naturally Developed Boundary Layer Cases Studied	6
2-1	Values of a and b in Equations (2-17) and (2-19)	34
3-1	Predicted Transition Points from Fully Rough to Transitionally Rough Behavior ($Re_k = Re_k^*$ where $Re_k^* = 55.0$ for $k_s = .079$ cm Uniform Spheres Roughness)	76
4-1	Recommended Values of Re_k'' for Different Types of Roughness	146
III-1	Hot-Wire Sensing Elements	184

List of Figures

Figure		Page
1-1	Schematic of HMT-1 wind tunnel - smooth test surface	9
1-2	Schematic of HMT-18 wind tunnel - rough test surface	10
2-1	Coordinate system for artificially thickened boundary layers .	42
2-2a	Smooth-wall artificial thickening apparatus (Design C)	43
2-2b	Smooth-wall spire dimensions (Design C)	43
2-3	Effects of spire streamlining on mean velocity profiles, x_1 = 2.08 m	44
2-4	Effect of barrier height, h, on mean velocity profiles in boundary layer coordinates, x_1 = 1.57 m (all profiles with Design C spires)	45
2-5	Displacement thickness and momentum thickness development, smooth-wall artificially thickened boundary layer	46
2-6a & b	Skin friction development, smooth-wall artificially thickened boundary layer	47
2-7	Development of velocity profiles in boundary layer coordinates, smooth-wall artificially thickened boundary layer	48
2-8a	Clauser shape factor variation with downstream distance, smooth-wall artificially thickened boundary layer	49
2-8b	Variation of Karman shape factor with U_∞/U_τ - comparison of Hama's (1954) data with smooth-wall artificially thickened boundary layer data	49
2-9	Development of velocity profiles in velocity defect coordinates, smooth-wall artificially thickened boundary layer . . .	50
2-10a	Development of longitudinal turbulence intensity profiles, smooth-wall artificially thickened boundary layer	51
2-10b	Development of turbulence kinetic energy profiles, smooth-wall artificially thickened boundary layer	51
2-10c	Development of Reynolds shear stress profiles, smooth-wall artificially thickened boundary layer	52
2-10d	Cross-correlation coefficient for the turbulent shear stress, and the Reynolds shear stress/turbulence kinetic energy ratio, smooth-wall artificially thickened boundary layer	52
2-11	Heat transfer behavior in Stanton number vs. enthalpy thickness Reynolds number coordinates, smooth-wall artificially thickened boundary layer	53
2-12	Comparison of smooth-wall artificially thickened heat transfer data with Reynolds (1958) unheated starting length data and correlation	54
2-13	Rough-wall artificial thickening apparatus (Design E)	55

Figure | Page

2-14 Effect of artificial thickening apparatus geometry changes on turbulence profiles 56

2-15 Effect of bar distance from wall, γ, on turbulence profiles . 57

2-16 Skin friction variation as a function of downstream distance in naturally developed and artificially thickened rough-wall boundary layers 58

2-17 Variation of momentum thickness with downstream distance, U_∞ = 26.8 m/sec 59

2-18 Variation of momentum thickness with downstream distance, U_∞ = 15.8 m/sec 60

2-19 Variation of momentum thickness with downstream distance, U_∞ = 10.1 m/sec 61

2-20 Variation of the shape factor with U_∞/U_τ - comparison of Hama's (1954) data with rough-wall artificially thickened boundary layer data 62

2-21 Spanwise uniformity and two-dimensionality of turbulence profiles, rough-wall artificially thickened boundary layer U_∞ = 26.8 m/sec 63

2-22 Downstream development and variation with freestream velocity of velocity profiles in velocity defect coordinates, rough wall artificially thickened boundary layers 64

2-23 Reynolds shear stress profile downstream development and variation with freestream velocity, rough-wall artificially thickened boundary layers 64

2-24 Cross-correlation coefficient for the Reynolds shear stress, and the ratio of the Reynolds shear stress to the turbulence kinetic energy in naturally developed and artificially thickened rough-wall boundary layers 65

2-25 Spectra in artificially thickened and naturally developed fully rough turbulent boundary layers, U_∞ = 26.8 m/sec . . . 66

2-26 Clauser shape factor variation with downstream distance, rough wall artificially thickened boundary layers 67

3-1 Variation of B with roughness Reynolds number 103

3-2 Rough-wall boundary layer skin friction variation as a function of momentum thickness 104

3-3 Rough-wall boundary layer skin friction variation as a function of Reynolds number based on downstream distance . . . 105

3-4 Fully rough, transitionally rough, and smooth mean velocity profiles 106

3-5 Rough-wall mean velocity profiles - smooth-wall, inner region coordinates 107

3-6 Transitionally rough mean velocity profiles - fully rough, inner region coordinates 108

3-7 Fully rough mean velocity profiles - fully rough, inner region coordinates 109

Figure		Page
3-8	Stanton number behavior in smooth, transitionally rough, and fully rough turbulent boundary layers	110
3-9	Effect of unheated starting length on Stanton number behavior in a fully rough turbulent boundary layer	111
3-10	Downstream development of mean temperature profiles in a fully rough turbulent boundary layer with an unheated starting length	111
3-11	Effect of downstream development on mean temperature profiles in a fully rough boundary layer with an unheated starting length	112
3-12	Effect of unheated starting length on mean temperature profiles having approximately the same enthalpy thickness in a fully rough turbulent boundary layer	112
3-13	Effect of freestream velocity on Stanton number behavior in rough-wall boundary layers having unheated starting length .	113
3-14	Effect of freestream velocity on mean temperature profiles in rough-wall boundary layers having unheated starting length	113
3-15	Variation of Stanton numbers with downstream distance, U_∞ = 26.8 m/sec	114
3-16	Variation of Stanton numbers with downstream distance, U_∞ = 15.8 m/sec	115
3-17	Variation of Stanton numbers with downstream distance, U_∞ = 10.1 m/sec	116
3-18	Profiles of longitudinal component of turbulence intensity from Klebanoff (1954), Pimenta (1975), Coleman (1976), and the present study	117
3-19	Summary of profiles of longitudinal component of turbulence intensity, normalized using the freestream velocity, for transitionally rough and fully rough turbulent boundary layers	118
3-20	Summary of profiles of longitudinal component of turbulence intensity, normalized using the friction velocity, for transitionally rough and fully rough turbulent boundary layers	119
3-21a	Profiles of longitudinal component of turbulence intensity, normalized using the freestream velocity, compared at different freestream velocities and at different downstream locations	120
3-21b	Profiles of normal and transverse components of turbulence intensity, normalized using the freestream velocity, compared at different freestream velocities and at different downstream locations	120

Figure Page

3-22 Profiles of longitudinal component of turbulence intensity normalized using the friction velocity, compared at different freestream velocities and at different downstream locations . 121

3-23 Transitionally rough and smooth (Orlando (1974)) normal Reynolds stress tensor components, U_∞ = 10.1 m/sec 122

3-24 Downstream development of transitionally rough profiles of longitudinal component of turbulence intensity, U_∞ = 10.1 m/sec 122

3-25 Profiles of turbulence kinetic energy normalized using the friction velocity, compared at different freestream velocities and at different downstream locations 123

3-26 Profiles of turbulence kinetic energy, normalized using the freestream velocity, compared at different freestream velocities and at different downstream locations 123

3-27 Spectra of longitudinal turbulence intensity in a fully rough turbulent boundary layer and in smooth-wall boundary layer and channel flows 124

3-28 Dissipation and production of turbulence kinetic energy in fully rough turbulent boundary layers 125

3-29 Spectra of longitudinal turbulence intensity normalized using Kolmogorov length and velocity scales in a fully rough turbulent boundary layer and in a smooth-wall channel flow . . . 126

3-30 Dissipation spectra in a fully rough turbulent boundary layer and a smooth-wall channel flow 127

4-1 Conduction sublayer temperature drop as a function of roughness Reynolds number 151

4-2 Prediction of Nikuradse's (1933) pipe skin friction coefficient data 152

4-3 Prediction of Dipprey and Sabersky's (1963) pipe heat transfer data 153

4-4 Pre iction of skin friction coefficients in naturally developed boundary layers with and without transpiration, and in artificially thickened boundary layers 154

4-5 Prediction of Stanton numbers in naturally developed boundary layers with and without transpiration 155

4-6 Prediction of mean velocity profiles in a transitionally rough boundary layer, fully rough boundary layers, and a fully rough boundary layer with transpiration 156

4-7 Prediction of mean temperature profiles in a transitionally rough boundary layer, a fully rough boundary layer, a fully rough boundary layer with transpiration, and a fully rough boundary layer with an unheated starting length 157

4-8a Prediction of skin friction coefficients and Stanton numbers in an accelerated fully rough boundary layer, $K_R = .15 \times 10^{-3}$ 158

Figure Page

4-8b Prediction of skin friction coefficients and Stanton numbers in an accelerated fully rough boundary layer, $K_R = .29 \times 10^{-3}$. 158

4-9 Prediction of mean temperature and mean velocity profiles in an accelerated fully rough boundary layer, $K_R = .15 \times 10^{-3}$. 159

4-10a Stanton number prediction in a boundary layer with acceleration, steps in blowing, and variable blowing 160

4-10b Stanton number prediction in a boundary layer with acceleration, steps in blowing, variable blowing, and a wall temperature step 160

4-10c Freestream velocity and blowing distributions 160

II-1 Schematic of equipment used for spectra measurements 182

III-1 Longitudinal turbulence intensity profiles in a fully rough turbulent boundary layer measured using hot wires with different sensing lengths 187

III-2 Longitudinal turbulence intensity profiles in a fully developed two-dimensional channel flow measured using hot wires with different sensing lengths 187

III-3 Spectra of longitudinal turbulence intensity in a fully rough turbulent boundary layer, $y'/\delta = .078$, measured using hot wires with different sensing lengths 188

III-4 Spectra of longitudinal turbulence intensity in a fully rough turbulent boundary layer, $y'/\delta = .600$, measured using hot wires with different sensing lengths 188

NOMENCLATURE

A	Smooth-wall sublayer thickness.
A^+	AU_τ/ν.
A_f	Spire frontal area.
A_R	Rough-wall sublayer thickness.
A_R^+	$A_R U_\tau/\nu$.
A_{th}	Thermal sublayer thickness.
A_{th}^+	$A_{th} U_\tau/\nu$.
B	Constant in fully rough law of the wall.
C	Constant in smooth law of the wall.
C_D	Drag coefficient based on area A, $2g_c F_D/\rho_\infty U_\infty^2 A$.
$C_f/2$	Local skin friction coefficient, $\tau_w g_c/\rho_\infty U_\infty^2$.
$\overline{C_f}/2$	Average skin friction coefficient.
C_p	Specific heat of fluid.
d	Diameter of sensing portion of hot-wire sensor.
D	Constant in transitionally rough law of the wall.
D	Pipe diameter.
e	Parameter in rough-wall mixing length equation.
$f_u(k_1)$	$\overline{u'^2}$ turbulent enerty associated with k_1.
$f_u(n)$	$\overline{u'^2}$ turbulent energy associated with n.
$F_u(k_1)$	Percent of $\overline{u'^2}$ turbulent energy associated with k_1.
$F_u(n)$	Percent of $\overline{u'^2}$ turbulent energy associated with n.
F	Blowing fraction, $\rho_w V_o/\rho_\infty U_\infty$.
G	Clauser shape factor, $\dfrac{1}{\int_o^\infty \left(\frac{U-U_\infty}{U_\tau}\right) dy} \int_o^\infty \left(\frac{U-U_\infty}{U_\tau}\right)^2 dy$.
h	Barrier height.
H	Shape factor, δ_1/δ_2.

k	Thermal conductivity.
k	Mean roughness height.
δ_k	Fully rough conduction sublayer thickness.
$(\delta_k)^+$	$(\delta k)U_\tau/\nu$.
k_1	One-dimensional wave number, $2\pi n/U$.
k_f	Dipprey Sabersky constant.
k_s	Equivalent sand grain roughness.
K_r	Fully rough acceleration parameter, $(r/U_\infty)(dU_\infty/dx)$.
ℓ	Sensing length of hot-wire probe.
ℓ	Mixing length.
L	Hydrodynamic starting length upstream of test surface, or distance between effective virtual origin of the flow and upstream edge of test surface, $x_2 - x_1$.
$\mathcal{L}$	General length scale.
n	Frequency.
$\mathcal{P}$	Production of turbulent kinetic energy.
Pe_t	Turbulent Peclet number.
Pr	Molecular Prandtl number, $\rho C_p \nu/k$.
Pr_t	Turbulent Prandtl number, $\varepsilon_M/\varepsilon_H$.
$\overline{q^2}$	Turbulent kinetic energy, $\overline{u'^2} + \overline{v'^2} + \overline{w'^2}$.
$\dot{q}''_w$	Wall heat flux.
r	Radius of spheres comprising test surface.
R	Distance from centerline of pipe.
R_o	Pipe radius.
Re_k	Roughness Reynolds number, $k_s U_\tau/\nu$.
$\overline{Re_k}$	$Re_k[1 + 16.0\ e\ V_o^+]$.
Re'_k	Roughness Reynolds number constant in rough-wall mixing-length equation.

Re_k''	Transitionally rough roughness Reynolds number at onset of smooth behavior.
Re_k^*	Transitionally rough roughness Reynolds number at onset of fully rough behavior.
Re_λ	$\sqrt{\overline{u'^2}}\lambda/\nu$.
Re_{δ_2}	Momentum thickness Reynolds number, $\delta_2 U_\infty/\nu$.
Re_D	Pipe diameter Reynolds number, $\overline{U}D/\nu$.
Re_{Δ_2}	Enthalpy thickness Reynolds number, $\Delta_2 U_\infty/\nu$.
Re_{x_2}	x_2-Reynolds number, $x_2 U_\infty/\nu$.
Re_ξ	Unheated starting length Reynolds number, $\xi U_\infty/\nu$.
R_{uv}	$-\overline{u'v'}/\sqrt{\overline{u'^2}\ \overline{v'^2}}$.
R_{q^2}	$-\overline{u'v'}/\overline{q^2}$.
St	Stanton number, $\dot{q}_w''/[\rho_\infty U_\infty C_p(T_w - T_{\infty,o})]$.
St_k	Conduction sublayer Stanton number, $\dot{q}_w''/(T_w - T_k)\rho C_p U_\tau$.
t	Time.
δt_o	Fully rough wall temperature step, $T_w - T_k$.
$(\delta t_o)^+$	$\delta t_o/T_\tau$.
T	Mean temperature.
T^+	$(T_w - T)/T_\tau$.
T_w	Wall temperature.
T_∞	Static freestream temperature.
$T_{\infty,o}$	Total freestream temperature.
T_τ	$\dot{q}_o''/\rho C_p U_\tau$.
T_k	Temperature at edge of conduction sublayer.
u	Instantaneous longitudinal velocity.
u'	Longitudinal velocity fluctuation.
u_{eff}	Instantaneous effective velocity sensed by the hot wire.
U	Mean longitudinal velocity.
U^+	U/U_τ.
U_s^+	Fully rough slip velocity.

U_∞	Freestream velocity.
U_τ	Friction velocity, $U_\infty \sqrt{C_f/2}$.
$\mathcal{U}$	General velocity scale.
v	Instantaneous velocity normal to surface.
v'	Normal velocity fluctuation.
$\mathcal{v}$	Kolmogorov velocity scale.
V	Mean normal velocity.
V_o	Velocity of transpired fluid at the wall.
V_o^+	V_o/U_τ.
w	Instantaneous transverse velocity.
w'	Transverse velocity fluctuation.
x	Longitudinal coordinate.
x_1	Longitudinal coordinate measured from upstream edge of test surface, actual x.
x_2	Longitudinal coordinate measured from effective virtual origin of the hydrodynamic flow field, apparent x, $x_1 + L$.
y	Coordinate normal to surface, measured from velocity virtual origin, $y' + \Delta y$.
y'	Coordinate normal to surface, measured from crests of spherical roughness elements.
y^+	yU_τ/ν.
Δy	Distance between the ball crests and the virtual origin of the velocity profiles.
δy_o	Mixing-length offset y shift.
z	Transverse coordinate.
z_o	Fully rough corrected roughness size, $k_s e^{-\kappa B}$.
α	Thermal diffusivity.
β	Spire height.
γ	Distance between bar and wall.

δ	Hydrodynamic boundary layer thickness, $U/U_\infty = 0.99$.
δ_1	Displacement thickness, $\int_0^\infty \left(1 - \frac{\rho U}{\rho_\infty U_\infty}\right) dy$.
δ_2	Momentum thickness, $\int_0^\infty \frac{\rho U}{\rho_\infty U_\infty} \left(1 - \frac{U}{U_\infty}\right) dy$.
Δ	Thermal boundary layer thickness, $(T_w - T)/(T_w - T_\infty) = 0.99$.
Δ_2	Enthalpy thickness, $\int_0^\infty \frac{\rho U}{\rho_\infty U_\infty} \left(\frac{T - T_\infty}{T_w - T_\infty}\right) dy$.
ε	Dissipation of turbulent kinetic energy.
ε_H	Eddy diffusivity for heat.
ε_M	Eddy diffusivity for momentum.
η	Kolmogorov length scale.
θ	Upstream spire blade angle.
κ	Karman constant.
λ	Taylor microscale.
ν	Kinematic viscosity.
ξ	Unheated starting length.
ρ	Density.
τ	Shear stress.
τ^+	τ/τ_w.
τ_w	Local wall shear stress.
ω	Transverse distance between the centerlines of spires.
$\omega(n)$	Cole's wake function, $1 - \cos(\pi n)$.

Subscripts		Superscripts	
o	Transpiration.	——	Mean (time-averaged) value.
w	Wall.		
∞	Freestream.		

Chapter 1

INTRODUCTION

The importance of roughness in practical boundary layer applications and the need for fundamental information on the response of a turbulent shear layer to wall roughness have motivated a rough-wall boundary layer program at Stanford and at many other institutions (see prior work, Chapters 2, 3, and 4). The Stanford program began with studies of the thermal and hydrodynamic behavior of flows in zero pressure gradients (Healzer (1974) and Pimenta (1975)) and later included a study of accelerated layers (Coleman (1976)). In the present work, the experimental domain investigated by these studies is extended to thicker boundary layers developing in zero pressure gradients. Mixing-length turbulent Prandtl number models are also developed from experimental data to predict the experimental cases studied. This prediction scheme can be used for transpired and accelerated rough wall boundary layers, as well as for zero pressure gradient flows without transpiration. The prediction scheme and the experimental data provide means for better understanding of the important turbulence processes which control events in rough-wall boundary layer flows.

1.1 BACKGROUND

Rough-wall turbulent boundary layers can be classified into different regimes of behavior which are distinguished by different ranges of the roughness Reynolds number. The roughness Reynolds number is given by

$$Re_k = \frac{k_s U_\tau}{\nu} \tag{1-1}$$

where k_s is the equivalent sand grain roughness size. For values of Re_k ranging from 0 to 5-20, the wall over which the boundary layer is developing is considered smooth. When Re_k is greater than values ranging from 55-90, the boundary layer is considered to be fully rough. Turbulent boundary layers having values of the roughness Reynolds number between the smooth and fully rough regimes are categorized as transitionally rough. As the roughness Reynolds number increases and the flows move from smooth to fully rough behavior, roughness elements are said to protrude

farther into the viscous sublayer, until it is eventually completely destroyed. The near-wall thermal resistance decreases and form drag on roughness elements increases, and the Stanton numbers and skin friction coefficients in flows over rough walls increase above the smooth-wall values for the same Reynolds number. The growth and entrainment of freestream fluid of rough-wall boundary layers are also increased. The effects of roughness thus result in significant alterations of boundary layer characteristics which may extend across the entire thickness of the layers.

Healzer (1974) showed the Stanton number and skin friction coefficients to be unaffected by the freestream velocity, being dependent only on the enthalpy thickness and momentum thickness. The momentum thickness and enthalpy thickness then show dependence on downstream distance, which does not change as the freestream velocity changes.

For the uniform-spheres roughness of the present study, Pimenta (1975) determined the equivalent sandgrain roughness size to be .079 cm. To do this, Pimenta used Schlichting's (1968) tabulations of k_s for different types of roughness, which are based on Nikuradse's (1933) earlier experiments in pipes. The value of k_s determined by Pimenta is used for all analysis in the present work.

In addition, Pimenta (1975) suggested that, as fully rough layers become very thick, Stanton numbers seem to asymptotically approach values invariant with downstream distance. However, if Pimenta's boundary layers developed to become thicker, it would probably become evident that the Stanton numbers decrease slowly with downstream distance. The skin friction coefficients would also decrease slowly with downstream distance, along with the roughness Reynolds number. A viscous sublayer would eventually begin to cover the roughness elements, causing the fully rough flow to become transitionally rough. If allowed to develop far enough downstream, the boundary layer would then behave as if it were flowing over a smooth surface.

Pimenta (1975) also investigated the Reynolds stress tensor components in fully rough and transitionally rough boundary layers. He found that, at $U_\infty = 15.8$ m/sec, the near-wall distribution of $\overline{u'^2}$ profiles showed qualitative characteristics similar to smooth behavior, since a near-wall

peak in $\overline{u'^2}$ was measured. At freestream velocities of 27.1 m/sec and 39.6 m/sec, the profiles of $\overline{u'^2}$ showed a fully rough character where the peak in $\overline{u'^2}$ is lowered, moved away from the wall, and spread over a greater portion of the layer. He pointed out that the differences in the near-wall profiles of $\overline{u'^2}$ offer the most definite possibility for distinguishing between fully rough and transitionally rough behavior.

1.2 OBJECTIVES

The present work is an extension of the studies of Healzer (1974), Pimenta (1975), and Coleman (1976), and has four principal objectives:

- To measure the Stanton number and skin-friction coefficients in boundary layers of greater thicknesses than those studied by previous investigators.
- To investigate the effects of downstream development on the mean and turbulence fields in transitionally rough and fully rough turbulent boundary layers.
- To investigate the mean and turbulence fields in transitionally rough boundary layers at different freestream velocities and further distinguish the differences between fully rough and transitionally rough behavior.
- To develop models for predicting scalar properties and mean profiles in rough-wall turbulent boundary layers, both with and without transpiration and with and without favorable pressure gradients.

In order to accomplish these objectives, the following sequence of tasks was undertaken:

- A technique was developed to artificially thicken smooth-wall turbulent boundary layers, so that the flow field produced was two-dimensional, at equilibrium, and having characteristics representative of natural behavior to the level of the turbulence quantities.
- The smooth-wall technique was then extended for use in studying thick rough-wall behavior, and verified to produce a two-dimensional, equilibrium flow field with properties representative of natural rough-wall boundary layer behavior.

- Data were obtained in the rough-wall boundary layers which include scalar quantities, mean profiles, the Reynolds stress tensor components, and spectra of longitudinal velocity fluctuations.
- The small-scale turbulence structure of rough-wall turbulent boundary layers was measured, and problems of measuring such characteristics using hot-wire anemometer techniques were examined.
- Mixing-length and turbulent Prandtl number closure models were developed which account for the effects of roughness in turbulent boundary layers over a broad range of the roughness Reynolds numebrs.
- The roughness closure model was then extended to predict rough-wall boundary layers with and without favorable pressure gradients, and with and without transpiration.
- The rough-wall prediction scheme was used as an extrapolation of experimental results to determine the behavior of boundary layers having thicknesses greater than the present range of experimental data.

Artificial thickening was made necessary for the study of thick, rough-wall, boundary layer behavior for a number of reasons. First, thicker boundary layers in fully rough flows cannot be obtained by changing the freestream velocity, since fully rough boundary layer behavior is not Reynolds number dependent. The Stanton number and skin friction coefficients in fully rough flows are dependent on thickness only, as Healzer (1974) pointed out, and thick boundary layers can be obtained only by increasing the length of the test surface or by augmenting the thickness of the layers in short wind tunnels. Since the cost of increasing the length of the rough surface was prohibitive, the logical alternative was to produce thick boundary layers at the upstream end of the test surface.

1.3 THE EXPERIMENT

The experimental cases studied, the experimental apparatus, and measurement techniques are now briefly discussed. Since both smooth-surface and rough-surface boundary layers were investigated, the apparatus and measurements section is divided into two parts. Additional details of the apparatus and measurement techniques are presented in Appendix II.

1.3.1 Cases Studied

The experimental cases investigated in artificially thickened boundary layers are listed in the table below.

Table 1-1

Artificially Thickened Boundary Layer Cases Studied

Designation	Freestream Velocity (m/sec)	Test Surface and Wind Tunnel	Artificially Thickened with Blowing
A*	10.2	Smooth - HMT-1	No
B	10.2	Smooth - HMT-1	F = .004 Plates 1-4
C*	26.8	Rough - HMT-18	No
D	26.8	Rough - HMT-18	F = .008 Plates 1-6
E	26.8	Rough - HMT-18	F = .0086 Plates 1-9
F	20.4	Rough - HMT-18	No
G*	15.8	Rough - HMT-18	No
H*	10.1	Rough - HMT-18	No

All of the boundary layer cases tabulated in Table 1-1 were artificially thickened using spire array-barrier devices described in Chapter 2. The cases designated B, D, and E were artificially thickened using spires in conjunction with blowing in upstream segments of the test surface, which provides an additional thickness increase. The technique of using blowing to augment boundary layer thickness is described by Pimenta (1975) and can be used to augment the thickness of thermal as well as hydrodynamic boundary layers.

The experimental cases investigated in naturally developed boundary layers are listed in Table 1-2.

Table 1-2

Naturally Developed Boundary Layer Cases Studied

Designation	Freestream Velocity (m/sec)	Surface - Wind Tunnel
I*	26.8	Rough - HMT-18
J	20.4	Rough - HMT-18
K	15.8	Rough - HMT-18
L*	10.1	Rough - HMT-18

The cases designated A, C, G, H. I, and L in Tables 1-1 and 1-2 are labeled with an asterisk to indicate that turbulence profiles and the downstream development of scalar quantities and mean profiles are completely documented for these cases. The other cases in Tables 1-1 and 1-2 were not fully documented because only minimal information was required for these cases to fill in or extend the experimental domain maps of the asterisk cases. For the K case in Table 1-2, complete documentation was not required, since Pimenta (1975) previously studied rough-wall boundary layers at this freestream velocity. Case I in Table 1-2 was used as a baseline data check to be compared with the existing measurements of Pimenta (1975) and Coleman (1976).

1.3.2 Apparatus and Measurement Techniques

1.3.2a. Smooth Surface. The wind tunnel used for the smooth-wall studies (Cases A and B) is the HMT-1 heat transfer tunnel, which is shown in Fig. 1-1. The apparatus was first described by Moffat (1967), and later by Anderson (1972) and Blackwell (1972), after more recent modifications were made.

The HMT-1 wind tunnel is an open-circuit tunnel and contains a test surface 2.44 meters long, consisting of 24 porous plates. Each plate may be heated individually to control the thermal boundary condition, and also may be used for transpiration studies, since air may be injected through each plate. The freestream velocity distribution may be controlled using slots located along the top wall of the test surface channel. Stanton numbers are determined by performing an energy balance on each plate: the

power into each segment of the test surface is measured and then plate losses are subtracted. Temperature measurements were made using thermocouples imbedded within each plate.

Mean velocities were measured in the smooth-wall wind tunnel using a boundary layer pitot probe of 0.508 mm outer diameter in conjunction with a micromanometer. Measurements of $\overline{u'^2}$ were made using a horizontal hot-wire probe, and measurements of $\overline{v'^2}$, $\overline{w'^2}$, and $-\overline{u'v'}$ were made using a rotatable, 45° slanted, hot-wire probe. The pitot probe and the two hot-wire probes were mounted on individual traversing mechanisms, each with a micrometer for adjusting probe position relative to the wall.

1.3.2b. Rough Surface. The wind tunnel used for the rough-surface studies (Cases C-L) is the HMT-18 wind tunnel, which is shown in Fig. 1-2. The apparatus was originally constructed by Healzer (1974) and also described by Pimenta (1975) and Coleman (1976). Modifications made to the wind tunnel for the present study are discussed in Appendix I.

The test surface of the wind tunnel is 2.44 meters long and consists of 24 plates which can be electrically heated individually to maintain a given temperature or transpiration boundary conditions. Each plate consists of 11 layers of 1.27 mm-diameter oxygen-free, high-conductivity (OFHC) copper spheres packed in the most dense array and brazed together. HMT-18 is a closed-circuit tunnel with a plexiglass top wall, which is flexible for alteration of freestream velocity. As for the smooth-wall wind tunnel, Stanton numbers are determined using an energy balance, and temperatures are measured using thermocouples installed in the plate.

The same probe used for measurement of $\overline{u'^2}$ in the smooth-wall boundary layer was used for measurement of mean velocity, $\overline{U}$, and $\overline{u'^2}$ in the rough-wall flow. Profiles of $\overline{v'^2}$, $\overline{w'^2}$, $\overline{u'v'}$, $\overline{v'w'}$, and $\overline{u'w'}$ were measured using the same probe used for the smooth-wall measurement of Reynolds stress tensor components. Spectra of the longitudinal velocity fluctuations were determined from the $\overline{u'^2}$ signals using a fast Fourier transform subroutine stored on an HP-2100 minicomputer.

1.4 PREDICTIONS

The prediction of rough-wall boundary layer skin-friction coefficients, Stanton numbers, mean velocity profiles, and mean temperature profiles were made by altering the mixing length and turbulent Prandtl number distributions to account for the effects of roughness in a boundary layer prediction program called STAN5. STAN5 is based on the Spalding-Patankar code and is discussed in detail by Crawford and Kays (1975). Generally, the program can be used to predict a large variety of two-dimensional boundary layer flows. For the present study, predictions of naturally developed and artificially thickened rough-wall boundary layers were made along with flows with and without favorable pressure gradients and flows with and without positive transpiration.

1.5 ORGANIZATION

The organization of the material presented in the following chapters is as follows. In Chapter 2 the details of the techniques used to artificially thicken turbulent boundary layers, and a discussion of qualification of the flow fields produced by the artificial thickening apparatus are presented. Chapter 3 then contains experimental results for artificially thickened boundary layers and naturally developed boundary layers. Chapter 4 presents a discussion of the closure schemes used for prediction of rough-wall boundary layer data, along with prediction results. Conclusions of the study are then listed in Chapter 5. Finally, tabular data, wind tunnel modifications, and measurement-technique details are presented in the appendices.

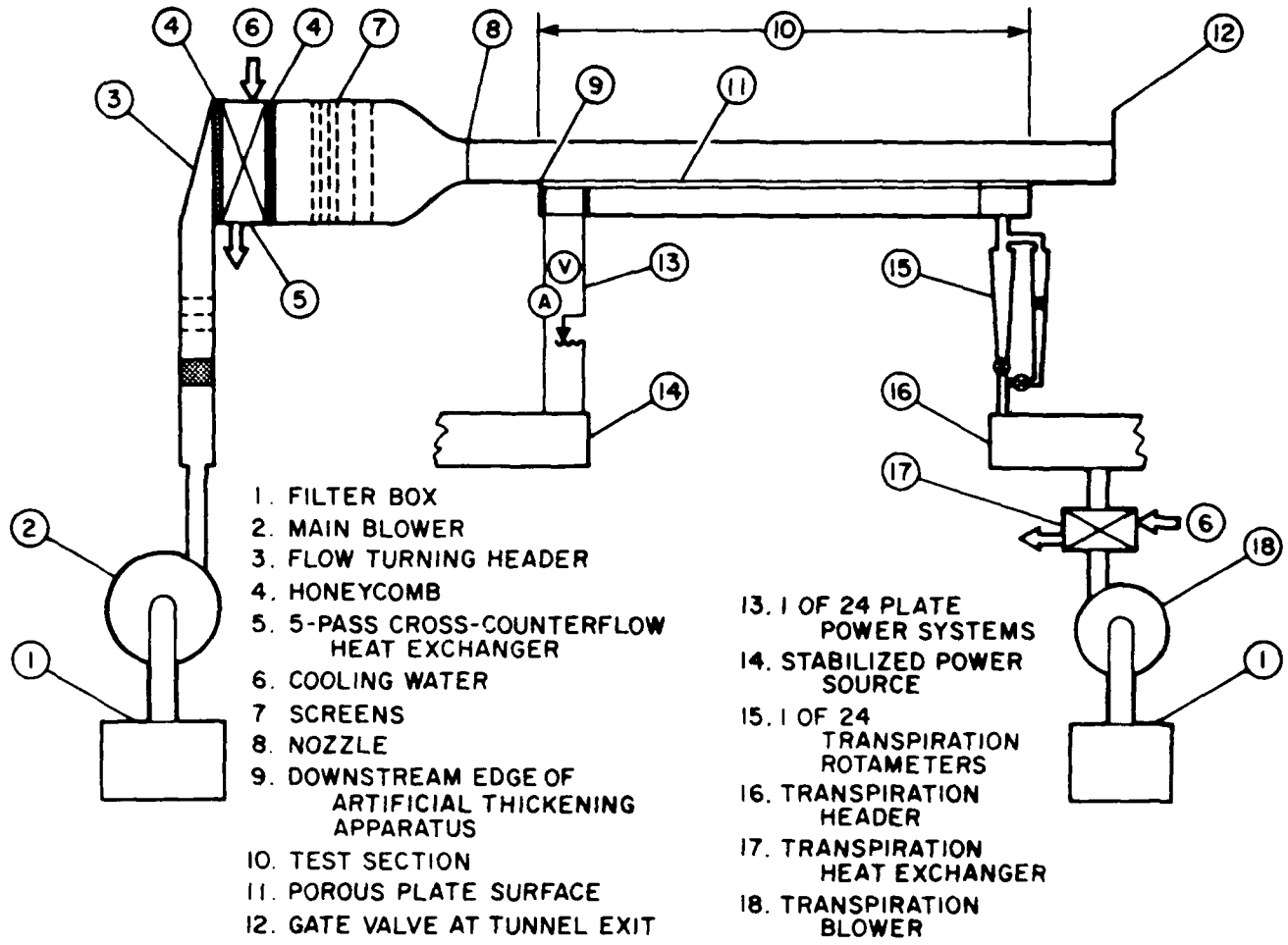

Fig. 1-1. Schematic of HMT-1 wind tunnel - smooth test surface.

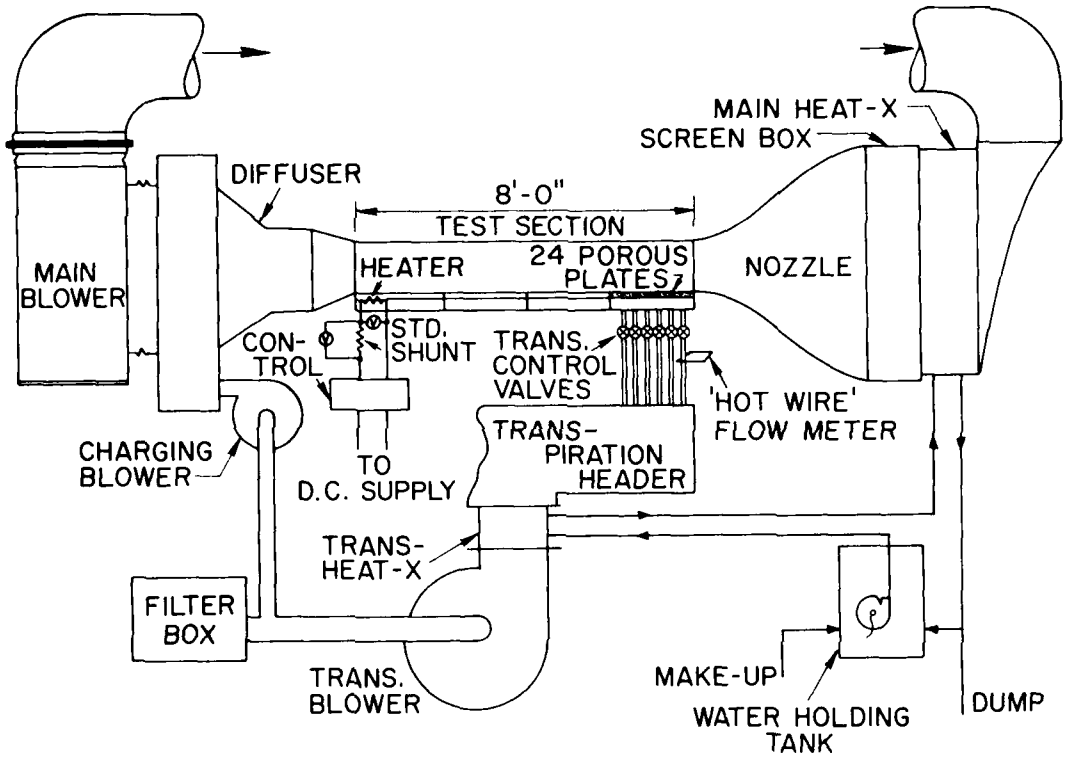

Fig. 1-2. Schematic of the experimental apparatus.

Chapter 2

ARTIFICIALLY THICKENED TURBULENT BOUNDARY LAYERS

2.1 INTRODUCTION

2.1.1 Classification of Techniques

Interest in thick shear layers has led several prior investigators to develop means of artificially thickening turbulent boundary layers. These can be compared by considering the type of fluid disturbance caused by the thickening device, and how these disturbances interact with shear layers which would be present in a wind tunnel without a thickening device. Three different categories can be defined, depending on whether the inner region, the outer region, or the potential flow region outside the existing boundary layer is disturbed by the thickening device. These differences are important in determining the characteristics of the artificially thickened boundary layer, and may be discussed by considering Townsend's (1956a) two-layer model for turbulent shear layers near walls.

Artificial thickening devices of the first category are the simplest and function either by altering the surface condition to increase the shear (thus accelerating the growth of the already existing turbulent boundary layer), or by producing an abrupt momentum deficit in the inner region. Boundary layer trips or increased surface roughness can be used to accomplish this effect. Only the inner layer of the boundary layer is disturbed using these methods, and the effects eventually diffuser towards the outer regions. Devices of this category are generally successful in preserving natural boundary layer properties, but require considerable downstream length considering the augmentation they produce. Only small net increases in thickness can be obtained, since limited momentum deficits can be added to the flow by changing wall characteristics.

The second type of device is one which alters both the inner and outer regions of the boundary layer, as, for example, using wall jets. The turbulence field of the naturally developed flow is enlarged, since regions of influence of the large eddies are extended farther from the wall to engulf larger portions of non-turbulent fluid than in a naturally developed

flow at the same location. Mixing is increased, which aids diffusion of turbulent kinetic energy from the inner regions to the outer regions, and the boundary layer thickness is augmented, since the mean flow field is retarded by increased Reynolds stress levels. The outer region of the turbulent boundary layer then behaves like a wake, where the principal source of turbulent energy is diffusion from the inner layer. The levels of production and dissipation are of comparable magnitude with advection and diffusion. Any disturbance to this region which creates additional turbulence would persist a considerable distance downstream before previously existing levels of production and dissipation are resumed.

The third type of boundary layer augmentation device is one which produces a momentum deficit and derives turbulent energy from previously irrotational potential flow. This technique usually uses an array of protrusions extending far from the wall, outside the approaching boundary layer. The wakes from these protrusions convect downstream to merge with existing wall boundary layer turbulence, to form an apparent extension on the region of influence by the wall. This method requires the merging of two turbulence fields, and the wake from the devices should resemble the behavior of the wake of a normal, flat-plate, turbulent boundary layer. Of the three techniques discussed, the largest momentum deficits can be produced using this method. However, simulation of given structural characteristics is most difficult, since abnormal turbulence structures shed from the solid obstacles may convect far downstream before decaying and blending with the wall turbulence field. Additionally, it is necessary to design the obstacles such that both the velocity and turbulence fields simultaneously attain specified distributions.

2.1.2 Prior Work

Two general types of shear flows have been simulated by previous investigators: atmospheric boundary layers and two-dimensional, flat-plate boundary layers. The two types of shear layers are vastly different, as indicated by Cockrell and Lee (1969), who describe the large-scale velocity field in the atmosphere as being more like a vortex with its axis perpendicular to the earth than a boundary layer flow with straight streamlines. In addition, the structural and equilibrium characteristics of atmospheric

boundary layers are less well understood than those of two-dimensional flows over flat plates. Simulations of atmospheric boundary layers are aimed at velocity profiles generally described by a power law equation (i.e., $U/U_\infty = (y/\delta)^{1/n}$), whereas correct flat plate simulations are required to produce flows with velocity profiles following the law of the wall, and the law of the wake. Many atmospheric simulation techniques are discussed in the literature (see the review article by Hunt and Fernholtz (1975)), whereas only a few methods are available for simulation of thick, flat-plate, turbulent boundary layers.

Klebanoff and Diehl (1952) artificially thickened zero-pressure gradient, turbulent boundary layers along smooth, flat plates using strips of sandpaper, an example of the first category discussed in Section 2.1.1. "Simplicity of method and adequacy of tests" were emphasized, and a remarkable degree of success was accomplished. The structural properties measured in the thickened flow field became exactly similar to those in a naturally grown boundary layer after the flow had passed over a 0.61 m strip of roughness and 0.91 m of smooth test surface. Measurements included mean velocity profiles, profiles of longitudinal velocity fluctuations, and spectra of longitudinal velocity fluctuations. Since the method affected only the near-wall region of the turbulent boundary layers, no extraneous turbulent structures were produced in the wake region and normal behavior eventually developed. However, the roughness caused only a relatively small increase in momentum deficit, and only a 30% increase in effective wind-tunnel length was produced.

Examples of the second type of boundary layer augmentation device have been developed by Nagib, Morkovin, Yung, and Tan-Atichat (1974). They developed a technique for wind-tunnel simulation of neutral atmospheric shear layers. Instead of drag-producing obstacles placed in the flow, wall jets were used to manipulate and control the turbulence field. The device provided good flexibility in manipulating the turbulence structure, but reproduction of a given set of data was felt to be potentially difficult, since it would require fine adjustment of counter-jet orientations and velocities. The active devices used by Nagib et al. (1974) are suited to the simulation of the high turbulent-fluctuation levels in the atmosphere, because additional energy is ejected into the flow from the wall

jets. In contrast, the fluctuating and mean-field energy immediately downstream of passive devices are derived entirely from the mean flow field upstream of the device, and the turbulent levels downstream of such apparatus are lower than those which also incorporate wall-jet thickeners.

Most techniques discussed in the literature are augmentation devices of the third type. Of these, Otten and Van Kuren (1976) used configurations of vertical pins to thicken flat-plate boundary layers at high subsonic velocities. The thickened boundary layers had power-law mean velocity profiles with exponents between 1/4 and 1/9, and they were spanwise uniform as a result of the simplicity of the geometry of the thickening device. The fluctuating velocity component data showed scatter, but measurements were generally similar to results reported for naturally grown boundary layers. Spectra of static pressure fluctuations for the artificially thickened layer agreed with flat-plate spectra below 1700 Herz, except for spikes due to tunnel noise. No evidence of low-order equilibrium, such as similarity of the velocity defect profiles in the flow direction, was indicated by the authors.

Peterka and Cermak (1974) used spires of simple geometry followed by either smooth or rough walls to simulate the earth's shear layer. Using this technique, building wind loading and particle dispersion around scaled-down versions of urban complexes were studied. Their method produced a spanwise-uniform mean flow field and streamwise velocity profile similarity in five or six spire heights downstream of the thickening apparatus over rough surfaces. Counihan (1969a, 1969b, 1970, 1973) used elliptic wedge generators following a specially constructed barrier to simulate the atmospheric boundary layer. His measurements on rough walls indicate that the shear layer behind the spires does not reach a low-order equilibrium such as that described by a constant Clauser shape factor. Counihan's vortex generators have been further investigated by the present authors. Smooth-wall tests indicated that the velocity profiles had not reached similarity within 14 spire heights downstream, and, at the same location, the Reynolds stress was characterized by a large region of constant stress near the wall, which extended over approximately 50% of the boundary layer thickness. The magnitude of the shear stress was also higher than in naturally developed smooth-wall turbulent boundary layers for comparable boundary layer thickness. Counihan, Hunt, and Jackson (1974) have also

used the elliptic wedge generators to create an environment for the study of wakes behind two-dimensional surface obstacles in turbulent boundary layers. Cockrell and Lee (1969) demonstrated that any required velocity profiles could be produced almost immediately downstream of properly spaced grids of rods. However, they pointed out that only small-scale turbulent structures are produced and that, as turbulence diffuses outward from the wall, the consequent Reynolds stress causes the mean velocity profile to be modified.

2.1.3 Present Approach

In the present study, we are interested in learning about the behavior of thick, rough-wall, turbulent boundary layers as they might develop along a test section which was much longer than the available apparatus. An artificial thickening device was needed which would produce a flow with properties which are representative of natural behavior and which, at the same time, would provide substantial thickness increases over the naturally grown boundary layers over the same test surface. Klebanoff and Diehl's (1952) method is not useful for the present study, since it provides only small increases in thickness and has not been demonstrated to be useful in augmenting boundary layer flows over rough walls.[1] Other boundary layer augmentation techniques for two-dimensional, flat-plate, boundary layer simulation, such as that described by Otten and Van Kuren (1976), do not yield the right high-order properties and do not result in streamwise equilibrium. Atmospheric boundary layer simulations are not relevant, since these flows have a different character than that desired for the present study. A new boundary layer augmentation approach was required which would produce an equilibrium flow field with scalar, mean profile, and turbulence characteristics resembling natural flat-plate behavior.

2.1.3a Coordinate System. The coordinate system used for the present study is shown in Fig. 2-1. On the figure, the effective increase in wind-tunnel length, L, is shown along with the coordinates x_1 and x_2, which represent actual distance along the test surface, and distance measured from the virtual origin of the hydrodynamic flow field, respectively. In the artificially thickened boundary layer shown in the figure, normal

boundary layer properties are considered to be those which would exist in a boundary layer which developed naturally from its virtual origin to the same thickness as that produced by artificial thickening. Also indicated on 2-1 is ξ, the unheated starting length. In artificially thickened boundary layers, the thermal boundary layer is always thinner than the hydrodynamic boundary layer, as shown in 2-1, because ξ is always greater than L.

2.1.3b Equilibrium. In the present study, two levels of equilibrium are considered: first-order equilibrium, which is related to mean profile behavior, and second-order equilibrium, which is related to turbulence profile behavior. Requirements for first-order equilibrium are considered satisfied in a zero pressure gradient if G, the Clauser shape factor (1954, 1956), is independent of downstream location and (for smooth walls) the measured local skin friction is equivalent to that determined using a "Clauser plot" (see Clauser (1954)). Second-order equilibrium is indicated by longitudinal similarity of the non-dimensionalized Reynolds stress tensor component profiles.

The Clauser shape factor, G, is based on the universality of mean velocity profiles in $(U_\infty - U)/U_\tau$ versus y/δ coordinates and is defined using

$$G = \frac{1}{\int_0^\infty \left(\frac{U_\infty - U}{U_\tau}\right) dy} \int_0^\infty \left(\frac{U_\infty - U}{U_\tau}\right)^2 dy \qquad (2\text{-}1)$$

which is equivalent to

$$G = \frac{1}{\sqrt{C_f/2}} \left(1 - \frac{1}{H}\right) \qquad (2\text{-}2)$$

The shape factor definition given by (2-1) was first presented by Rotta (1953, 1955) in a theoretical analysis. Later, Clauser (1954, 1956) experimentally verified that G becomes invariant when $(\delta_1/\tau_w)(dP/dx)$ is constant, using his own adverse pressure gradient data and the zero pressure gradient data of Schultz-Grunow (1941), Hama (1954), Klebanoff and Diehl (1952), and Moore (1951).

The first-order and second-order requirements for equilibrium in the present study are also consistent with Townsend's (1956a) ideas of self-preservation in turbulent boundary layers. According to Gartshore and

de Croos (1976), self-preservation "describes a turbulent shear flow whose turbulence is in exact dynamic equilibrium so that the mean distributions of turbulence, non-dimensionalized by a single velocity and length scale, do not change at all in the streamwise direction." Townsend (1956a) developed this idea by first non-dimensionalizing mean and turbulence quantities such that

$$\frac{U_\infty - U}{(U_\tau/\kappa)} = f_1\left(\frac{y}{\delta}\right) \tag{2-3}$$

$$\frac{\overline{u'v'}}{(U_\tau/\kappa)^2} = g_1\left(\frac{y}{\delta}\right) \tag{2-4}$$

$$\frac{\overline{u'^2}}{(U_\tau/\kappa)^2} = g_2\left(\frac{y}{\delta}\right) \tag{2-5a}$$

and

$$\frac{\overline{v'^2}}{(U_\tau/\kappa)^2} = g_3\left(\frac{y}{\delta}\right) \tag{2-5b}$$

The boundary layer equation was then rearranged by expressing it in terms of the functions given by Eqns. (2-3) through (2-5). Then, for zero-pressure gradient flows, Townsend (1956a) showed that the equations of motion would be exactly satisfied such that the functions f_1, g_1, g_2, and g_3 are self-preserving and independent of downstream distance when the velocity deficit

$$\frac{U_\infty - U}{U_\infty} = \frac{U_\tau}{U_\infty \kappa} f_1\left(\frac{y}{\delta}\right) \tag{2-6}$$

is small. He showed that $(U_\infty - U)/U_\infty$ can be considered small over most of the boundary layer thickness, including part of the constant stress region when Reynolds numbers $U_\infty x/\nu$ are large. He explained the lack of similarity at low Reynolds numbers to be a consequence of large transverse mean velocities, V, which transport appreciable momentum due to the large transverse mean velocity gradient. Townsend (1956a, 1956b) also extended this analysis to flows with pressure gradients, by showing that the self-preserving functions f_1, g_1, g_2, and g_3 also exactly satisfy the equations of motion for certain freestream velocity distributions. It is

interesting to note that second-order equilibrium expressed by self-preservation of g_1, g_2, and g_3, is often achieved only downstream of first-order equilibrium when a turbulent boundary layer is developing downstream of a slight perturbation. Thus, even though the lower-order properties in the boundary layer, such as the mean velocity profile, may appear to be normal, the higher-order structure may not yet have normal equilibrium characteristics.

2.1.3c Information Hierarchy. The four different levels of boundary layer information considered for the present study are: (0) scalar quantities, (1) mean profiles, (2) Reynolds stress tensor components, and (3) one-dimensional turbulence spectra. It is assumed here that if the $n+1$ level of boundary layer information has normal characteristics, then all lower levels $(n, n-1, n-2)$ would also be expected to have natural behavior. More specifically, if all spectra, turbulence distributions, and mean profiles are representative of natural behavior, two-dimensional, and at equilibrium, one can strongly argue that the Stanton number and skin friction distributions will also be representative of natural behavior. This is because the transport properties for heat and momentum (i.e., mixing length and turbulent Prandtl number) are determined by these higher-ordered properties. This is consistent with the levels of assumption currently used in boundary layer prediction schemes. In non-equilibrium situations, as pointed out earlier, the different levels of information may not display this relationship.

2.2 SMOOTH-SURFACE, ARTIFICIALLY THICKENED BOUNDARY LAYERS

2.2.1 Objective

The objective of the smooth-wall study is to show that normal mean and turbulence properties can be produced simultaneously in an artificially thickened boundary layer developing from a device of the third type discussed in Section 2.1.1. Experience is to be gained in artificially thickening boundary layers before such methods are used to study thick, rough-wall behavior. The smooth-wall environment provides a good qualification test for the flow field, since all artificially thickened boundary layer measurements can be compared to baseline data. Both thermal and hydrodynamic

behavior on smooth walls is documented extensively throughout the literature by many authors, and is characterized by Reynolds number dependence. The Reynolds number dependence allows lower-order properties, such as $C_f/2$ and St, to be compared in two different boundary layers having the same momentum or enthalpy thickness Reynolds number, even though the two cases may have differing boundary layer thickness or freestream velocity.

2.2.2 Apparatus

2.2.2a Final Design. The final design of the apparatus used to artificially thicken turbulent boundary layers over smooth surfaces is shown in Figs. 2-2a and 2-2b and is designated Design C. The apparatus consists of a trip, an array of spires, and a barrier, each of which extends across the width of the wind tunnel, just upstream of the test surface. The trip is .025 cm high and is located just downstream of the exit plane of the nozzle of the wind tunnel. The spires are 3.0 cm downstream of the trip, and the barrier is 3.016 cm downstream of the spires.

The apparatus was developed and used in the HMT-1 wind tunnel, as discussed in Chapter 1.

2.2.2b Component Effects. In general, the functions of the artificial thickening apparatus are to slow down the flow and to augment the turbulence, hastening the development of small-scale and large-scale eddy structures. Fluctuations are produced using energy from the mean velocity flow upstream of the thickening apparatus. The eddies caused by this mixing are convected downstream and mix with eddies from the near-wall regions. Turbulence levels are increased over previous potential flow levels and near-wall turbulence is transported more readily into the outer portions of the augmented boundary layer.

Specific effects of some of the components of the artificial thickening apparatus are now presented in a discussion divided into sections on adjustment of particular boundary layer properties.

Hydrodynamic starting length adjustment. The hydrodynamic starting length (or the effective increase in tunnel length), L, associated with an artificial thickening apparatus can be altered by changing the form drag on the apparatus. An estimate of the dependence of L on geometry can be

obtained by equating the form drag from the thickening device to the skin friction which would exist for a test section of length L

$$\frac{\overline{C_f}}{2} L = \frac{C_D}{2} \frac{A_f}{\omega} \tag{2-7}$$

In (2-7), ω is the spacing between the centerlines of the spires and C_D is the drag coefficient for the thickening appratus based on the frontal area of one spire, A_f. If the Schultz-Grunow (1941) correlation for $\overline{C_f}/2$ is then substituted in (2-7) and the result is rearranged, we have

$$\frac{(0.427)L}{(2.0)\left(-0.407 + \log\left(\frac{U_\infty L}{\nu}\right)\right)^{2.64}} = \frac{C_D}{2} \frac{A_f}{\omega} \tag{2-8}$$

From (2-8), the hydrodynamic starting length L increases whenever the frontal area of the spires increases, the spire drag coefficient increases, or the spacing between the spires decreases. Increased barrier height, h, and increased spire height, β, also result in increased magnitudes of L. In the present study, for the Fig. 2-2 spire design, $C_D \sim 1.0$.

Adjustment of the momentum thickness just downstream of the spires. The momentum thickness just downstream of the spires, $\delta_2\big|_L$ (δ_2 at $x_2 = L$) can be adjusted in the same way in which the hydrodynamic starting length is changed. This becomes apparent, first, by considering that thicker boundary layers require greater downstream distances to develop, and secondly, by substituting for $\overline{C_f}/2$ in (2-7) using the momentum integral equation to give

$$\delta_2\Big|_L = \frac{C_D}{2} \frac{A_f}{\omega} \tag{2-9}$$

A comparison of (2-8) and (2-9) then shows the same qualitative dependence of $\delta_2\big|_L$ and L on artificial thickening apparatus characteristics.

Mean velocity profile adjustment. The mean velocity profiles can be adjusted by changing the shape or spacing of the spires. As the spacing between spires is increased, the differences between the boundary layer velocities and the freestream velocity decrease. As the shapes of the spires are changed, the velocity profiles are altered depending on how the local streamlining of the spires is altered.

Figure 2-3 shows velocity profiles measured downstream of different spire arrays, where the shapes of the spires are drastically changed by adding blades on upstream and downstream sides. The velocity profile with the largest differences relative to the freestream velocity is obtained with Design A, which has a blunt trailing edge and no upstream blade. The velocity profile with the smallest differences relative to the freestream velocity is obtained using Design B, which is fully streamlined with upstream and downstream blades. A velocity profile which is between those produced by A and B, and also shows agreement with Simpson's (1967) data at the same momentum thickness Reynolds number, is produced by Design C.

Finer adjustments of the velocity profiles than those produced by adding upstream and downstream blades can be made by altering the upstream total angle of each blade, θ. This is possible since the spanwise momentum flux of fluid diverted between spires is dependent upon direction relative to the freestream, which is a function of θ at the spire upstream edges.

The tapered nature of the spires shown in Fig. 2-2 also has important consequences regarding the velocity profiles in the augmented boundary layer. Because the spires are thinner at the top than at the bottom, less momentum is taken from the flow near the top of the spires than at the bottom, resulting in increasing velocities as distance from the wall increases.

Adjustment of the relation between the skin friction and the mean velocity profile. The relation between the skin friction and mean velocity profiles can be adjusted by changing the barrier height, h. Alterations in barrier height result in simultaneous changes in both the inner and outer regions of the boundary layer. The effect on the inner regions is shown in Fig. 2-4, which shows that the log regions of the velocity profiles in U^+ versus y^+ coordinates shift as h is changed. In other words, the relationship is varied between the skin friction determined from near wall measurements of the shear stress (see Appendix II) and the skin friction determined from a "Clauser plot" (see Clauser (1954)). Barrier height adjustments affect the outer region by changing the relation between the skin friction and mean velocity such that the dependence of G, the Clauser (1954, 1956) shape factor, on downstream distance is altered. G will increase or decrease with downstream distance, depending on whether the U^+

versus y^+ plots are above or below the law of the wall, which is given by

$$U^+ = \frac{1}{\kappa} \ln y^+ + C \qquad (2\text{-}10)$$

where $\kappa = 0.41$ and $C = 5.10$. Thus, changing the barrier height is a means by which the flow field can be adjusted to have first-order equilibrium, which occurs when G is a constant with downstream distance and the inner regions of the boundary layer agree with the law of the wall. Fig. 2-4 and 2-8a show that this occurs using design C spires when the barrier height, h, is 0.476 cm.

Turbulence profile adjustment. Any modification which changes the mixing around the artificial thickening apparatus will affect the downstream turbulence. One component of the apparatus which has a large influence on the downstream turbulence structure is the upstream blade on each spire. The angle of each blade, θ, (see Fig. 2-2) influences the mixing in the fluid diverted by the blade. Generally, it seems that turbulence levels increase as θ increases.

2.2.2c. Design Development. The first trial in the design of the present artificial thickening apparatus is shown as Design A in Fig. 2-3. It was based on a scaled-down version of the spire design used by Peterka and Cermak (1974). Subsequent alterations followed an iterative scheme in which the drag-producing shapes were placed in the flow and the downstream properties were then examined with respect to their similarity to the structure of a naturally developing boundary layer. This was followed by modification to produce behavior more closely resembling the desired lower-order flow field characteristics, and then the procedure was continued, eventually to higher levels of information until convergence to the desired flow structure was accomplished.

During design development, it was found that small geometric variations in the spire array can cause large spanwise variations of the mean velocity and of the turbulence structure in the downstream flow field, particularly at high velocities. Equilibrium is also a major problem which becomes more difficult as higher freestream velocities and smoother test

sections are used. Because the wake region is strongly dependent on upstream history effects and responds only slowly to wall boundary conditions, it will be the last region to reach equilibrium. Any unnatural velocity or turbulence effects produced in the wake by the spires may be convected far downstream before a semblance of natural behavior develops.

2.2.3 Boundary Layer Characteristics

The final design of the smooth-wall, artificial thickening apparatus (Design C) produces a flow field with properties representative of normal behavior to the level of the cross-correlation coefficient for the turbulent shear stress, and the Reynolds shear stress-turbulent kinetic energy ratio. All measurements concerning the smooth-plate work are presented in this section and compared to measurements by other investigators in naturally developed zero-pressure-gradient flows. Predictions of Stanton number distributions and skin-friction coefficient distributions have also been made using STAN5, a finite-difference numerical scheme for smooth-wall, two-dimensional boundary layer flows. The prediction method is based on the Spalding-Patankar code and is discussed in detail by Crawford and Kays (1975). The program was used with the usual Van Driest (1955) mixing-length scheme, without adjustment or deviation from a normal turbulent boundary layer run.

2.2.3a. Hydrodynamic Results. All of the measurements made downstream of the smooth-wall thickening apparatus were made in air at a free stream velocity of 10.1 m/sec and at an approximate free stream temperature of 22.8°C.

Displacement thickness and momentum thickness data are compared with the correlations of Schultz-Grunow (1941) in Fig. 2-5. The effective hydrodynamic starting length upstream of the thickening apparatus, L, was determined to be 2.60 m, based on the displacement "match point" shown in Fig. 2-5, interpreted through the Schultz-Grunow correlation. Using the same value of L for remaining data points, agreement is maintained between the thickened flow field measurements and the correlations for $x_1 > 0.9$ m. The growth rate is thus shown to be consistent with natural equilibrium behavior. Agreement with Simpson's (1967) mean velocity profiles in U/U_∞ versus y/δ coordinates also occurs at the measuring stations downstream

of $x_1 = 0.9$ m (see Fig. 2-3). Spanwise velocity profiles at $x_1 = 1.22$ m for $z = -5.08$ cm, $z = 0$ cm (centerline), and $z = 10.16$ cm, showed a variation of momentum thickness of less than 3% about the mean.

The local skin friction was determined from measurements of the Reynolds shear stress near the wall using a rotatable, slanted, hot-wire anemometer. The details of the measurement procedure are discussed in Appendix II.

Results of skin friction measurements from the present study are shown in Figs. 2-6a and 2-6b. Fig. 2-6a indicates that the skin friction agrees with the Schultz-Grunow (1941) correlation, calculated using the same L discussed above. In Fig. 2-6b, measured data agree with the well-known relation

$$\frac{C_f}{2} = 0.0128\left(Re_{\delta_2}\right)^{-0.25}$$

where the constant 0.0128 is that suggested by Kays (1966). Figs. 2-6a and 2-6b further show agreement between predictions and the data. At the last four downstream stations, the measured skin friction is also closely equivalent to the skin friction determined from the velocity profiles using a "Clauser plot" (1954). Agreement with the momentum integral equation for average skin friction is also maintained within ± 10% at the same locations, where the equation is given by

$$\frac{\overline{C_f}}{2} = \frac{\delta_2}{x} \tag{2-11}$$

Velocity profiles in wall coordinates are shown in Fig. 2-7. These profiles were non-dimensionalized using measured skin friction, and show excellent agreement with the law of the wall, given by

$$U^+ = \frac{1}{\kappa} \ln y^+ + C \tag{2-12}$$

where $\kappa = 0.41$ and $C = 5.10$, for the stations where $x_1 > 0.9$ m. The value of y^+ where data points begin to vary from the law of the wall (at the edge of the wake) is approximately 500. Clauser (1956) indicates that the appropriate value of momentum thickness Reynolds number for deviation

at this point is 5000, which is consistent with thickened flow-field measurements. Fig. 2-7 also indicates that in the transition or buffer region of the artificially thickened boundary layer, the velocity measurements fall within the scatter of Laufer's (1954) data for pipe flow. Thus, for $y^+ \lesssim 500$, the velocity profiles in boundary layer coordinates are consistent with normal behavior at the four measuring stations farthest downstream

Each equilibrium turbulent boundary layer corresponds to a certain value of G, the Clauser shape factor (1954, 1956), where the value of G depends on the pressure gradient. Fig. 2-8a indicates that the artificially thickened boundary layer reaches a Clauser-type of equilibrium for $x_1 > 0.9$ m, since G becomes constant at approximately 6.8, a value consistent with natural zero-pressure-gradient boundary layer behavior. Values of G are shown on the figure which are determined both from measured values of the local skin friction and values determined using a "Clauser plot" (see Clauser (1954)).

The definitions of the momentum thickness, displacement thickness, and Karman shape factor can be substituted into the defining equation for G, and the result rearranged to produce an equation for the Karman shape factor

$$H = \left(1 - G\sqrt{\frac{C_f}{2}}\right)^{-1} \tag{2-13}$$

A boundary layer flow with a value of G consistent with natural behavior assures that the dependence of the Karman shape factor with skin friction is also normal. This is demonstrated in Fig. 2-8b for the artificially thickened boundary layer. The data show agreement with Eqn. (2-13), and the measurements fall within the scatter of Hama's (1954) data for smooth-wall flows.

Since the Clauser shape factor is independent of x-location in the artificially thickened boundary layer, the velocity profiles, when plotted in defect coordinates, should show downstream similarity. Such behavior exists for $x_1 > 0.9$m, as indicated in Fig. 2-9. Agreement is also found, for the same locations, with Coles' (1956) law of the wake, given by

$$\frac{U_\infty - U}{U_\tau} = -\frac{1}{\kappa}\ln\left(\frac{y}{\delta}\right) + \frac{\pi}{\kappa}\left[2 - \omega\left(\frac{y}{\delta}\right)\right] \tag{2-14}$$

where $\pi = 0.55$ for zero-pressure-gradient flows, and $\kappa = 0.41$. Measured skin friction values were used to non-dimensionalize velocities in Fig. 2-9.

The profiles of longitudinal turbulent intensity, turbulent shear stress, and turbulent kinetic energy are closely similar to those of naturally developing boundary layers at $x_1 = 1.98$ m and $x_1 = 2.29$ m. Measurements 1.17 meters and 1.57 meters downstream of the thickening apparatus indicate that the turbulence in the augmented boundary layer is not fully developed at these two locations. Profiles at all four locations are shown in Figs. 2-10a through 2-10c, along with Klebanoff's (1954) measurements at $U_\tau/U_\infty = 0.037$ and Orlando's (1974) measurements at $U_\tau/U_\infty = .043$ for comparison. The slight deficits which exist for $0.14 < y/\delta < 0.60$ at $x_1 = 1.17$ m and at $x_1 = 1.57$ m disappear farther downstream, where streamwise similarity of the profiles indicates that second-order equilibrium has developed.

It appears that Klebanoff's (1954) definition of δ is based on $U/U_\infty \sim .999$ rather than $U/U_\infty = .99$, which is used in the present study. The Klebanoff data in Figs. 2-10a through 2-10c have been corrected to account for differences in definitions of δ used for the two studies.

Figure 2-10d indicates that measurements taken at all four locations for $0.10 < y/\delta < 0.90$ agree with the cross-correlation coefficient for the turbulent shear stress, and the ratio of the Reynolds shear stress to the turbulent kinetic energy within $\pm 10\%$, where the correlations are given by

$$\frac{\overline{-u'v'}}{\sqrt{\overline{u'^2}\ \overline{v'^2}}} = 0.46 \quad \text{and} \quad \frac{\overline{-u'v'}}{\overline{q^2}} = 0.145 \qquad (2\text{-}15)$$

2.2.3b. Heat Transfer Results. The results of heat transfer studies in the artificially thickened boundary layer, shown in Figs. 2-11 and 2-12, indicate that normal behavior exists for $x_1 > 0.6$ m. An unheated starting-length effect is evident as measured Stanton numbers are located below the curve for constant wall temperature, when plotted against enthalpy thickness Reynolds number. The virtual origin of the hydrodynamic boundary layer is upstream of the point where the thermal boundary layer begins to develop.

Consequently, a greater portion of the thermal boundary layer downstream of the step change in wall temperature is immersed in the laminar sublayer, when compared to a constant wall temperature flow at the same enthalpy thickness Reynolds number.

Flows with three different unheated starting lengths, ξ, were created by heating different segments of the test section downstream of the spires. The apparent origin of the thermal flow field is determined with respect to the hydrodynamic origin by adding the starting length based on displacement thickness, L, to the distance between the spires and the upstream edge of the first heated plate, x_1, as shown in Fig. 2-1. Plotted on Fig. 2-11a are data for $\xi = 2.603$ m, in which all plates were heated at constant temperature without transpiration. The thermal boundary layer begins to develop just downstream of the augmentation apparatus, and the first four plates are in a region of high mixing and eddy interaction. First-order equilibrium has not yet developed in the flow, the heat transfer in this region is augmented, and measured Stanton numbers are greater than predicted values. Eventually, data and prediction agree, as the unnatural mixing effects subside from the thermal boundary layer. Farther downstream, at $Re_{\Delta_2} \sim 2500$, the influence of the unheated starting length also subsides, as shown when the data approach the isothermal flat-plate solution. Figs. 2-11b and 2-11c, for $\xi = 3.213$ m and $\xi = 3.822$ m, show similar trends, with predictions and measurements in good agreement for all data points.

The data for $\xi = 2.603$ m, $\xi = 3.213$ m, and $\xi = 3.822$ m are also plotted as functions of Re_{x_2} in Fig. 2-12a, which demonstrates agreement with the well-known correlation developed by Reynolds (1958). Agreement with Reynolds' (1958) data is shown in Fig. 2-12b, where Re_ξ is a Reynolds number based on ξ. In Fig. 2-12b coordinates, unheated starting length effects persist at all measured data points, evidenced by the fact that they are located above the constant wall-temperature solution.

Figure 2-11a shows the results of a test in which all of the plates were heated and $F = .004$ transpiration was used on the first four plates. The lowered Stanton numbers at these four data points recover to values for a non-transpired flow within two plates downstream of the blown region. This is consistent with normal behavior and significant, since it demonstrates

that the artificially thickened boundary layer behaves normally when subject to a blowing perturbation. Transpiration also increases the thickness of the thermal boundary layer compared to the non-transpired flow, as evidenced by the increase in enthalpy thickness Reynolds number at the farthest downstream plate from 3900 to 4400. Transpiration can thus be used to augment the thermal boundary layer without causing unnatural effects in the downstream heat transfer behavior.

2.2.3c. Conclusions. Measurements have shown that the artificially thickened boundary layer has a hydrodynamic field which is similar to that of a naturally developed smooth-wall, turbulent boundary layer. The similarity extends up to the level of the cross-correlation coefficient for the turbulent shear stress and the ratio of Reynolds shear stress to turbulent kinetic energy. An effective increase in the wind tunnel test section length of 2.60 m is provided at a free-stream velocity of 10.1 m/sec. The final displacement thickness is 1.74 times greater than that which would exist at the downstream end of the same test surface at the same free-stream velocity.

Normal thermal behavior has been demonstrated by Stanton number measurements, which agree for $x_1 > 0.6$ m with predictions and data for naturally developing boundary layer flows having unheated starting lengths. Heat transfer with transpiration ($F = .004$ for $x_1 < .406$ m) also indicates normal behavior, indicating that the augmented thermal layer responds normally when subjected to a blowing perturbation.

The above-mentioned tests indicate that it is possible to successfully simulate boundary layer behavior over smooth walls, using an artificial thickening device of the type presented here. The techniques can then be extended to the study of thick, turbulent boundary layers which develop over rough walls.

2.3 ROUGH-SURFACE, ARTIFICIALLY THICKENED BOUNDARY LAYERS

The flow field downstream of the artificial thickening device can be viewed as a natural differential equation solver for thick, rough-wall, turbulent boundary layers. The flow produces a "solution" to the boundary layer equations which is dependent on the boundary conditions and initial conditions, and is measurable at any downstream location. The boundary conditions for the solution are set by the distribution of freestream velocity with downstream distance and the characteristics of the roughness elements which comprise the test surface. The initial conditions consist of the profiles of mean velocity and the six Reynolds stress tensor components, produced at some distance downstream of the artificial thickening device. In order for the solution to be representative of normal behavior, these initial condition properties produced by the artificial thickening apparatus must be two-dimensional, and in an equilibrium relationship which matches those of a naturally developed boundary layer of the same thickness.

2.3.1 Objectives

The objective of the rough-wall, artificial thickening apparatus is to produce a flow field sufficiently normal that it allows studies to be made of the turbulence and mean properties of thick, rough-wall boundary layers. In order to be sufficiently normal, the artificially thickened boundary layer must be at equilibrium, must be two-dimensional, and must show growth characteristics typical of a natural flow. In addition, the turbulent boundary layer structure must also be consistent with that which would exist in a natural flow at the same thickness.

Proof that the artificially thickened rough-wall layer structure is normal requires a different approach than did the smooth-wall flows. No prior studies have been reported concerning thick boundary layers over sphere-type roughness, whereas smooth-wall layers have been extensively documented. Thus there is no data base available which can be used directly to verify that the flow field is normal. It is necessary to make the proof indirectly, using whatever properties are well known for thick, rough-wall layers. The most sensible properties to be used for this purpose are those which have been indicated to be invariant with downstream development in naturally developing boundary layers. If the artificially

thickened boundary layer is in fact an extension of a naturally developed boundary, these should be also invariant in the augmented boundary layer. Demonstration of this invariance can then be used as part of the qualification of the structural behavior of the artificial boundary layer.

In the present study, we are interested in learning not only about the effects of downstream development on thick, rough-wall boundary layers, but also effects of changing the freestream velocity. Qualification of the structure must therefore not only investigate downstream development, but also the response to changes in freestream velocity. Response to changes in freestream velocity is checked by investigating properties invariant with freestream velocity at different freestream velocities.

Qualification of the thick boundary layer is to be made by showing that the flow field has normal growth, two-dimensionality, equilibrium, and structural characteristics. The properties of the thick, rough-wall layers to be used for qualification of the structure are those known to be independent of both freestream velocity and downstream distance in naturally developing layers. These are four: the law of the wake, the Reynolds shear stress profile, the Reynolds shear stress/turbulent kinetic energy ratio, and the correlation coefficient for the Reynolds shear stress. The law of the wall cannot be used to qualify the structural behavior of thick, rough-wall layers, since the law is dependent on Re_k in transitionally rough flows, and Re_k may vary with downstream distance.

2.3.2 Apparatus

2.3.2a. Final Design. The final design of the apparatus is designated Design E and is shown in Fig. 2-13. The dimensions and characteristics of the design are similar to those of the smooth-wall design shown in Figs. 2-2a and 2-2b, with three exceptions: (1) a square bar having a width of .238 cm was added on the downstream side of the spires a distance 2.064 cm away from the wall; (2) the barrier height was changed to .635 cm; and (3) the trip was located 3.49 cm upstream of the spires, and its thickness was increased to 0.16 cm.

The final design was developed at a freestream velocity of 26.8 m/sec, The details of this development are presented in Section 2.3.2c. No additional changes were needed, as the final design was used at other freestream velocities.

The rough-wall, artificial thickening apparatus was developed and used in the HMT-18 wind tunnel, as mentioned in Chapter I.

2.3.2b. Component Effects. The components of the Fig. 2-13 apparatus are now discussed with regard to adjustment of rough-wall boundary layer characteristics.

Turbulence profile adjustment. As in the smooth-wall study, the turbulence characteristics of the augmented rough-wall boundary layer can be changed by altering the way fluid mixes. Two characteristics which have been found to change the turbulence profiles are the barrier height, h, and the bar location, γ. Fig. 2-14 shows a comparison of turbulence profiles over the rough surface downstream of three different configurations: Designs C, D, and E. The figure shows that Design C produces lower values of $-\overline{u'v'}/U_\tau^2$ and $\overline{u'^2}/U_\infty^2$ than Designs D and E, although magnitudes of $\overline{u'w'}/U_\tau^2$ are significantly higher. These differences for $y/\delta > 0.1$ are caused by the bar which is included on Designs D and E, and left off of Design C. Fig. 2-14 also shows that the magnitude of $\overline{u'^2}/U_\infty^2$ for $0.02 < y/\delta < 0.10$ is higher for Design E than for Design D. The differences between the two profiles are as large as 7% and are a result of a barrier height change of 0.08 cm.

Figure 2-15 shows profiles of $\overline{u'^2}/U_\infty^2$ downstream of the rough-wall design as the distance between the bar and wall, γ, is changed, where the γ coordinate is illustrated on Fig. 2-13. As the bar is moved farther from the wall and γ increases, the magnitudes of $\overline{u'^2}$ in the outer regions of the profile increase and the magnitudes of $\overline{u'^2}$ in the inner regions of the profile decrease. Thus, from these geometry alterations, we see that quantitative adjustments of the turbulence structure can be made by altering apparatus characteristics.

Adjustment of the relation between the skin friction and the mean velocity profile. As for the smooth-wall flow, the relation between the skin friction and the mean velocity can be altered by changing the barrier height. In fully rough flows at 26.8 m/sec, the barrier can be adjusted so that G is invariant with downstream distance simultaneously when the near-wall velocities follow the fully rough law of the wall

$$U^+ = \frac{1}{\kappa} \ln \left(\frac{y' + \Delta y}{k_s} \right) + 8.5 \qquad (2\text{-}16)$$

where $\Delta y = .023$ cm and $k_s = .079$ cm. Thus, for both the smooth and fully rough flows investigated, the barrier height can be altered to change the relation between $C_f/2$ and $U(y)$ so that the flow field produced has first-order equilibrium.

2.3.2c. Design Development. The first trial in the design of the rough-wall, artificial thickening apparatus was the smooth-wall design (Design C) shown in Fig. 2-2. The flow produced over the rough surface by the design in Fig. 2-2 had reasonably normal mean properties, but displayed some spanwise non-uniformities. The turbulence profiles also varied significantly with downstream development, and the three-dimensional Reynolds stress components showed $\overline{u'w'}$ and $\overline{v'w'}$ magnitudes as large as 40% of $-\overline{u'v'}$.

The iterations in apparatus development which led to improved flow behavior began with design modifications to achieve a two-dimensional flow field. Generally, the two-dimensionality depends on the details of the geometry, spacing, and shape of the spires and other components of the artificial thickening apparatus. The two-dimensionality is particularly affected if these geometric characteristics are not uniform across the entire width of the wind tunnel. After the two-dimensionality of the flow was acceptable, a bar was added across the downstream side of the spires to alter the turbulence structure (Design D). Then barrier height adjustments were made to change the relation between the mean velocity and the skin friction, to produce first-order equilibrium and agreement with the fully rough law of the wall (Design E).

2.3.3 Boundary Layer Characteristics

The boundary layer characteristics used to qualify the behavior of the artificially thickened boundary layer are presented in this section. The layer is produced from the Design E device shown in Fig. 2-13. Boundary layer growth, two-dimensionality, structure, and equilibrium are discussed for free stream velocities of 10.1 m/sec, 15.8 m/sec, and 26.8 m/sec. Some structural characteristics are also presented for a freestream velocity of 20.4 m/sec.

2.3.3a. Growth. Boundary layer growth can be represented using two different characteristics of boundary layers which are related through the momentum integral equation. These two characteristics are the variation of the skin friction coefficient, $C_f/2$, with momentum thickness, δ_2, and the variation of momentum thickness with downstream distance, x.

Skin friction is shown in Fig. 2-16 as a function of momentum thickness in naturally developed and artificially thickened boundary layers for freestream velocities of 10.1 m/sec, 15.8 m/sec, and 26.8 m/sec. The skin friction coefficients were determined from measurements of the Reynolds shear stress and mean velocity near the wall, as discussed in Appendix II. Momentum thickness values were determined independently of the $C_f/2$ measurements using the definition of δ_2 and the mean velocity profiles. On 2-16, the artificially thickened data forms a natural extension of the naturally developed data. Thus, the artificially thickened layer has normal growth characteristics with respect to $C_f/2$ versus δ_2. At a given freestream velocity, data can be represented using

$$\frac{C_f}{2} = a\left(\frac{\delta_2}{r}\right)^{-b} \tag{2-17}$$

where the constants a and b are presented in Table 2-1. The constants in Table 2-1 for $U_\infty = 26.8$ m/sec are the same as those suggested by Pimenta (1975) for a naturally developed flow.

The variation of the momentum thickness with downstream distance (measured from the virtual origin of the hydrodynamic flow field, $x_2 = 0$) is now determined. The right-hand side of Eqn. (2-17) is set equal to the two-dimensional momentum integral equation

$$\frac{C_f}{2} = \frac{d\delta_2}{dx} \tag{2-18}$$

which produces a result which can then be integrated to give

$$\frac{\delta_2}{r} = \left[a(b+1)\right]^{1/b+1} \left(\frac{x_2}{r}\right)^{1/b+1} \tag{2-19}$$

The effective increase in wind tunnel length, L, can then be calculated using (2-19) for a given free stream velocity. This is done by matching

(2-19) to one data point per augmentation ("match point") and then extrapolating to $x_2 = 0$, the virtual origin of the hydrodynamic flow field. The values of L for the artificially thickened measurements are shown for free stream velocities of 26.8 m/sec, 15.8 m/sec, and 10.1 m/sec in Figs. 2-17, 2-18, and 2-19, respectively. Also shown are Eqns. (2-19) and measurements. The figure shows that the data points not fitted to Eqn. (2-19) also match the equation. Thus, the growth properties of the artificially thickened boundary layer seem normal with respect to variations of δ_2 with x_2.

Table 2-1

Values of a and b
in Eqns. (2-17) and (2-19)

U_∞ (m/sec)	a	b	Roughness Regime
10.1	.00381	.332	Transitionally rough
15.8	.00327	.217	Transitionally rough
26.8	.00328	.175	Fully rough

If the Karman shape factor, H, is plotted versus U_∞/U_τ as in Fig. 2-20, we find that the artificially thickened results fall within the scatter of Hamm's results (1954) for rough walls. Thus, the variations of δ_1, the displacement thickness, with U_∞/U_τ are not inconsistent with other measurements, and we can conclude that these growth characteristics of the thickened boundary layer are also representative of normal behavior.

2.3.3b. Two-dimensionality. The two-dimensionality of the artificially thickened flow field was checked by measuring the three-dimensional Reynolds shear stress components, $\overline{v'w'}$ and $\overline{u'w'}$, at all turbulent kinetic energy measurement locations on the rough surface. More extensive two-dimensionality checks, consisting of spanwise measurements of the mean velocity and Reynolds stress tensor components, were made at 26.8 m/sec.

The spanwise velocity profiles at $U_\infty = 26.8$ m/sec were made at $x_1 = 1.168$ m and $x_1 = 2.083$ m. The three momentum thickness values show variations of $\pm 3.9\%$ about the mean value and $\pm 4.6\%$ about the mean value at

these respective locations. The spanwise variation of momentum thickness then increases in the downstream direction and thus shows a trend which is qualitatively consistent with data of Osaka, Shimizu, Nakamura, and Furaya (1977).

Figure 2-21 shows that the profiles of the Reynolds stress tensor components are spanwise uniform at $x_1 = 1.168$ m and $U_\infty = 26.8$ m/sec. The figure also indicates that $\overline{u'w'}$ and $\overline{v'w'}$ are insignificant compared to $-\overline{u'v'}$ at all profile positions at this location. These small values of $\overline{u'w'}$ and $\overline{v'w'}$ are consistent with the spanwise uniformity of $\overline{w'^2}$. The three-dimensional shear stress components are also negligible compared to $-\overline{u'v'}$ at all other traverse locations in the rough-wall, artificially thickened boundary layer, for the four free stream velocities studied.

An additional check on the two-dimensionality of the flow is provided by the momentum integral equation, where qualitative agreement with the data was indicated in the previous section. A quantitative comparison can be made by substituting δ_2 values at sequential measuring stations into Eqn. (2-11), in order to compare with measured skin friction values. Agreement with Eqn. (2-11) is maintained within 10% for free stream velocities of 26.8 m/sec and 15.8 m/sec. The data for 10.1 m/sec shows a maximum deviation from Eqn. (2-11) of 13%.

2.3.3c. Structural Similarity. The mean velocity and turbulence structure of the augmented boundary layer are further qualified by comparing measurements to those known to exist in boundary layers which developed naturally to the same thickness as that produced by artificial thickening. Since known characteristics are required, only those boundary layer characteristics indicated to be invariant with thickness in naturally developing flows can be used for this purpose. Since conclusions will be drawn regarding the effect of using different free stream velocities, the characteristics must also be invariant as the free stream velocity changes.

Mean velocity profiles -- velocity defect coordinates. The first of these boundary layer characteristics to be discussed is the velocity profile in defect or wake coordinates. According to Clauser (1956), when $(\delta_1/\tau_w)(dP/dx)$ is equal to any constant and the boundary layers are at equilibrium, velocity profiles in $(U_\infty - U)/U_\tau$ versus y/δ coordinates are

universally similar in shape, where the shape is dependent on the value of $(\delta_1/\tau_w)/(dP/dx)$. Profiles having a given shape are then characterized by a given value of the shape factor G given by Eqn. (2-1). In the present study, a G which is invariant in the downstream direction is taken to indicate first-order equilibrium, and thus first-order equilibrium is closely connected to the streamwise similarity of $(U_\infty - U)/U_\tau$ versus y/δ profiles. Clauser first argued the plausibility of these concepts and then provided experimental verification for zero-pressure-gradient flows using the smooth-wall data of Schultz-Grunow (1941), Hama (1954), and Klebanoff and Diehl (1951), as well as the rough-wall data of Hama (1954) and Moore (1951). Clauser showed that equilibrium velocity profiles in $(U_\infty - U)/U_\tau$ versus y/δ coordinates are invariant both with downstream development and with changes in surface roughness. Later, Coles (1956) produced a functional relation to describe these profiles in various equilibrium pressure gradients, which is given by Eqn. (2-14) and referred to as the law of the wake. Pimenta (1975) showed that Eqn. (2-14) was valid for turbulent boundary layers developing over the uniform-spheres roughness of the present study. Other investigators, such as Perry and Joubert (1963) show the law of the wake also represents boundary layer behavior over additional types of roughness. Thus, the law of the wake and similarity of profiles in $(U_\infty - U)/U_\tau$ versus y/δ coordinates are important criteria for qualification of the augmented flow field, and experimental agreement is necessary if the properties of the flow field are to be considered representative of natural behavior.

The velocity profiles in defect coordinates measured at all four free stream velocities of the present study show excellent agreement with the law of the wake, as shown in Fig. 2-22. An example of the downstream development of these velocity measurements is also shown in the figure for U_∞ = 26.8 m/sec. The profiles show agreement with the law of the wake and have downstream similarity for $x_1 > 1.0$ m. The friction velocities used to nondimensionalize the profiles were calculated using local skin friction coefficients determined from near-wall shear stress and mean velocity measurements (see Appendix II).

The value of y used for the plots in Fig. 2-22 and all subsequent mean profile plots is measured from the apparent or virtual origin of the

mean velocity profiles. This origin is located a distance Δy below the crests of the roughness elements, and is determined using the method suggested by Monin and Yaglom (1971), which was also used by Pimenta (1975) and Coleman (1976). Briefly, it is assumed that a corrected roughness size, z_o, does not change with y near the wall for fully rough flows, where z_o is defined using

$$U^+ = \frac{1}{\kappa} \ln \left(\frac{y' + \Delta y}{z_o} \right) \tag{2-20}$$

The value of Δy determined from measurements in naturally developed and artificially thickened boundary layers in the present study is .023 cm. Pimenta (1975) and Coleman (1976) suggest values of Δy ranging from .015 cm to .018 cm. In Eqn. (2-20), y' is measured from the crests of the roughness elements, and hence $y = y' + \Delta y$.

Reynolds shear stress profiles. In a theoretical analysis, Clauser (1956) showed that if a universal velocity profile (such as that given by the law of the wake equation (2-14)) exists, then a shear stress distribution exists which is nearly universal. Clauser said that the variations of these nearly similar profiles of $-\overline{u'v'}/U_\tau^2$ versus y/δ would depend on the skin friction coefficient, $C_f/2$, but that "great care would have to be taken experimentally to distinguish between the curves." Thus, shear stress profiles are expected to be approximately invariant in equilibrium boundary layers whenever the law of the wake is valid. As discussed in the previous section, the law of the wake represents equilibrium boundary layer profile behavior, regardless of variations of surface roughness, freestream velocity, or downstream development.

Experimental verification of Clauser's (1956) analysis can be made using results of several investigations. These investigations are discussed by first considering the downstream development of shear stress profiles and then by considering the invariance of shear stress profiles with roughness size and freestream velocity.

The invariance of $-\overline{u'v'}/U_\tau^2$ versus y/δ profiles with downstream development in equilibrium flows is shown by Pimenta's (1975) measurements and by the measurements from the present study in naturally developed boundary layers. Such characteristics are consistent with Townsend's (1956a) structural similarity hypothesis, as discussed earlier.

The approximate invariance of shear stress profiles with roughness is demonstrated by comparing the smooth-wall measurements of Klebanoff (1954) and Orlando (1974) with the rough-wall measurements of Liu (1966), Pimenta (1975), and the present work (after correction for differences in the definition of δ). Invariance of shear stress profiles as roughness changes is also demonstrated by Grass (1971), who determined the profiles of Reynolds shear stress from hydrogen-bubble flow tracers in a free-surface channel flow. His measurements in flows developing over surfaces with different roughness sizes showed that $-\overline{u'v'}/U_\tau^2$ versus y/δ profiles were closely similar in smooth, transitionally rough, and fully rough flows.

Measurements from the present study and Pimenta's (1975) study also show the $-\overline{u'v'}/U_\tau^2$ versus y/δ profiles are invariant as U_∞ changes. In these studies, the variation of U_∞ is the principal means by which the roughness Reynolds number, Re_k, is varied, since k_s is held constant. Thus, the profiles of $-\overline{u'v'}/U_\tau^2$ versus y/δ are invariant as different roughness regimes are investigated in these studies.

From these experimental studies and Clauser's (1956) analysis, profiles of $-\overline{u'v'}/U_\tau^2$ versus y/δ in thick, rough-wall boundary layers are expected to be the same as in naturally developing flows, and approximately invariant as flows at different freestream velocities are investigated.

The Reynolds shear stress profiles were measured at three downstream locations in the artificially thickened boundary layer at freestream velocities of 26.8 m/sec, 15.8 m/sec, and 10.1 m/sec. The measurements at the two locations farthest downstream show excellent agreement with measurements by the present author in a naturally developed flow, where an example of such behavior at U_∞ = 26.8 m/sec is shown in Fig. 2-23. Fig. 2-23 also shows that the artificially thickened Reynolds shear stress profiles are invariant as the freestream velocity varies and show agreement with Pimenta's (1975) measurements from a naturally developed flow.

<u>Turbulence correlation coefficients:</u> R_{uv} <u>and</u> R_{q^2}. The values of the turbulence correlations expressed by Eqn. (2-15) have been demonstrated to be constant for equilibrium smooth and rough-wall boundary layers by many investigators, including Orlando (1974), Pimenta (1975), Coleman (1976), Bradshaw (1966), and Townsend (1956). Since the correlations seem to have the same values regardless of surface condition, free-stream velocity

distribution, and magnitude of wall transpiration, the correlations appear to have universal form in representing the physical mechanisms which control the distribution of turbulence in wall shear flows. The significance of the Reynolds shear stress-turbulent kinetic energy ratio, and the possibility of its constant magnitude in wall shear flows was first suggested in a similarity hypothesis concerning the structure of turbulence by von Karman (see Hinze (1975)).

Measurements in the rough-wall, augmented boundary layer indicate that the values of the correlation for the Reynolds shear stress and the Reynolds shear stress-turbulent kinetic energy ratio are consistent with values in naturally developing flows within $\pm 5\%$, as indicated in Fig. 2-24. The measurements of Orlando (1974) and Pimenta (1975) are also shown in the figure for comparison. Consequently, the universal structural characteristics represented by the magnitude of the correlations appear to exist in the rough-wall, artificially thickened boundary layers.

Spectra of streamwise velocity fluctuations. Qualification of the structural characteristics of the rough-wall, artificially thickened boundary layer can be extended to include spectra of the longitudinal velocity fluctuations. Spectra were measured using the fast Fourier transform, as discussed in Appendix II. Measurements were made at $x_1 = 1.78$ m in a naturally developing flow for comparison with augmented boundary layer results at the same value of x_1 for a freestream velocity of 26.8 m/sec. Comparison of these measurements at four different values of y/δ is shown in Fig. 2-25. In the figure, spectra magnitudes are normalized such that

$$\int_0^\infty \frac{F_u(k_1)}{y}\, d(yk_1) = \int_0^\infty F_u(k_1)\, dk_1 = 1.0 \qquad (2\text{-}21)$$

where the one-dimensional wave number, k_1, is determined from frequency, using

$$k_1 = \frac{2\pi n}{U} \qquad (2\text{-}22)$$

In Fig. 2-25, the non-dimensionalization given by (2-21) should be viewed as a normalization with respect to boundary layer thickness, since spectra

are compared at the same y/δ. It should also be mentioned that the lines in Fig. 2-25 represent a graphical fit to closely spaced data points.

Figure 2-25 indicates that the broad-band spectra characteristics of the artificially thickened boundary layer show excellent agreement with baseline measurements for $y/\delta = .078$, 0.150, and 0.600. The spectra at $y/\delta = 1.00$ for the augmented boundary layer and the naturally developing flow show differences which are related to differences in the intermittency characteristics of the two flows, and differences in large-scale eddy structures at the boundary layer edge. These differences are not surprising, since the structures with the largest scales require the longest time to stabilize downstream of the augmentation device. In fact, Bradshaw (1971) points out that the lifetime of the larger eddies in a boundary layer is approximately $30\delta/U_\infty$, or a downstream distance of 30δ. Such values are based on the idea that the total duration of a phenomenon is of the order of three times the time constant, where the time constant is calculated from the ratio of the turbulent kinetic energy to the production rate.

2.3.3d. Structural Equilibrium. First-order equilibrium in a zero-pressure-gradient flow is indicated by a Clauser shape factor which is independent of downstream distance. The artificially thickened boundary layer reaches such equilibrium for $x_1 > 1.0$ m for freestream velocities of 26.8 m/sec, 15.8 m/sec, and 10.1 m/sec, as shown in Fig. 2-26.

As for the smooth-wall flow, the turbulence structure requires a greater downstream distance than mean profiles to relax to normal equilibrium behavior. Fig. 2-23 shows that second-order equilibrium occurs for $x_1 > 1.46$ m since the Reynolds shear stress profiles show downstream similarity. Downstream similarity is also indicated by normalized spectra of the longitudinal velocity fluctuations for $y/\delta = 0.78$, 0.150, and 0.600, as shown in Fig. 2-25.

The equilibrium behavior of the normal Reynolds stress tensor components is discussed in Section 3.3.5.

2.3.3e. Conclusions. The growth, two-dimensionality, structural similarity, and structural equilibrium characteristics of the rough-wall, artificially thickened boundary layer indicate that all measurements of lower order than one-dimensional $\overline{u'^2}$ spectra have characteristics representative

of natural behavior. Thus, skin friction and Stanton number distributions, mean-velocity and temperature profiles in inner coordinates, and the normal Reynolds stress tensor components can be discussed regarding the influences of variations in the freestream velocity (and also Re_k) and downstream development.

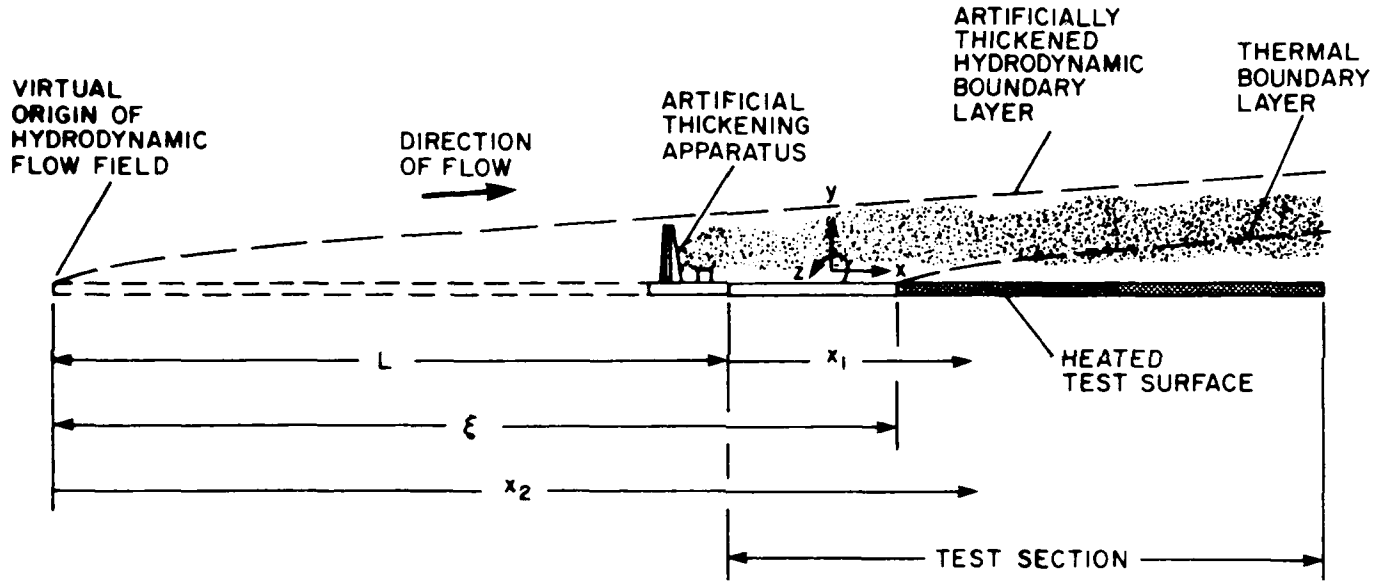

Fig. 2-1. Coordinate system for artificially thickened boundary layers.

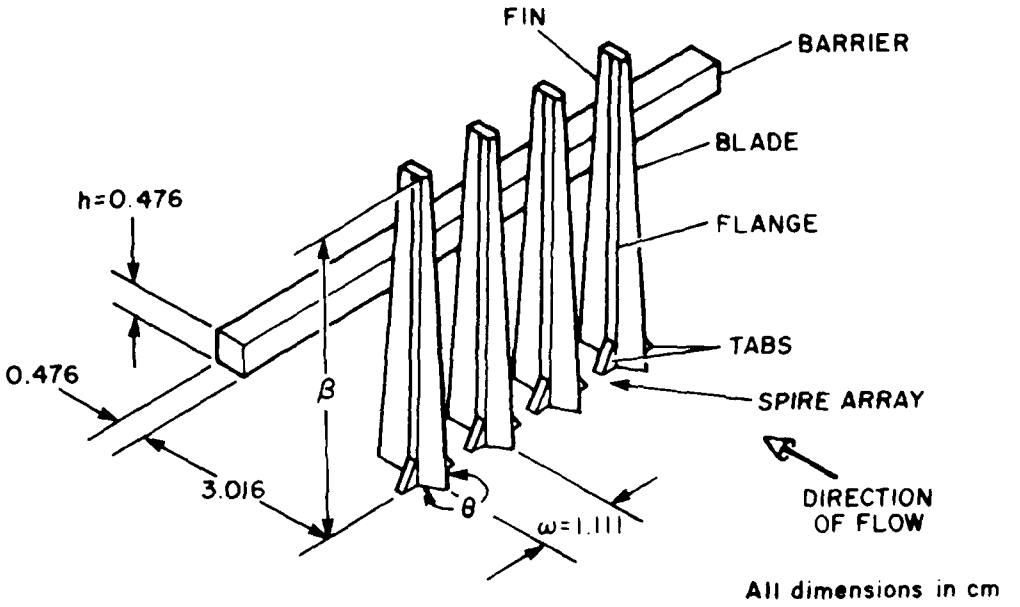

Fig. 2-2a. Smooth-wall artificial thickening apparatus (design C).

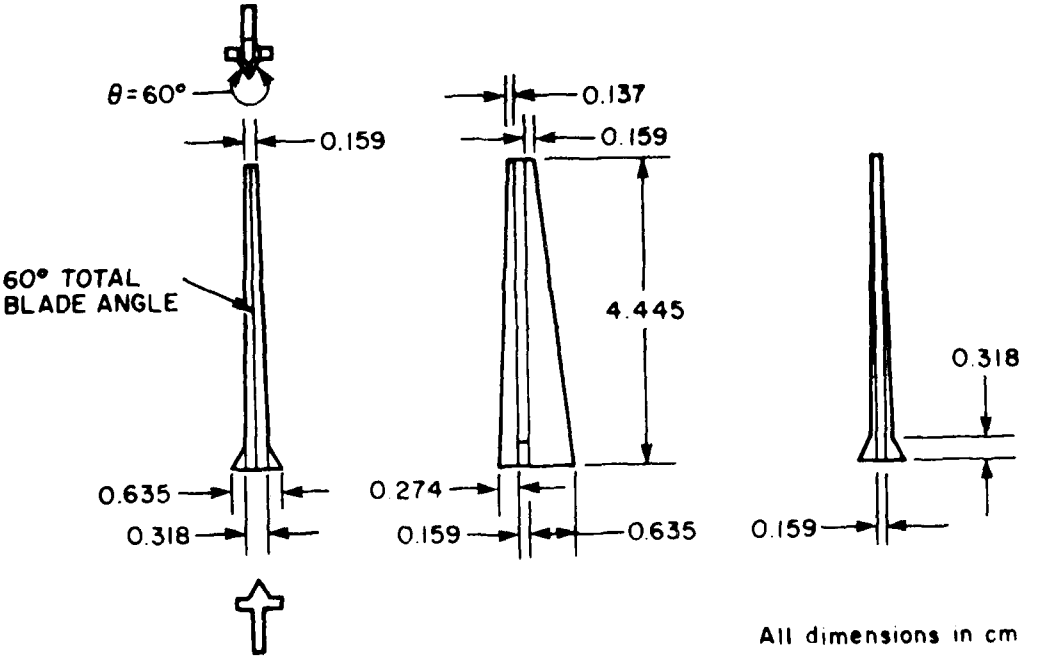

Fig. 2-2b. Smooth-wall spire dimensions (design C).

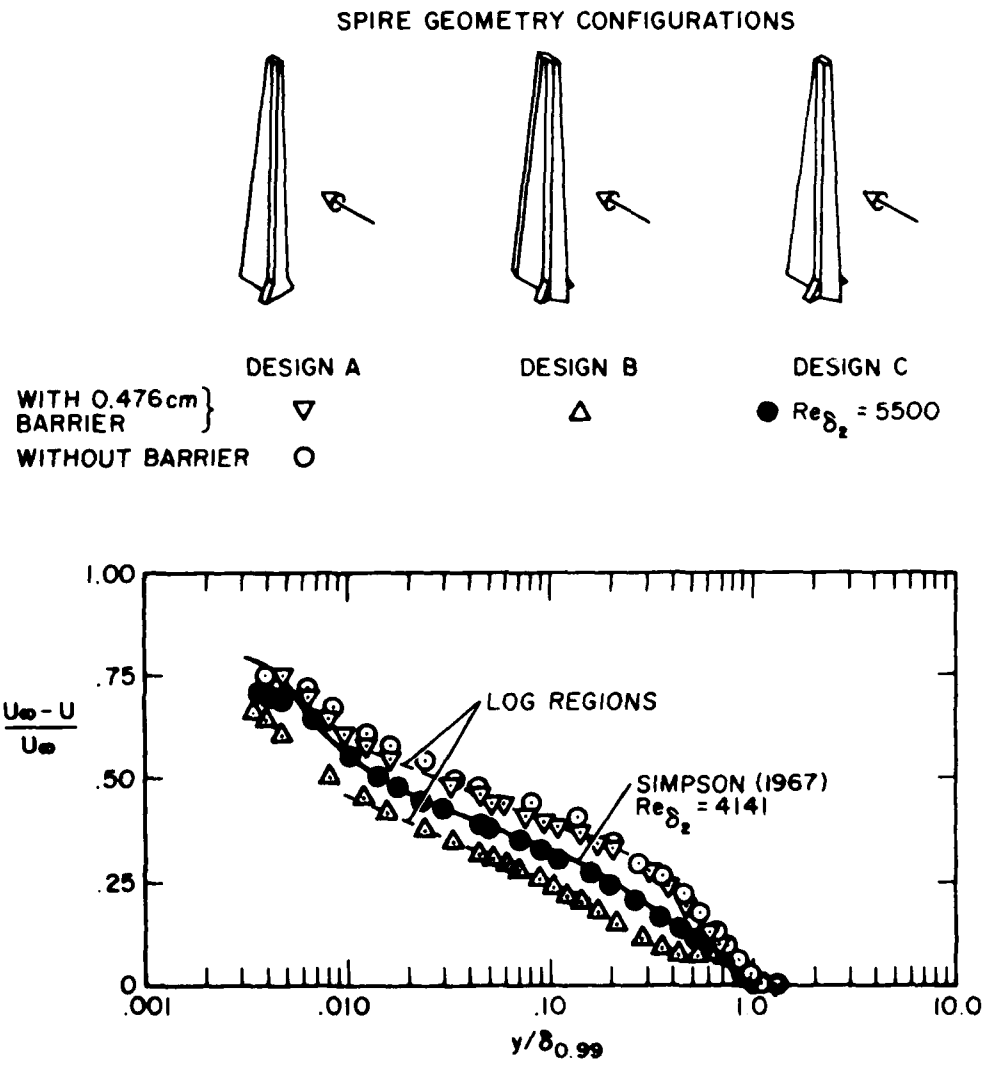

Fig. 2-3. Effects of spire streamlining on mean velocity profiles, x_1 = 2.08 m.

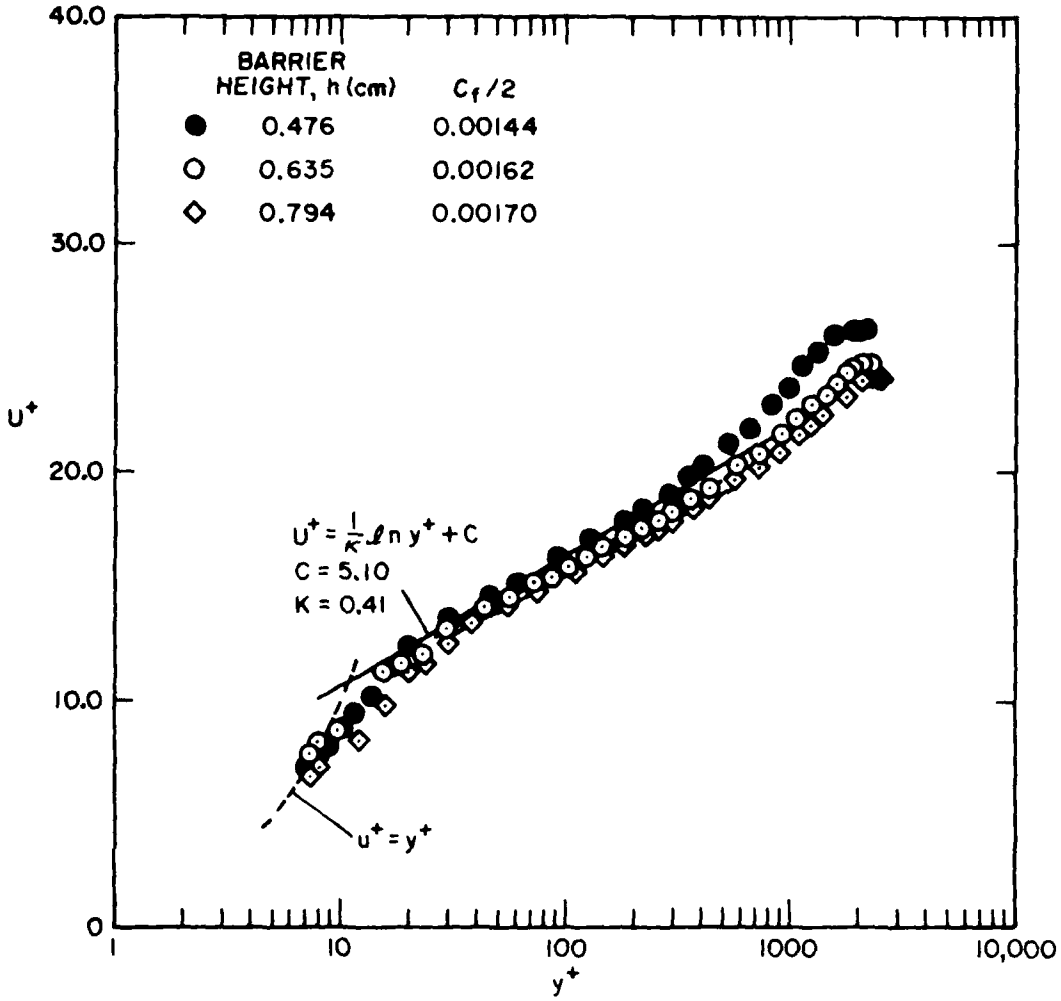

Fig. 2-4. Effect of barrier height, h , on mean velocity profiles in boundary layer coordinates, x_1 = 1.57 m (all profiles with design C spires).

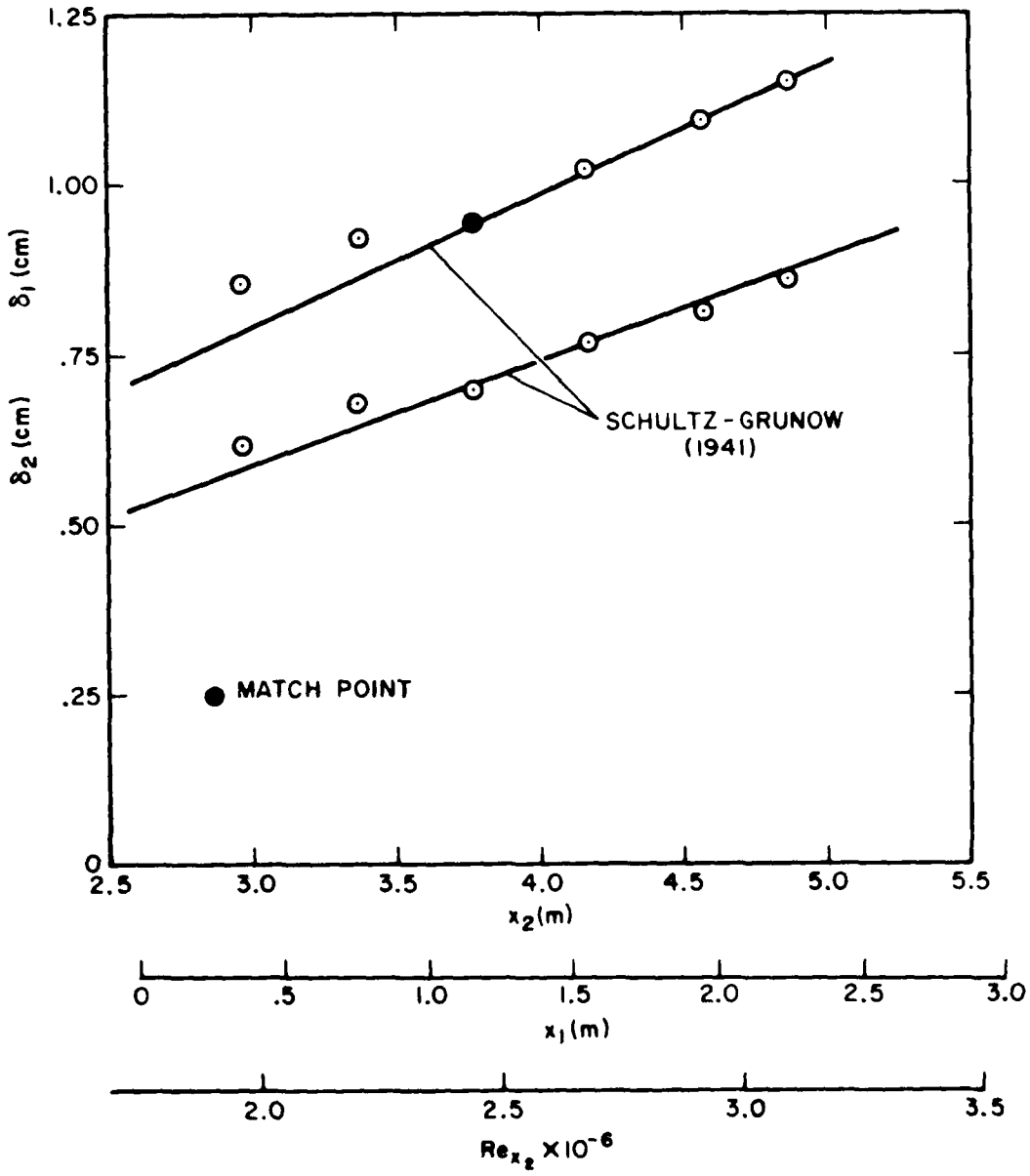

Fig. 2-5. Displacement thickness and momentum thickness development, smooth-wall artificially thickened boundary layer.

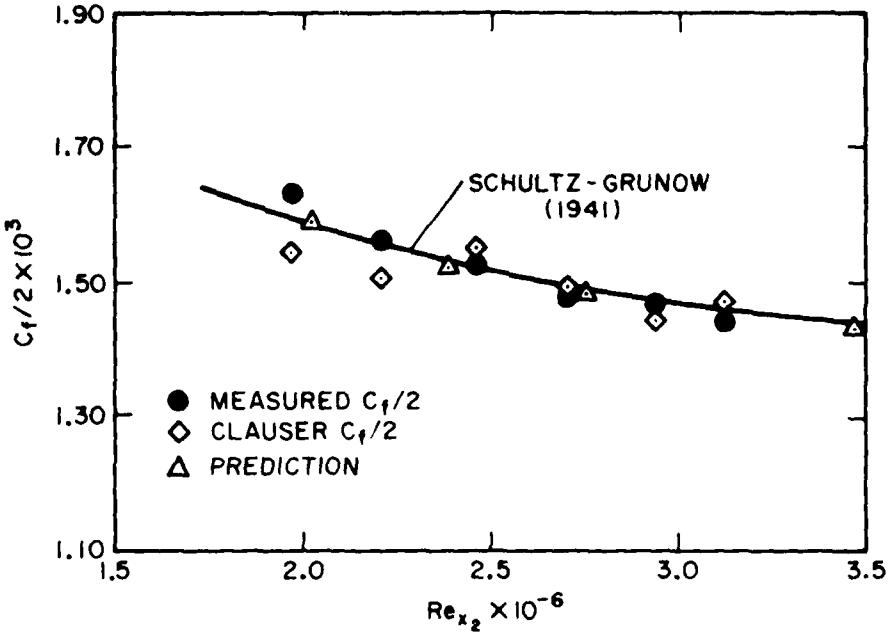

Fig. 2-6a. Skin friction development, smooth-wall artificially thickened boundary layer.

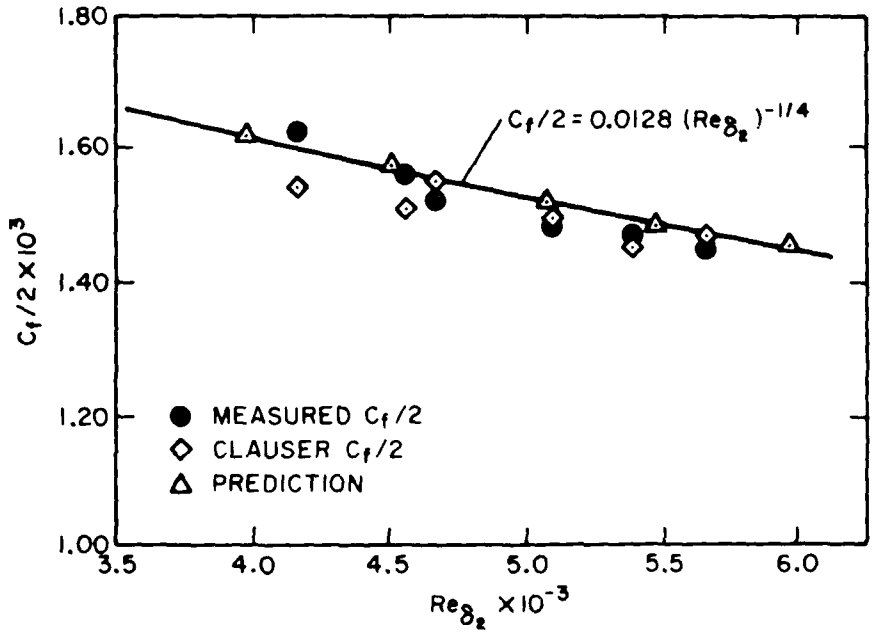

Fig. 2-6b. Skin friction development, smooth-wall artificially thickened boundary layer.

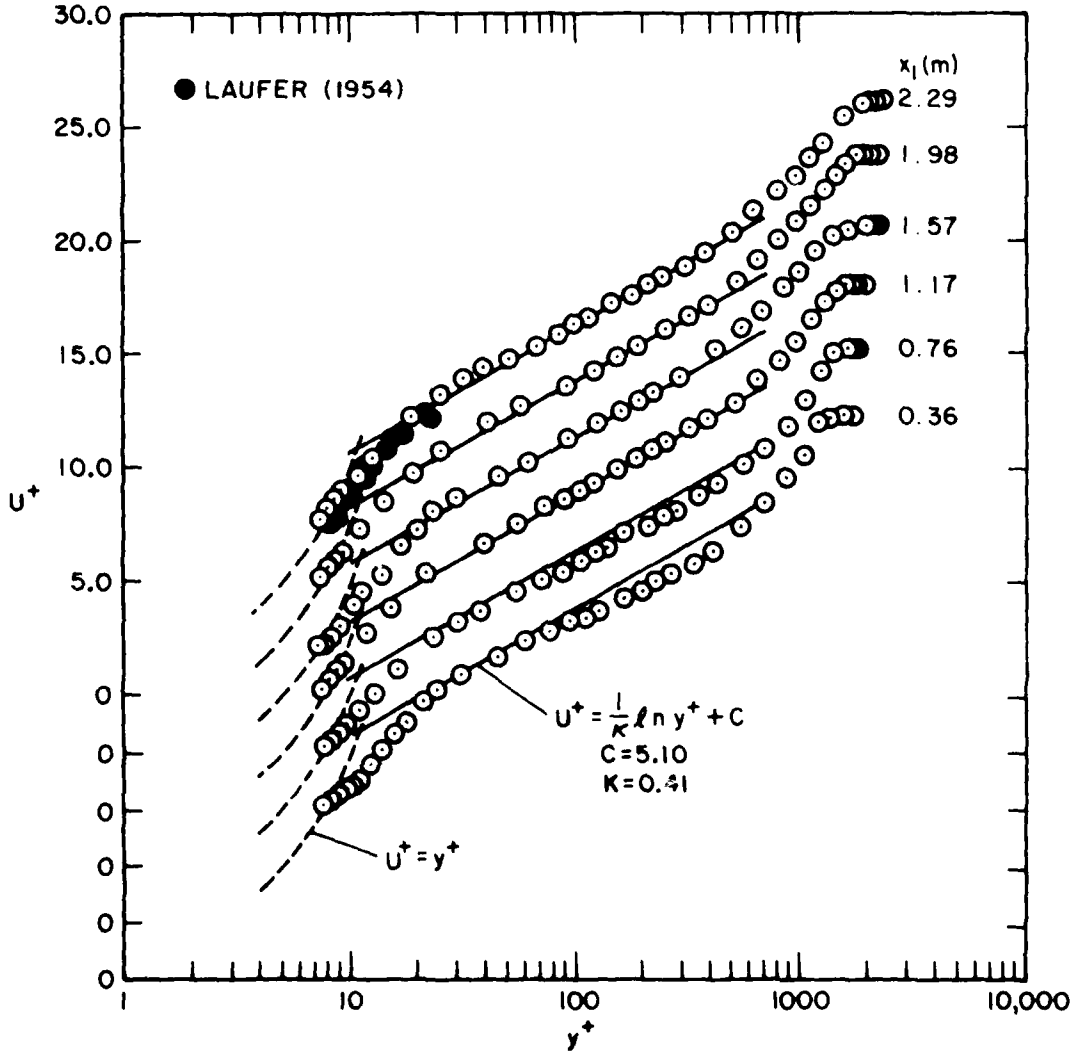

Fig. 2-7. Development of velocity profiles in boundary layer coordinates, smooth-wall artificially thickened boundary layer.

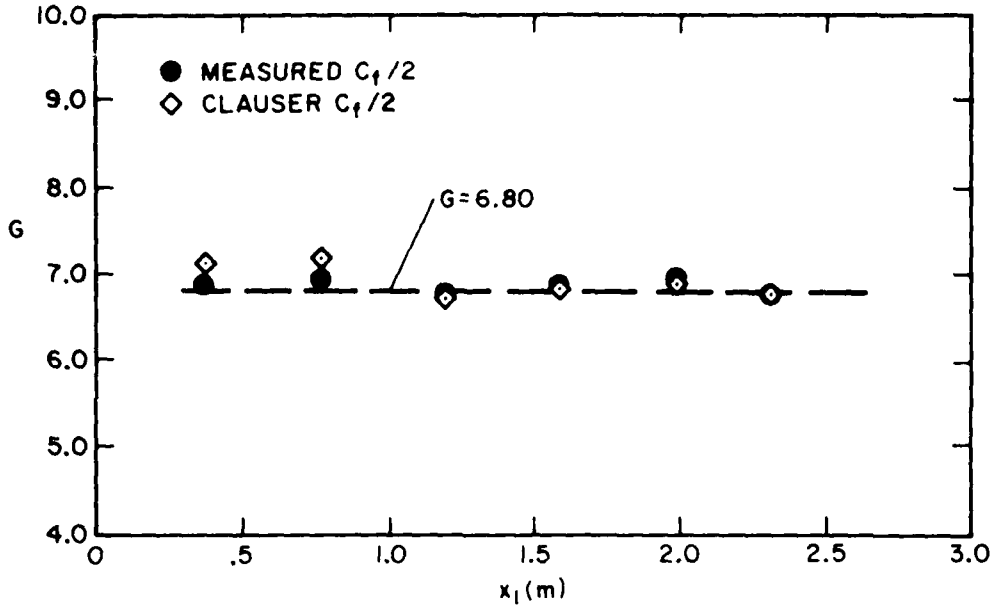

Fig. 2-8a. Clauser shape factor variation with downstream distance, smooth-wall artificially thickened boundary layer.

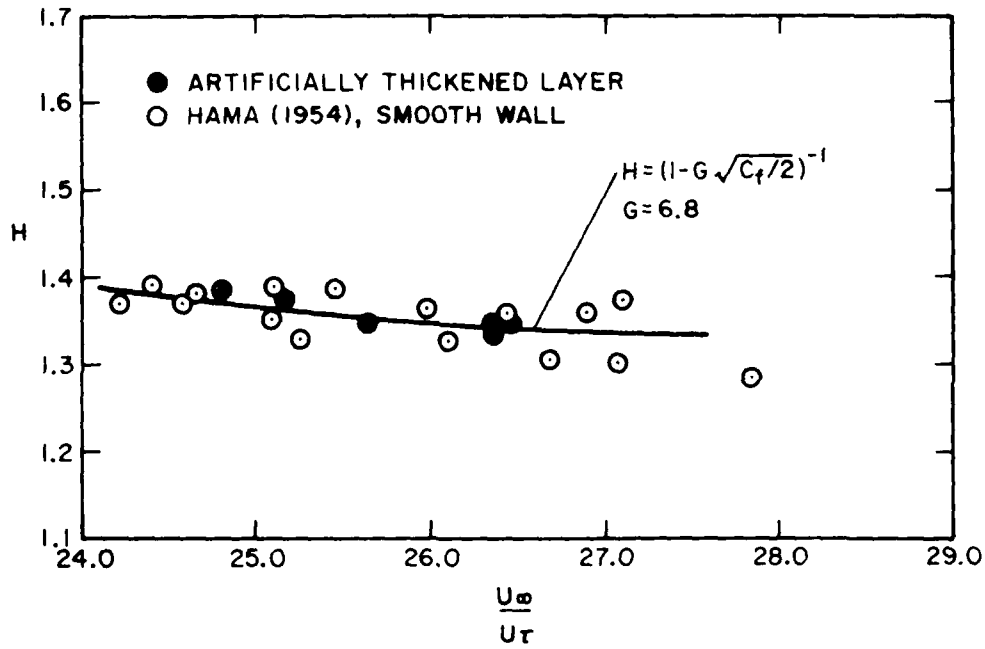

Fig. 2-8b. Variation of Karman shape factor with U_∞/U_τ - comparison of Hama's (1954) data with smooth-wall artificially thickened boundary layer data.

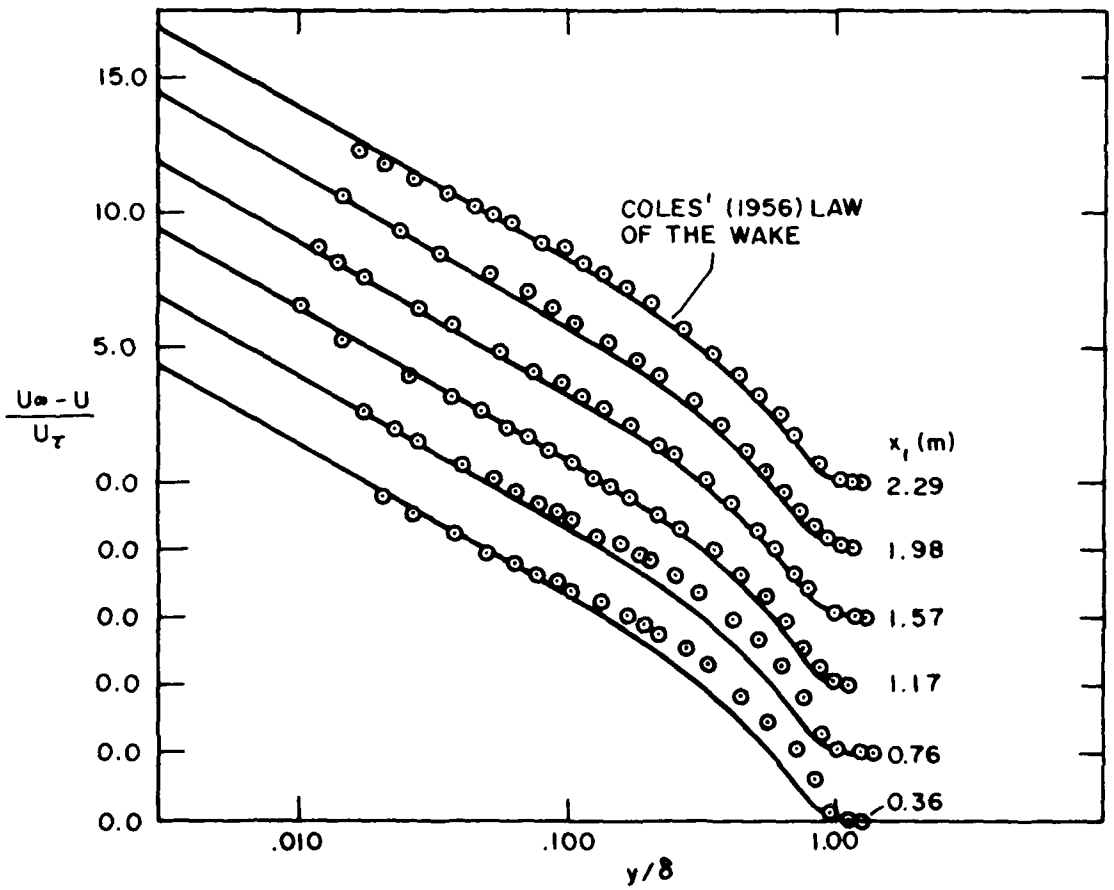

Fig. 2-9. Development of velocity profiles in velocity defect coordinates, smooth-wall artificially thickened boundary layer.

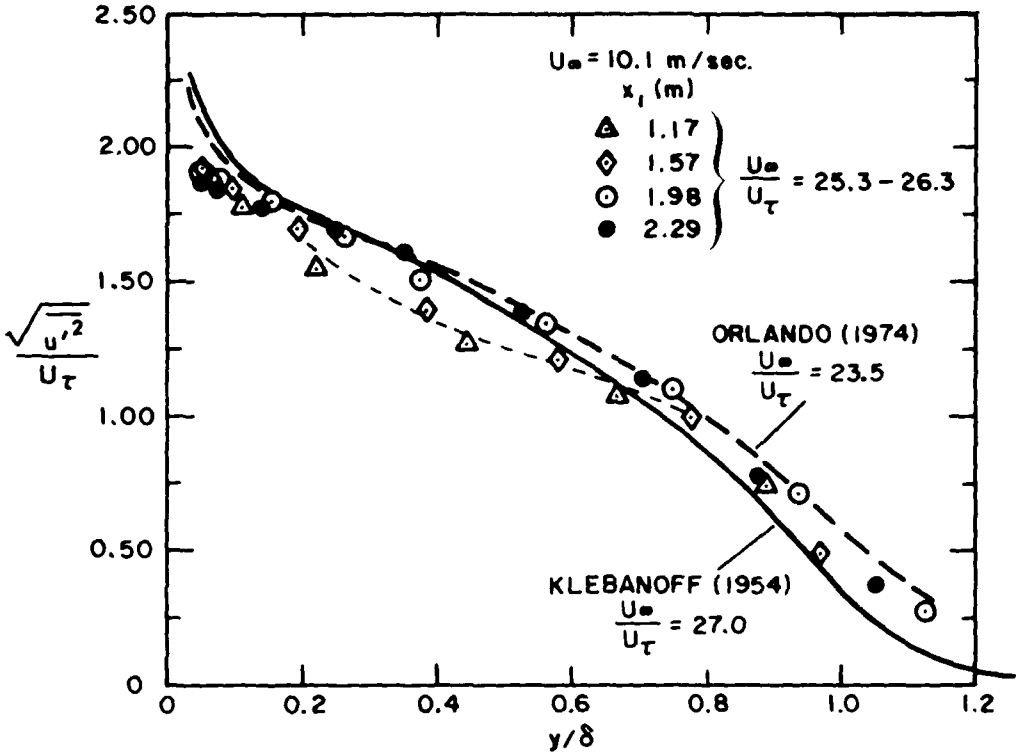

Fig. 2-10a. Development of longitudinal turbulence intensity profiles, smooth-wall artificially thickened boundary layer.

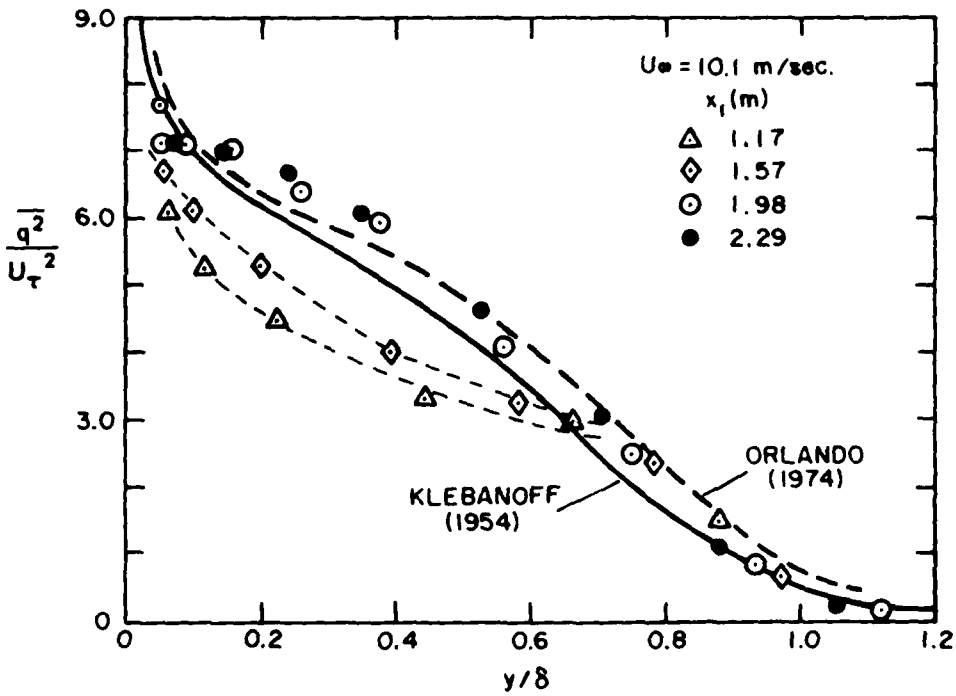

Fig. 2-10b. Development of turbulence kinetic energy profiles, smooth-wall artificially thickened boundary layer.

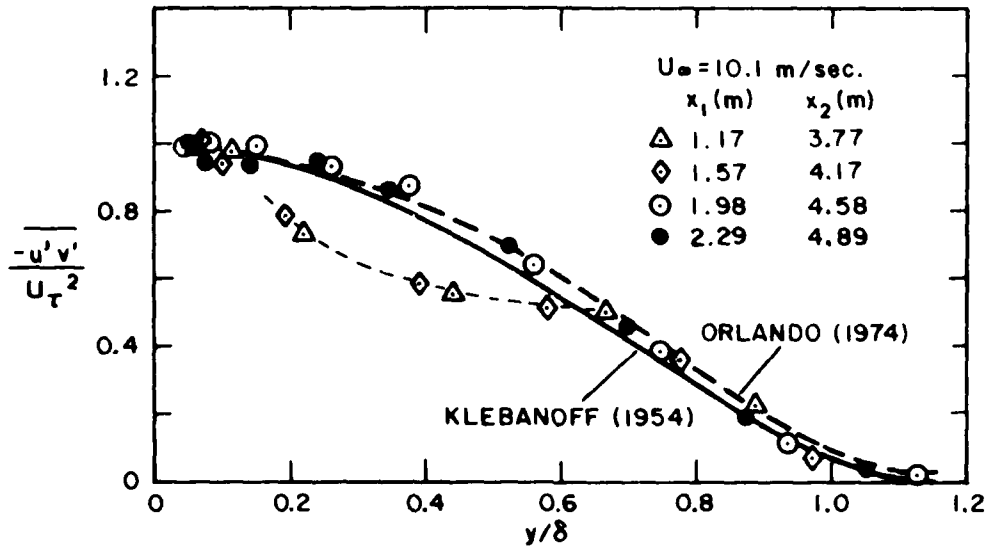

Fig. 2-10c. Development of Reynolds shear stress profiles, smooth-wall artificially thickened boundary layer.

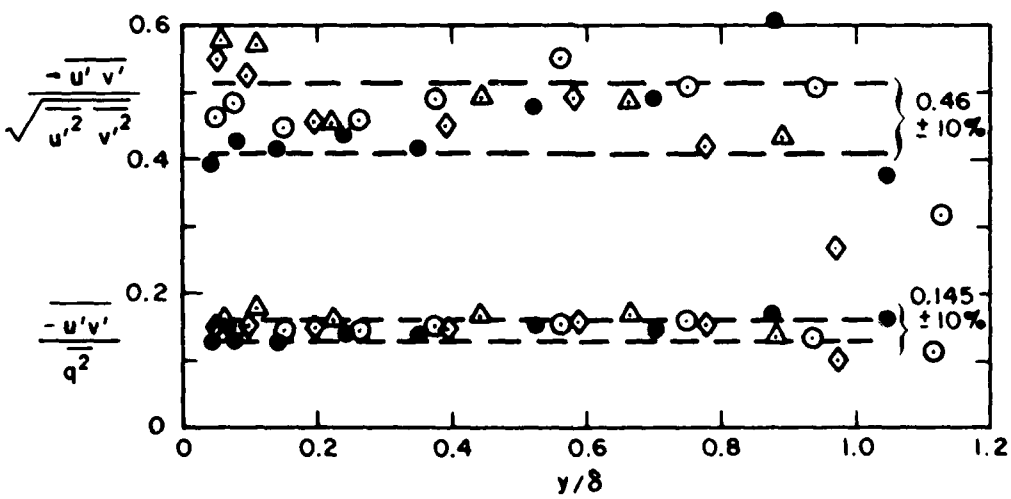

Fig. 2-10d. Cross-correlation coefficient for the turbulent shear stress, and the Reynolds shear stress/turbulence kinetic energy ratio, smooth-wall artificially thickened boundary layer.

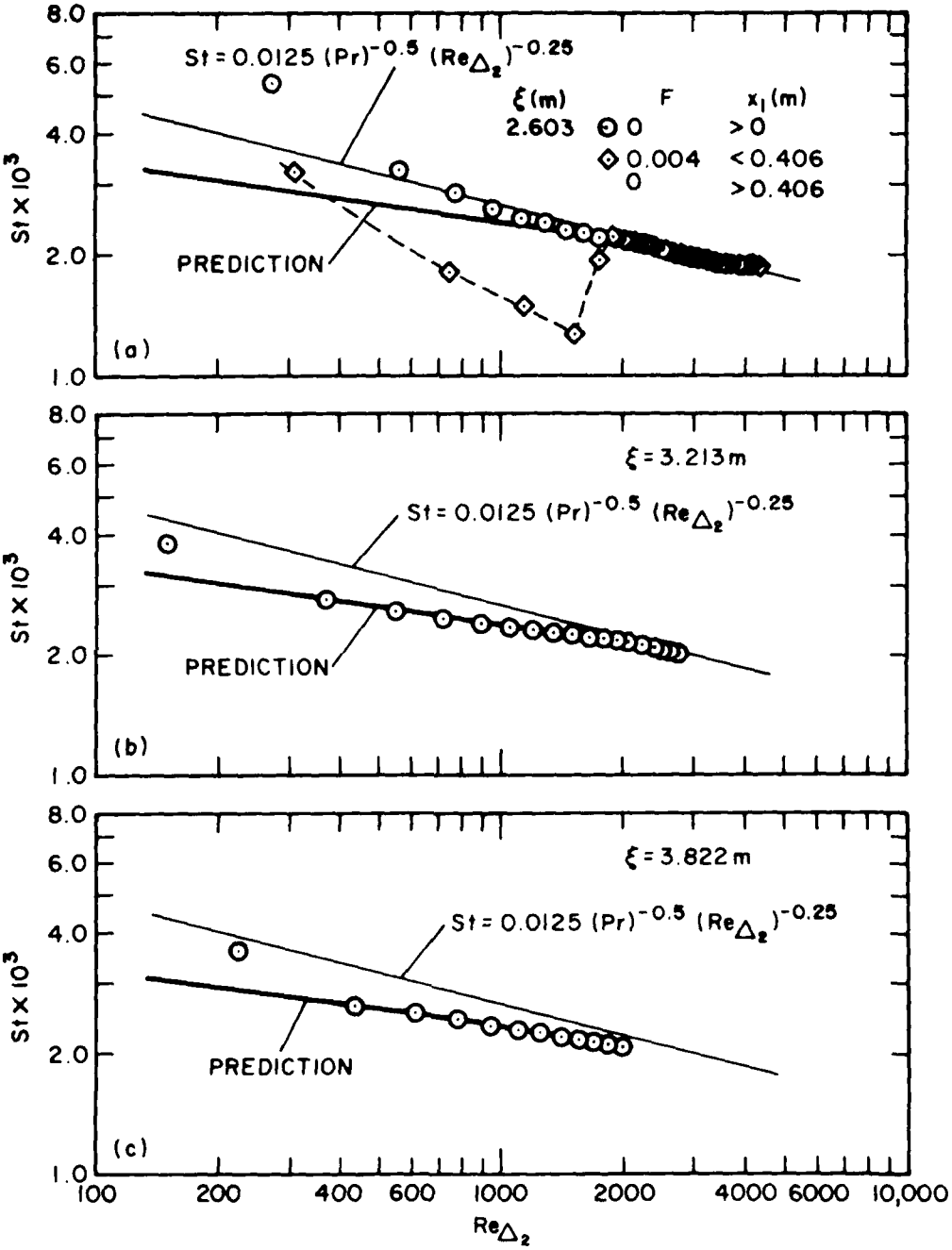

Fig. 2-11. Heat transfer behavior in Stanton number versus enthalpy thickness Reynolds number coordinates, smooth-wall artificially thickened boundary layer.

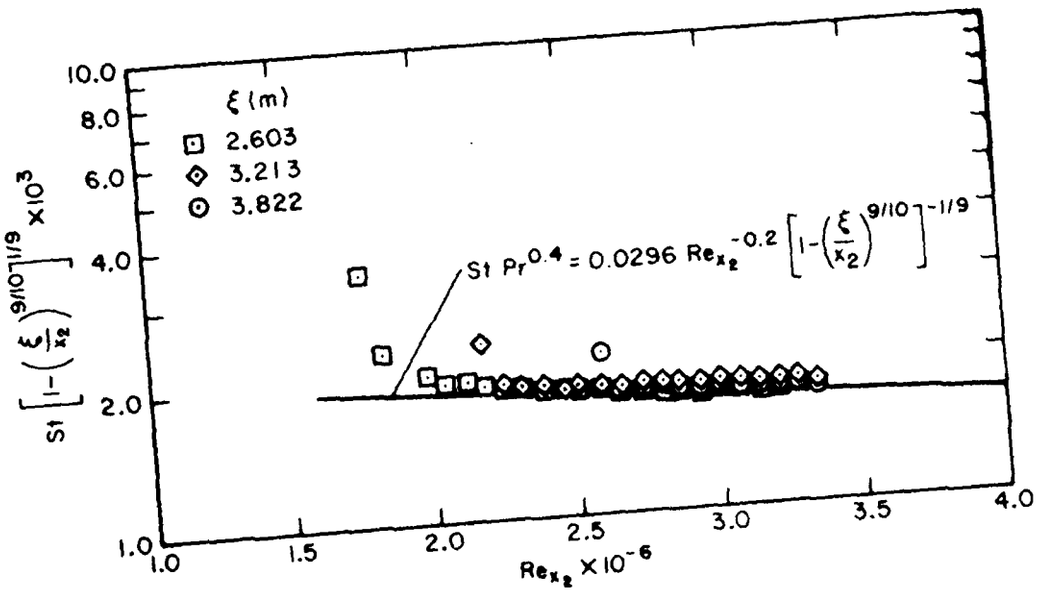

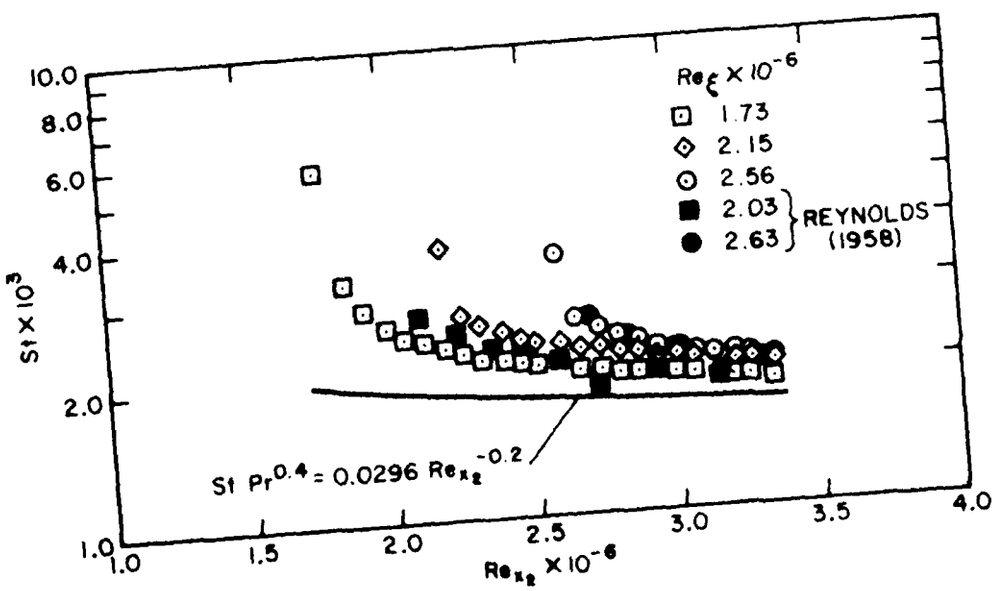

Fig. 2-12. Comparison of smooth-wall artificially thickened heat transfer data with Reynolds' (1958) unheated starting length data and correlations.

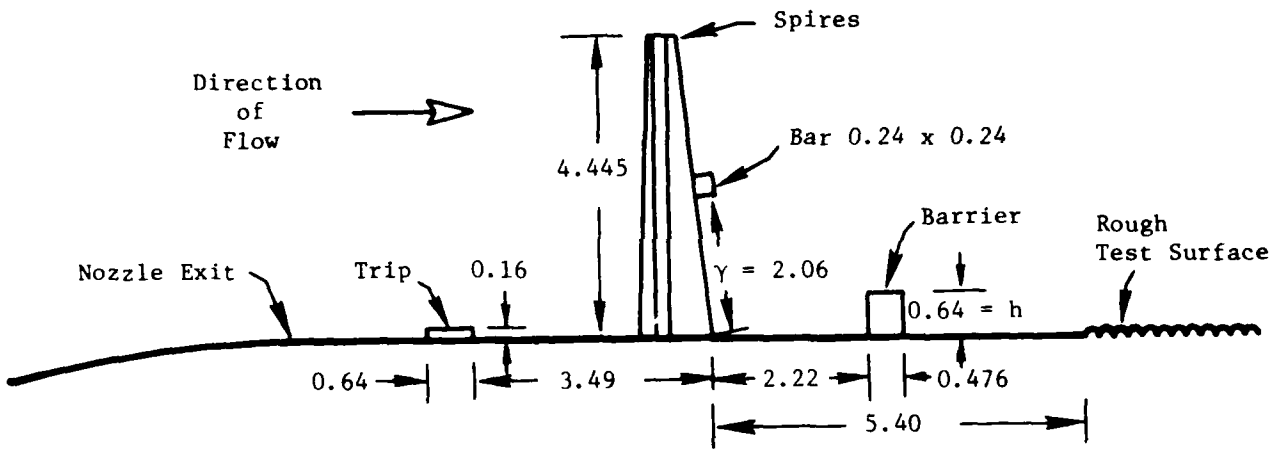

All dimensions in cm.

Fig. 2-13. Schematic of rough wall artificial thickening apparatus (design E).

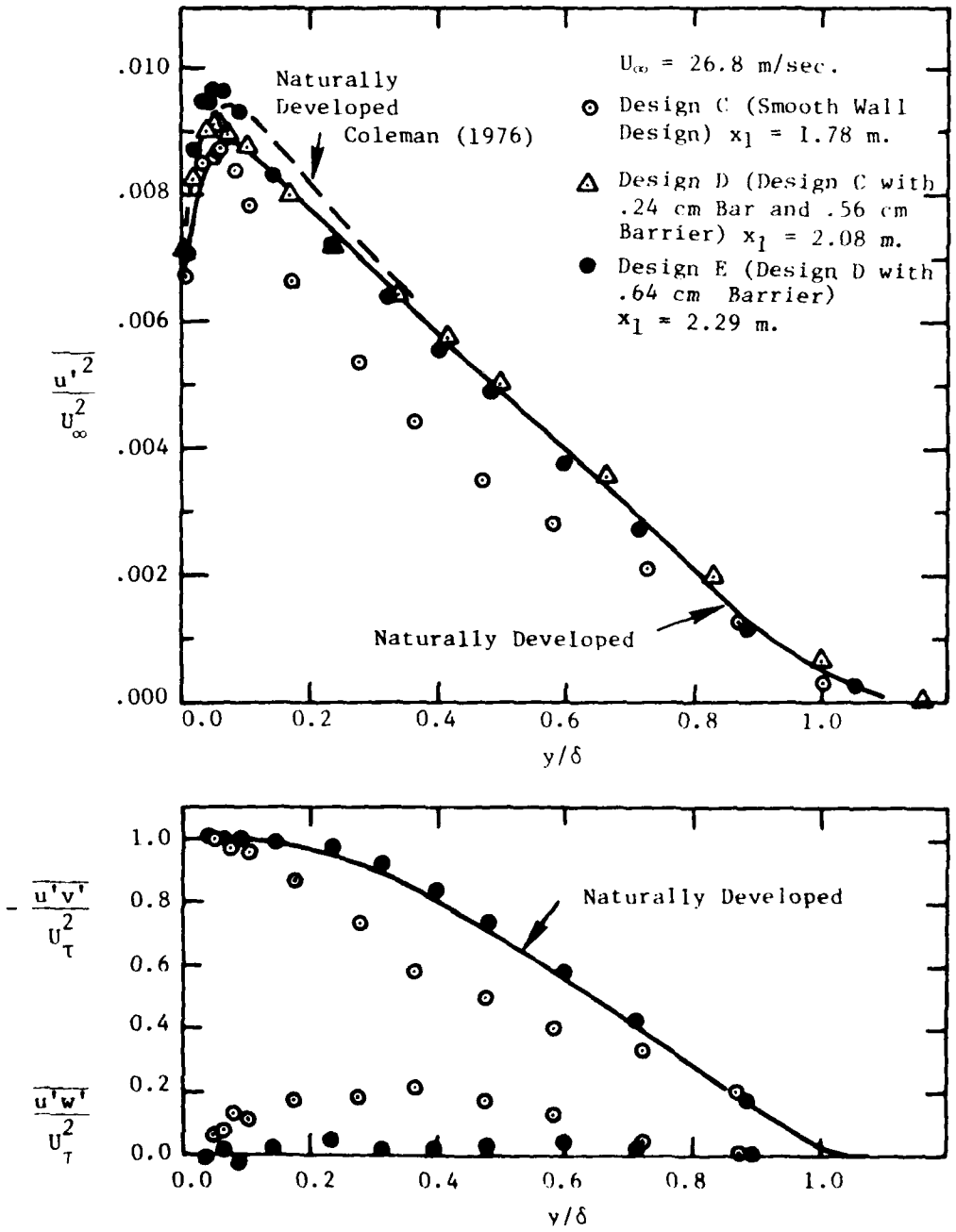

Fig. 2-14. Effect artificial thickening apparatus geometry changes on turbulence profiles.

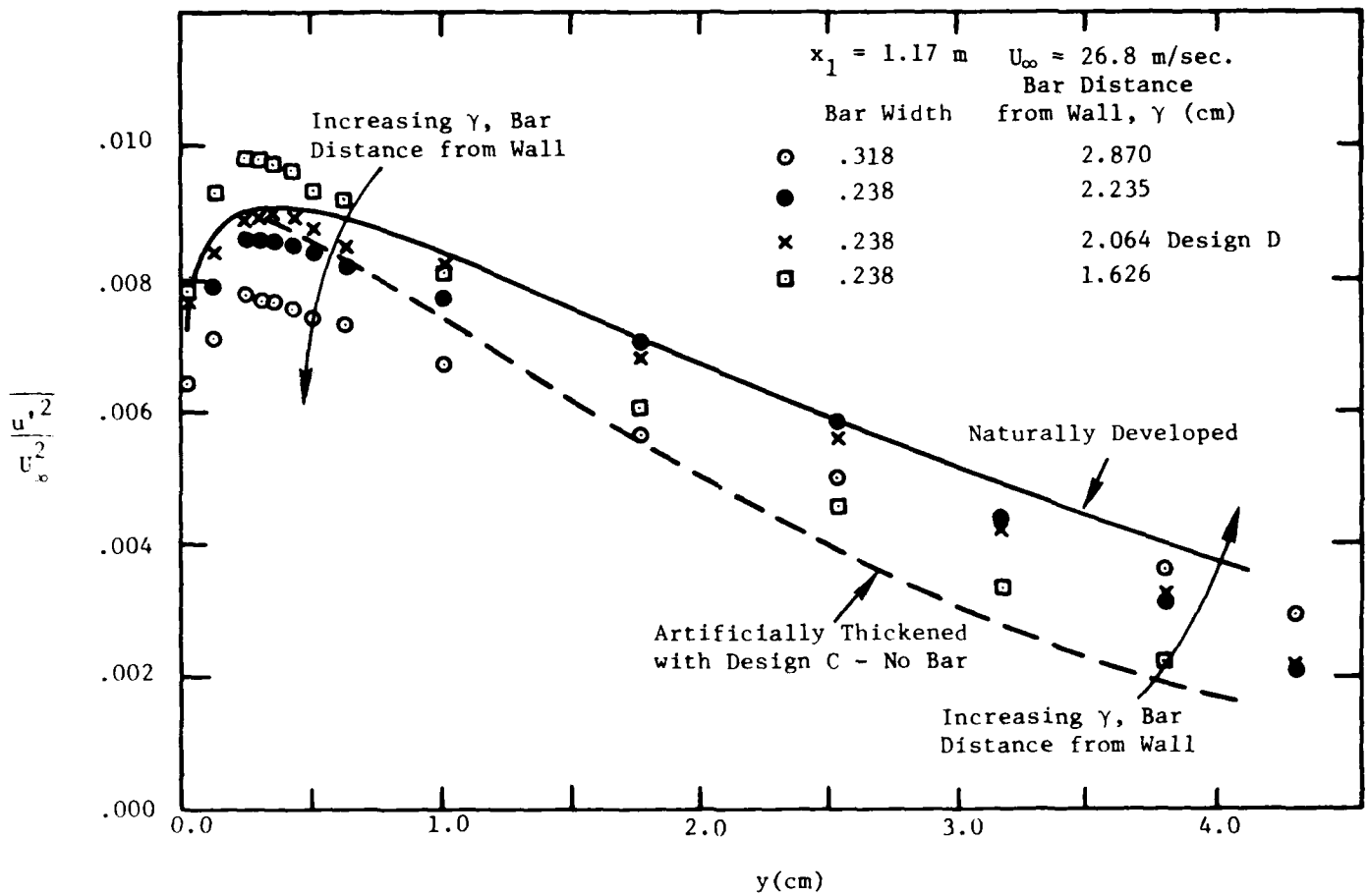

Fig. 2-15. Effect of bar distance from wall, γ, on turbulence profiles.

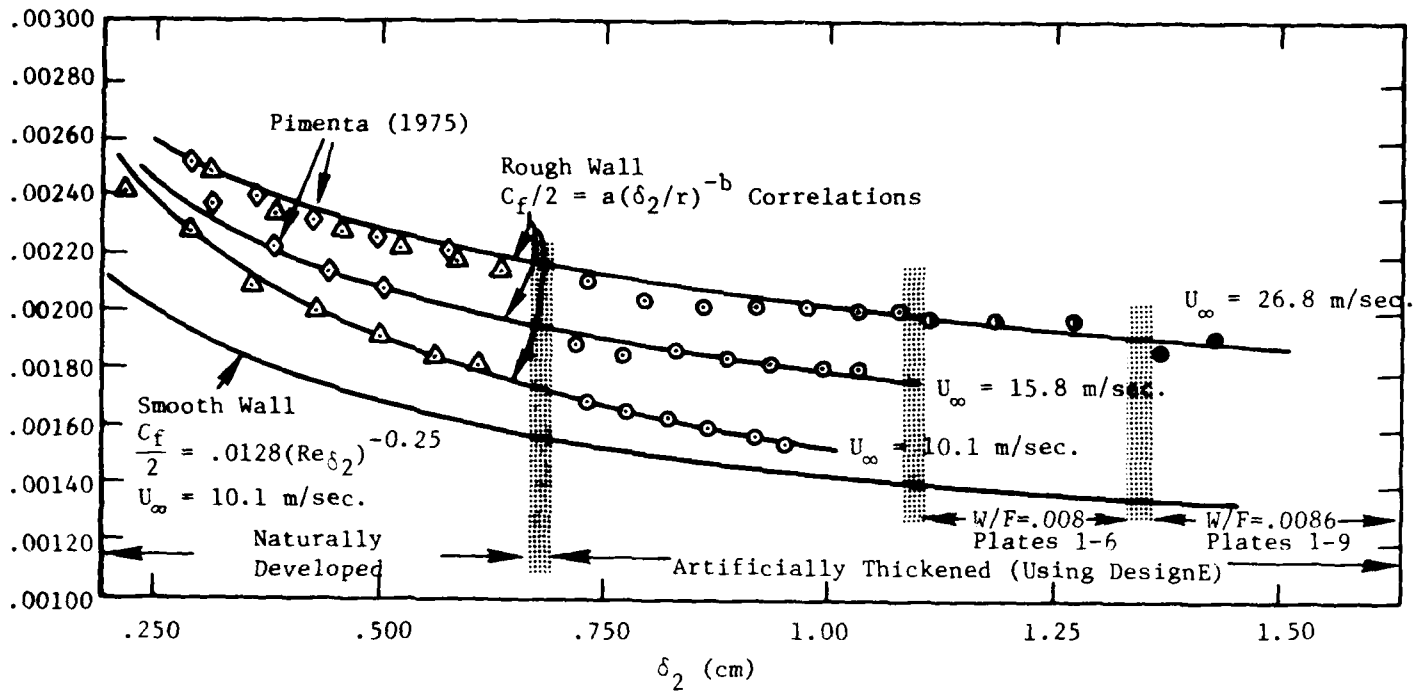

Fig. 2-16. Skin friction variation as a function of downstream distance in naturally developed and artificially thickened rough wall boundary layers.

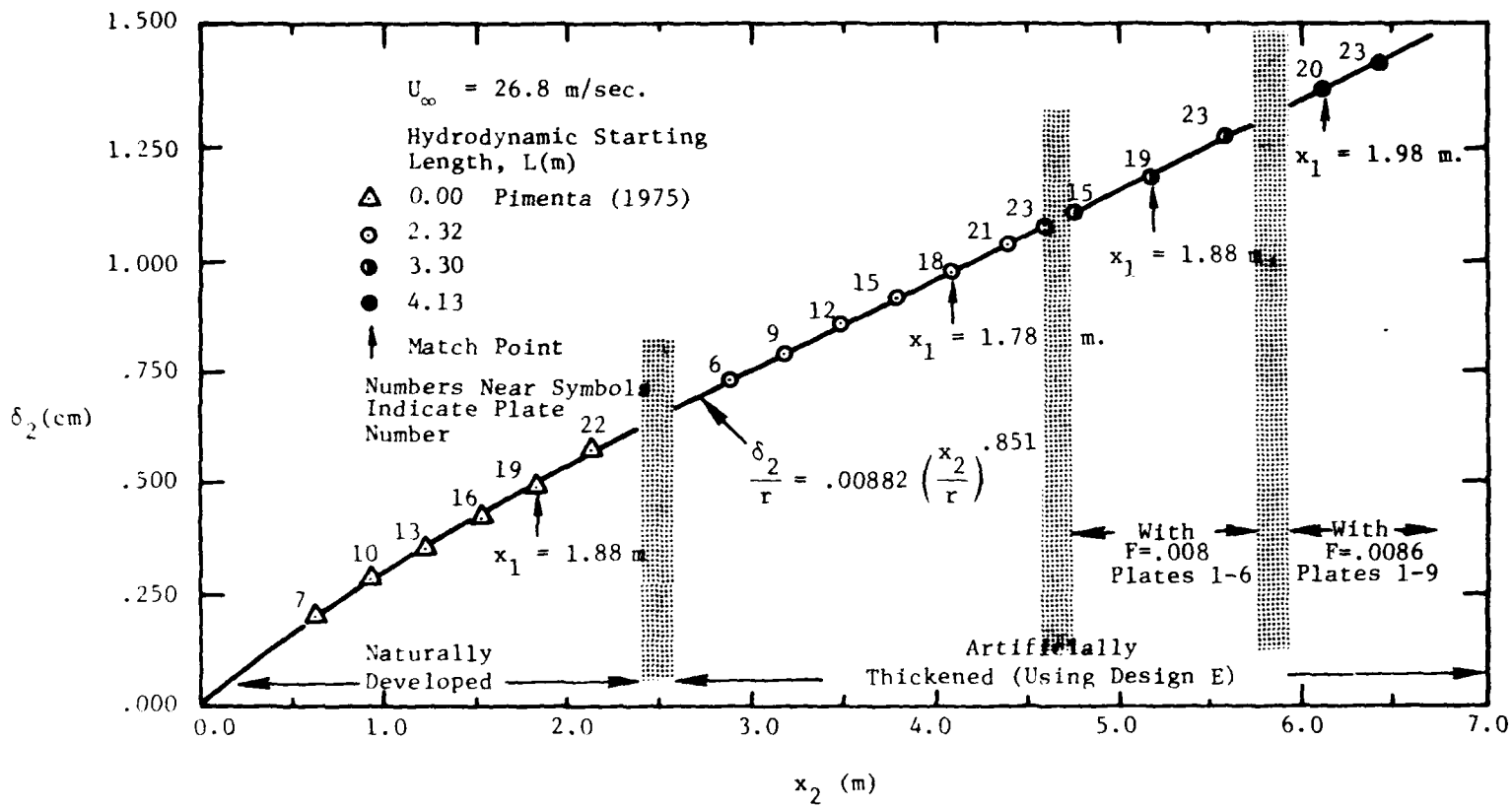

Fig. 2-17. Variation of Momentum Thickness with Downstream Distance, U_∞ = 26.8 m/sec.

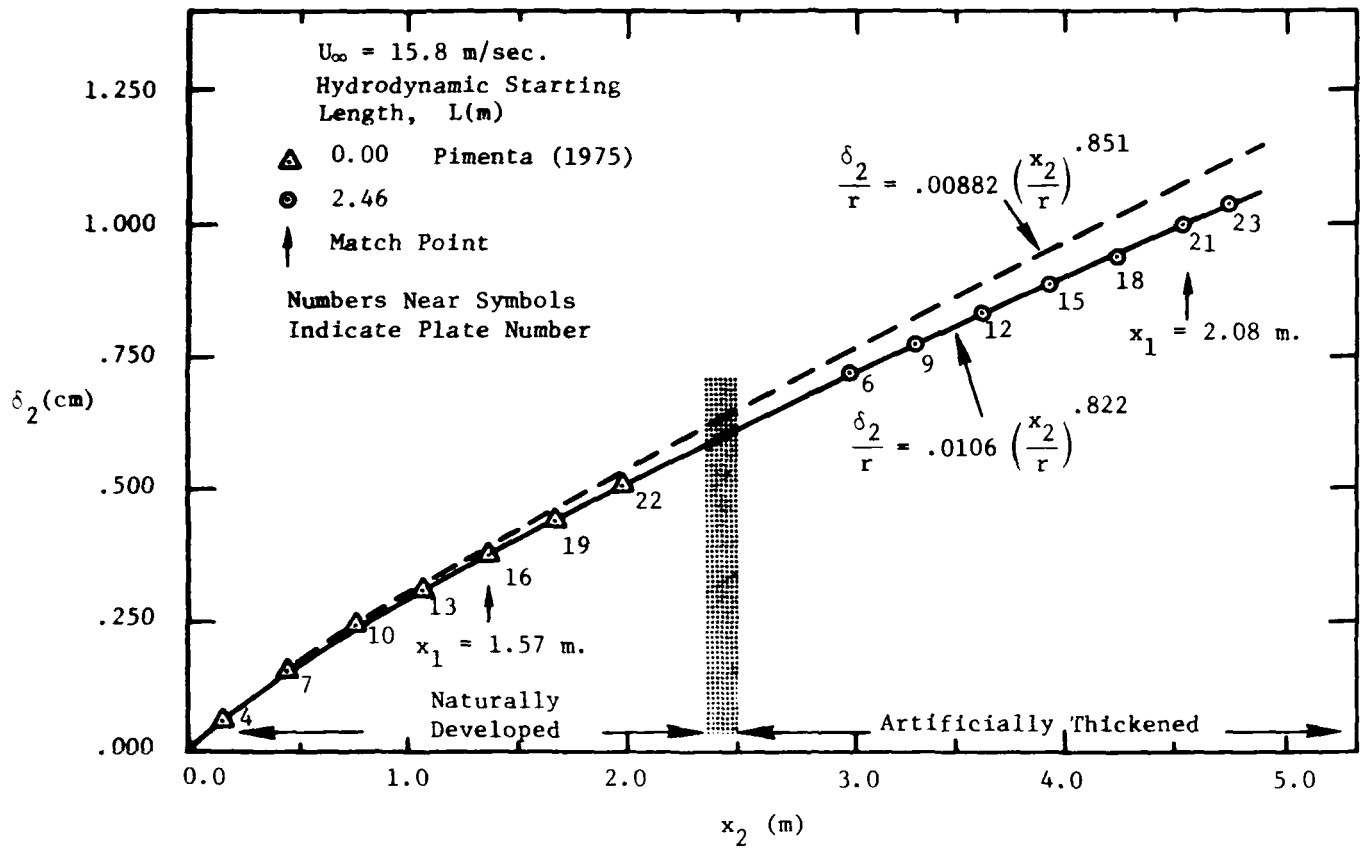

Fig. 2-18. Variation of momentum thickness with downstream distance, U_∞ = 15.8 m/sec.

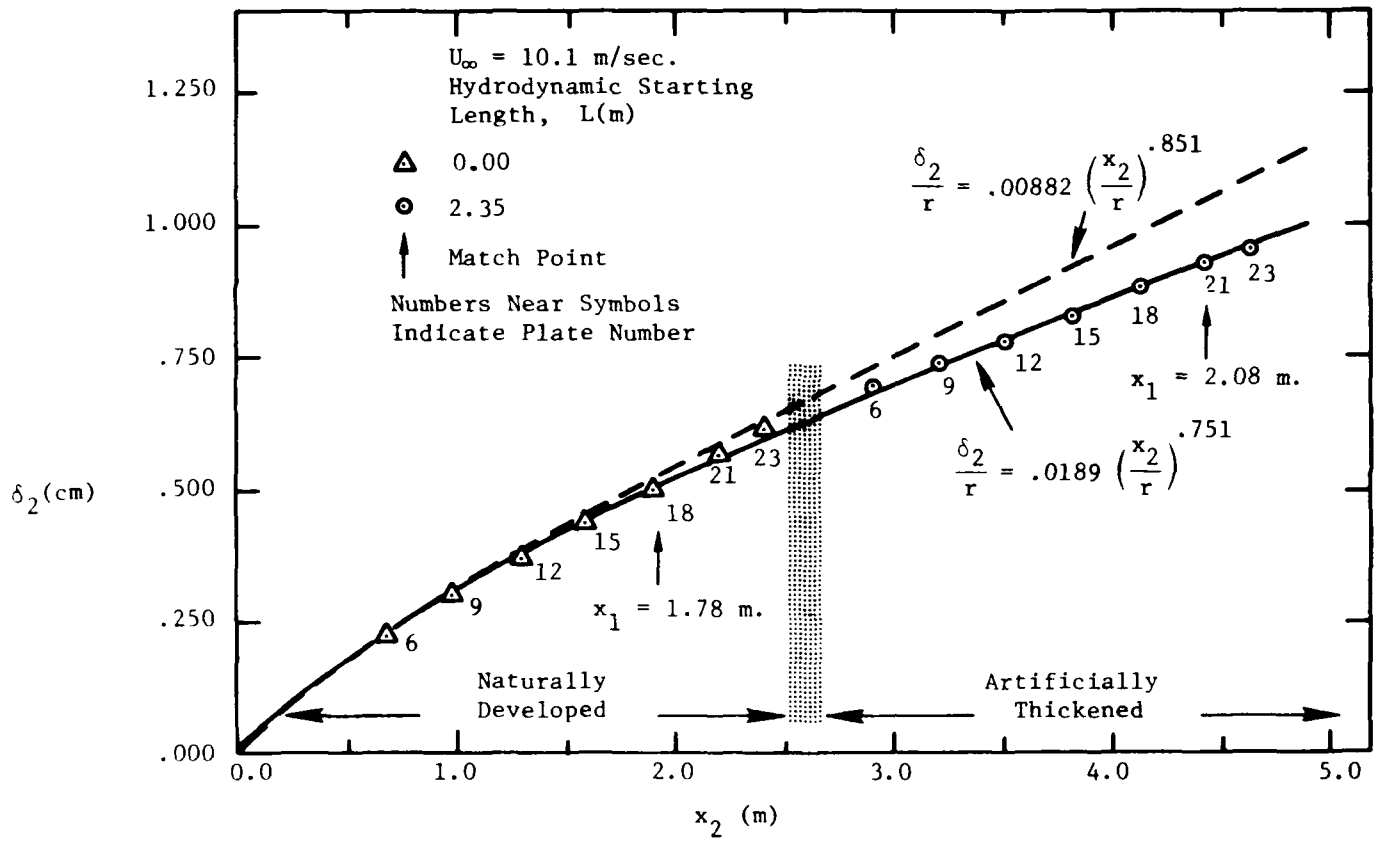

Fig. 2-19. Variation of momentum thickness with downstream distance, U_∞ = 10.1 m/sec.

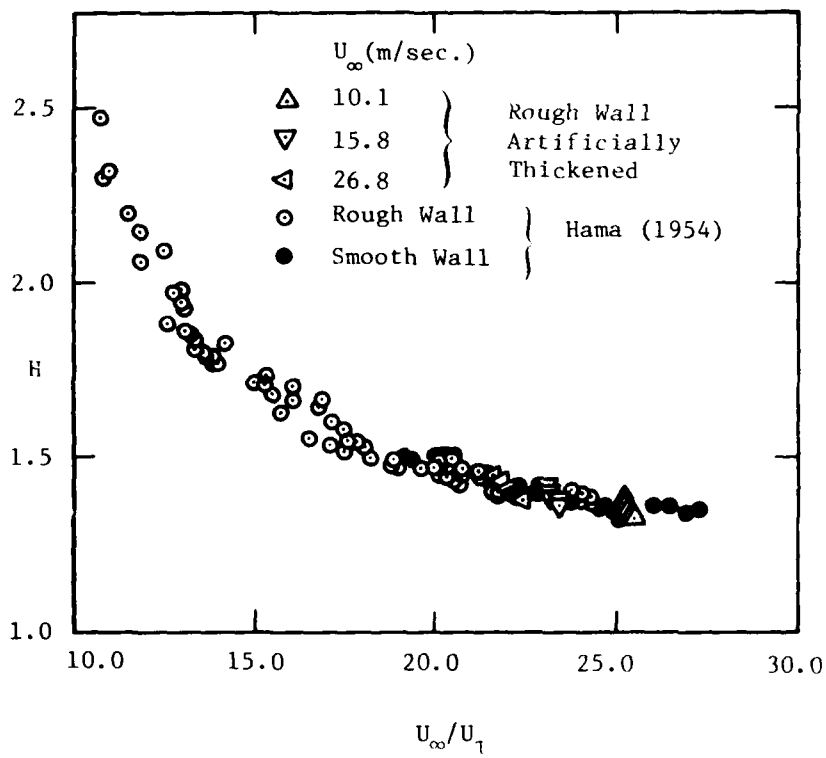

Fig. 2-20. Variation of the shape factor with U_∞/U_τ -- comparison of Hama's (1954) data with rough-wall artificially thickened boundary layer data.

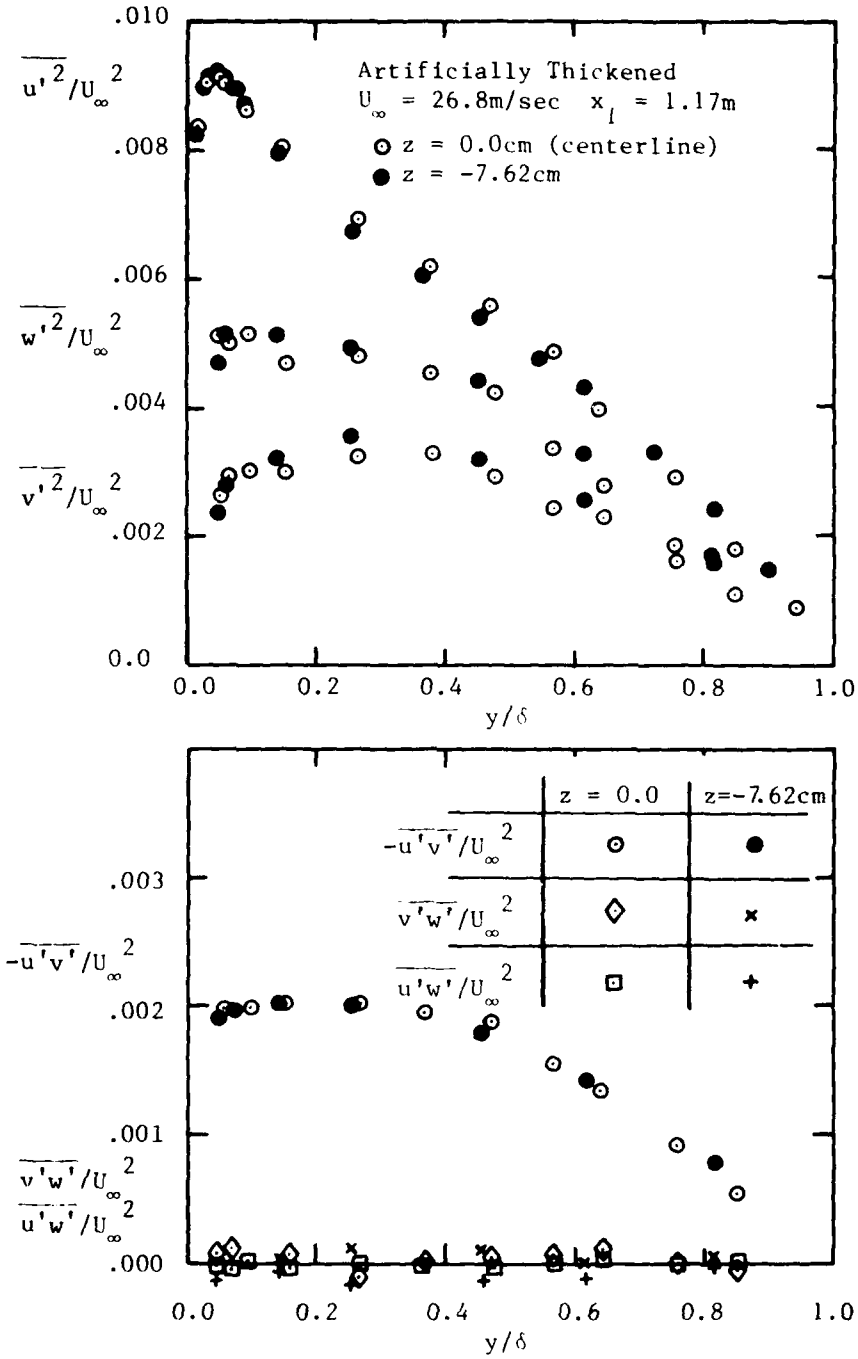

Fig. 2-21. Spanwise uniformity and two-dimensionality of turbulence profiles, rough-wall artificially thickened boundary layer U_∞ = 26.8 m/sec.

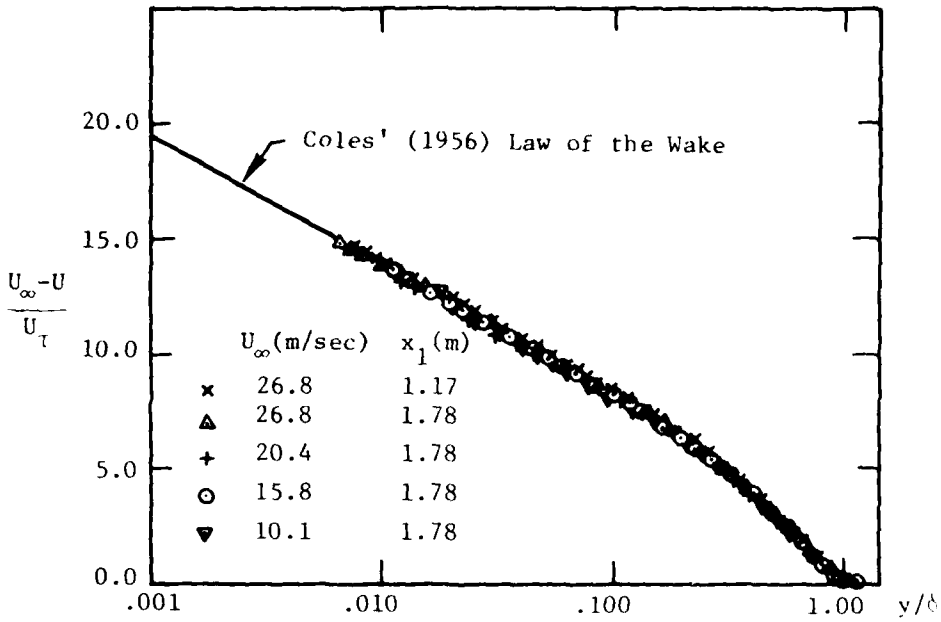

Fig. 2-22. Downstream development and variation with freestream velocity of velocity profiles in velocity defect coordinates, rough wall artificially thickened boundary layers.

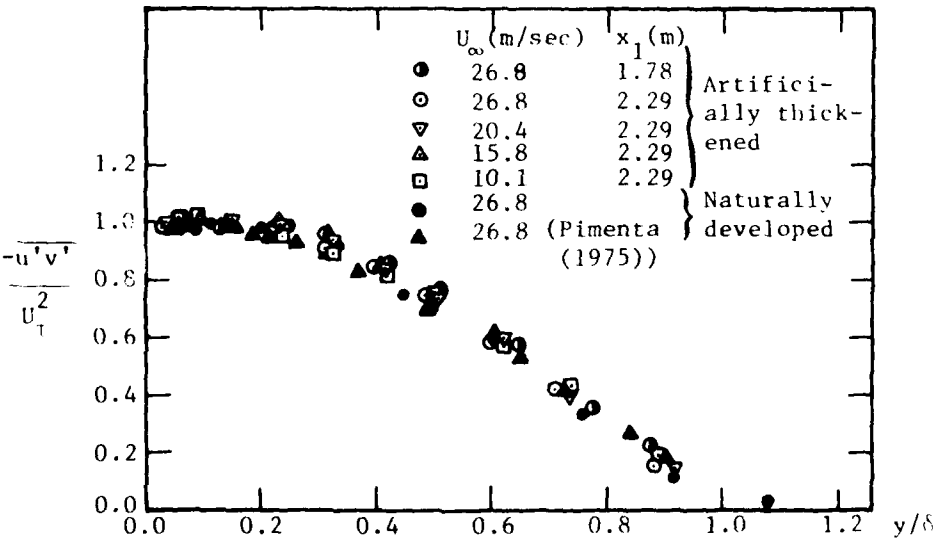

Fig. 2-23. Reynolds shear stress profile downstream development and variation with freestream velocity, rough-wall artificially thickened boundary layers.

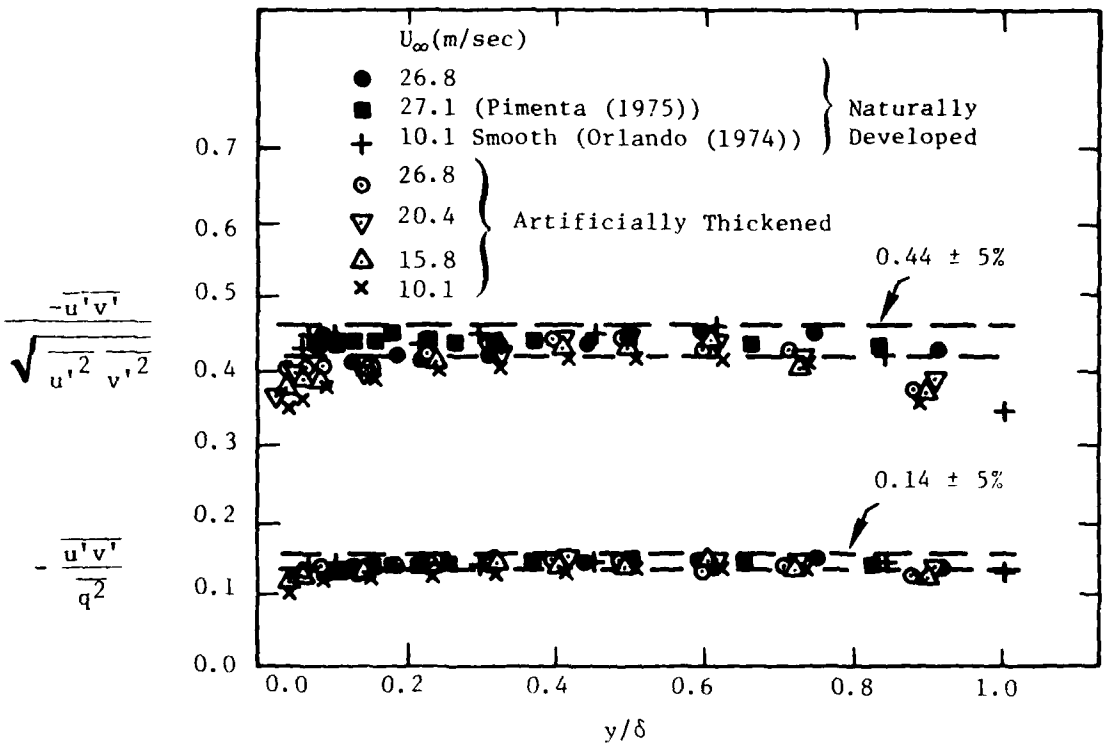

Fig. 2-24. Cross correlation coefficient for the Reynolds shear stress, and the ratio of the Reynolds shear stress to the turbulent kinetic energy in naturally developed and artificially thickened rough wall boundary layers.

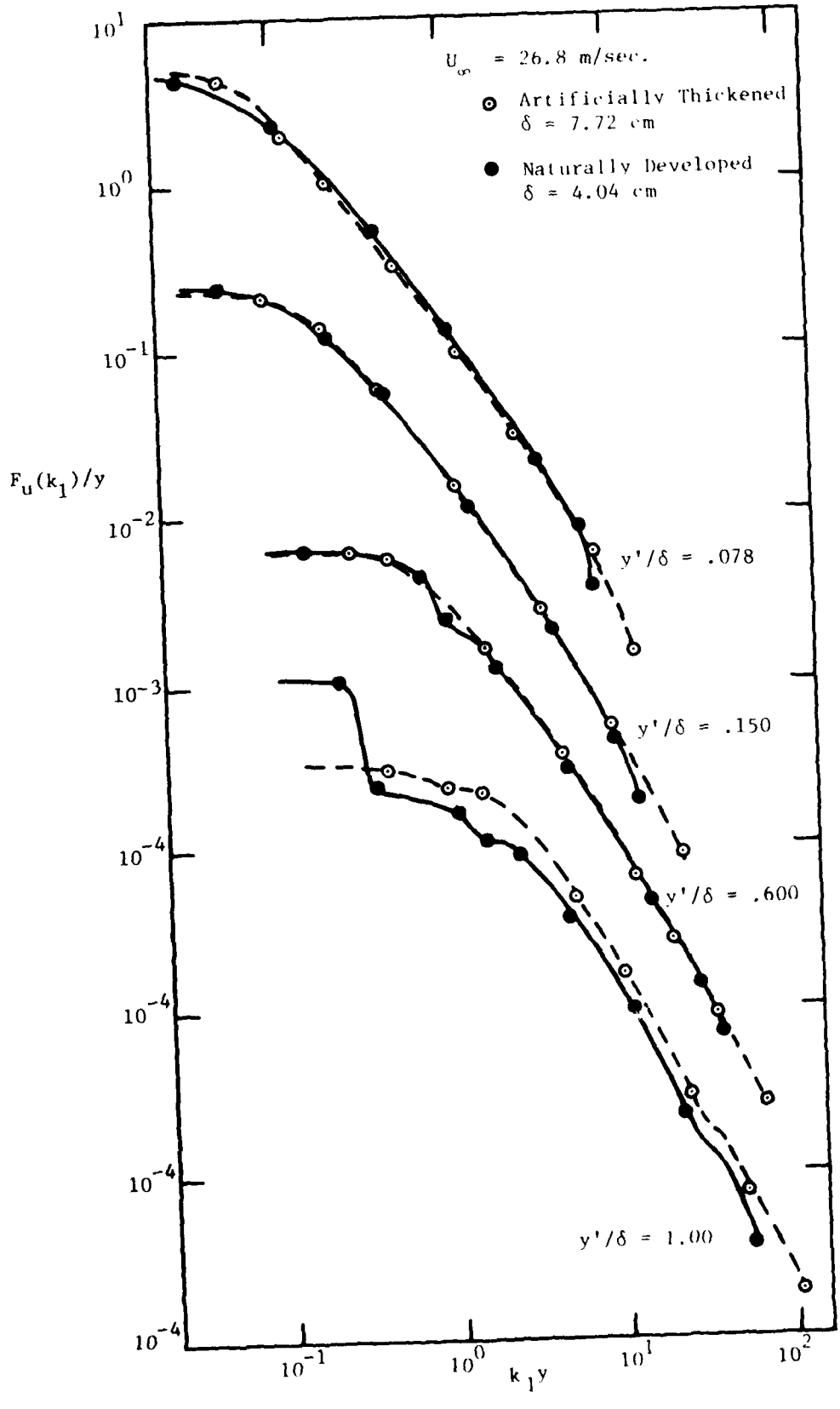

Fig. 2-25. Spectra in artificially thickened and naturally developed fully rough turbulent boundary layers.

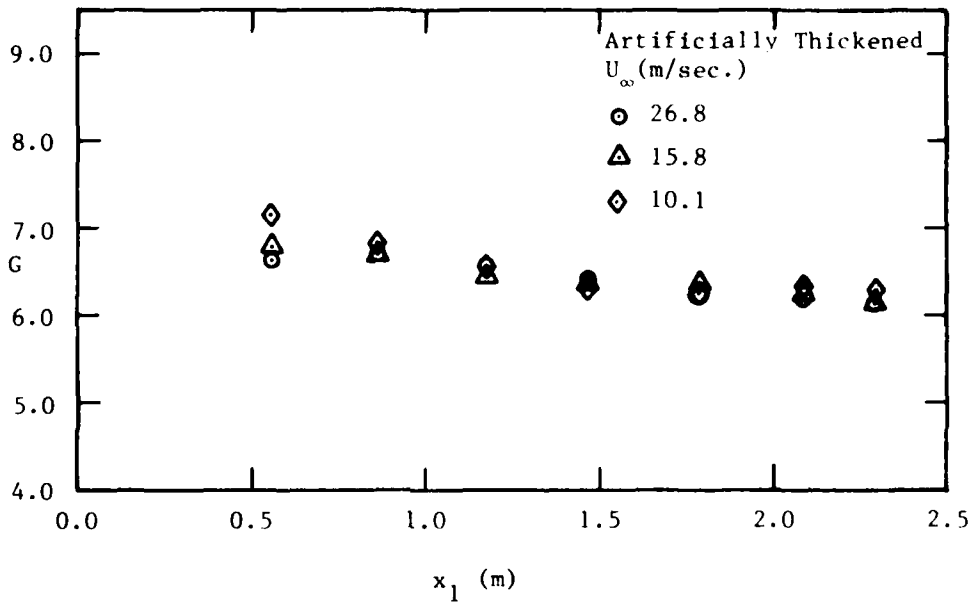

Fig. 2.26. Clauser shape factor variation with downstream distance, rough-wall artificially thickened boundary layers.

Chapter 3

EXPERIMENTAL RESULTS: FULLY ROUGH AND TRANSITIONALLY ROUGH TURBULENT BOUNDARY LAYERS

The influence of roughness on hydrodynamic and thermal boundary layer properties is discussed in this chapter, both for naturally developed and artificially thickened boundary layers. The discussion emphasizes the effect of downstream development and the differences between transitionally rough and fully rough flows, and is divided into four parts. Each part contains a summary of the relevant prior studies not included in Pimenta's (1975) literature survey. These four parts are:

- Hydrodynamic Scalar Properties and Mean Velocity Profiles
- Thermal Scalar Properties and Mean Temperature Profiles
- Turbulence Structure
- Spectra of Longitudinal Velocity Fluctuations

3.1 HYDRODYNAMIC SCALAR PROPERTIES AND MEAN VELOCITY PROFILES

3.1.1 Introduction

Scalar quantities, such as the skin friction coefficient, momentum thickness, and displacement thickness, have been investigated in rough-wall turbulent boundary layers and turbulent pipe flows since the early experiments of Nikuradse (1933) and Hama (1954). This study is still continuing with recent work at Stanford (see Healzer (1974), Pimenta (1975), and Coleman (1976)) and by other investigators such as Voisinet (1978, 1979). However, analysis and understanding of rough-wall turbulent boundary layers is still far from complete, as pointed out by Cebeci and Chang (1979). According to Clauser (1956), one of the most challenging problems of boundary layer research is to determine why different types of roughness produce different types of mean profile behavior. This problem still exists today.

The present section presents measurements of scalar quantities and mean velocity profiles measured in a boundary layer developing over uniform spheres. Recent prior work is first mentioned. Then background information is presented, and the functional dependence of the velocity profile

shift for the present roughness is determined as a function of Re_k, the roughness Reynolds number. The results from these sections are then used to determine functional forms for the skin friction coefficient and the viscous sublayer thickness. Finally, mean profile behavior is discussed in U/U_∞ versus y/δ_2 coordinates, smooth law of the wall coordinates, and fully rough law of the wall coordinates.

3.1.2 Prior Work

Hydrodynamic studies of rough-wall boundary layers since 1975 have been made by several investigators, including Furuya, Miyata, and Fujita (1976), Narayana (1977), Schetz and Nerney (1977), and Voisinet (1978, 1979). Of these, the Schetz and Nerney study and Voisinet study are the most relevant to the Stanford roughness program, since these studies deal with the combined effects of roughness and transpiration. Schetz and Nerney (1977) conducted experiments to measure the skin friction, mean velocity, and longitudinal turbulence intensity in turbulent boundary layers developing over the surface of an axisymmetric body. The authors found that the skin friction of a boundary layer developing over a rough surface is considerably reduced by blowing. With high blowing, the rough-wall skin friction goes below smooth-wall values, when the flows are compared at the same Reynolds number. Voisinet (1978, 1979) studied the combined effects of surface roughness and transpiration in boudnary layers with freestream Mach numbers as high as 2.95. For his study, Voisinet used a specially designed balance for direct measurement of skin friction. He found that blowing shifted the velocity profiles below those which would be expected with roughness and no blowing, and also that blowing affects skin friction results in the same way, regardless of the freestream Mach number.

3.1.3 Experimental Background

There is a log region in the velocity profile over a rough wall, and the velocity profiles can be described using

$$U^+ = \frac{1}{\kappa} \ln \left(\frac{y}{k_s}\right) + B \qquad (3\text{-}1)$$

where the value of B varies with roughness Reynolds number, Re_k, and roughness geometry characteristics. There is an upper critical value of the roughness Reynolds number, Re_k^*, above which the value of B is constant and the flow is known as "fully rough". According to Pimenta (1975), for fully rough boundary layers over uniform spheres roughness, and Schlichting (1968), for fully rough flows in pipes with sandgrain roughness,

$$B = 8.5 \tag{3-2}$$

There is also a lower critical value, Re_k'', below which the flow obeys the smooth-wall law of the wall. If $Re_k < Re_k''$, B has the form

$$B = \frac{1}{\kappa} \ln(Re_k) + C \tag{3-3}$$

where $C = 5.10$. For $Re_k'' < Re_k < Re_k^*$, the flow is transitionally rough and, according to Clauser (1956) and Rotta (1962), B is then a function of Re_k and roughness geometry.

The U^+ versus y/k_s coordinates of Eqn. (3-1) are most appropriate for plotting velocity profiles from flows which are fully rough. Eqn. (3-1) can be rearranged to express the profiles in boundary layer or wall coordinates, allowing a comparison to be made between the smooth law of the wall and rough behavior. This rearranged equation is given as

$$U^+ = \frac{1}{\kappa} \ln\left(\frac{yU_\tau}{\nu}\right) - \frac{1}{\kappa} \ln\left(\frac{k_s U_\tau}{\nu}\right) + C + D \tag{3-4}$$

where $D = B - C$. The difference between Eqn. (3-4) and the smooth law of the wall can then be expressed as a velocity profile shift, which is given by

$$\frac{\Delta U}{U_\tau} = -D + \frac{1}{\kappa} \ln\left(\frac{k_s U_\tau}{\nu}\right) \tag{3-5}$$

so that (3-4) becomes

$$U^+ = \frac{1}{\kappa} \ln\left(\frac{yU_\tau}{\nu}\right) + C - \frac{\Delta U}{U_\tau} \tag{3-6}$$

From (3-5) it is evident that the velocity profile shift from the smooth law of the wall is dependent on the value of B in Eqn. (3-1) and the roughness Reynolds number, Re_k. This approach was first suggested by Nikuradse (1933) for flows in pipes and by Hama (1954) for boundary layers. Clauser (1956), Rotta (1962), and Schlichting (1962) also discuss the velocity profile shift.

3.1.4 B versus Re_k

Using Eqn. (3-1), the values of B can be determined from boundary layer velocity profiles. Values of B versus Re_k for the roughness of the present boundary layer study, from Pimenta's (1975) study, and from Healzer's (1974) study (uniform spheres) are plotted in Fig. 3-1, along with B versus Re_k data for sandgrain roughness in pipes from Nikuradse (1933) (also see Schlichting (1968)). Data for both types of roughness can be represented by a parameter correlation

$$B = C + \frac{1}{\kappa}\,\ell n(Re_k) + \left[8.5 - C - \frac{1}{\kappa}\,\ell n\, Re_k\right] \sin\left[\frac{\pi}{2}\left(g(Re_k)\right)\right] \qquad (3\text{-}7)$$

where

$$g(Re_k) = \frac{\ell n\, Re_k - \ell n\, Re_k''}{\ell n\, Re_k^* - \ell n\, Re_k''} \quad \text{for} \quad Re_k'' \le Re_k \le Re_k^* \qquad (3\text{-}8a)$$

$$g(Re_k) = 1 \quad \text{for} \quad Re_k > Re_k^* \qquad (3\text{-}8b)$$

and

$$g(Re_k) = 0 \quad \text{for} \quad Re_k < Re_k'' \qquad (3\text{-}8c)$$

Predictions based on Eqn. (3-7) are shown in Fig. 3-1, using $Re_k'' = 15.0$ and $Re_k^* = 55.0$ for uniform spheres roughness, and $Re_k'' = 2.25$ and $Re_k^* = 90.0$ for sandgrain roughness. These values for sandgrain roughness were suggested by Ioselevich and Pilipenko (1974) and give their B vs. Re_k equation when substituted into (3-7) (see Cebeci and Bradshaw (1977)). Thus, in Eqn. (3-7), Re_k^* and Re_k'' are fixed by the roughness geometry. In

the transitionally rough regime, both the data and Eqn. (3-7) approach fully rough behavior as Re_k increases. As Re_k decreases, the value of B increases for the spheres roughness, indicating an approach to smooth behavior represented by Eqn. (3-3).

For the uniform spheres roughness, Fig. 3-1 shows that transitionally rough behavior occurs over a smaller range of Re_k than for the sandgrain roughness. The abrupt change from smooth to fully rough behavior occurs as a result of the uniformity of the spheres roughness in contrast to the more gradual transition caused by sandgrains having a more irregular distribution of sizes and shapes. However, both types of behavior are well represented by Eqn. (3-7), where the different geometric characteristics of the two types of roughness are accounted for by using appropriate values of Re_k^* and Re_k''.

3.1.5 Skin Friction

By combining Eqn. (3-1) with Coles' law of the wake, given by Eqn. (2-14), an equation can be determined for the skin friction coefficient of rough-wall boundary layers. In the log region of the velocity profile, Eqn. (2-14) becomes

$$\frac{U_\infty - U}{U_\tau} = -\frac{1}{\kappa}\,\ell n\left(\frac{y}{\delta}\right) + \frac{2\pi}{\kappa} \tag{3-9}$$

which, when added to Eqn. (3-1), produces

$$\frac{U_\infty}{U_\tau} = -\frac{1}{\kappa}\,\ell n\left(\frac{y}{\delta}\right) + \frac{2\pi}{\kappa} + \frac{1}{\kappa}\,\ell n\left(\frac{y}{k_s}\right) + B \tag{3-10}$$

or, alternatively,

$$\sqrt{\frac{2}{C_f}} = \frac{1}{\kappa}\,\ell n\left(\frac{\delta_2}{k_s}\right) - \frac{1}{\kappa}\,\ell n\left(\frac{\delta_2}{\delta}\right) + \frac{2\pi}{\kappa} + B \tag{3-11}$$

Skin friction equations for smooth, fully rough, and transitionally rough flows can then be expressed by substituting appropriate equations for B into (3-11). The skin friction equations are:

$$\sqrt{\frac{2}{C_f}} + \frac{1}{\kappa}\,\ell n\left(\sqrt{\frac{2}{C_f}}\right) = \frac{1}{\kappa}\,\ell n\left(Re_{\delta_2}\right) - \frac{1}{\kappa}\,\ell n\left(\frac{\delta_2}{\delta}\right) + \frac{2\pi}{\kappa} + C \tag{3-12}$$

for $Re_k < Re_k''$,

$$\sqrt{\frac{2}{C_f}} = \frac{1}{\kappa} \ln\left(\frac{\delta_2}{k_s}\right) - \frac{1}{\kappa} \ln\left(\frac{\delta_2}{\delta}\right) + \frac{2\pi}{\kappa} + 8.5 \tag{3-13}$$

for $Re_k > Re_k^*$, and

$$\sqrt{\frac{2}{C_f}} = \frac{1}{\kappa} \ln\left(\frac{\delta_2}{k_s}\right) - \frac{1}{\kappa} \ln\left(\frac{\delta_2}{\delta}\right) + \frac{2\pi}{\kappa} + C + \frac{1}{\kappa} \ln(Re_k) + \left[8.5 - C - \frac{1}{\kappa} \ln(Re_k)\right] \sin\left[\frac{\pi}{2}\left(g(Re_k)\right)\right] \tag{3-14}$$

for $Re_k'' < Re_k < Re_k^*$. For transitionally rough flows, Eqn. (3-14) is in an implicit form since Re_k depends on the skin friction coefficient, $C_f/2$.

Equations (3-13) and (3-14) are compared to experimental measurements of the skin friction coefficient in Fig. 3-2. Fig. 3-2 also contains $C_f/2$ versus δ_2 data for naturally developed and artificially thickened boundary layers. The value of δ_2/δ recommended for all calculations is 0.12, which is estimated from the velocity profile measurements. The constants π and κ are the same as those used in the law of the wake and the smooth law of the wall. Fig. 3-2 indicates that Eqns. (3-12), (3-13), and (3-14) for skin friction show good agreement with the data, with a maximum deviation of approximately 6 per cent. Eqns. (3-12), (3-13), and (3-14) then indicate that the equations for the skin friction coefficient may be expressed in the forms

$$\frac{C_f}{2} = f\left(Re_{\delta_2}\right) \tag{3-15a}$$

$$\frac{C_f}{2} = f\left(\frac{\delta_2}{k_s}, \frac{U_\infty k_s}{\nu}, Re_k'', Re_k^*\right) \tag{3-15b}$$

and

$$\frac{C_f}{2} = f\left(\frac{\delta_2}{k_s}\right) \tag{3-15c}$$

for smooth, transitionally rough, and fully rough turbulent boundary layers, respectively.

Figure 3-3 shows skin friction data plotted in the $C_f/2$ versus Re_{x_2} coordinates used by Prandtl and Schlichting (see Schlichting (1968)) to show predicted skin friction behavior for flows over smooth and rough surfaces. On the figure, a line of constant $U_\infty k_s/\nu$ represents data for a boundary layer at constant freestream velocity developing over a uniformly rough surface. Also, the constant x/k_s lines of the Prandtl and Schlichting treatment are replaced by lines of constant momentum thickness, δ_2. These lines of constant momentum thickness indicate that the skin friction is constant and therefore consistent with Eqn. (3-15c) for fully rough conditions since fully rough $C_f/2$ values are dependent on δ_2 only for a given roughness size. Transitionally rough and smooth $C_f/2$ also depend on momentum thickness, but also on viscosity and other properties.

According to calculations by Prandtl and Schlichting (see Schlichting (1968)), a fully rough boundary layer will eventually become transitionally rough if the boundary layer develops along a uniformly rough test surface long enough to allow the layer to become sufficiently thick. This would occur when the skin friction coefficient, $C_f/2$, decreases to a value such that Re_k is less than or equal to Re_k^*, the roughness Reynolds number which separates fully rough and transitionally rough behavior.

Skin friction data in Fig. 3-3 for all $U_\infty k_s/\nu$ values studied show trends consistent with the Prandtl-Schlichting hypothesis. The skin friction coefficients decrease as δ_2 and Re_{x_2} increase. However, the Prandtl-Schlichting hypothesis is not completely verified by the results in Fig. 3-3 since experimental uncertainties for $C_f/2$ (± 10 per cent) do not allow one to conclude whether or not $C_f/2$ data for $U_\infty k_s/\nu = 1437$ are constant or decreasing lightly with downstream distance for $Re_{x_2} > 6 \times 10^6$. If $C_f/2$ were constant with downstream distance, lines of constant $U_\infty k_s/\nu$ on Fig. 3-3 would be parallel to lines of constant $C_f/2$, and different δ_2 lines would collapse on one curve.

The skin friction behavior of boundary layers which are thicker than those investigated experimentally in the present study can be estimated using the prediction schemes discussed in Chapter 4. However, it is important to remember that the prediction results represent an extrapolation of the data and are not verified beyond the range of the measurements. Predictions for values of $U_\infty k_s/\nu$ of 1130, 1210, and 1437 show that, when

fully rough layers become thick enough, the value of Re_k drops to Re_k^*, and the fully rough plate becomes transitionally rough, as Prandtl and Schlichting suggest. Results of these calculations, shown in Table 3-1, indicate that the downstream distance required for a fully rough layer to become transitionally rough increases as $U_\infty k_s/\nu$ increases. At $U_\infty k_s/\nu = 1437$, this value is 20.8 m, which is equivalent to a downstream Reynolds number of 3.8×10^7 or a momentum thickness of 3.78 cm.

Table 3-1

Predicted Transition Points

from Fully Rough to Transitionally Rough Behavior

($Re_k = Re_k^*$ where $Re_k^* = 55.0$ for $k_s = .079$ cm uniform spheres roughness)

U_∞ (m/sec)	$\frac{U_\infty k_s}{\nu}$	x_2 (m)	Re_{x_2}	δ_2 (cm)	Re_{δ_2}
21.3	1130	1.44	2.1×10^6	.46	6.6×10^3
22.8	1210	2.86	4.5×10^6	.78	1.2×10^4
27.1	1437	20.8	3.8×10^7	3.78	6.9×10^4

3.1.6 Viscous Sublayer

The variation of B with Re_k and the differences between fully rough and transitionally rough skin friction behavior can both be described in terms of changes in the viscous sublayer thickness, A^+. These changes occur as Re_k changes, where the value of A^+ decreases as Re_k increases. In this section, the relation between A^+ and Re_k is first discussed on a qualitative basis. Then equations relating A^+ to B and to Re_k are determined.

Qualitative comparison between roughness size and viscous sublayer thickness can be made by considering that Re_k represents the y^+ value of the height of the roughness elements, where height is expressed as the equivalent sandgrain roughness size. Without roughness, the influence of viscosity extends to a value of y^+ as large as 40-50. The value of Re_k can then be compared to this y^+ range to determine if the non-dimensionalized

AD-A094 011 STANFORD UNIV CALIF THERMOSCIENCES DIV F/G 20/4
THE THERMAL AND HYDRODYNAMIC BEHAVIOR OF THICK, ROUGH-WALL, TUR--ETC(U)
AUG 79 P M LIGRANI, R J MOFFAT, W M KAYS N00014-67-A-0112-0072
UNCLASSIFIED HMT-29 NL

2 OF 3
AD A
094011

roughness height is greater or less than the thickness of the region near the wall, where laminar stresses are significant compared to turbulent stresses. When $Re_k \geq 55\text{-}90$, the viscous sublayer is completely destroyed, the influence of viscosity on the hydrodynamic behavior of the flow is negligible, and the flow is fully rough. When $Re_k < 55\text{-}90$, the flow is transitionally rough and viscosity influences boundary layer behavior.

The relation between the effective sublayer thickness and the velocity profile shift can be determined by referring to Fig. 3-4. On the figure, y^* is the intersection point between the equation

$$U^+ = y^+ \tag{3-16}$$

and Eqn. (3-6)

$$U^+ = \frac{1}{\kappa} \ln y^+ + C - \frac{\Delta U}{U_\tau} \tag{3-17}$$

which represents the log region of rough-wall mean velocity profiles. Combining yields

$$y^* = \frac{1}{\kappa} \ln y^* + C - \frac{\Delta U}{U_\tau} \tag{3-18}$$

The mean velocity over a rough surface for $y^+ < y^*$ can never be greater than that given by $U^+ = y^*$, due to limitations on the motion of the fluid caused by viscosity. The value of y^* can be related to the thickness of the viscous sublayer over rough walls using

$$A_R^+ = \phi y^* \tag{3-19}$$

where the parameter ϕ represents the ratio of the effective value of transitionally rough sublayer thickness in the van Driest mixing length equation (4-16) to the distance from the wall at which viscosity dominates momentum transport. The value of ϕ was determined to be 2.39 based on smooth-wall flows where $y^* = 10.8$ and $A^+ = 26.0$. Substituting for y^* in (3-18), using (3-19), and then rearranging produces

$$\frac{\Delta U}{U_\tau} = C - \left(\frac{A_R^+}{\phi}\right) + \frac{1}{\kappa} \ln \left(\frac{A_R^+}{\phi}\right) \tag{3-20}$$

which shows the dependence of the rough-wall velocity profile shift on the thickness of the viscous sublayer. Substituting for $\Delta U/U_\tau$ in (3-20) using (3-5), and rearranging gives

$$B = \frac{1}{\kappa} \ln\left(\frac{Re_k}{A_R^+}\right) + \frac{A_R^+}{\phi} + \frac{1}{\kappa} \ln(\phi) \qquad (3\text{-}21)$$

which relates B and A_R^+. From (3-21), B is a function of the magnitude of the viscous sublayer thickness which exists on a rough wall, A_R^+, and of the ratio of Re_k to A_R^+.

For fully rough profiles, shown in Fig. 3-4 for $Re_k = 55.0$, the profiles are shifted so far below the smooth law of the wall that intersection with Eqn. (3-16) is not possible. In this case, y^* would be physically located far below the crests of the roughness elements, and consequently Eqns. (3-18)-(3-20) are not valid. This leads to the condition that Eqns. (3-19), (3-20), and (3-21) are valid only when $y^* > 1/\kappa$ or when $\left[B - \frac{1}{\kappa} \ln (Re_k)\right] > 0.264$.

The dependence of A_R^+ on Re_k can be determined by substituting (3-7) into (3-5) and then using this result to replace $\Delta U/U_\tau$ in (3-20), which, after rearrangement, becomes

$$\left(\frac{A_R^+}{\phi}\right) - \frac{1}{\kappa} \ln\left(\frac{A_R^+}{\phi}\right) = C + \left[8.5 - C - \frac{1}{\kappa} \ln Re_k\right] \sin\left[\frac{\pi}{2}\left(g(Re_k)\right)\right] \qquad (3\text{-}22)$$

Eqn. (3-22) can be compared to Eqn. (4-64), a correlation used to produce values of A^+ which correctly predict transitionally rough hydrodynamics. The two curves have the same trends for A^+ versus Re_k, where agreement is maintained within 10%. Eqn. (4-64) is discussed in Chapter 4, and was developed by Healzer (1974) in a different form than is used in the present study.

3.1.7 Mean Velocity Profiles -- U/U_∞ versus y/δ_2 Coordinates

Mean velocity profiles in U/U_∞ versus y/δ_2 coordinates for artificially thickened boundary layers at freestream velocities of 26.8 m/sec, 15.8 m/sec, and 10.1 m/sec show downstream similarity. The downstream similarity is within $\pm .02$ units of U/U_∞ for all y/δ_2 values in the profiles. Such behavior is expected, since both Pimenta's (1975) data for

constant freestream mean velocity and Coleman's (1976) data for equilibrium accelerations show downstream similarity for individual runs at sufficient distances from the front edge of the test surface.

The values of y used for the U/U_∞ versus y/δ_2 plots were measured from the virtual origin of the velocity profiles, as discussed in Section 2.3.3c. All subsequent profiles plotted versus y are measured from the same location. All subsequent profiles plotted versus y' are measured from the crests of the spherical balls which comprise the rough surface of the present study. The virtual origin of the velocity profiles is located a distance Δy below the crests of the roughness elements, where the value of Δy for the present study was determined to be .023 cm.

3.1.8 Mean Velocity Profiles -- Smooth-Wall Coordinates

Transitionally rough and fully rough velocity profiles are shown in inner region smooth-wall coordinates, U^+ versus y^+ in Fig. 3-5. The smooth law of the wall and the equation $U^+ = y^+$, which represents the viscous sublayer, are also shown on the figure. Data in the log regions of the velocity profiles are well represented using Eqn. (3-4), given as

$$U^+ = \frac{1}{\kappa} \ln(y^+) - \frac{1}{\kappa} \ln(Re_k) + B(Re_k) \qquad (3\text{-}23)$$

where appropriate values of $B(Re_k)$ are determined using Eqn. (3-2) for $Re_k > Re_k^*$ or using the correlation given by Eqn. (3-7) for $Re_k'' < Re_k < Re_k^*$. The agreement between (3-23) and velocity profiles in (3-5) then depends on the match between Eqns. (3-2) and (3-7) and data in Fig. 3-1.

In Fig. 3-5, there is evidence of a buffer layer in the velocity profiles for freestream velocities less than or equal to 16.0 m/sec. The buffer layer is indicated by data points for $y^+ \lesssim 30$, which fall below the line which represents the log regions. Existence of a buffer layer indicates that viscous stresses are becoming significant compared to stresses caused by turbulent fluid motion in the near-wall region of the boundary layer.

In U^+ versus y^+ coordinates, fully rough mean velocity profiles do not collapse on one line, as shown in Fig. 3-5 for $U_\infty \gtrsim 26$ m/sec. Collapse of these profiles on the same curves occurs only when the values of B and Re_k for the profiles are the same. An example of such behavior

is indicated by the fully rough boundary layer profiles at $U_\infty = 26.8$ m/sec and $U_\infty = 27.1$ m/sec. Since all smooth-wall data collapse on one curve in U^+ versus y^+ coordinates, and transitionally rough data shift below the smooth law of the wall, the coordinates are most appropriate for showing differences between smooth and transitionally rough mean velocity profiles.

3.1.9 Mean Velocity Profiles -- Fully Rough Coordinates

The same velocity profiles which are plotted in Fig. 3-5 are shown in Figs. 3-6 and 3-7 in fully rough velocity coordinates, U^+ versus y/k_s. The log regions of all profiles for freestream velocities of approximately 26 m/sec and greater collapse on the fully rough law of the wall,

$$U^+ = \frac{1}{\kappa} \ln \frac{y}{k_s} + 8.5 \qquad (3\text{-}24)$$

as shown in Fig. 3-7. When profiles are transitionally rough, they are shifted above Eqn. (3-24) and, thus, U^+ versus y/k_s coordinates are most appropriate for showing the differences between fully rough and transitionally rough mean profile data. In Fig. 3-7, the values of y^+ where data points begin to diverge from the fully rough law of the wall (at the edge of the wake) increase as momentum thickness increases. This trend is qualitatively similar to Clauser's (1956) observation for smooth walls, where the y^+ value of the divergence point increases with momentum thickness Reynolds number. The near-wall data in Fig. 3-7 also show no indication of a buffer layer. Thus, for $U_\infty \gtrsim 26$ m/sec the viscous stresses seem to be negligible compared to the turbulent stresses as near as mean velocity measurements can be made to the roughness elements.

Transitionally rough mean velocity profiles in fully rough coordinates are shown in Fig. 3-6. The log regions of the profiles lie between the smooth law of the wall and the fully rough law of the wall, as expected. The transitionally rough velocity profiles in U^+ versus y/k_s coordinates in the figure are represented using a correlation obtained by substituting Eqn. (3-7) for B into the general expression for rough-wall profiles, Eqn. (3-1), which is given by

$$U^+ = \frac{1}{\kappa} \ln \left(\frac{y}{k_s}\right) + B(Re_k) \qquad (3\text{-}25)$$

The comparison between (3-25) and data in Fig. 3-6 is essentially the same as was made between Eqn. (3-23) and data in Fig. 3-5.

Equation (3-25) and Fig. 3-6 indicate that transitionally rough velocity profiles at a freestream velocity of approximately 10 m/sec are approaching the smooth law of the wall as the boundary layer develops with downstream distance. The value of B is increasing and approaching smooth-wall behavior given by Eqn. (3-3) as Re_k decreases. This qualitative trend of B versus Re_k behavior at $U_\infty = 10$ m/sec is also evident in Fig. 3-1 and is a consequence of changes in the viscous sublayer thickness, as discussed earlier.

3.2 THERMAL SCALAR PROPERTIES AND MEAN TEMPERATURE PROFILES

3.2.1 Introduction

Heat transfer in turbulent boundary layers developing over rough surfaces is important for the design of many engineering components, including reentry vehicles, nuclear reactors, gas turbines, aircraft, and ships. This study is applicable in situations where steps in wall temperature exist, or where the boundary layers over rough surfaces become very thick.

In this section, other recent work is first briefly summarized. Then the differences between Stanton number behavior in smooth, transitionally rough, and fully rough boundary layers developing over rough surfaces are discussed. Variations in Stanton number behavior in boundary layers having unheated starting lengths are then presented. Finally, Stanton numbers in thick, rough-wall, turbulent boundary layers are determined from skin-friction measurements using a Reynolds analogy.

3.2.2 Prior Work

Recent studies of the thermal behavior of rough-wall turbulent boundary layers have been made by Donne and Meyer (1977), Siedman (1978), Kader and Yaglom (1977), and Keel (1977). Kader and Yaglom (1977) and Donne and Meyer (1977) studied turbulent boundary layers developing over two-dimensional, rib-type roughness. Siedman (1978) developed new correlations

to predict heat transfer in rough-wall turbulent boundary layers. Keel (1977) directly measured the skin friction, heat transfer, and mean velocity in a boundary layer at freestream Mach number of 2.5 and 5.0 developing over a 5° cone with sandgrain roughness. The author found that Stanton numbers show the same dependence on enthalpy thickness Reynolds number for two different sizes of sandgrain roughness. Keel observed similar behavior for $C_f/2$ data plotted versus Re_{δ_2}, where the $C_f/2$ data were nearly constant as Re_{δ_2} changed.

3.2.3 Fully Rough, Transitionally Rough, and Smooth Behavior of Thermal Boundary Layers

Rough-wall Stanton number measurements from the present study are shown in Fig. 3-8 for naturally developed boundary layers without an unheated starting length. Freestream velocities of 10.1 m/sed and 26.8 m/sec are shown. The data at the two freestream velocities show the same qualitative trends with downstream development, although the data for U_∞ = 26.8 m/sec (fully rough) are slightly higher than the data at 10.1 m/sec (transitionally rough). Also shown are: (1) the Kays Stanton number equation for smooth walls

$$St = .0125\ Pr^{-0.5}\ Re_{\Delta_2}^{-0.25} \tag{3-26}$$

for $5.0 \times 10^2 < Re_{\Delta_2} < 1.15 \times 10^4$, which is plotted for freestream velocity of 26.8 m/sec, 10.1 m/sec, and 5.0 m/sec, and (2) Pimenta's fully rough Stanton number equation

$$St = .00317 \left(\frac{\Delta_2}{r}\right)^{-.175} \tag{3-27}$$

for $1.5 < \Delta_2/r < 10.0$. Eqn. (3-27) shows excellent agreement with measurements from the present rough-wall study at U_∞ = 26.8 m/sec for $\Delta_2/r \gtrsim 3$.

In the coordinates of Fig. 3-8, smooth-wall Stanton numbers increase in magnitude at a given enthalpy thickness, as the freestream velocity is lowered, with the smooth-wall thermal data approaching the rough behavior. This becomes evident from Fig. 3-10 after a comparison of smooth- and rough-wall results is made at 10.1 and 26.8 m/sec. At 10.1 m/sec, Stanton numbers

closely approximate smooth behavior. The flow is transitionally rough, and the data lie only 4-6% above Eqn. (3-26). If the freestream velocity becomes low enough so that $Re_k \lesssim Re_k''$, the thermal boundary layer will behave as though it is flowing over a smooth surface. Under such circumstances, rough-wall Stanton number data would be represented using Eqn. (3-26). Fig. 3-8 also shows that, for freestream velocities such as 5.0 m/sec, there is the possibility that smooth Stanton numbers may be greater than fully rough Stanton numbers, when the flows are compared at the same value of enthalpy thickness.

3.2.4 Effect of Unheated Starting Length on Rough-Wall Thermal Boundary Layers

Stanton number and mean temperature data in rough-wall, augmented boundary layers show the typical characteristics of flows having unheated starting lengths. The value of the unheated starting length, ξ, is determined for rough walls using the same method discussed in Chapter 2 for smooth walls.

The effect on Stanton numbers of varying the unheated starting length in a flow at a constant freestream velocity of 26.8 m/sec (fully rough) is shown in Fig. 3-9. In the figure, Stanton numbers for flows with an unheated starting length lie below the constant wall temperature curve, when $\Delta_2/r < 3\text{-}4$; that is, when the thermal boundary layers are thin and just beginning to develop. As ξ increases, the values of St at a given enthalpy thickness decrease in magnitude. As the thermal boundary layers become thick, data from flows having unheated starting lengths approach the isothermal boundary layer behavior. Thus, the influence of the unheated starting length disappears with sufficient downstream distance for data in St versus Δ_2/r coordinates. Comparison of the rough data in Fig. 3-9 with smooth-wall results in Fig. 2-11 shows that the same qualitative trends with respect to the effect of ξ are demonstrated by the thermal data regardless of surface roughness. Examination of the transitionally rough St versus Δ_2/r data at 15.9 m/sec and 10.0 m/sec confirm this observation.

Compared with normal, flat-plate boundary layers, boundary layers with unheated starting lengths have lower Stanton numbers at a given enthalpy thickness, because of two physical mechanisms. First, the average mixing length over the thickness of the thermal boundary layer is less than if

$\Delta \sim \delta$, because the thermal boundary layer is contained in the inner regions of a hydrodynamic boundary layer. This follows, because a greater percentage of the layer has a mixing length given by $\ell = ky$ instead of $\ell = \lambda\delta$ than is the case for $\xi = 0$ layers. Consequently, the net eddy diffusivity for heat has an effectively reduced value, and the thermal resistance between $y = 0$ and $y = \Delta$ is increased. The second physical mechanism is that the mean convective velocities are lower in flows where $\Delta < \delta$ than in those where the thermal and hydrodynamic boundary layers are of comparable thickness. The lower mean velocities result in reduced downstream convection of heat, which limits the amount of heat which can be transported by turbulent mixing in the y direction away from the wall. This second effect can also be viewed as a net lower freestream velocity, since the mean velocity at the edge of the thermal layer is less than if $\Delta = \delta$. This effectively lowered freestream velocity decreases as ξ increases.

Figure 3-10 shows typical mean temperature profiles in a thermal boundary layer with an unheated starting length ($\xi = 3.54$ m) at $U_\infty = 26.7$ m/sec. In the $(T_w-T)/(T_w-T_\infty)$ versus y/Δ_2 coordinates of the figure, the $\xi > 0$ temperature profiles show downstream similarity. Similar behavior is shown by other rough-wall profiles with unheated starting lengths, measured at freestream velocities of 10.1 m/sec, 15.8 m/sec, and 26.8 m/sec. The streamwise similarity which occurs at these freestream velocities seems to coincide with invariant Δ_2/Δ with downstream distance.

Another interesting feature of the $\xi > 0$ mean temperature profiles in Fig. 3-10 is that the log regions extend almost to the edge of the thermal boundary layer. The profiles do not have the typical flat-plate wake behavior shown by one of Pimenta's profiles also included on 3-10. This behavior is a consequence of the fact that the $\xi > 0$ thermal boundary layers are thinner than the hydrodynamic boundary layers. A comparison with mean velocity profiles at the same downstream positions supports this explanation, since the log regions of the temperature and velocity profiles cover the same range of y locations.

The mean temperature profiles which are plotted in Fig. 3-10 are also shown in $(T_w-T)/(T_w-T_\infty)$ versus U/U_∞ coordinates in Fig. 3-11. As the profiles develop downstream and x increases, the profiles move closer to the $\xi = 0$ profile. This downstream development trend occurs because the

young thermal boundary layer is growing faster than the older hydrodynamic layer within which it is contained, and δ/Δ is decreasing. The temperature profiles in 3-11 coordinates are approaching $\xi = 0$ behavior in the same sense that the Stanton number approached constant wall temperature behavior in Fig. 3-9. However, temperature profiles in unheated starting length flows are not likely to resemble the $\xi = 0$ profile in Fig. 3-11, unless $\delta \sim \Delta$, which would occur only after considerable downstream development.

Figure 3-12 shows the effect of variations in the magnitude of ξ on mean temperature profiles in $(T_w-T)/(T_w-T_\infty)$ versus U/U_∞ coordinates. The profiles are compared at approximately the same values of Δ_2 and $(x_2 - \xi)$ to eliminate differences between the profiles due to the effects of downstream development. Also included on Fig. 3-12 is a profile from Pimenta (1975) for $\xi = 0$, which shows characteristics consistent with Reynolds analogy, except that the data approach a temperature above T_w at $U = 0$. As the magnitude of ξ increases, δ/Δ increases and the profiles in Fig. 3-12 shift upwards and to the left to diverge from the $\xi = 0$ profile. However, both the $\xi > 0$ profile and the $\xi = 0$ profile show a wall temperature step if the data are extrapolated to $U = 0$.

3.2.5 Effect of Freestream Velocity on Thermal Boundary Layers with an Unheated Starting Length

Figures 3-9 through 3-12 showed the effect of an unheated starting length on flows with constant freestream velocity. The effect of variable velocity on thermal boundary layers having nearly the same magnitudes of unheated starting length are presented in Figs. 3-13 and 3-14. Figure 3-13 shows Stanton number data and Fig. 3-14 shows temperature profile data in the same coordinates used for Figs. 3-9 and 3-10. The unheated starting length is approximately 3.0 m. Data are compared at freestream velocities of 10.1 m/sec, 15.8 m/sec, and 26.8 m/sec.

A comparison of the data in Fig. 3-13 with data in Fig. 3-8 shows that the $\xi > 0$ data in 3-13 have approximately the same trends with freestream velocity variations as the $\xi = 0$ data. In both figures, the fully rough data at $U_\infty = 26.8$ m/sec are slightly higher than the transitionally rough data at the lower velocities. Such qualitative behavior would probably also

exist in a $\xi = 0$ boundary layer at the same x_2 location as for the $\xi > 0$ layer, since such behavior is highly dependent on local hydrodynamic conditions. Dependence on local hydrodynamic conditions is evident on St versus Δ_2/r plots of $\xi > 0$ data by the amount of shift below the $\xi = 0$ solution. The amount of this shift is a function of Δ/δ, the ratio of the thermal boundary layer thickness to the hydrodynamic boundary layer thickness.

The temperature profiles which show the effects of different freestream velocities on flows with a constant unheated starting length are presented in Fig. 3-14. The $\xi > 0$ temperature profiles in the figure are from the same flows shown in Fig. 3-13, where an arrow indicates the approximate Δ_2 location where all the profiles are measured. As the freestream velocities decrease, the log regions of the profiles shift upwards in the $(T-T_w)/(T_w-T_\infty)$ versus y/Δ_2 coordinates of Fig. 3-14. The variations in the temperature profiles which occur for $y/\Delta_2 < 0.30$ are a consequence of the influence of molecular properties on thermal transport near the wall. The region of molecular influence extends to larger y as the freestream velocity decreases, since Re_k is becoming smaller and the viscous sublayer thickness is increasing.

3.2.6 The Behavior of Thick, Rough-Wall Thermal Boundary Layers Without an Unheated Starting Length

Experimentally, thermal boundary layers with enthalpy thickness greater than 0.65 cm $(\Delta_2/r = 10.0)$ cannot be produced on the present rough surface with zero pressure gradient and zero transpiration boundary conditions. Artificially thickened hydrodynamic boundary layers of the present study have reached momentum thicknesses as large as 1.45 cm. Consequently, it is not possible to directly measure Stanton numbers in $\xi = 0$ thermal boundary layers which have thicknesses comparable to those of augmented hydrodynamic layers. However, it is possible to deduce Stanton number behavior for such flows using a Reynolds analogy applied to skin friction coefficient measurements. A discussion of this approach and Stanton number data determined using this approach is now presented.

For turbulent boundary layers, the Reynolds analogy is given by the equation

$$St = \frac{C_f}{2} \tag{3-28}$$

for thermal and hydrodynamic boundary layers of approximately the same thickness which develop from the same origin ($\xi = 0$). Assumptions used in the derivation of (3-28) are that the molecular Prandtl number is approximately unity and the turbulent eddy diffusivity for heat approximately equals the turbulent eddy diffusivity for momentum ($Pr_T \sim 1.0$).

Figures 3-15, 3-16, and 3-17 show Stanton number and skin friction coefficient measurements at freestream velocities of 26.8 m/sec, 15.8 m/sec, and 10.1 m/sec. The data in the naturally developed boundary layers ($x_2 < 2.44$ m) are consistent with the Reynolds analogy, since data agree with Eqn. (3-28) at a given value of x_2. Such behavior is expected, since the assumptions for the derivation of (3-28) are valid for the present experimental conditions in air. Since the Reynolds analogy is expected to be valid regardless of downstream location, Stanton numbers can be determined for $x_2 > 2.44$ m using Eqn. (3-28) and $C_f/2$ measurements from artificially thickened boundary layers. Rough-wall Stanton number behavior in thermal boundary layers having enthalpy thicknesses greater than 0.65 cm are then shown by $C_f/2$ data in Figs. 3-15, 3-16, and 3-17.

Also shown in Figs. 3-15, 3-16, and 3-17 are predictions of rough-wall Stanton numbers which are made using the boundary layer equations closure schemes described in Chapter 4. The thermal predictions show excellent agreement sith St and $C_f/2$ measurements in naturally developed boundary layers, and with $C_f/2$ measurements in the artificially thickened boundary layers. Consequently, the Stanton number behavior deduced from $C_f/2$ measurements for $x_2 > 2.44$ m is further validated by the prediction results. The Stanton number predictions also show agreement with unheated starting length measurements for both naturally developed and augmented boundary layers. Since unheated starting length thermal behavior is highly dependent on local hydrodynamic conditions, the accurate prediction of $\xi > 0$ behavior at a given x_2 strengthens the credibility of the $\xi = 0$ predictions at the same value of x_2.

Figure 3-15 for $U_\infty = 26.7$ m/sec also includes the equation

$$St = .00728 \left(\frac{x_2}{r}\right)^{-.149} \tag{3-29}$$

which was deduced using the energy integral equation in conjunction with Eqn. (3-27). Fig. 3-15 indicates that (3-29) is consistent with deduced fully rough Stanton numbers at all boundary layer thicknesses studied experimentally. Thus, Pimenta's correlation for fully rough thermal layers (Eqn. (3-27)) is expected to represent $U_\infty = 26.7$ m/sec Stanton number behavior in $\xi = 0$ thermal boundary layers whenever $x_2 < 6.55$ m.

The same conclusions regarding the hydrodynamic behavior of fully rough boundary layers as they develop downstream and become very thick can be made regarding fully rough thermal boundary layers. For the range of experimental measurements of the present study, it is not possible to conclude whether Stanton numbers are constant with downstream distance, or decrease with a low power law dependence. However, as Table 3-1 and Section 3.1.5 demonstrated for the $C_f/2$ predictions, predicted Stanton numbers decrease with downstream development and eventually approach transitionally rough and then smooth-wall behavior. However, the predictions represent only an extrapolation of experimental results, and are not verified to represent real boundary layer behavior beyond enthalpy thickness of 1.43 cm, which is the effective limit of the present experimental measurements at $U_\infty = 26.8$ m/sec.

3.3 TURBULENCE STRUCTURE

3.3.1 Introduction

In this section, the structural characteristics of the normal Reynolds stress tensor components, $\overline{u'^2}$, $\overline{v'^2}$, and $\overline{w'^2}$, are discussed. Pimenta's (1975) conclusions regarding the structural characteristics of rough-wall boundary layers are first presented, along with a brief summary of the results of the present study. The detailed characteristics of the normal Reynolds stress tensor components are then given in three-part discussion: (1) the effect of freestream velocity on the normal Reynolds stress tensor components, (2) downstream development of the normal Reynolds stress tensor components, and (3) turbulence kinetic energy.

3.3.2 Prior Work

Figure 3-18 shows Pimenta's (1975) measurements of the longitudinal velocity fluctuations for a fully rough boundary layer at $U_\infty = 27.1$ m/sec, and a transitionally rough layer at $U_\infty = 15.8$ m/sec. Also shown are Coleman's (1976) measurements at $U_\infty = 27.1$ m/sec, measurements from the present study at about the same U_∞, and Klebanoff's (1954) data for a smooth-wall flow. The measurements shown in Fig. 3-18 by Pimenta, Coleman, and the present author for $U_\infty = 27.1$ m/sec are in excellent agreement for $y/\delta > 0.20$. For $y/\delta < 0.20$, differences exist for the three sources which amount to a few percent.

From Klebanoff's (1954) data and his own measurements at 27.1 m/sec and 15.8 m/sec, several important characteristics of fully rough and transitionally rough boundary layers were noted by Pimenta (1975). The fully rough distribution of $\overline{u'^2}$ differs from that of smooth flows, since the peak of $\overline{u'^2}$ is moved out from the wall, lowered, and spread over a greater portion of the layer. In constrast, the transitionally rough $\overline{u'^2}$ profile has distinctively different near-wall characteristics from the fully rough profile, qualitatively similar to smooth behavior, as indicated by a near-wall peak in turbulent intensity. Both the transitionally rough and fully rough flows have higher levels of $\overline{u'^2}/U_\infty^2$ throughout the boundary layers than do smooth-wall flows. Pimenta noted these differences and stated that the near-wall characteristics of $\overline{u'^2}$ offer the most definitive distinction between transitionally rough and fully rough flows.

Grass (1971) also studied the structural characteristics of fully rough and transitionally rough flows in a free-surface channel. Grass varied the roughness Reynolds number by changing the size of the roughness elements, and deduced velocity and stress measurements from hydrogen-bubble flow tracers. The results of his study are discussed and compared to results from this study in Section 3.3.4.

3.3.3 Summary of Results

The present study produced the following observations regarding the structural characteristics of the normal Reynolds stress tensor components:

- The distributions of $\overline{u'^2}/U_\tau^2$ in rough-wall boundary layers approach invariance with U_∞, both as U_∞ decreases and increases. The invariant $\overline{u'^2}$ profiles at high velocities correspond to fully rough behavior, and the invariant $\overline{u'^2}$ profiles at low velocities approach smooth behavior. In between, the flows are transitionally rough, and the distributions of $\overline{u'^2}/U_\tau^2$ change continuously from fully rough behavior to smooth behavior, as the freestream velocity of the flow changes. Fully rough $\overline{u'^2}/U_\tau^2$ profiles can then be distinguished from transitionally rough profiles, since the transitionally rough profiles vary significantly as U_∞ changes, whereas fully rough profiles do not.

- The normalizing variable U_τ collapses the outer regions of profiles of $\overline{u'^2}$ for boundary layers at different downstream locations and at different freestream velocities. U_τ is considered a more universal normalizing variable for $\overline{u'^2}$ profiles than U_∞, but, when normalized using U_∞, the profiles of $\overline{u'^2}$ show approximate downstream similarity for flows at a given freestream velocity. This is largely because the skin friction coefficient, $C_f/2$, changes only slightly with downstream distance.

- When normalized using U_τ, profiles of $\overline{q^2}$ collapse for boundary layers at different freestream velocities which are approximately the same thickness. Profiles of $\overline{q^2}$ show downstream similarity when normalized using U_∞, for flows at a given freestream velocity. Generally, U_τ is considered a more universal normalizing variable for $\overline{q^2}$ profiles than U_∞.

- For $U_\infty \geq 15.8$ m/sec, the normalizing variable U_∞ collapses profiles of $\overline{v'^2}$ and $\overline{w'^2}$ for flows at different downstream locations and at different freestream velocities better than U_τ.

- As the freestream velocity decreases less than 15.8 m/sec, profiles of $\overline{v'^2}/U_\infty^2$ and $\overline{w'^2}/U_\infty^2$ are different from the universal behavior shown by fully rough and transitionally rough flows with freestream velocities greater than or equal to 15.8 m/sec. These profiles are diverging from the $U_\infty \geq 15.8$ m/sec behavior to approach smooth-wall behavior.

- A comparison of profiles of $\overline{u'^2}$ at different downstream locations indicates that fully rough flows do not approach transitionally rough behavior, and transitionally rough flows do not approach smooth behavior for $U_\infty \gtrsim 15$ m/sec and $\delta_2 < 1.45$ cm.

- Measurements at $U_\infty = 10.1$ m/sec indicate that transitionally rough profiles of $\overline{u'^2}$ are approaching smooth-wall behavior with downstream development.

3.3.4 Effect of Freestream Velocity on the Normal Reynolds Stress Tensor Components

Comparisons of profiles of $\overline{u'^2}$, $\overline{v'^2}$, and $\overline{w'^2}$ at different freestream velocities are made in Figs. 3-21, 3-22, and 3-23 for naturally developed and artificially thickened boundary layers. Summaries of the distributions of $\overline{u'^2}$ in transitionally rough and fully rough turbulent boundary layers are also shown in Figs. 3-19 and 3-20, along with Orlando's (1974) smooth-wall data at 9.7 m/sec and Pimenta's (1975) fully rough data at 39.5 m/sec.

3.3.4a Qualitative data trends. Figures 3-19 and 3-20 show, respectively, profiles of $\overline{u'^2}/U_\infty^2$ and $\overline{u'^2}/U_\tau^2$ versus y'/δ for different freestream velocities. When $\overline{u'^2}$ is normalized using U_∞^2, as in Fig. 3-19, the shape of the $\overline{u'^2}$ surface seems to vary for all freestream velocities shown. However, if U_τ^2 is used as a normalization parameter, as in Fig. 3-20, the outer 97-98% of $\overline{u'^2}$ profiles are invariant as the freestream velocity changes for $U_\infty > 25.0$ m/sec. This is a characteristic of fully rough flows. For freestream velocities less than 10.1 m/sec, the $\overline{u'^2}$ profiles are also expected to become invariant as U_∞ changes to approach smooth behavior. The profile of $\overline{u'^2}$ for $U_\infty = 10.1$ m/sec in Figs. 3-19 and 3-20 is similar to that for smooth behavior. There is a peak located near that shown in Orlando's (1974) profile. The similarity to smooth behavior can also be seen in Fig. 3-23. In between the smooth and fully rough regions, the $\overline{u'^2}$ profiles are transitionally rough, and the distributions of $\overline{u'^2}$ change continuously from fully rough behavior to smooth behavior, as the freestream velocity of the flow changes. Fully rough $\overline{u'^2}/U_\tau^2$ profiles can then be distinguished from transitionally rough profiles, since the transitionally rough profiles vary significantly as U_∞ changes, whereas fully rough profiles do not.

The fully rough profiles which exist for $U_\infty \geq 25$ m/sec have a broad, flat hump with a maximum value around $y'/\delta = 0.100$. For $y'/\delta < 0.02$-0.05, the values of $\overline{u'^2}$, normalized using U_τ or U_∞, decrease with increasing freestream velocity and are always lower than for transitionally rough flows. As the freestream velocity decreases below 25.0 m/sec and the boundary layers become transitionally rough, the value of $\overline{u'^2}$ at the measurement location nearest the wall increases as the freestream velocity drops. The "hump" of turbulence, which characterizes fully rough flows, decreases in magnitude and eventually flattens out. These characteristics are shown in Figs. 3-21 and 3-22, as well as in Figs. 3-19 and 3-20.

The variations in the structural characteristics of $\overline{u'^2}$ in transitionally rough boundary layers may be caused by differences in the near-wall turbulent bursting, the source of turbulent kinetic energy. The bursting mechanisms change as the thickness of the viscous sublayer changes. For smooth-wall flows and low-velocity, transitionally rough flows, the bursts develop from the viscous sublayer and move vertically outward from the wall to collide with high-velocity fluid and produce vigorous mixing near $y^+ \sim 10$-30. For such flows, if roughness is present, it is essentially invisible to the flow, since it is completely immersed within a layer of viscous dominated fluid. The viscous film acts as a "cushion" to insulate the wall from fast-moving, turbulent fluid. However, as the flow moves closer to fully rough behavior, the roughness elements begin to protrude through the sublayer. In this case, the turbulent fluid interacts with the wall, since sweeps of fast-moving fluid moving to the wall $(u' > 0, v' < 0)$ may collide with roughness elements. Low-velocity fluid is then ejected from between roughness elements $(u' < 0, v' > 0)$ to be pushed farther from the wall and collide with fast-moving fluid in larger quantities than is the case for smooth-wall flows. The result for such flows is that the region of greatest mixing is moved farther from the wall and spread over a greater portion of the layer. Fully rough profiles of $\overline{u'^2}$ are then characterized by the large, flat "humps" whose maximum values occur around $y'/\delta = 0.10$, as discussed earlier.

According to Grass (1971), the differences in the bursting process near smooth and rough surfaces are "mainly associated with the detailed mechanisms of low momentum fluid entrainment at the bed surface, following inrush phases." He observed that the entrainment near rough surfaces is

more violent than near smooth surfaces. He also noted that the "long, twisting, streamwise vortices", very apparent close to the smooth boundary, are less apparent in the transitionally rough and fully rough flows. These "long, twisting, streamwise vortices" observed by Grass may be responsible for the near-wall peaks of $\overline{u'^2}$ observed at low velocities over the present rough-wall surface. These decrease in magnitude as the freestream velocity increases and the surface appears to become more rough.

3.3.4b Normalizing parameters. The friction velocity, U_τ, is the appropriate normalization parameter for the outer regions of profiles of $\overline{u'^2}$, when comparing boundary layers of approximately the same thickness at different freestream velocities. Fig. 3-22 shows that the distributions of $\overline{u'^2}/U_\tau^2$ at different U_∞ collapse on the same curve for $y'/\delta > 0.35$ for naturally developing boundary layers, and for $y'/\delta > 0.20$ for boundary layers of augmented thickness. Thus, in examining Fig. 3-22, it becomes evident that the artificially thickened data show a better collapse than measurements from naturally developed boundary layers. When normalized using the freestream velocity, U_∞, the $\overline{u'^2}$ profiles at different freestream velocities show significant differences throughout the boundary layers, as shown in Fig. 3-21a. In Fig. 3-21a, $\overline{u'^2}/U_\infty^2$ is plotted with the abscissa in linear coordinates; in 3-22, the abscissa is in log and linear coordinates. Thus, inner-region $\overline{u'^2}$ behavior is magnified in 3-22. Referring to Figs. 3-19 and 3-20, normalization of $\overline{u'^2}$ using U_τ creates a more regular and simple three-dimensional, experimental surface than that produced when $\overline{u'^2}$ is normalized using U_∞. Grass (1971) also found $\overline{u'^2}$ measurements in fully rough, transitionally rough, and smooth-wall flows to be invariant when scaled on U_τ for $y'/\delta > 0.2$. Inside of $y'/\delta = 0.2$, Grass's measurements were qualitatively similar to those of the present study in that $\overline{u'^2}$ profiles vary with Re_k.

The freestream velocity, U_∞, is the appropriate normalization parameter for $\overline{v'^2}$ and $\overline{w'^2}$ profiles plotted versus y/δ when they are compared at different values of U_∞ and when $U_\infty \gtrsim 15.8$ m/sec. Such behavior is indicated by Fig. 3-21b, which shows that profiles of $\overline{v'^2}/U_\infty^2$ and $\overline{w'^2}/U_\infty^2$ collapse on the same curves, regardless of the value of the freestream velocity. In Grass's (1971) study, $\overline{v'^2}$ profiles for different Re_k are invariant when scaled on U_τ.

As the freestream velocity becomes less than 15.8 m/sec, Fig. 3-23 shows that profiles of $\overline{v'^2}/U_\infty^2$ and $\overline{w'^2}/U_\infty^2$ are different from the universal behavior shown by fully rough and transitionally rough flows with freestream velocities greater than or equal to 15.8 m/sec. The $\overline{w'^2}/U_\infty^2$ and $\overline{v'^2}/U_\infty^2$ profiles for 10.1 m/sec are lower than profiles taken at higher freestream velocities for $0.1 < y/\delta < 0.5$. Transitionally rough behavior for $U_\infty \gtrsim 15.8$ m/sec is then characterized by distributions of $\overline{w'^2}$ and $\overline{v'^2}$ which are similar to fully rough flows. For $U_\infty < 15.8$ m/sec, the profiles approach the smooth-wall profiles of Orlando (1974).

3.3.5 Downstream Development of the Normal Reynolds Stress Tensor Components

Figure 3-21 shows the downstream development of profiles of $\overline{u'^2}$, $\overline{v'^2}$ and $\overline{w'^2}$ normalized using U_∞ and plotted versus y/δ for freestream velocities of 26.7 m/sec, 20.4 m/sec, 15.8 m/sec, and 10.1 m/sec. The downstream development of $\overline{u'^2}/U_\infty^2$ for $U_\infty = 10.1$ m/sec is also shown plotted versus y^+ in Fig. 3-24.

3.3.5a Qualitative data trends. Profiles of $\overline{u'^2}/U_\infty^2$, $\overline{v'^2}/U_\infty^2$, and $\overline{w'^2}/U_\infty^2$ in the artificially thickened boundary layer show the same qualitative trends with downstream development as profiles of $\overline{u'v'}/U_\infty^2$ for freestream velocities of 10.1 m/sec, 15.8 m/sec, and 26.8 m/sec. Initially, at $x_1 = 1.17$ m, the normal Reynolds stress tensor components have magnitudes higher than for a naturally developed boundary layer for $y/\delta > 0.2$. As the layer develops downstream at $x_1 = 1.78$ m and $x_1 = 2.29$ m, the profiles are closely similar, a characteristic indicating an approach to second-order equilibrium. Thus, the normal Reynolds stress tensor components eventually relax to normal equilibrium behavior, after having slightly higher magnitudes just downstream of the artificial thickening apparatus.

Figures 3-21a and 3-22 show that, for freestream velocities of 15.8 m/sec and greater, there is no significant change in the qualitative character of the inner 10% of equilibrium profiles of $\overline{u'^2}$ as the boundary layers develop downstream. The artificially thickened results are higher than the naturally developed measurements, but the same trends with downstream development were shown by Pimenta's (1975) measurements in a naturally developing flow at $U_\infty = 27.1$ m/sec. In addition, the changes in boundary layer behavior

with downstream distance shown in 3-21 and 3-22 are not significant enough to indicate a change in roughness regime (i.e., fully rough to transitionally rough). Thus, with regard to near-wall $\overline{u'^2}$ properties, the fully rough flow at 26.8 m/sec is not approaching transitionally rough behavior as the layer becomes thick, and the transitionally rough flows at 20.4 m/sec and 15.8 m/sec are not becoming "smoother" with downstream development.

The near-wall $\overline{u'^2}$ characteristics in the rough-wall boundary layer at 10.1 m/sec seem to have more significant changes with downstream development. Fig. 3-24 shows profiles of $\overline{u'^2}/U_\infty^2$ versus y^+ at two different downstream locations along with Orlando's (1975) smooth-wall measurements for comparison. The peak in $\overline{u'^2}$, which occurs at approximately the same y^+ for all profiles, is increasing with downstream distance in the rough-wall flow, and, since the increase is much larger than observed at other U_∞, it may indicate that the turbulence structure in the transitionally rough flow is approaching smooth-wall behavior as the boundary layer develops downstream (also see Fig. 3-22). The B versus Re_k data and U^+ versus y/k_s profiles discussed in Section 3.1 for the same flow at U_∞ = 10.1 m/sec show similar characteristics, in that they also approach smooth-wall behavior as the boundary layer increases in thickness.

3.3.5b Normalizing parameters. In Section 3.3.4, the friction velocity, U_τ, was indicated to be the appropriate scaling parameter to collapse profiles of $\overline{u'^2}$ compared at different freestream velocities and approximately the same thickness. The friction velocity, U_τ, is also the appropriate normalization parameter for the outer regions of profiles of $\overline{u'^2}$ when comparing boundary layers at different downstream locations, as shown in Fig. 3-22. Similarly, the freestream velocity, U_∞, collapses profiles of $\overline{v'^2}$ and $\overline{w'^2}$ at different downstream locations, as well as for different freestream velocities, as shown in Fig. 3-21b.

The outer 90% of profiles of $\overline{u'^2}/U_\infty^2$ versus y/δ are invariant at different downstream locations for flows at a given freestream velocity, when the skin friction coefficient, $C_f/2$, is approximately constant for these locations. Such behavior is indicated on Fig. 3-21a for freestream velocities of 26.7 m/sec, 20.4 m/sec, 15.8 m/sec, and 10.1 m/sec. Such an observation is sensible, since (1) the outer regions of profiles of $\overline{u'^2}$

at different downstream locations collapse on one curve when $\overline{u'^2}$ is non-dimensionalized using the friction velocity, U_τ, and (2)

$$\frac{\overline{u'^2}}{U_\infty^2} = \frac{C_f}{2} \frac{\overline{u'^2}}{U_\tau^2} \tag{3-30}$$

Coleman's (1976) measurements and Pimenta's (1975) measurements are also consistent with this observation, where the degree of downstream similarity depends on the differences between $C_f/2$ for the locations compared.

3.3.6 Turbulence Kinetic Energy

Profiles of the turbulence kinetic energy, $\overline{q^2}$, are shown in Figs. 3-25 and 3-26 for naturally developed and artificially thickened boundary layers.

Many of the qualitative trends indicated by $\overline{u'^2}$ data are also shown by the turbulence kinetic energy profiles. First, as for $\overline{u'^2}$ profiles, the most appropriate similarity variable for $\overline{q^2}$ profiles is the friction velocity, U_τ. This result is not surprising, since $-\overline{u'v'}/U_\tau^2$ profiles have near-universal behavior and $-\overline{u'v'}/\overline{q^2} = 0.145 \pm 5\%$. Fig. 3-25 shows that the outer 60-70% of $\overline{q^2}/U_\tau^2$ versus y/δ profiles are similar for measurements at approximately the same thickness compared at different free-stream velocities. The figures also show that all profiles except at $U_\infty = 10.1$ m/sec collapse when they are compared at different downstream locations. Such dependence of $\overline{q^2}$ profiles on U_τ is interesting, since the only component of $\overline{q^2}$ which scales on U_τ is $\overline{u'^2}$, whereas $\overline{v'^2}$ and $\overline{w'^2}$ generally scale on U_∞.

Figure 3-26 shows profiles of $\overline{q^2}$ non-dimensionalized using the free-stream velocity, U_∞, and plotted versus y/δ. When normalized in this way, the $\overline{q^2}$ profiles show significant differences throughout the boundary layers when compared at different values of U_∞ and approximately the same thickness. However, the $\overline{q^2}/U_\infty^2$ versus y/δ profiles show similarity when compared at different downstream locations for a given freestream velocity. Such behavior may be related to skin friction coefficient variations with downstream distance, as discussed earlier in regard to $\overline{u'^2}$ profiles.

3.4 SPECTRA OF THE LONGITUDINAL VELOCITY FLUCTUATIONS

3.4.1 Introduction

Spectra of the longitudinal velocity fluctuations, $\overline{u'^2}$, are presented for a fully rough boundary layer developing naturally (not artificially thickened) over uniform-spheres roughness at a freestream velocity of 26.8 m/sec. The differences between these and spectra from flows over smooth surfaces are shown, with particular attention given to the high wave number characteristics. Since measurements in boundary layer and channel flows over smooth surfaces are presented, estimation can be made of transitionally rough behavior by interpolation between the smooth and fully rough results. The spectra were measured using a fast Fourier transform. Details of the measurements technique are presented in Appendix II.

3.4.2 Prior Work

Recent spectral studies of flows over rough surfaces have been made by Perry and Abell (1977), Champagne (1978), and Sabot, Saleh, and Comte-Bellot (1977). Perry and Abell (1977) studied flow in pipes with hexagonal weave roughness, and attempted to show that rough-wall spectra can be predicted from smooth-wall results by properly scaling the measurements. Their paper is based on Townsend's (1976) Reynolds-number similarity hypothesis, which according to the authors means that "all mean relative motions and energy-containing components of the turbulent motions are independent of viscosity and of surface roughness except in so far as these variables may affect boundary conditions on the flow." Champagne's (1978) measurements were made in a variety of flows, including atmospheric boundary layers developing over surfaces with known roughness characteristics. Champagne examined the universal similarity of the fine-scale structure of turbulent velocity fields as related to Kolmogorov's original theories. Sabot, Saleh, and Comte-Bellot (1977) report the results of a study of the effects of roughness on the intermittent maintenance of Reynolds shear stress in pipe flow. In their paper, the authors present the frequency distribution of $-\overline{u'v'}$ at various distances from a rough wall, and also compare the magnitudes of integral-length scales in flows over smooth and rough surfaces. Spectral

studies in boundary layer and pipe flows over smooth walls have been made by Klebanoff (1952, 1954), Laufer (1954), and many others.

3.4.3 Experimental Background

In the present study, the spectra are normalized such that

$$\int_0^\infty f_u(k_1)\, dk_1 = \int_0^\infty f_u(n)\, dn = \overline{u'^2} \tag{3-31}$$

and

$$\int_0^\infty F_u(k_1)\, dk_1 = \int_0^\infty F_u(n)\, dn = 1.0 \tag{3-32}$$

where

$$F_u(k_1) = \frac{f_u(k_1)}{\overline{u'^2}} \tag{3-33a}$$

and

$$F_u(n) = \frac{f_u(n)}{\overline{u'^2}} \tag{3-33b}$$

The one-dimensional wave number, k_1, is determined using

$$k_1 = \frac{2\pi n}{U} \tag{3-34}$$

which is one way of expressing Taylor's "frozen-flow" approximation. Alternatively, Taylor's hypothesis may be expressed as

$$\frac{\partial(\ )}{\partial t} = -U \frac{\partial(\ )}{\partial x} \tag{3-35}$$

A derivation of Eqns. (3-34) and (3-35) is presented by Champagne (1978), developed from the assumption that the time variation of the turbulent structure in a moving reference frame is small relative to the motion produced by convection of the turbulent structure.

Aside from the normalization given by Eqns. (3-31) and (3-32), spectra can also be normalized using

$$\frac{f_u(k_1)}{\mathcal{U}^2\mathcal{L}} = f_1(k_1\mathcal{L}) \tag{3-36}$$

where $\mathcal{U}$ and $\mathcal{L}$ are velocity and length scales which may pertain to the physical parameters which affect the transport of turbulent energy. Alternatively, $\mathcal{U}$ and $\mathcal{L}$ may be based on scales related to eddy size and eddy structure in the flow. In either case, the physical parameters for $\mathcal{U}$ and $\mathcal{L}$ will vary as different wave number ranges are considered. Examples of appropriate scaling parameters applicable to low wave numbers for flows over both smooth and rough surfaces are given by Tennekes and Lumley (1972), Hinze (1975), and by Perry and Abell (1977).

For high wave numbers, Kolmogorov's two hypotheses concerning the fine-scale structure of turbulence describe spectrum behavior (see Champagne (1978) and Tennekes and Lumley (1972)). The first hypothesis states that the motion of small-scale turbulent structures is uniquely determined by ε, the viscous dissipation of turbulent energy, and by ν, the kinematic viscosity. One-dimensional spectra should then be similar for all turbulent velocity fields when normalized such that

$$\frac{f_u(k_1)}{v^2\eta} = \frac{f_u(k_1)}{(\varepsilon\nu^5)^{1/4}} = f_2(k_1\eta) \tag{3-37}$$

where $\eta = (\nu^3/\varepsilon)^{1/4}$ is the Kolmogorov length scale and $v = (\nu\varepsilon)^{1/4}$ is the Kolmogorov velocity scale. This hypothesis is valid for an equilibrium range of wave numbers characterized by large Re_λ, where

$$Re_\lambda = \frac{\overline{(u'^2)}^{1/2}\,\lambda}{\nu} \tag{3-38}$$

and λ is the Taylor microscale given by

$$\lambda^2 = \overline{u'^2} \Big/ \overline{\left(\frac{\partial u'}{\partial x}\right)^2}$$

The second Kolmogorov hypothesis speaks to the behavior of a range of wavenumbers (within the equilibrium range) called the inertial subrange. In the inertial subrange, negligible dissipation occurs, the effects of viscosity are negligible, and energy is transferred principally by inertial forces. The spectra are given by

$$f_u(k_1) = \alpha_1 \varepsilon^{2/3} k_1^{-5/3} \tag{3-39}$$

or, alternatively,

$$\frac{f_u(k_1)}{(\varepsilon\nu^5)^{\frac{1}{4}}} = \alpha_1 (k_1\eta)^{-5/3} \tag{3-40}$$

where α_1 is a universal constant. From Pao's (1965) results, α_1 was estimated to be equal to 0.47.

3.4.4 Effects of Roughness

In Figs. 3-27a and 3-27b, rough-wall boundary layer spectra of $\overline{u'^2}$ are compared to smooth-wall measurements for $y'/\delta = .078$ and $y'/\delta = 0.600$. As for Fig. 2-25, the lines in Fig. 3-27 and all subsequent spectra plots represent a graphical fit to closely spaced data points. The data in 3-27 are plotted in $F_u(k_1)$ versus k_1 coordinates, and thus the figures show the distribution of energy with respect to wave number. For both values of y/δ, smooth-wall channel measurements show reasonable agreement with Klebanoff's (1954) smooth-wall boundary layer measurements. Additionally, all data sets exhibit behavior characteristic of the inertial subrange, since $F_u(k_1)$ varies with $k_1^{-5/3}$ for the part of the wave number range shown. However, the inertial subrange seems to persist at much higher values of k_1 for the fully rough flow than is the case for the smooth-wall flows. This is evident from the figures, since the smooth $F_u(k_1)$ decrease faster than $k_1^{-5/3}$ for $k_1 > 10^1$. The rough-wall boundary layer has more energy at higher wave numbers than do smooth-wall flows, when the boundary layers are compared at the same y/δ. This indicates that the small-scale turbulent motions from the spheres roughness may be more numerous or more energetic than eddies produced from the bursting which originates from a viscous sublayer.

Since the present rough-wall spectra have a wave number region where $f_u(k_1)$ varies with $k_1^{-5/3}$, the viscous dissipation of turbulent energy may be determined using Eqn. (3-39) or (3-40). In doing so, we are assuming that the rough-wall spectra have an inertial subrange, and that Kolmogorov's second hypothesis is applicable. The dissipation calculations are

shown as data points in Fig. 3-28 for a naturally developed rough-wall flow (δ_2 = .557 cm) and an artificially thickened rough-wall flow (δ_2 = .978 cm). Also included in the figure is $\mathcal{P}$, the production of turbulent kinetic energy, estimated from measurements using

$$\mathcal{P} = -\overline{u'v'}\,\frac{\partial U}{\partial y} \tag{3-41}$$

Production seems to match dissipation everywhere within the layer, not only in the inner region. Diffusion and convection of turbulent kinetic energy may then have approximately the same magnitudes at every measurement location as well.

Figure 3-29 shows rough-wall boundary layer spectra and smooth-wall channel spectra normalized with respect to Kolmogorov's length and velocity scales, η and $\mathcal{V}$. Since Eqn. (3-39) was used to determine ε for calculation of η and $\mathcal{V}$, the spectra in Fig. 3-29 show excellent agreement with Eqn. (3-39) in the inertial subrange ($1 \times 10^{-2} - 2 \times 10^{-2} < k_1\eta < 10^{-1}$). For $k_1\eta < 1 \times 10^{-2} - 2 \times 10^{-2}$, significant variations between different spectra are shown as a consequence of the large-scale turbulent motions in the flows. For values of $k_1\eta$ greater than 10^{-1} (outside of the inertial subrange), the smooth-wall channel measurements and the rough-wall boundary layer measurements agree with Pao's (1965) equation for $f_u(k_1)$. Thus, if the values of the dissipation of turbulent kinetic energy determined from Eqn. (3-39) represent real behavior, then the smooth-channel and rough boundary layer spectra show universal small-scale characteristics consistent with Kolmogorov's first and second hypotheses.

For isotropic turbulence, the viscous dissipation of turbulent kinetic energy is given by

$$\varepsilon = 15\nu\,\overline{\left(\frac{\partial u'}{\partial x}\right)^2} \tag{3-42}$$

If Taylor's "frozen-flow" hypothesis is then applied to (3-42), ε can be expressed as

$$\varepsilon = 15\nu\int_0^\infty k_1^2 f_u(k_1)\,dk_1 \tag{3-43}$$

Dissipation spectra then consist of plots of $k_1^2 f_u(k_1)$ versus k_1 and are often used to magnify the high wave number part of a spectrum. The dissipation spectrum for a rough-wall boundary layer at $y'/\delta = .078$ is compared to smooth-channel measurements at $y/\delta = .086$ in Fig. 3-30. Estimation of behavior at large k_1 using Pao's (1965) equation for universal small-scale behavior (see Fig. 3-29) is also shown for the two sets of measurements. From the figure, it is evident that the peak in $k_1^2 f_u(k_1)$, which is where viscous dissipation is most significant, occurs at much higher one-dimensional wave number values for the rough-wall flow than for the smooth-wall flow. This is related to the fact that more energy exists at higher frequencies in flows over rough surfaces and, at the same time, the magnitude of the Kolmogorov length scale for the rough surface flow is approximately half the magnitude for the smooth-wall flow.

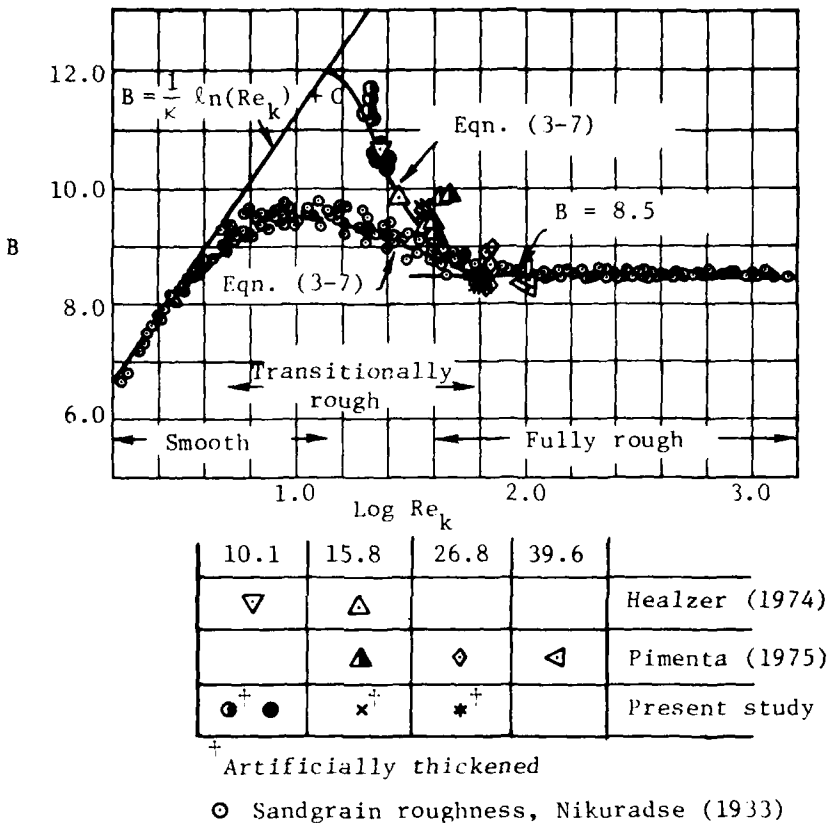

Fig. 3-1. Variation of B with roughness Reynolds number.

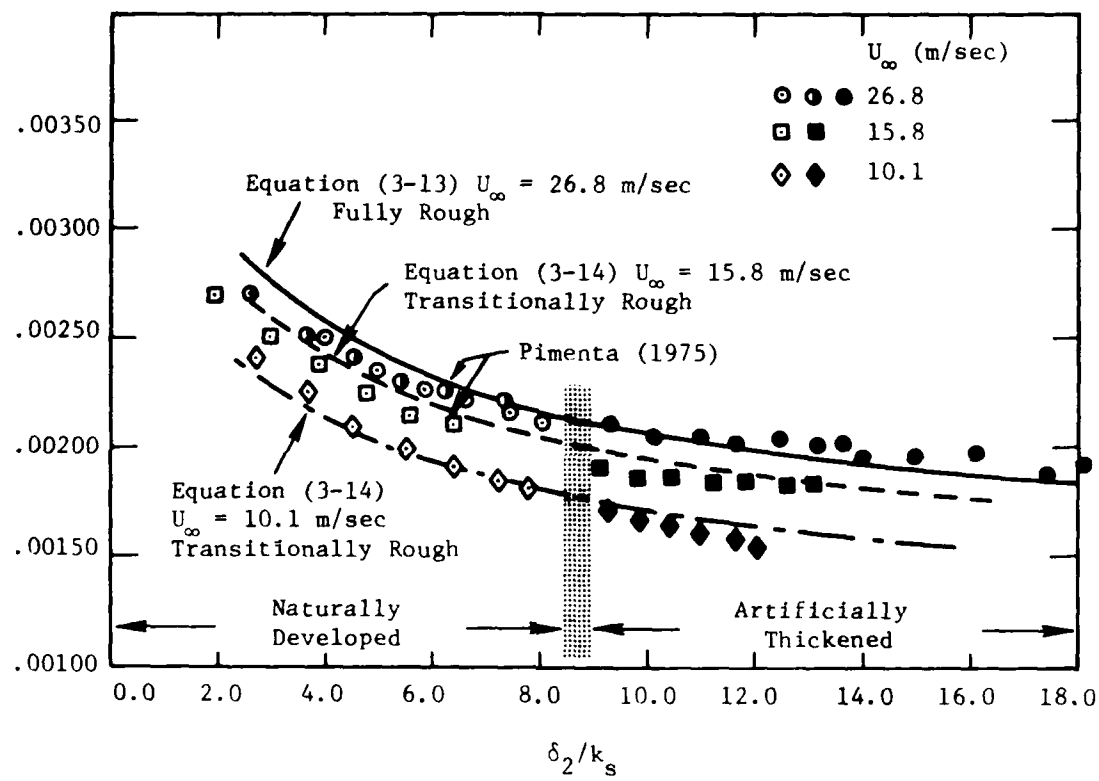

Fig. 3-2. Rough wall boundary layer skin friction variation as a function of momentum thickness.

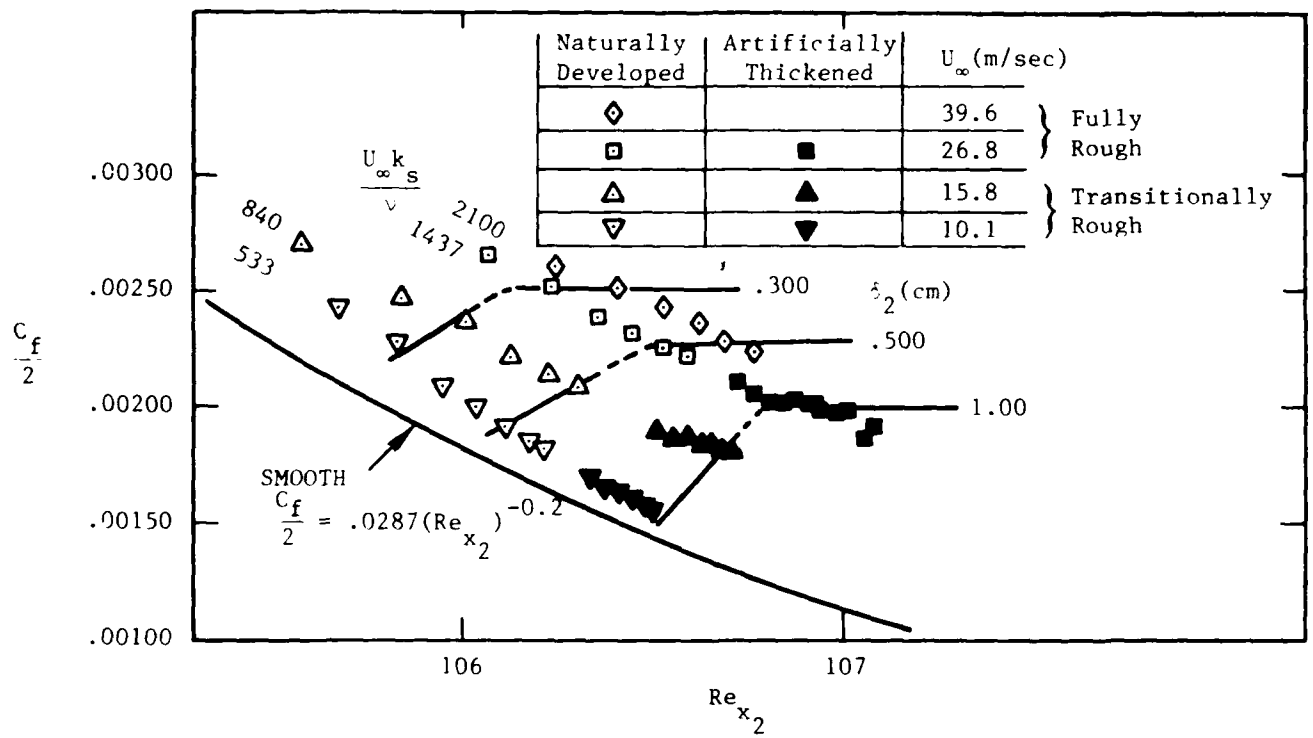

Fig. 3-3. Rough-wall boundary layer skin friction variation as a function of Reynolds number based on downstream distance.

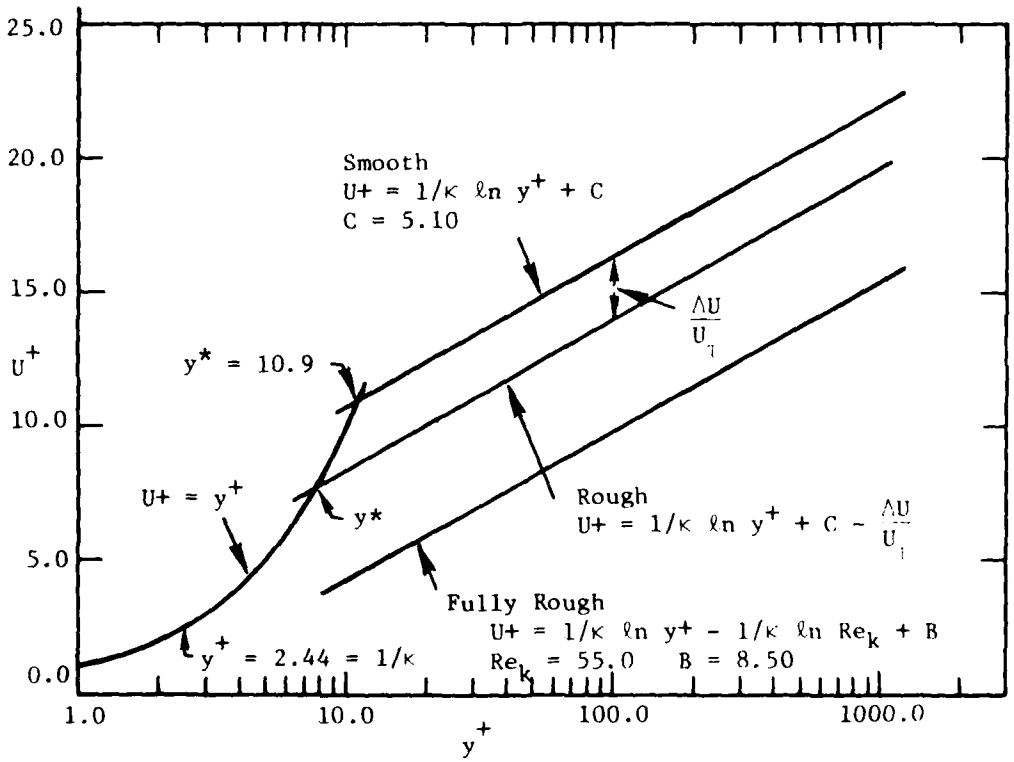

Fig. 3-4. Fully rough, transitionally rough, and smooth mean velocity profiles.

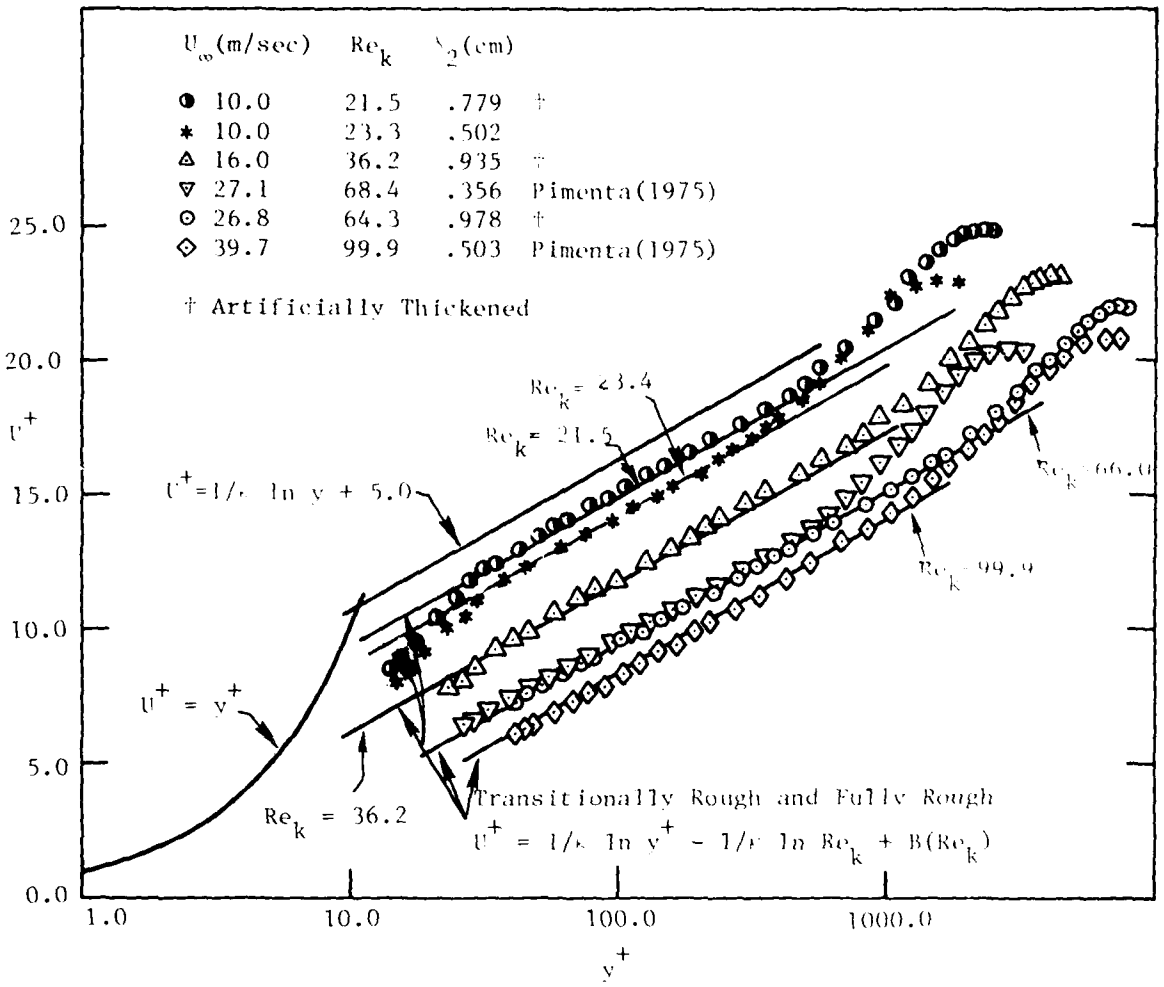

Fig. 3-5. Rough-wall mean velocity profiles - smooth-wall inner region coordinates.

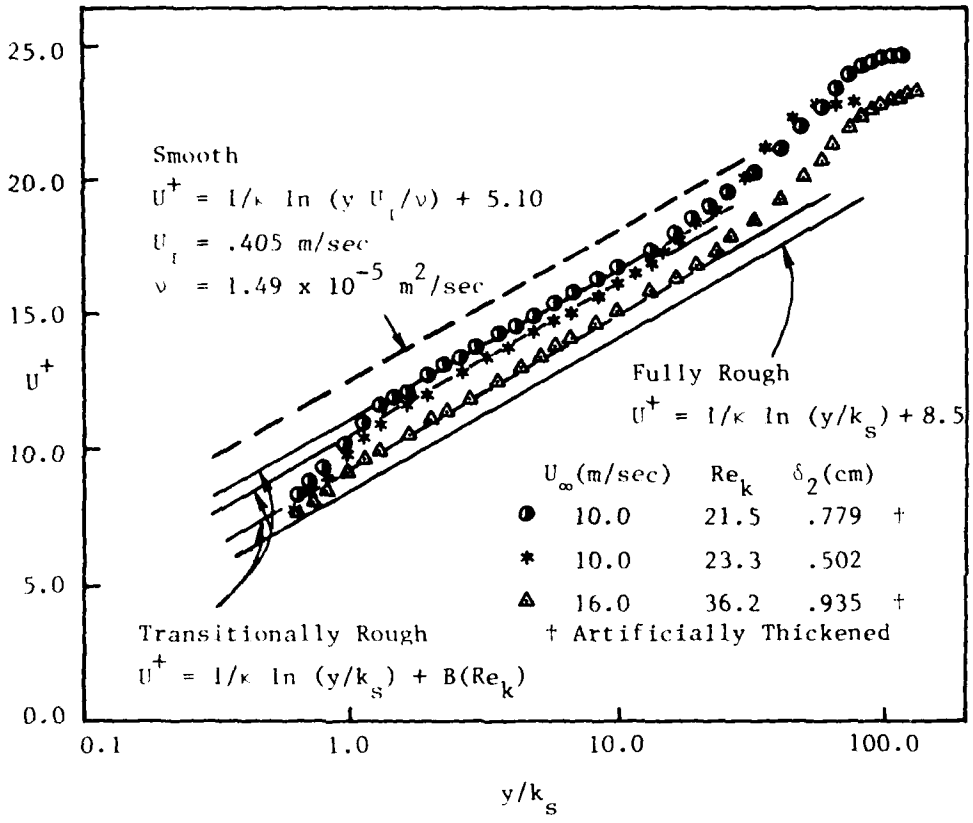

Fig. 3-6. Transitionally rough mean velocity profiles - fully rough, inner region coordinates.

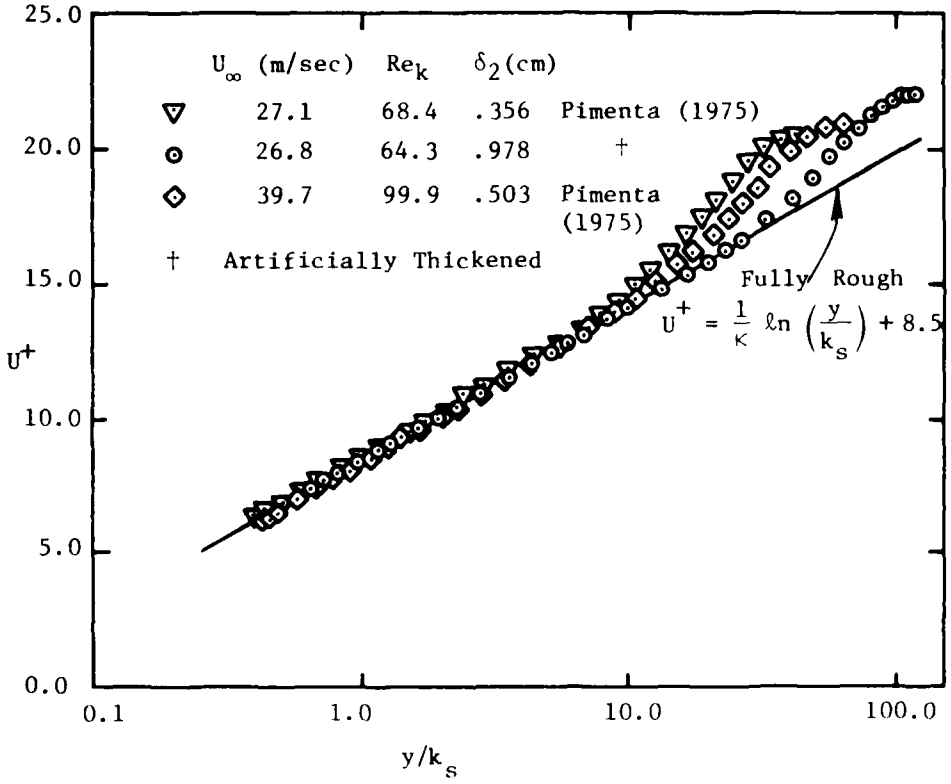

Fig. 3-7. Fully rough mean velocity profiles - fully rough, inner region coordinates.

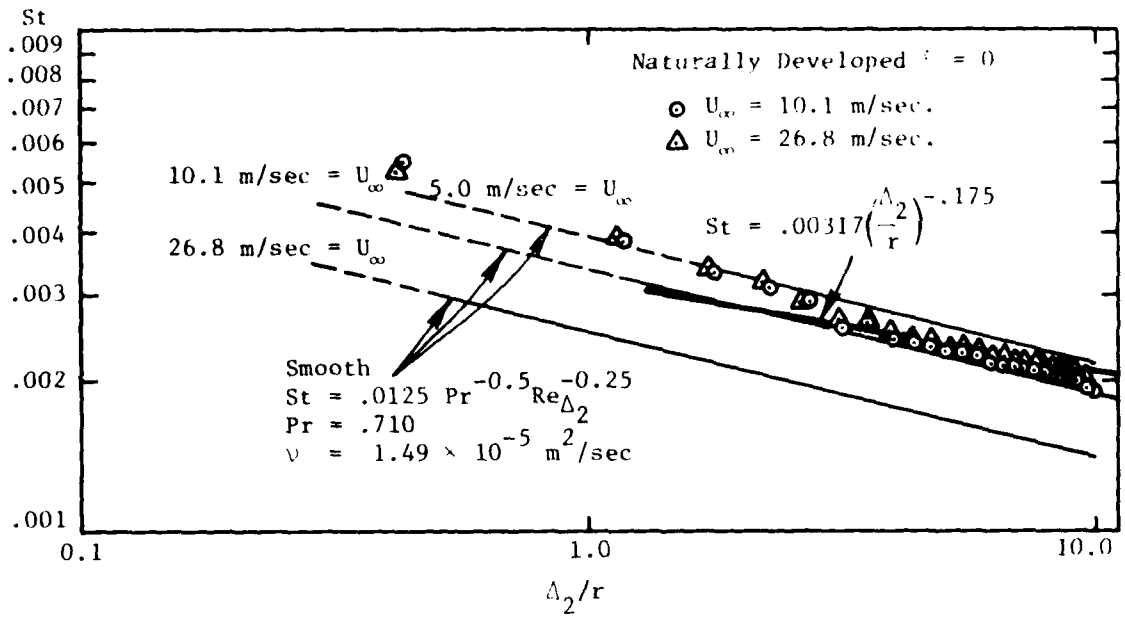

Fig. 3-8. Fully rough, transitionally rough, and smooth Stanton number behavior.

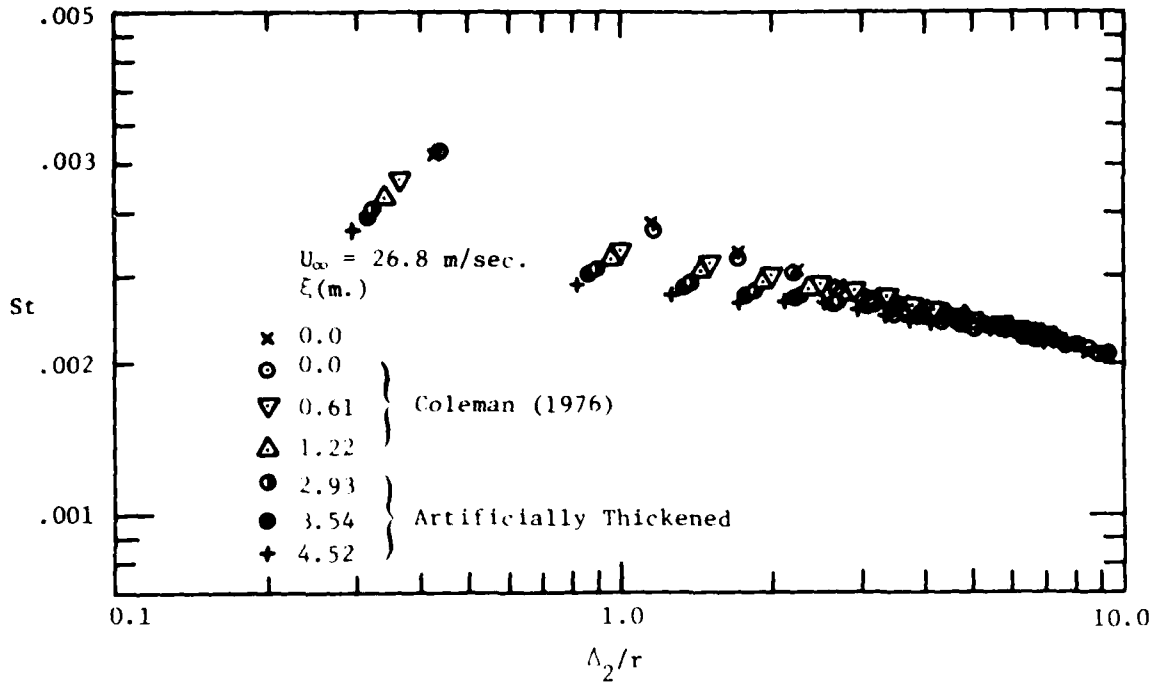

Fig. 3-9. Effect of unheated starting length on Stanton number behavior in a fully rough turbulent boundary layer.

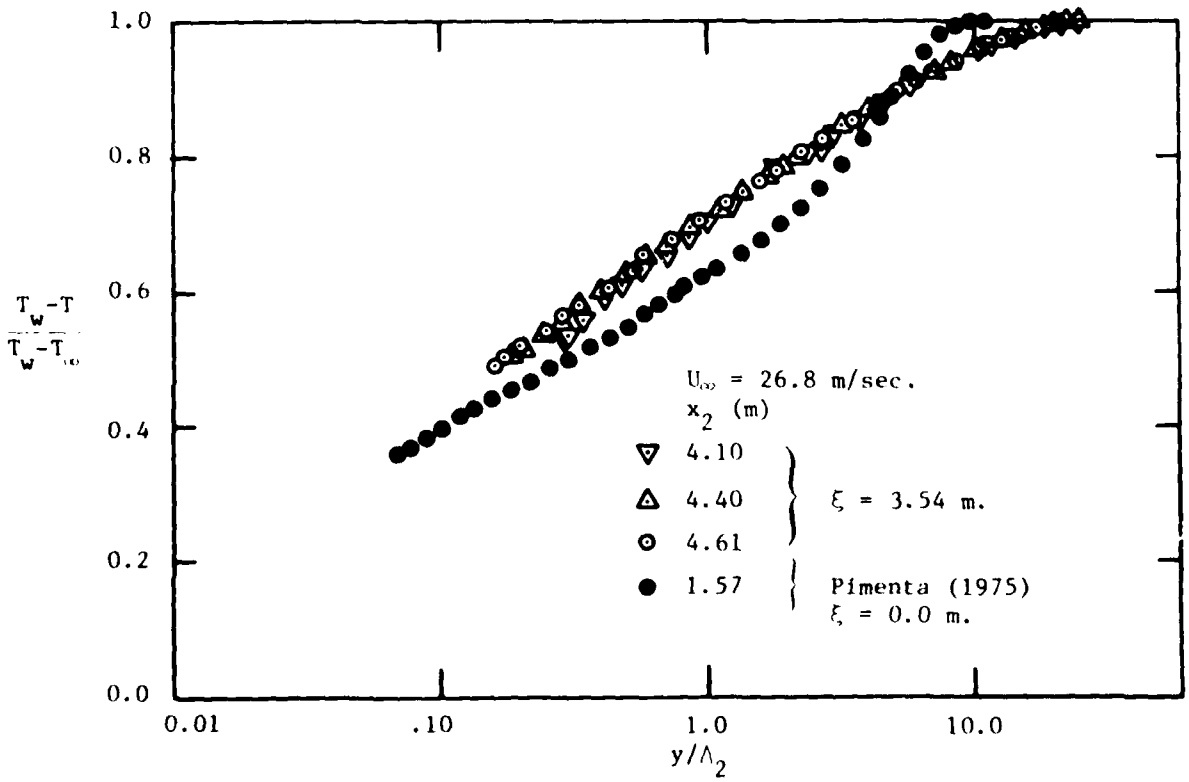

Fig. 3-10. Downstream development of mean temperature profiles in a fully rough turbulent boundary layer with an unheated starting length.

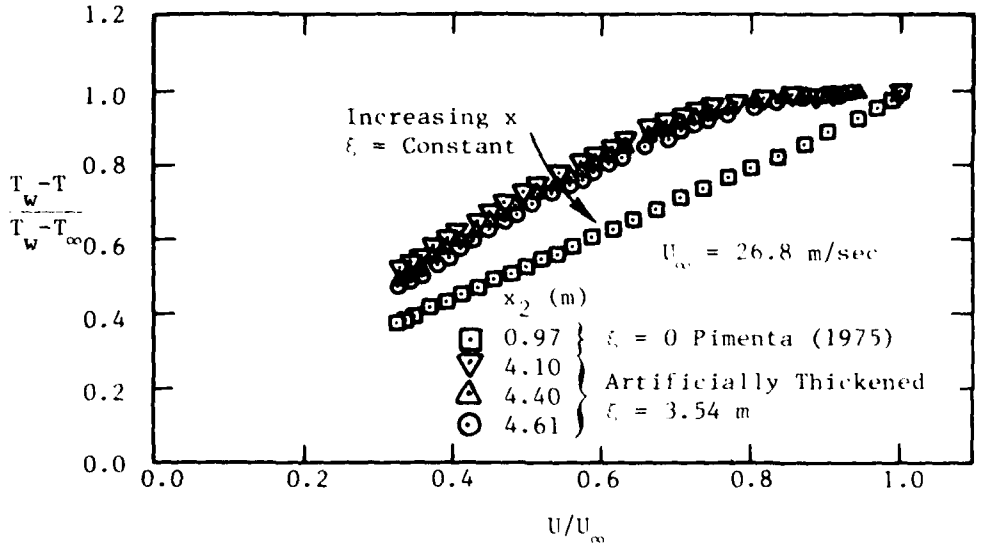

Fig. 3-11. Effect of downstream development on mean temperature profiles in a fully rough boundary layer with an unheated starting length.

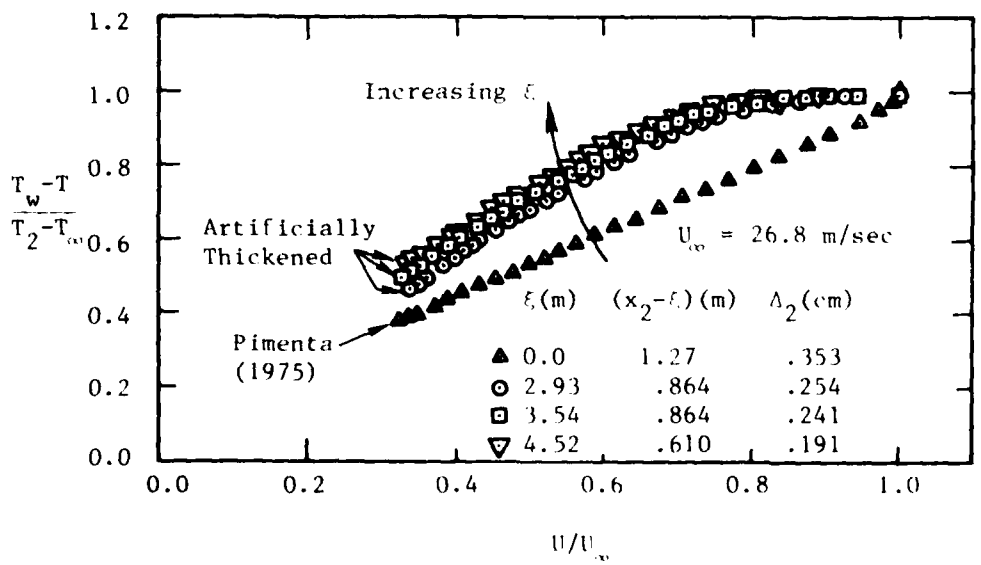

Fig. 3-12. Effect of unheated starting length on mean temperature profiles having approximately the same enthalpy thickness in a fully rough turbulent boundary layer.

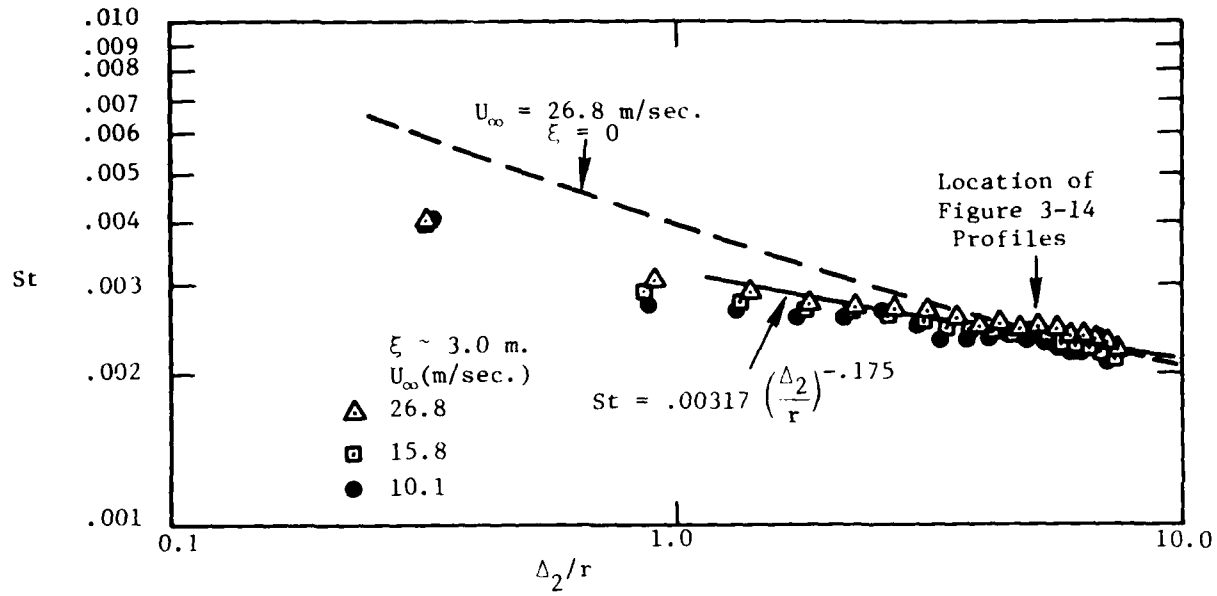

Fig. 3-13. Effect of freestream velocity on Stanton number behavior in rough-wall boundary layers having unheated starting length.

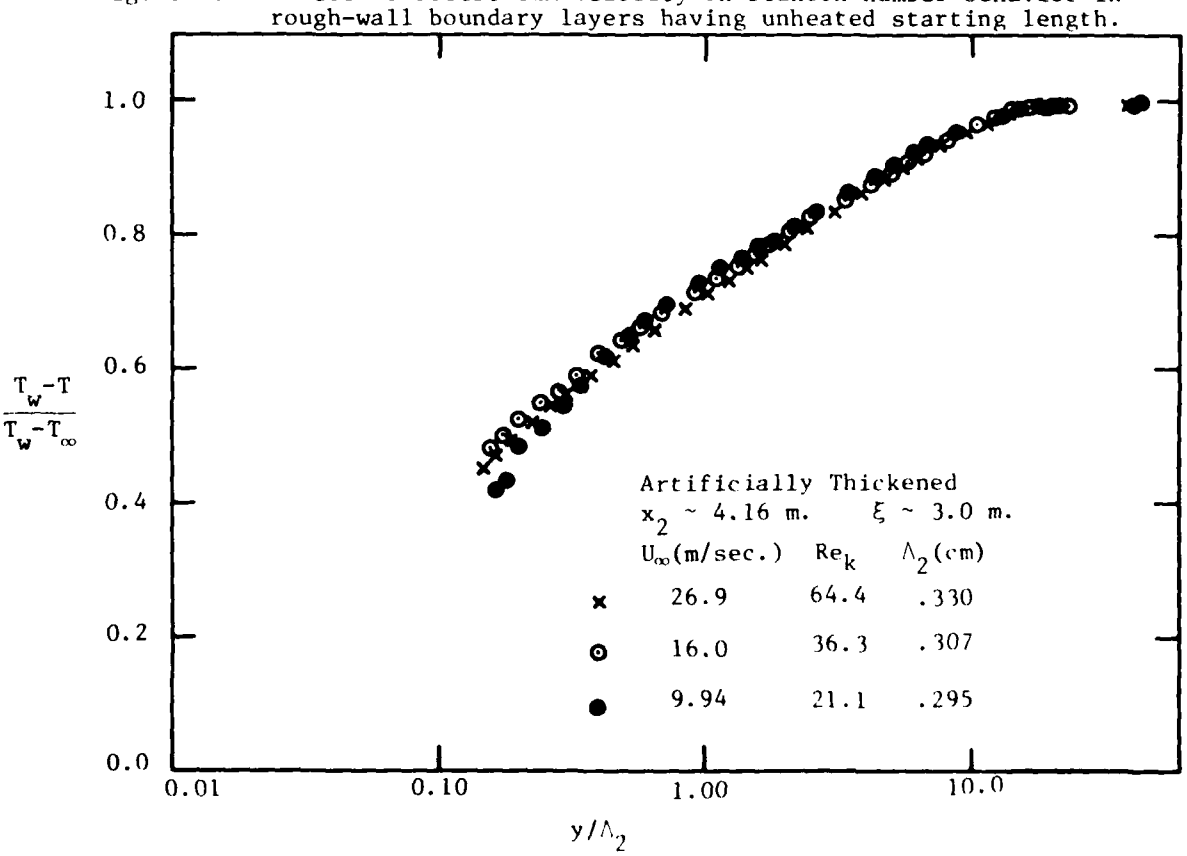

Fig. 3-14. Effect of freestream velocity on mean temperature profiles in rough-wall boundary layers having unheated starting length.

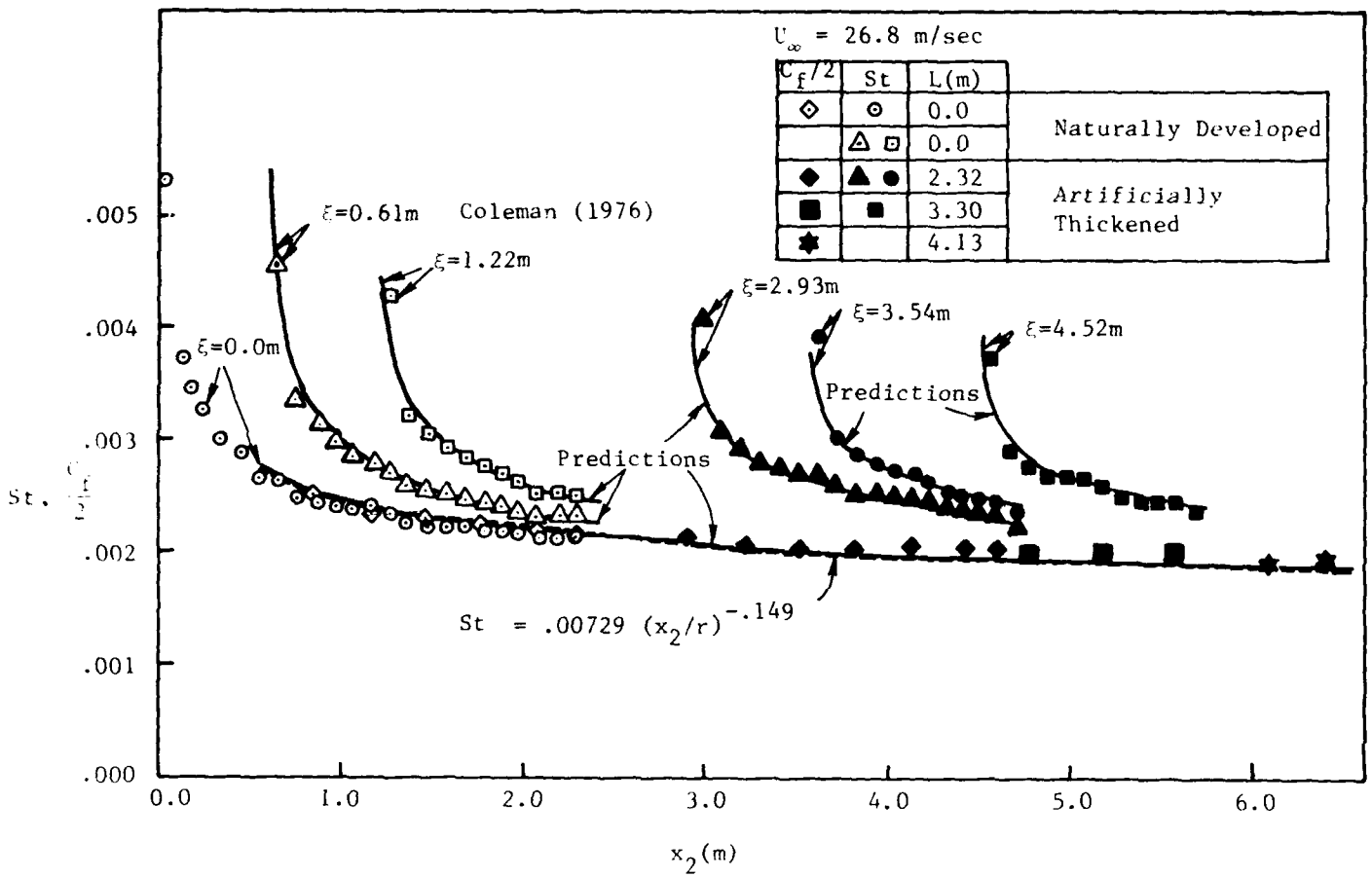

Fig. 3-15. Variation of Stanton numbers with downstream distance, U_∞ = 26.8 m/sec.

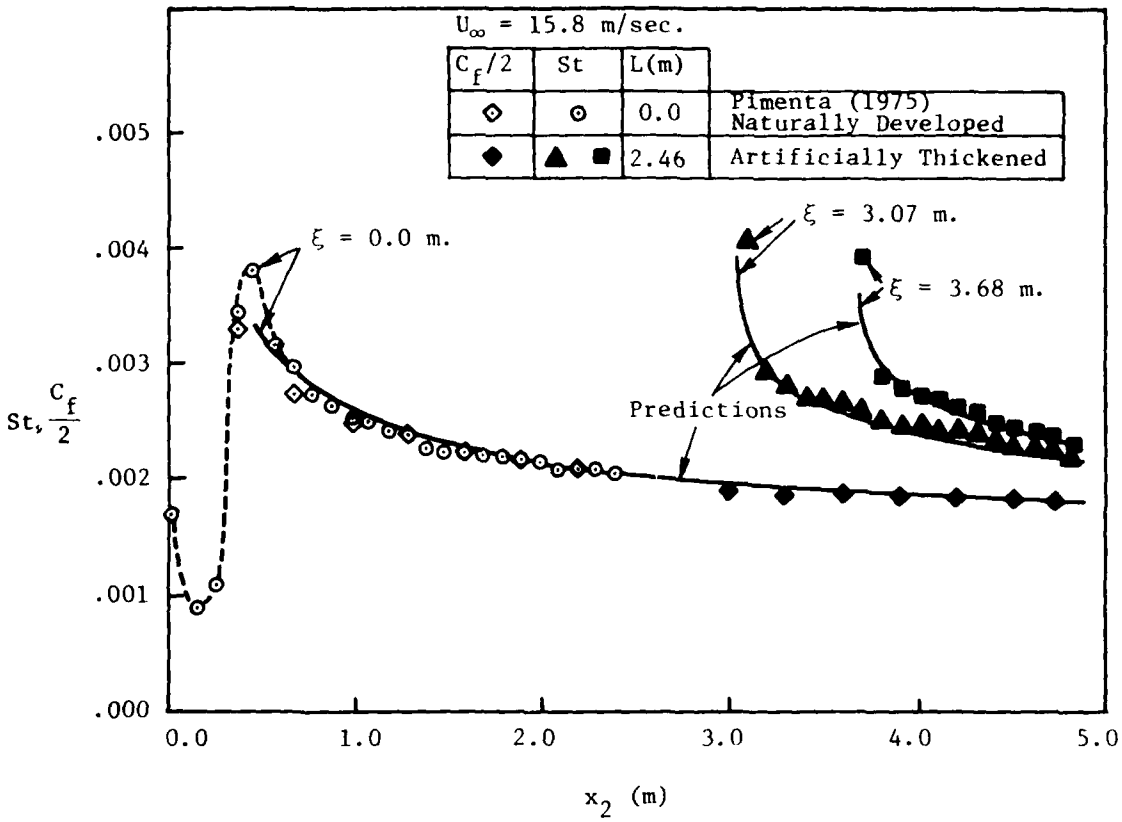

Fig. 3-16. Variation of Stanton numbers with downstream distance, U_∞ = 15.8 m/sec.

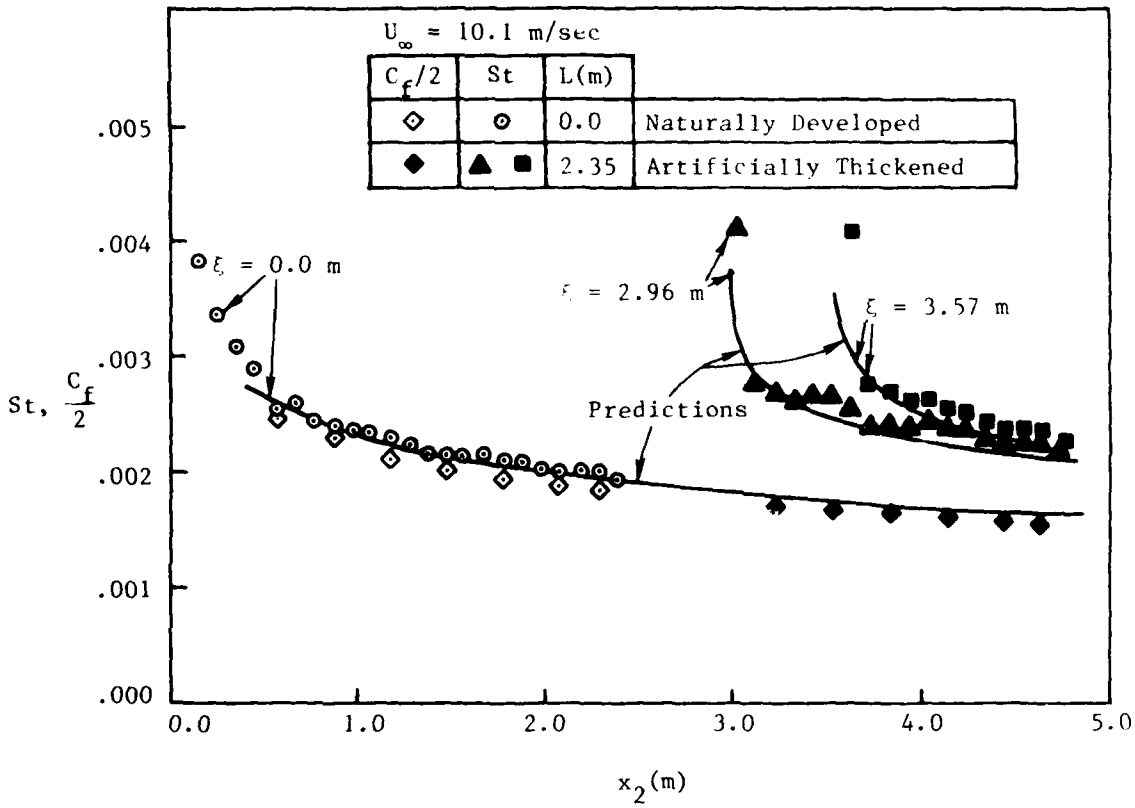

Fig. 3-17. Variation of Stanton numbers with downstream distance, U_∞ = 10.1 m/sec.

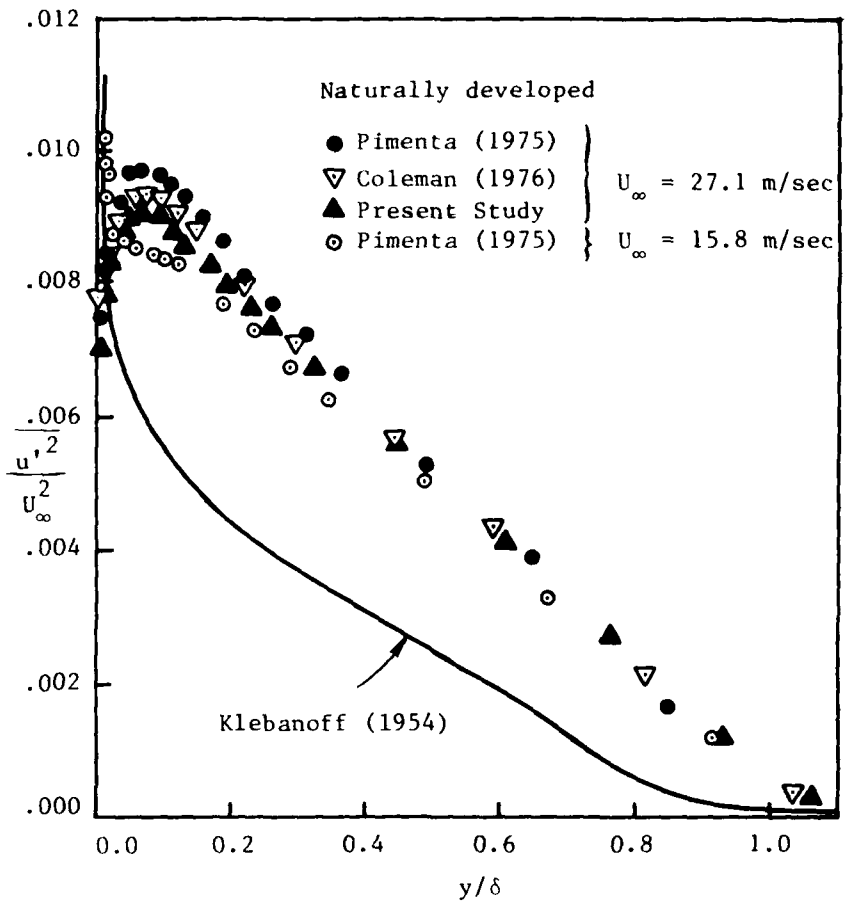

Fig. 3-18. Profiles of longitudinal component of turbulence intensity from Klebanoff (1954), Pimenta (1975), Coleman (1976), and the present study.

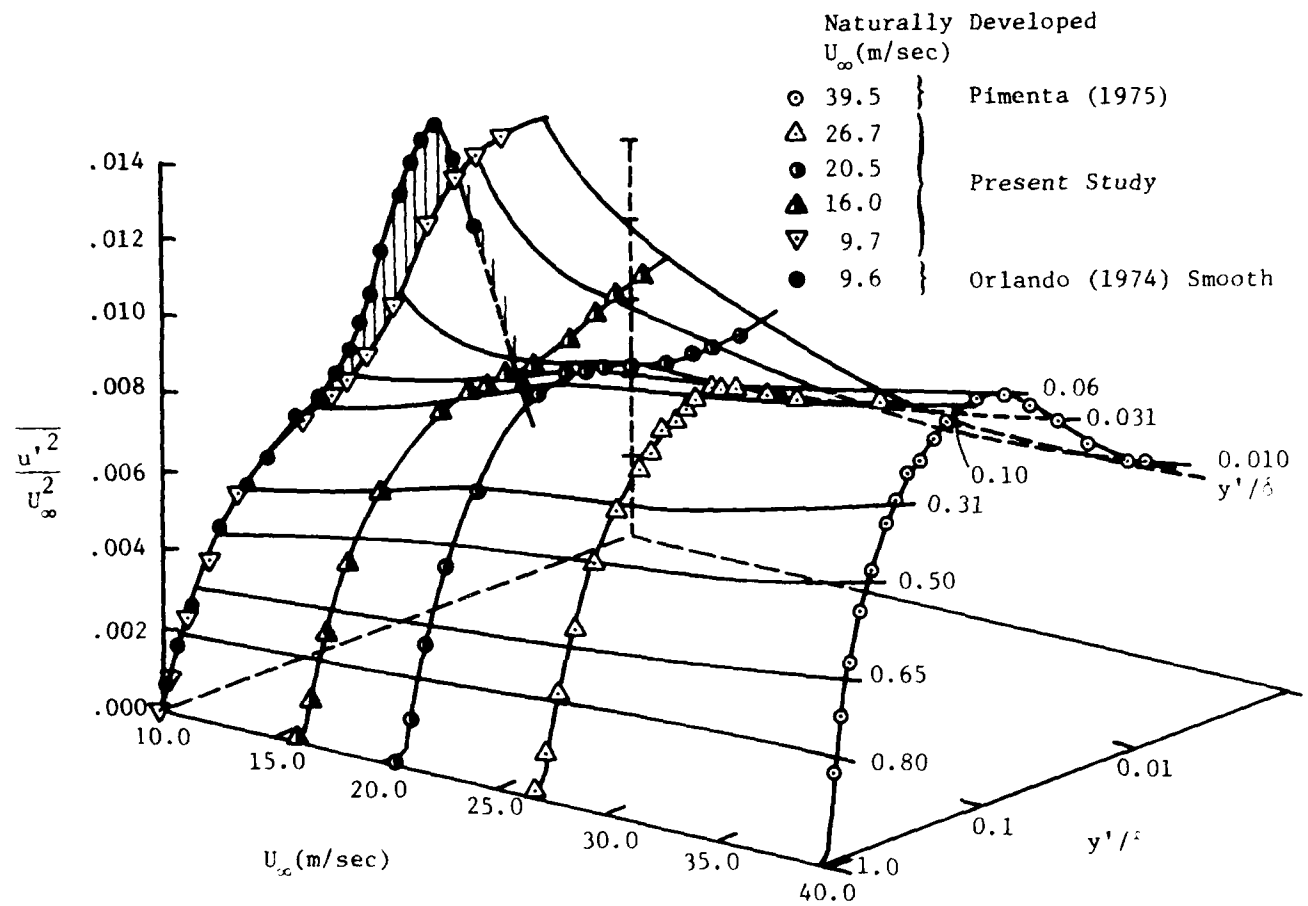

Fig. 3-19. Summary of profiles of longitudinal component of turbulence intensity, normalized using the freestream velocity, for transitionally rough and fully rough turbulent boundary layers.

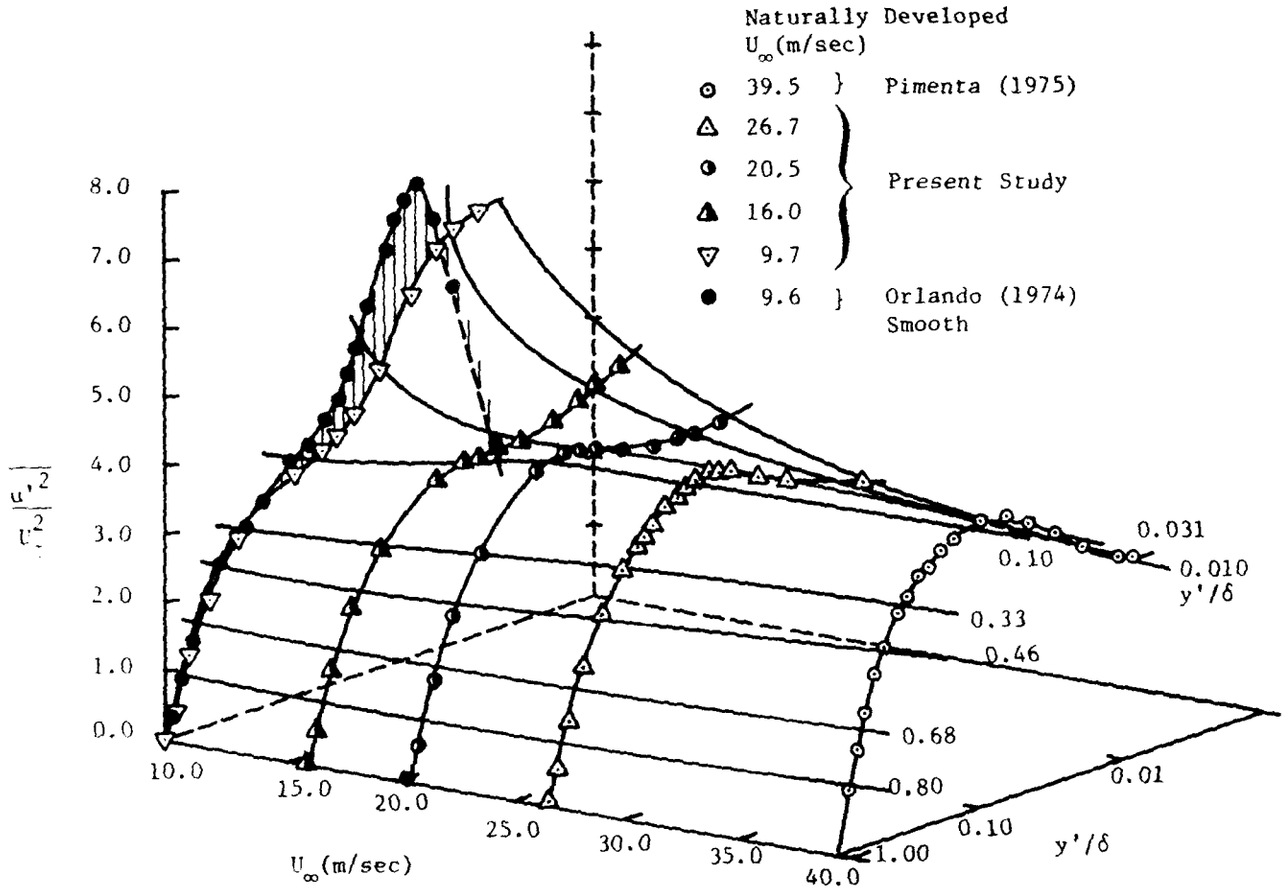

Fig. 3-20. Summary of profiles of longitudinal component of turbulence intensity, normalized using the friction velocity, for transitionally rough and fully rough turbulent boundary layers.

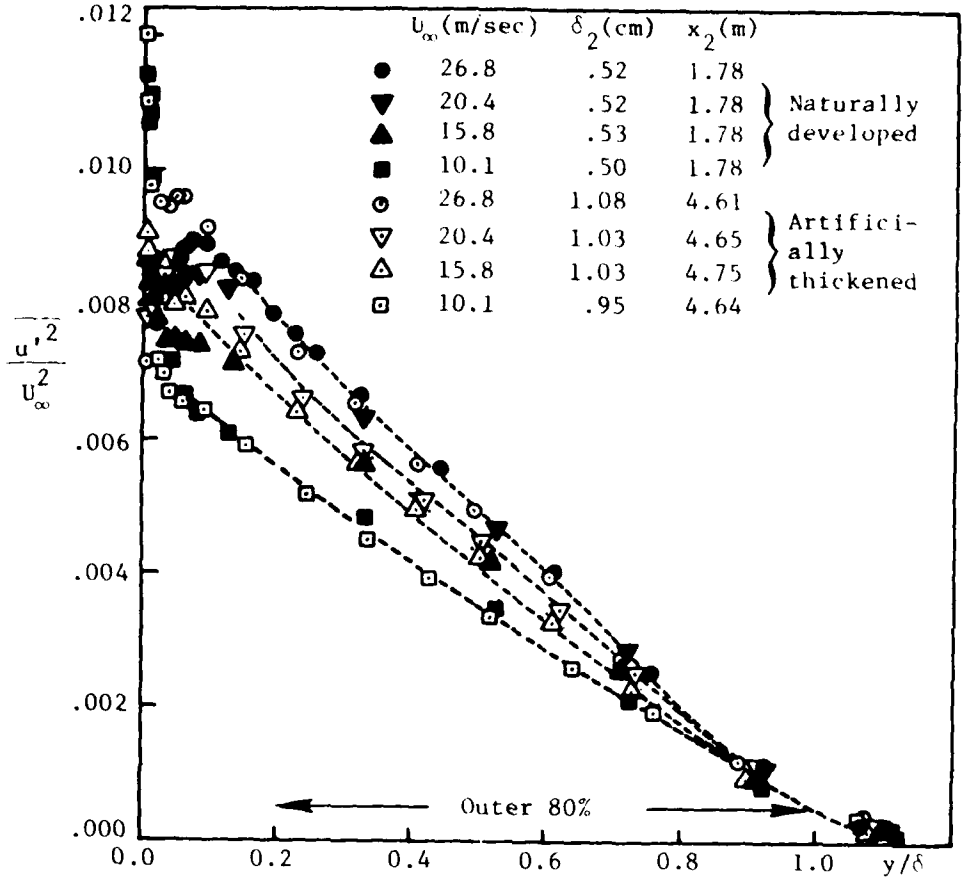

Fig. 3-21a. Profiles of longitudinal component of turbulence intensity, normalized using the freestream velocity, compared at different freestream velocities and at different downstream locations.

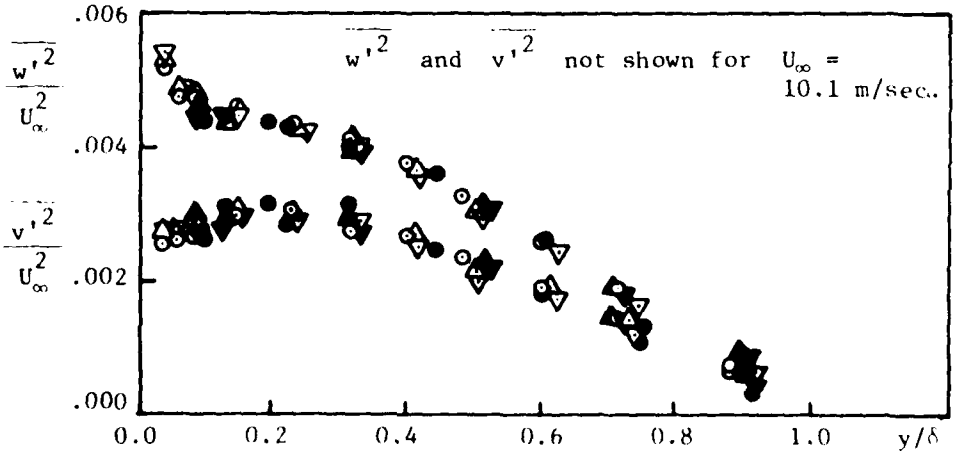

Fig. 3-21b. Profiles of normal and transverse components of turbulence intensity, normalized using the freestream velocity, compared at different freestream velocities and at different downstream locations.

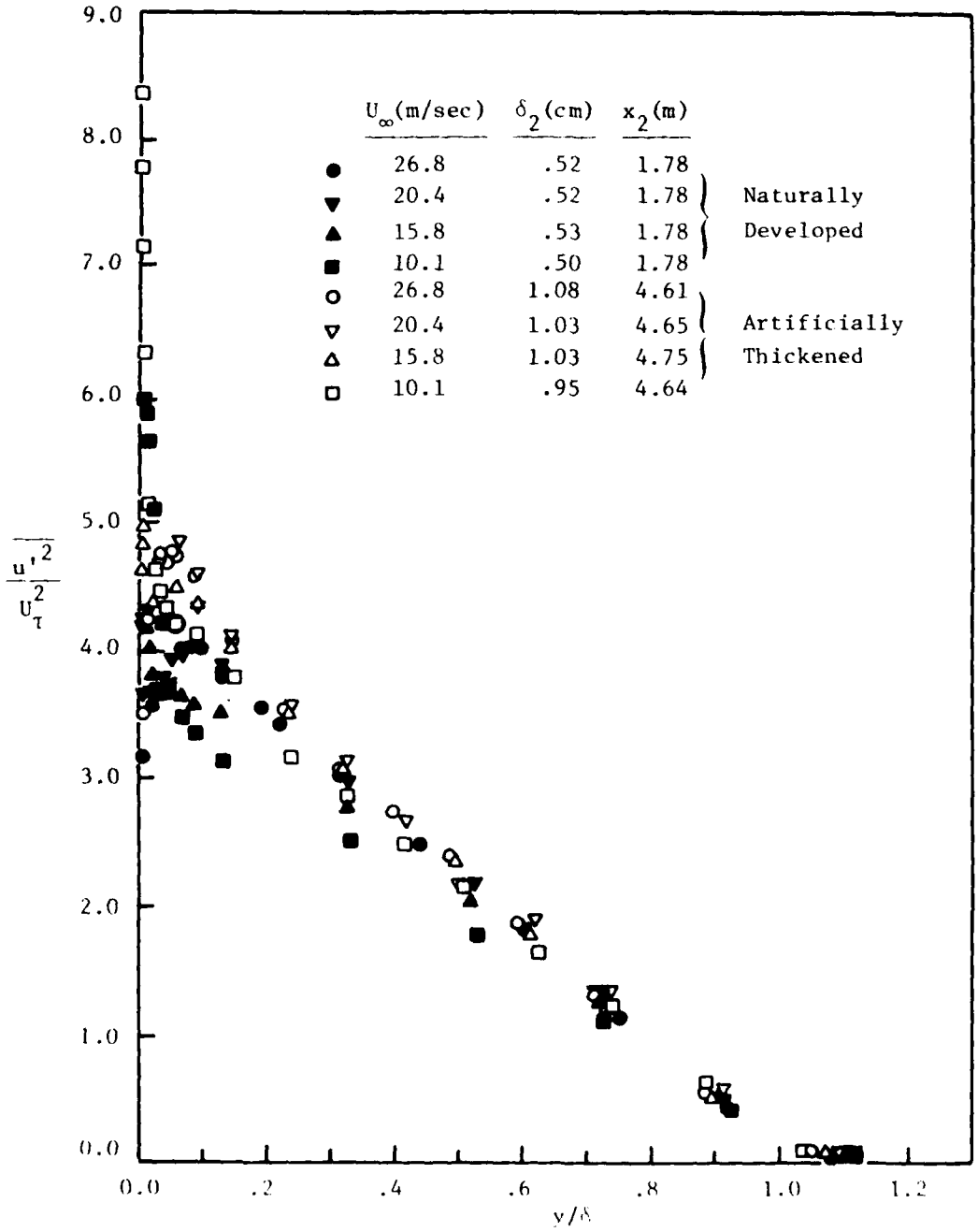

Fig. 3-22. Profiles of longitudinal component of turbulence intensity normalized using the friction velocity, compared at different freestream velocities and at different downstream locations.

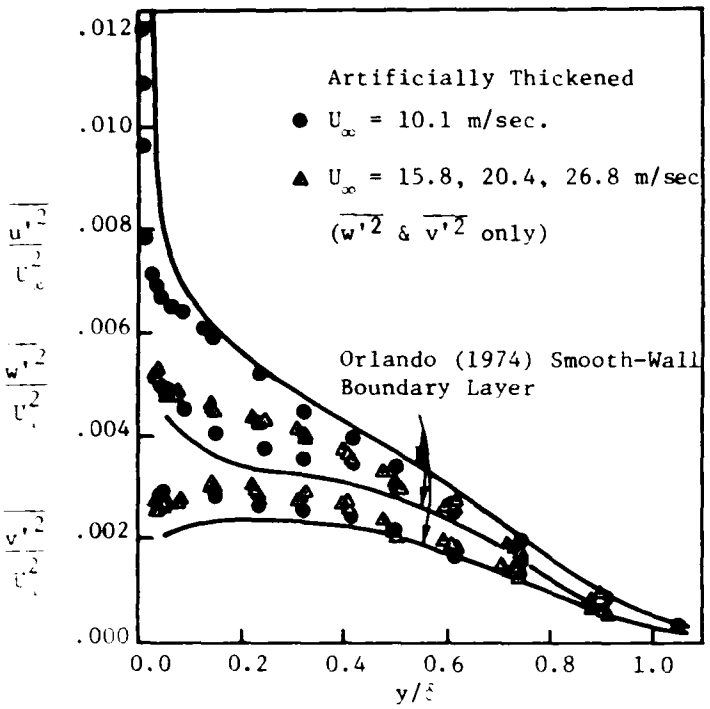

Fig. 3-23. Transitionally rough and smooth (Orlando (1974)) normal Reynolds stress tensor components, U_∞ = 10.1 m/sec.

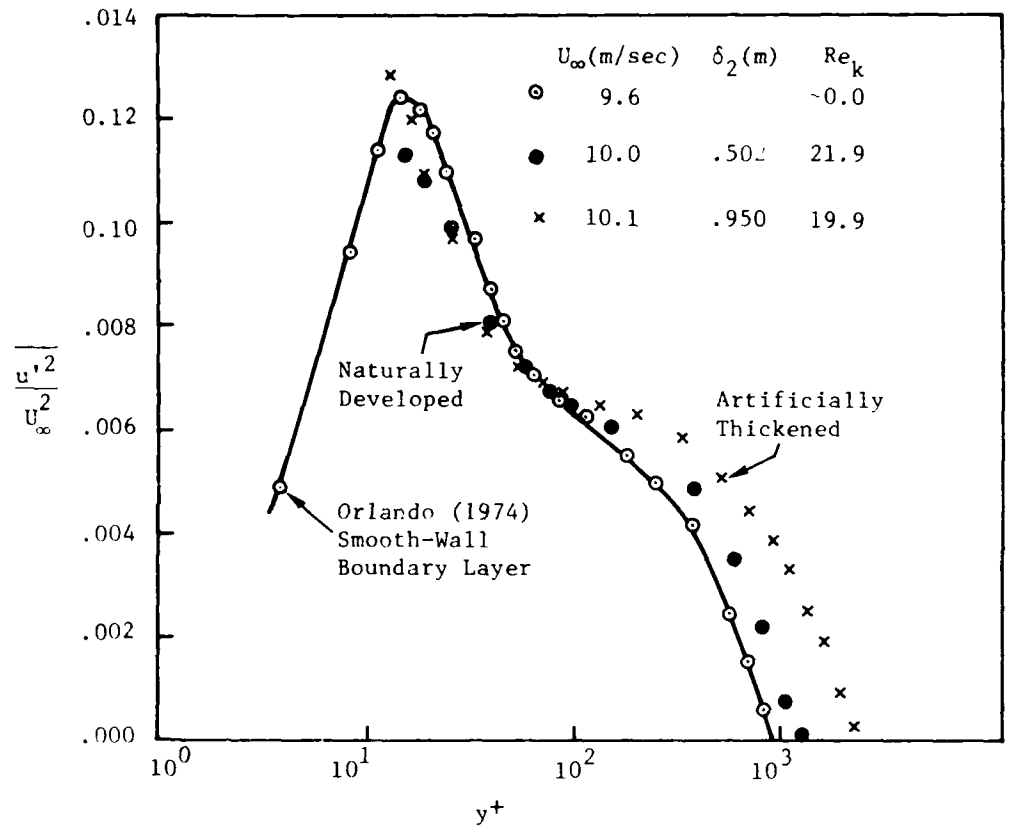

Fig. 3-24. Downstream development of transitionally rough profiles of longitudinal component of turbulence intensity, U_∞ = 10.1 m/sec.

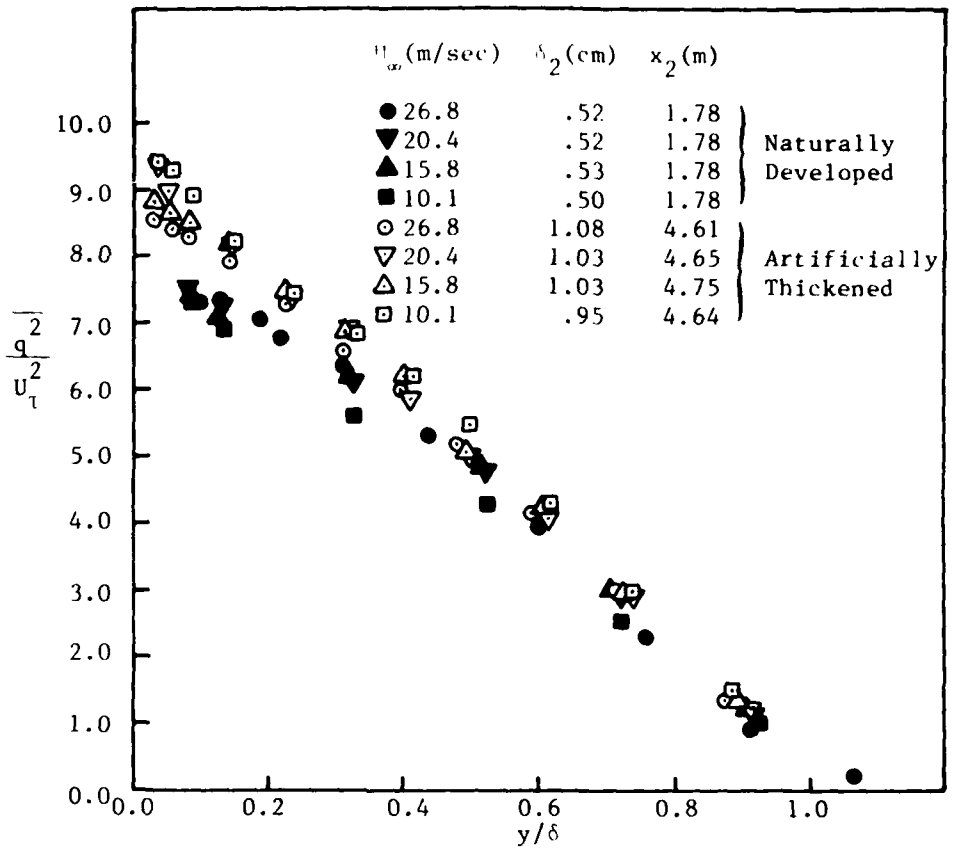

Fig. 3-25. Profiles of turbulence kinetic energy normalized using the friction velocity, compared at different freestream velocities and at different downstream locations.

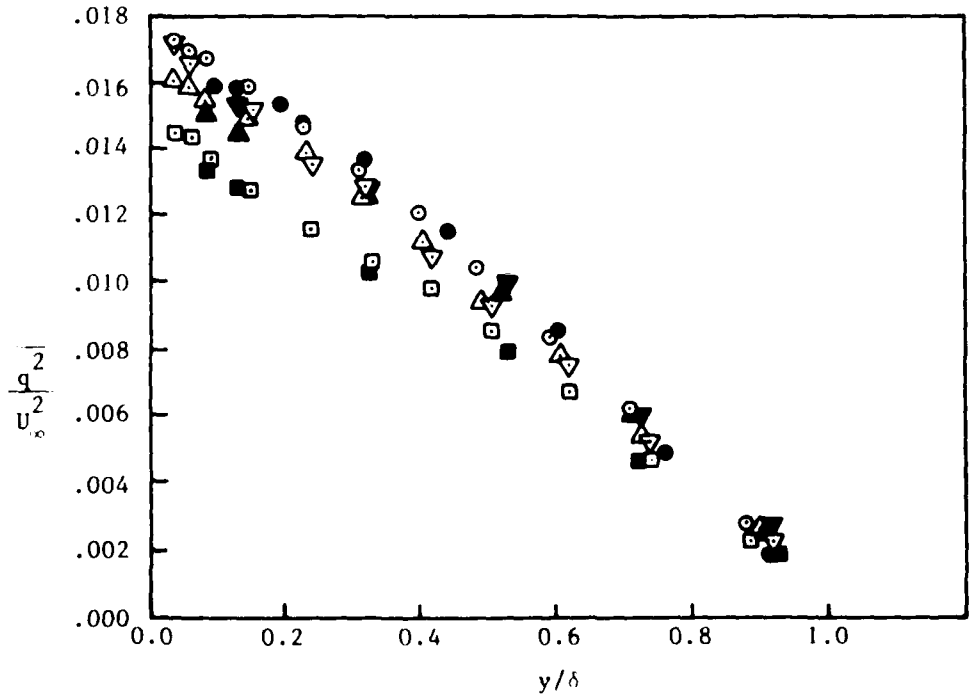

Fig. 3-26. Profiles of turbulence kinetic energy, normalized using the freestream velocity, compared at different freestream velocities and at different downstream locations.

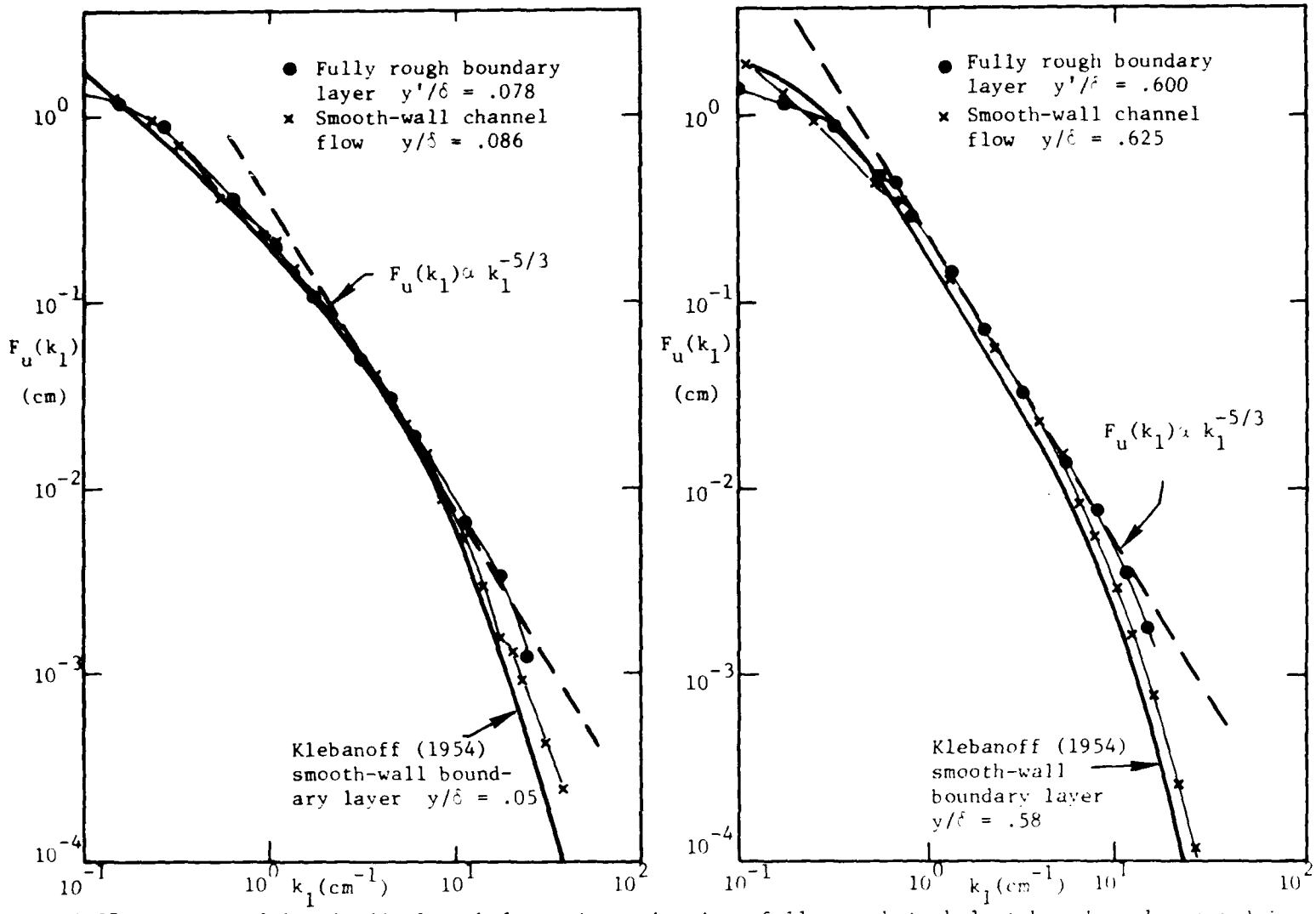

Fig. 3-27. Spectra of longitudinal turbulence intensity in a fully rough turbulent boundary layer and in smooth-wall boundary layer and channel flows.

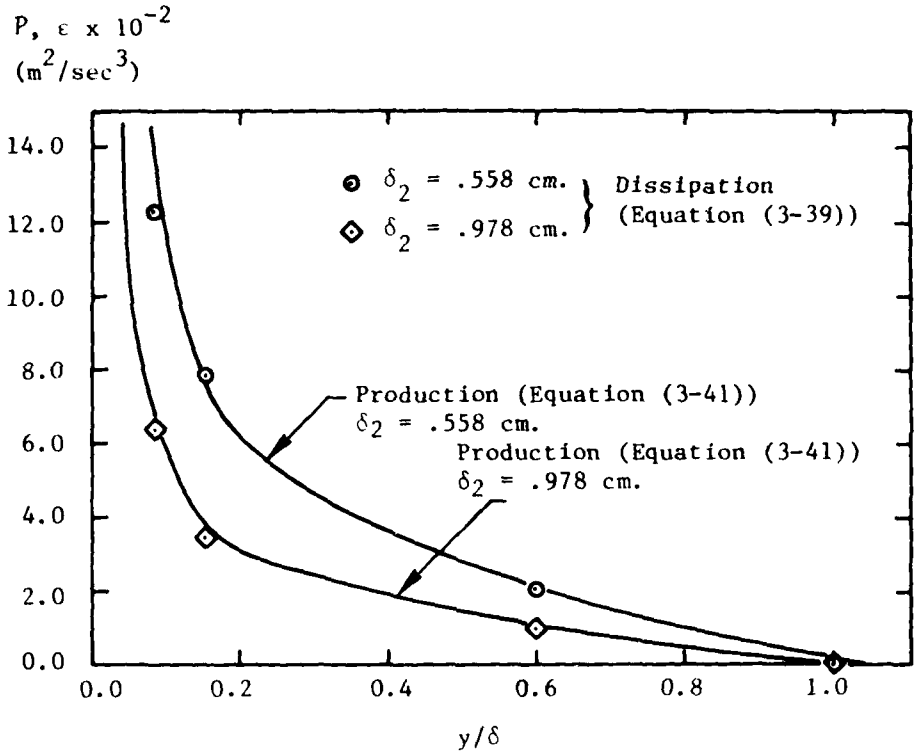

Fig. 3-28. Dissipation and production of turbulence kinetic energy in fully rough turbulent boundary layers.

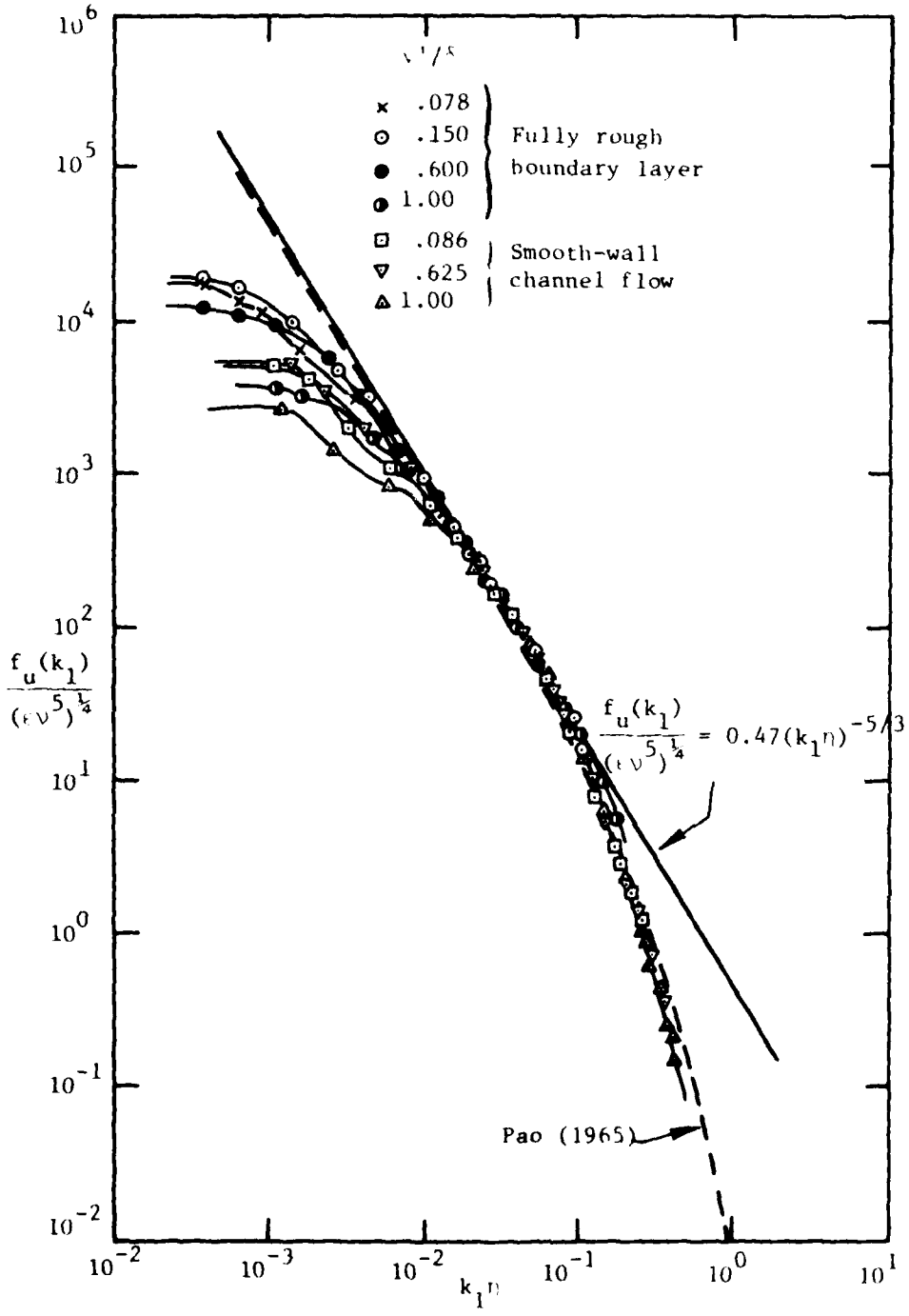

Fig. 3-29. Spectra of longitudinal turbulence intensity normalized using Kolmogorov length and velocity scales in a fully rough turbulent boundary layer and in a smooth-wall channel flow.

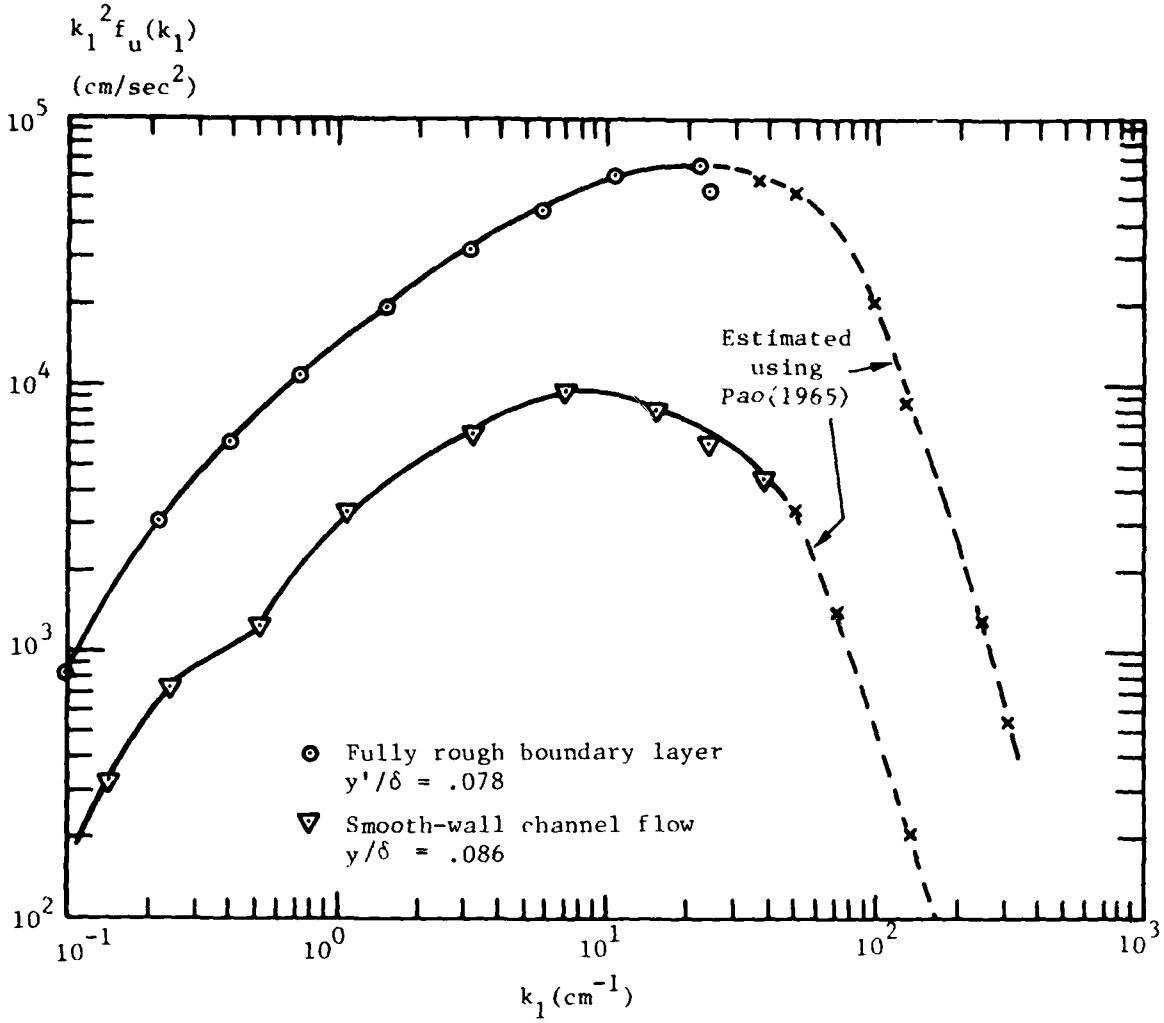

Fig. 3-30. Dissipation spectra in a fully rough turbulent boundary layer and a smooth-wall channel flow.

Chapter 4

ROUGH-WALL BOUNDARY LAYER PREDICTIONS

4.1 INTRODUCTION

The purpose of this chapter is to present a new prediction method to account for the effects of roughness on turbulent boundary layer flows. First, other work in this area and the prediction program which incorporates the new closure model are briefly described. Then transport property characteristics known from measurements away from the wall are summarized. This is followed by a discussion and derivations of the transport properties required for closure of the boundary layer equations to account for roughness effects near rough walls. Finally prediction results are discussed for thermal and hydrodynamic flow fields in pipes, and over flat plates with and without favorable pressure gradients, and with and without transpiration.

4.2 PRIOR WORK

In recent years there has been considerable interest in developing techniques which can be used to predict the effects of wall roughness on turbulent flows. Several methods are currently available, ranging from the integral techniques of Dvorak (1969, 1972) to differential boundary layer methods, such as that suggested by Antonia and Wood (1975). More elegant differential methods include the turbulent kinetic energy equation to calculate the downstream development of the mixing length, where an additional term may be included in the equation to account for increased turbulent production from the wakes of roughness elements. Engineering-oriented methods incorporate an empirically designed mixing-length closure for the momentum equation and a turbulent Prandtl number closure for the energy equation.

Many mixing-length schemes have appeared in the literature, and the roughness effects are usually included in fully rough flows by using a non-zero wall value of mixing length. The effects of roughness on heat transfer have generally been modeled by eliminating molecular transport in the

boundary layers except for a thin layer of film around the roughness elements. Comparison of the various mixing-length and turbulent Prandtl number schemes used to predict flows near rough walls can be made on the basis of how realistically they represent the actual physical processes of the flows, their simplicity, and the number of different physical situations and boundary conditions which can be handled using the particular method.

The only prediction scheme prior to the present work, which was developed to handle the effects of roughness with heat transfer and transpiration, has been that of Healzer, Moffat, and Kays (1974). Healzer's equations for the mixing length and turbulent Prandtl number produced agreement with his experimental measurement; however, there were two points deemed worthy of further study: (1) the mixing length offset used for fully rough conditions was dependent upon molecular viscosity, and (2) the heat transfer model did not account for conduction in the fluid adjacent to roughness elements. The mixing-length equations used in Healzer's work for fully rough flows was

$$\ell^+ = \sqrt{(\kappa y^+)^2 + (\Delta\ell_o^+)^2} \tag{4-1}$$

where

$$\Delta\ell_o^+ = \sqrt{\left(\frac{Re_k - 46}{39}\right)^2 - .05325} \tag{4-2}$$

Transitionally rough situations were handled by decreasing the value of the sublayer thickness from its smooth-wall value to zero, using a van Driest damping expression. Van Driest first suggested a mixing-length damping expression to simulate smooth-wall sublayer physics in a 1955 paper in which he also suggested that the conventional expression for mixing length also applied to fully rough flows. This mixing length is given as

$$\ell = \kappa y \tag{4-3}$$

However, if Eqn. (4-3) is incorporated into a prediction scheme using zero velocity at the wall, it can be used only to simulate behavior just at the onset of fully rough flow. Van Driest (1955) also proposed that a local

"vortex-generation factor" could be included within the damping expression to account for roughness effects in the transitionally rough regime. This scheme can be expressed as

$$\ell = \kappa y \left[1 - e^{-y^+/26} + e^{-60y^+/26Re_k} \right] \tag{4-4}$$

which becomes Eqn. (4-3) when $Re_k = 60.0$. Cebeci and Chang (1978) have recently developed a differential method with near-wall mixing-length modifications to account for the influence of roughness, related to methods suggested by Antonia and Wood (1975). According to Cebeci and Chang, the mixing-length equation in their method is based on earlier contributions by Rotta (1962). The mixing-length equation is valid for $4.535 < Re_k < 2000$ and can be expressed using

$$\ell = \kappa(y + \overline{\Delta\Gamma}) \left[1 - \exp\left(-(y + \overline{\Delta\Gamma})/A \right) \right] \tag{4-5}$$

where

$$(\Delta\Gamma)^+ = 0.90 \left[\sqrt{Re_k} - Re_k \exp\left(-\frac{Re_k}{5} \right) \right] \tag{4-6}$$

McDonald and Fish (1973) developed a turbulence model to predict transition between laminar and turbulent flow as influenced by surface roughness and freestream turbulence. The authors handled the influence of roughness on thermal and hydrodynamic boundary layers by adding a damping factor due to roughness, ΔD_k, to the damping factor used to account for the presence of the viscous sublayer, ΔD_s. The mixing length for this technique is

$$\ell = \kappa y(\Delta D_s + \Delta D_k) \tag{4-7}$$

with

$$\Delta D_k = \left(1.0 + \frac{k^+}{30y^+} \right) \exp\left(\frac{-2.3y^+}{k^+} \right) \tag{4-8}$$

Adams and Hodge (1977) used an integral form of the turbulent kinetic energy equation with a model based on the approach of Finson (1975) to simulate rough-wall behavior. A sink term was added to the streamwise momentum equation to

account for the increased form drag from roughness elements, in addition to a term added to the turbulence kinetic energy equation to represent the generation of turbulence which occurs in the wakes behind roughness elements. The method thus avoided representing the form drag on roughness elements by a non-zero mixing length at the wall. Schetz and Nerney (1977) used experimental data to extend the van Driest model and Reichardt model to predict the hydrodynamic behavior of flows over rough surfaces with and without transpiration. The investigators were most successful using Reichardt's equations. They reproduced velocity profiles and the Reichardt sublayer parameter as a function of V_o^+ using their prediction scheme. Hatton and Walklate (1976) suggest a mixing-length model, expressed as

$$\frac{\ell^+}{R_o^+} = \frac{\ell_o^+}{R_o^+} + \frac{\kappa y^+}{R_o^+}\left[1 - \exp\left(-\frac{y^+}{A^+}\right)\right] - B'\left(\frac{y^+}{R_o^+}\right)^2 \qquad (4\text{-}9)$$

where B' is a constant and ℓ_o^+ is given by

$$\ell_o^+ = 0.154(k^+)^{0.72} \qquad (4\text{-}10)$$

A constant turbulent Prandtl number of 0.90 was used in the outer flow regions of the pipe along with a wall-temperature step to account for conduction in the fluid adjacent to the roughness elements. The temperature step was expressed as the inverse of a "cavity Stanton number," where Dipprey and Sabersky's (1963) correlation was used with a Stanton number based on bulk velocity. The method was demonstrated to be useful in the fully developed and entrance regions of pipes with continuous roughness and either heat flux or constant temperature boundary conditions. Wassel and Mills (1979) have developed a method for calculation of variable-property turbulent friction and heat transfer in pipes. In their method, a mixing-length model is used in the turbulent core, whereas a roughness element drag coefficient and a sublayer Stanton number are used to represent near-wall behavior. Both sandgrain roughness and transverse repeated rib roughness are predicted, where an equation for St_k having the same power-law dependence as the Dipprey and Sabersky (1963) correlation is used for the sandgrain roughness.

4.3 PREDICTION PROGRAM

The present rough-wall boundary layer prediction method is incorporated into a program for numerical computation of two-dimensional internal/external boundary layer flows. The computer code, which is called STAN5, is based on the Spalding-Patankar code and is discussed in detail by Crawford and Kays (1975). In the program, the time-averaged continuity, momentum, and energy boundary layer equations for a flat plate with no body forces, viscous dissipation, or sources are expressed as

$$\frac{\partial}{\partial x}(\rho U) + \frac{\partial}{\partial y}(\rho V) = 0 \tag{4-11}$$

$$\rho U \frac{\partial U}{\partial x} + \rho V \frac{\partial U}{\partial y} = -g_c \frac{dP}{dx} + \frac{\partial}{\partial y}\left[\mu \frac{\partial U}{\partial y} - \rho \overline{u'v'}\right] \tag{4-12}$$

and

$$\rho U \frac{\partial T}{\partial x} + \rho V \frac{\partial T}{\partial y} = \frac{\partial}{\partial y}\left[k \frac{\partial T}{\partial y} - \rho \overline{t'v'}\right] \tag{4-13}$$

respectively. The turbulent shear stres, $-\overline{u'v'}$, is modeled using an eddy diffusivity for momentum, so that the total shear stress is

$$\frac{g_c \tau}{\rho} = (\nu + \varepsilon_M) \frac{\partial U}{\partial y} \tag{4-14}$$

where

$$-\overline{u'v'} = \varepsilon_M \frac{\partial U}{\partial y} \tag{4-15}$$

The eddy diffusivity for momentum, ε_M, is then replaced by a function of the mixing length, $\ell^2 \partial U/\partial y$, where, for smooth walls, ℓ is given by the classic van Driest (1955) expression

$$\ell^+ = \kappa y^+ (1 - e^{-y^+/A^+}) \tag{4-16}$$

The total heat flux normal to the surface is given by

$$\frac{\dot{q}''}{\rho c_p} = -(\varepsilon_H + \alpha) \frac{\partial T}{\partial y} \tag{4-17}$$

where the turbulent component is included as

$$-\overline{v't'} = \varepsilon_H \frac{\partial T}{\partial y} \tag{4-18}$$

ε_M/Pr_t is then substituted for ε_H and closure of the energy equation is accomplished by specifying the turbulent Prandtl number. The turbulent Prandtl number distribution recommended by Crawford and Kays (1975) for smooth walls is given by

$$Pr_t = \left[\frac{\alpha^2}{2} + \alpha c\ Pe_t - (cPe_t)^2 \left(1.0 - \exp\left[\frac{-\alpha}{cPe_t}\right]\right)\right]^{-1} \tag{4-19}$$

in which $Pe_t = (\varepsilon_M/\nu)Pr$, $c = 0.20$, $\alpha = \sqrt{1/PRT}$, and $PRT = 0.860$.

4.4 ROUGH-WALL TRANSPORT PROPERTIES -- OUTER REGIONS OF THE BOUNDARY LAYER

The distributions of mixing length and turbulent Prandtl number for the outer 94-98% of rough-wall turbulent boundary layers have been determined from measurements of mean velocity, mean temperature, turbulent shear stress, and turbulent heat flux. The inner 2-6% of the flows has not been studied because of restrictions due to size of the probes used. Measurements for $y > 0.330$ cm indicate that the mixing length is well represented using

$$\ell = \kappa y \tag{4-20}$$

for $y/\delta < 0.10$ in fully rough flows. Pimenta (1975), Coleman (1976), and the present study show Eqn. (4-20) to be valid in zero-pressure-gradient flows with and without transpiration, and in accelerated flows with and without transpiration. For the outer 90% of rough-wall boundary layers, the mixing length can be approximated using

$$\ell = \lambda\delta \tag{4-21}$$

where $\lambda = 0.080$.

Turbulent Prandtl numbers have been determined for $y^+ > 60\text{-}100$ for the same types of experimental conditions for which (4-20) is valid.

Rough-wall measurements show that Pr_t is reasonably approximated using Eqn. (4-19), when the smooth-wall eddy diffusivity for momentum is replaced by the appropriate rough-wall value in (4-19).

4.5 ROUGH-WALL TRANSPORT PROPERTIES -- INNER REGIONS OF THE BOUNDARY LAYER

4.5.1 Hydrodynamic Transport

Mixing-length distributions for the very near wall regions of fully rough turbulent boundary layers are derived in this section. Eqn. (4-14) and certain boundary layer assumptions are first used to give general mixing-length equations for fully rough conditions.

These general equations are determined by first assuming that Couette flow exists near the wall and that no transpiration or pressure gradients exist. Then U_τ can be substituted into (4-14) to give

$$U_\tau^2 = (\nu + \varepsilon_M) \frac{\partial U}{\partial y} \tag{4-22}$$

which is valid for the inner 10% of the boundary layer, except very close to roughness elements, where the flow is three-dimensional. In these three-dimensional regions, we shall represent transport properties using (4-22) for a two-dimensional flow field. Next, the viscosity contribution in (4-22) is neglected, an approach justified by fully rough hydrodynamic data which show the same behavior regardless of the molecular properties. If the eddy diffusivity for momentum in (4-22) is then replaced with the appropriate mixing-length function and this result is then rearranged, we have

$$U_\tau = \ell \frac{\partial U}{\partial y} \tag{4-23}$$

and the desired mixing-length equations can be determined.

Two mixing-length schemes which have been developed using Eqn. (4-23) to reproduce observed physics in fully rough flows are the mixing-length offset method and the slip-velocity method. In the mixing-length offset method, a non-zero mixing length and a zero velocity are used at $y = 0$. The slip velocity method uses a zero mixing length at $y = 0$, and a non-zero slip velocity at $y = \Delta y$. For both methods, y is measured from the

virtual origin of the velocity profile, which is located between the crests and the troughs of the roughness elements, as discussed in Chapter 3. $y = \Delta y$ then locates the crests of the roughness elements.

4.5.1a Mixing-length offset scheme. The mixing-length offset equation is now derived. This is done by first considering that at the onset of fully rough flow, the sublayer thickness is near zero, and, using the van Driest equation (Eqn. (4-16)), the mixing length is given by

$$\ell = \kappa y \tag{4-24}$$

As the roughness Reynolds number increases, the mixing length is increased to a non-zero value at the wall, and Eqn. (4-24) becomes

$$\ell = \kappa(y + \delta y_o) \tag{4-25}$$

where $\delta y_o = 0$ at $Re_k = Re_k'$. Thus, Re_k' is defined as the value of the roughness Reynolds number where Eqn. (4-25) becomes Eqn. (4-24). Substituting Eqn. (4-25) into Eqn. (4-23) and rearranging then produces

$$\frac{1}{\kappa}\int_o^y \frac{dy}{(y + \delta y_o)} = \int_o^{U^+} dU^+ \tag{4-26}$$

which, after integration, gives the fully rough velocity profile, expressed as

$$U^+ = \frac{1}{\kappa}\,\ell n(y + \delta y_o) - \frac{1}{\kappa}\,\ell n(\delta y_o) \tag{4-27}$$

Then, neglecting the δy_o contribution to $\ell n(y + \delta y_o)$, Eqn. (4-27) becomes

$$U^+ = \frac{1}{\kappa}\,\ell n(y) - \frac{1}{\kappa}\,\ell n(\delta y_o) \tag{4-28}$$

which can be set equal to the fully rough law of the wall

$$U^+ = \frac{1}{\kappa}\,\ell n\left(\frac{y}{k_s}\right) + 8.5 \tag{4-29}$$

in order to determine the functional dependence of the mixing-length offset on the equivalent sandgrain roughness. Thus, we have

$$\delta y_o = .0307\ k_s \tag{4-30}$$

and in wall coordinates,

$$(\delta y_o)^+ = .0307(Re_k) \tag{4-31}$$

Since $(\delta y_o)^+ = 0$ at $Re_k = Re_k'$, Eqn. (4-31) becomes

$$(\delta y_o)^+ = (.0307)(Re_k - Re_k') \tag{4-32}$$

and Re_k' should be approximately equal to the roughness Reynolds number at the onset of fully rough flow, Re_k^*. In Section 3.1, Re_k^* was defined as the value of Re_k where $B = 8.5$ and $A_R^+ = 0$. By rearranging Eqn. (4-32), one can then obtain

$$(\delta y_o) = .0307\ k_s\left(1 - \frac{U_\tau'}{U_\tau}\right) \tag{4-33}$$

where U_τ' is defined by Eqn. (4-34),

$$Re_k' = \frac{U_\tau' k_s}{\nu} \tag{4-34}$$

Substituting Eqn. (4-33) into Eqn. (4-25) then produces an equation for the mixing length for fully rough flows, which is given by

$$\ell = \kappa\left[y + .0307\ k_s\left(1 - \frac{U_\tau'}{U_\tau}\right)\right] \tag{4-35}$$

or, in wall coordinates,

$$\ell^+ = \kappa\left[y^+ + .0307(Re_k - Re_k')\right] \tag{4-36}$$

Equations (4-35) and (4-36) seem rational if one considers that form drag on roughness elements is significant for fully rough conditions and

can be represented by a non-zero eddy diffusivity at $y = 0$, which is between the crests and troughs of the roughness elements. In addition, Eqn. (4-35) contains no viscosity dependence and is therefore consistent with experimental observations. Also, as U_τ becomes large, the mixing length becomes dependent on the equivalent sandgrain roughness only, since U_τ' is a constant for a given roughness geometry.

It is also evident from (4-35) that very small values of $\kappa\delta y_o$ are required to simulate the increased mixing due to roughness. Thus, for $y > \Delta y$, or for regions of the boundary layer above the crests of the roughness elements, Eqn. (4-35) approaches $\ell = \kappa y$, and therefore is in excellent agreement with the measurements of Pimenta (1975), Coleman (1976), and the present author for fully rough conditions.

It is also interesting to compare $(\delta y_o)^+$ given by Eqn. (4-31) to some of the results of Rotta's (1962) analysis of rough-wall mean velocity profiles. Rotta explains that rough-wall mean velocity profiles can be represented using the smooth law of the wall (Eqn. (2-12)) "when the plane of reference is shifted beneath the surface by an amount Δy_r." Using this approach, rough-wall profiles are given by

$$U^+ = f\left(\frac{(y+\Delta y_r)U_\tau}{\nu}\right) - f\left(\frac{\Delta y_r U_\tau}{\nu}\right) \tag{4-37}$$

which in the log region becomes

$$U^+ = \frac{1}{\kappa}\,\ell n(y^+) + C - f\left(\frac{\Delta y_r U_\tau}{\nu}\right) \tag{4-38}$$

when $\ell n(y+\Delta y_r) \sim \ell n(y)$. The function $f(\Delta y_r U_\tau/\nu)$ in (4-38) is then equivalent to $\Delta U/U_\tau$, the rough-wall log region shift given by Eqn. (3-5). From (4-37) and (4-38), $f(\Delta y_r U_\tau/\nu)$ is also given as

$$f\left(\frac{\Delta y_r U_\tau}{\nu}\right) = \frac{1}{\kappa}\,\ell n(\Delta y_r^+) + C \tag{4-39}$$

Equating the right-hand side of (4-39) to $\Delta U/U_\tau$ for fully rough flows given by (3-5) produces

$$(\Delta y_r)^+ = (Re_k)\,\exp(-\kappa B) \tag{4-40}$$

and Rotta's Δy_r is then equivalent to the δy_o given by Eqn. (4-30).

$$\Delta y_r = \delta y_o \tag{4-41}$$

It is important to realize that Δy_r and δy_o are not the same as Δy, the experimentally determined value of the y shift described in Section 2.3.3c (see Eqn. (2-20)). This experimental Δy is required to shift fully rough U^+ versus y/k_s data to obtain linear behavior on semilog coordinates for data points near the wall.

4.5.1b Slip velocity scheme. The equations for the slip-velocity mixing length method are now determined. The slip-velocity prediction scheme uses a non-zero velocity near the wall, in conjunction with a mixing length to simulate fully rough boundary layer behavior. The mixing length for this method is given by Eqn. (4-24), and the slip velocity at $y = \Delta y$ is

$$U_s^+ = \frac{1}{\kappa} \ln\left(\frac{\Delta y}{k_s}\right) + 8.5 \tag{4-42}$$

Equation (4-42) is obtained simply by setting $y = \Delta y$ in (4-29), and thus we have assumed that the fully rough law of the wall extends from the outer regions of the boundary layer to the crests of the roughness elements. The slip-velocity concept can be represented using an equation given by

$$\frac{1}{\kappa} \int_{\Delta y}^{y} \frac{dy}{y} = \int_{U_s^+}^{U^+} dU^+ \tag{4-43}$$

which can be compared to the mixing-length offset method represented by Eqn. (4-26). In (4-26), the value of the wall mixing length, $\kappa(\delta y_o)$ is chosen to produce the fully rough law of the wall, and, in (4-43), the value of the near-wall velocity, U_s^+, is chosen to produce the fully rough law of the wall.

4.5.2 Thermal Transport

Molecular and turbulent transport properties for the near-wall regions of rough-wall turbulent boundary layers are now discussed. The presentation begins with a general discussion of the behavior of flows over smooth and rough walls. Then the details of fully rough transport behavior are presented in a discussion divided into sections on the conduction sublayer thickness, the conduction sublayer Stanton number, and the thermal fully rough law of the wall.

4.5.2a Thermal transport in smooth, transitionally rough, and fully rough boundary layers. For smooth and rough walls, the heat flux in turbulent boundary layers normal to the surface is represented by Eqn. (4-17). Using the assumptions made in the development of Eqn. (4-23) for momentum, Eqn. (4-17) can be expressed as

$$-\frac{dT}{T_\tau} = \frac{dy^+}{\left(\frac{\varepsilon_H}{\nu} + \frac{\alpha}{\nu}\right)} \tag{4-44}$$

For smooth walls, (4-44) can be rearranged into the form

$$T^+ = \int_o^{A^+_{th}} Pr\ dy^+ + \int_{A^+_{th}}^{y^+} \frac{dy^+}{(\varepsilon_H/\nu)} \tag{4-45}$$

which becomes the thermal law of the wall for smooth walls,

$$T^+ = 13.2\ Pr + \frac{Pr_t}{\kappa}\ \ell n\left(\frac{y^+}{13.2}\right) \tag{4-46}$$

after integration, with appropriate substitutions made for ε_H and A^+_{th} = 13.2.

When heat transfer is present in turbulent boundary layers which are fully rough, a conduction sublayer is present which can be described as a thin film of fluid surrounding the roughness elements, where heat transfer is principally by molecular conduction. The conduction sublayer would have a microscopic thickness on the high-pressure sides of roughness elements and become slightly thicker on the downstream sides and in cracks between roughness. Outside of the conduction sublayer, turbulent transport becomes

significant due to turbulent mixing and molecular transport is negligible. If heat is transferred from the wall to the freestream, the temperature variation in a fully rough turbulent boundary layer then consists of an abrupt drop across the conduction sublayer, followed by a more gradual temperature drop across the log and wake regions of the boundary layer, where turbulent mixing is the dominant transport mechanism. If we then assume that molecular effects account for all transport within the conduction sublayer, and no transport outside it, Eqn. (4-44) can be rearranged to become

$$T^+ = \int_o^{\delta_k^+} \frac{dy^+}{\alpha/\nu} + \int_{\delta_k^+}^{y^+} \frac{dy^+}{\varepsilon_H/\nu} \tag{4-47}$$

where δ_k^+ represents the thickness of the conduction sublayer in wall coordinates.

For transitionally rough situations, Eqn. (4-44) becomes

$$T^+ = \int_o^{\delta_k^+} Pr\ dy^+ + \int_{\delta_k^+}^{A_{th}^+} Pr\ dy^+ + \int_{A_{th}^+}^{y^+} \frac{dy^+}{\varepsilon_H/\nu} \tag{4-48}$$

where δ_k^+ is greater than zero and less than the value which would exist for fully rough flows, and A_{th}^+ is greater than δ_k^+ and less than the value which would exist for smooth walls. The first integral in Eqn. (4-48) represents the temperature step at the wall caused by the presence of the conduction sublayer, and the second integral represents the regions around and between roughness elements, where molecular effects are beginning to influence thermal transport behavior slightly away from the wall.

4.5.2b. Fully rough temperature profile. The fully rough temperature profile given by Eqn. (4-47) can be rearranged such that T^+ is a function of the conduction sublayer temperature drop and the hydrodynamic fully rough law of the wall. This is accomplished by first substituting ε_M/Pr_t for ε_H. Then the eddy diffusivity for momentum is replaced by an expression determined by substituting Eqns. (4-25) and (4-27) into $\varepsilon_M = \ell^2 \frac{\partial U}{\partial y}$ so that the second integral of (4-47) becomes

$$\int_{\delta_k^+}^{y^+} \frac{dy^+}{\varepsilon_H/\nu} = \frac{Pr_t}{\kappa} \int_{\delta_k}^{y} \frac{dy}{(y + \delta y_o)} \tag{4-49}$$

Integrating (4-49) then produces

$$\frac{Pr_t}{\kappa}\int_{\delta_k}^{y}\frac{dy}{(y+\delta y_o)} = \frac{Pr_t}{\kappa}\left[\ell n(y+\delta y_o) - \ell n(\delta_k+\delta y_o)\right] \qquad (4\text{-}50)$$

Assuming that δ_k is small compared to δy_o, (4-50) is equivalent to the fully rough velocity profile (Eqn. (4-29)) multiplied by Pr_t. Substituting this result into Eqn. (4-47) then gives the equation

$$T^+ = \int_o^{\delta_k^+}\frac{dy^+}{\alpha/\nu} + Pr_t\left[\frac{1}{\kappa}\,\ell n\,\frac{y}{k_s} + 8.5\right] \qquad (4\text{-}51)$$

or, alternatively,

$$T^+ = (\delta t_o)^+ + Pr_t(U^+) \qquad (4\text{-}52)$$

where

$$(\delta t_o)^+ = \int_o^{\delta_k^+}\frac{dy^+}{\alpha/\nu} \qquad (4\text{-}53)$$

Equations (4-51) and (4-52) are then the results we are seeking, where Eqn. (4-53) represents the non-dimensional temperature drop across the conduction sublayer, $(T_w-T_k)/(\dot{q}_w''/\rho C_p U_\tau)$.

4.5.2c. Fully rough conduction sublayer thickness. An equation for the average thickness of the conduction sublayer can now be produced by integrating the right-hand side of (4-53), assuming a constant molecular Prandtl number

$$(\delta_k)^+ = \frac{1}{Pr}\,(\delta t_o)^+ \qquad (4\text{-}54)$$

The conduction sublayer thickness represented by (4-54) is then an effective value which would exist over the area projected by the plane surface which contains the roughness elements. Actually, the average conduction sublayer thickness is spread over the roughness elements and is determined by multiplying $(\delta_k)^+$ by $\bar{\phi}$, where $\bar{\phi}$ is the ratio of the protected area of the

plane surface containing the roughness to the actual rough-wall surface area. Thus, we have

$$(\delta_k)^+_{actual} = \bar{\phi}\, \delta_k^+ \tag{4-55}$$

with $\bar{\phi} = 2.0/\pi$ for the densely packed uniform-spheres roughness of the present study.

4.5.2d. Fully rough conduction sublayer Stanton number. The fully rough conduction sublayer Stanton number, St_k, can be expressed in terms of the temperature drop across the conduction sublayer (Eqn. (4-53)) using

$$St_k = \frac{1}{(\delta t_o)^+} \tag{4-56}$$

For close-packed granular-type roughness in pipes, Dipprey and Sabersky (1963) suggest

$$St_k = \frac{1}{k_f} (k^+)^{-0.20} (Pr)^{-0.44} \tag{4-57}$$

where k_f is a constant for a given type of roughness geometry. Owen and Thomson (1963), Yaglom and Kader (1974), and Jayatilleke (1969) have also suggested forms for the functional dependence of St_k on non-dimensional roughness height and molecular properties. Of these, Owen and Thomson's (1963) result is particularly interesting, since it contains power-law dependence on Reynolds number and Prandtl number similar to that for laminar boundary layers ($St_k \propto Re_k^{-0.45}\, Pr^{-0.80}$). Substituting Eqn. (4-57) into Eqn. (4-56) and replacing k^+ with Re_k then produces

$$(\delta t_o)^+ = k_f'(Re_k)^{0.20} (Pr)^{0.44} \tag{4-58}$$

where a new geometry dependent constant, k_f', is used to replace k_f.

On Fig. 4-1, Eqn. (4-58) is plotted in $(\delta t_o)^+$ versus Re_k coordinates for $k_f' = 1.0$. Also shown are values of $(\delta t_o)^+$ determined using Pimenta's (1975) temperature profile data in Eqn. (4-52). Pimenta's

data are nearly constant as Re_k varies, and the low power-law dependence on Re_k given by (4-58) is then a more realistic representation of Stanford rough-wall data than other correlations, such as that suggested by Owen and Thompson (1963).

4.5.2e. Thermal, fully rough law of the wall. The thermal, fully rough law of the wall can now be determined using Eqn. (4-58) and the value of k_f' which fits Pimenta's data. Substituting (4-58) into (4-53) and then substituting this result in (4-51), the thermal, fully rough law of the wall is obtained

$$T^+ = k_f'(Re_k)^{0.20} (Pr)^{0.44} + Pr_t \left[\frac{1}{\kappa} \ln\left(\frac{y}{k_s}\right) + 8.5\right] \qquad (4\text{-}59)$$

where $k_f' = 1.00$ for the thermal boundary layers developing over the uniform spheres roughness of the present study. Eqn. (4-59) is compared to measured temperature profiles in Section 4.7.

4.6 PREDICTION MODEL

The rough-wall equations inserted into STAN5 are now presented. The first step in the prediction scheme is the calculation of the roughness Reynolds number, Re_k. A correction is then made to account for blowing, such that

$$\overline{Re_k} = Re_k \left[1 + 16.0\ e\ V_o^+\right] \qquad (4\text{-}60)$$

where $e = 1.0$ for $Re_k > 55.0$, and $e = Re_k/55.0$ for $Re_k \leq 55.0$. Re_k in Eqn. (4-60) is based on a value of $C_f/2$ reduced by the effects of transpiration. The correction in (4-60) is based on Healzer's (1974) method and can be viewed as replacing U_τ in the roughness Reynolds number with a new

velocity scale $(U_\tau + 16.0\ e\ V_o)$. If $\overline{Re_k}$ is then substituted for Re_k in Eqn. (4-36), the mixing length with and without blowing becomes

$$\ell^+ = \kappa\left[y^+ + .0307\ (\overline{Re_k} - Re_k')\right] \tag{4-61}$$

which is used for predictions whenever $\overline{Re_k} > Re_k'$ with $Re_k' = 46.0$. If Eqn. (4-61) is then multiplied by ν/U_τ, we have

$$\ell = \kappa\left[y + .0307(k_s)\left(1 + 16.0\ e\ \frac{V_o}{U_\tau} - \frac{U_\tau'}{U_\tau}\right)\right] \tag{4-62}$$

Using this approach, the effective value of the roughness Reynolds number, $\overline{Re_k}$, and the near-wall value of the mixing length are increased to values larger than exist without transpiration. On smooth walls, the effect of blowing is to decrease the thickness of the laminar sublayer, thus increasing the near-wall mixing length. The rough-wall model is consistent with observed physics, since the roughness model with transpiration makes the flow appear rougher rather than smoother. Eqn. (4-62) also seems consistent with observed physics, since fully rough velocity profiles with transpiration show no evidence of a viscous sublayer. The formation of a viscous sublayer is an unlikely possibility, since blowing increases near-wall turbulence intensity levels.

For high-velocity flows with strong blowing, $\overline{Re_k} \sim 16.0\ \frac{V_o k_s}{\nu}$ and the ratio of roughness effects to viscous effects is no longer dependent on U_τ. The behavior of the rough-wall boundary layer then is dependent upon the magnitude of transpiration and not on the wall shear forces. Thus, two regimes of fully rough behavior with blowing may be present: for weak blowing, the flow is characterized by a non-dimensional parameter which is a function of both U_τ and V_o, and, for strong blowing, the parameter is dependent upon V_o only.

An alternative to the mixing-length offset method expressed by Eqn. (4-61) for no blowing and $Re_k > Re_k'$ is the slip-velocity scheme. Using this technique, the mixing length is given by Eqn. (4-24), which is used in conjunction with a slip velocity expressed as Eqn. (4-42).

For $\overline{Re_k} < Re_k^*$, van Driest damping is used for predictions with a sublayer thickness less than the smooth-wall value to account for the effect

of roughness. If blowing is present, the sublayer thickness, A^+, is first modified to account for the transpiration, using a correlation recommended for smooth-wall flows by Crawford and Kays. The value of A^+ is then altered to include roughness effects using a rearranged form of Healzer's (1974) equation for transitionally rough flows. The mixing length is represented using Eqn. (4-16), with A_R^+ replacing A^+ to give

$$\ell^+ = \kappa y^+ \left[1 - e^{-y^+/A_R^+} \right] \tag{4-63}$$

The viscous sublayer thickness on rough walls, A_R^+, is then expressed using the empirical relation

$$A_R^+ = A^+ f(\overline{Re_k}) \tag{4-64}$$

where $f(Re_k) = 1 - g(Re_k)$ and $g(Re_k)$ was discussed earlier as Eqn. (3-8). In Eqn. (3-8), $g(\overline{Re_k})$ is dependent on Re_k'' and Re_k^*, as well as Re_k. Re_k^* and Re_k'' are constant for a given roughness geometry. Recommended values for Re_k'' are presented in the following table for different types of roughness.

Table 4-1

Recommended Values of Re_k'' for Different Types of Roughness

Re_k''	Roughness
2.25	Commercial
7.00	Sandgrain
15.0	Uniformly packed spheres

For Re_k^*, a value of 55.0 is used for prediction of flows over all three types of roughness.

For the outer regions of the rough-wall boundary layers, where

$$y > \frac{\lambda(\delta_{.99})}{\kappa} \tag{4-65}$$

the mixing length is given by

$$\ell = \lambda\delta \tag{4-66}$$

where δ is based on $U/U_\infty = 0.99$ and $\lambda = 0.080$. For pipe-flow predictions where $R/R_o < 0.90$, the Reichardt equation (see Kays (1966)) for the eddy diffusivity for momentum given by

$$\frac{\varepsilon_M}{\nu} = \frac{\kappa y^+}{6}\left[1 + \frac{R}{R_o}\right]\left[1 + 2\left(\frac{R}{R_o}\right)^2\right] \tag{4-67}$$

is incorporated into the prediction scheme.

For the rough-wall heat transfer predictions, a temperature step at the wall is used which is given by

$$(\delta t_o)^+ = g(\overline{Re_k})\, k_f'(\overline{Re_k})^{0.20}\, (Pr)^{0.44} \tag{4-68}$$

which becomes Eqn. (4-58) when $\overline{Re_k} > Re_k^*$ and $V_o^+ = 0$. As the flow approaches smooth-wall behavior for $\overline{Re_k} < Re_k^*$, the temperature step given by (4-68) decreases to zero inversely as the viscous sublayer thickness increases. The variation of $(\delta t_o)^+$ for this range of roughness Reynolds numbers is given by Eqn. (4-68), where $g < 1.0$ and g is given by Eqn. (3-8).

In Eqn. (4-68), $k_f' = 2.86$ is recommended to predict Dipprey and Sabersky's (1963) pipe heat transfer data, and $k_f' = 1.00$ provides good results for Stanford data. Dipprey and Sabersky recommend $k_f = 5.19$. However, it is important to realize that k_f and k_f' are not the same, since in (4-58), $(\delta t_o)^+$ is a function of equivalent sandgrain roughness, k_s, and in Dipprey and Sabersky's original equation, $(\delta t_o)^+$ is a function of mean roughness height, k.

The turbulent Prandtl number distribution used for the rough-wall predictions is given by Eqn. (4-19), where Pr_t was calculated using the rough-wall eddy diffusivity for momentum, instead of the smooth-wall value. The rough-wall Pr_t value increases for $y^+ < 30$, which represents an effective decrease of the transport of heat by turbulent mixing as the wall is approached. Eventually, ε_H becomes insignificant as the wall is approached, and molecular properties dominate thermal transport in the conduction sublayer.

4.7 PREDICTION RESULTS

The validity of the rough-wall closure scheme is first demonstrated by predicting hydrodynamic and heat transfer behavior in pipe flows. Prediction results are then presented for the present rough-wall boundary layer data with and without transpiration, and with and without favorable pressure gradients. Input data required for the predictions are k_s, the equivalent sandgrain roughness of the surface, the type of roughness (commercial, sandgrain, or uniformly packed spheres), and the geometry-dependent constant for heat transfer, k_f', defined by Eqn. (4-58).

Prediction results for Nikuradse's (1950) data for pipe flows are shown in Fig. 4-2, using the mixing-length offset method. For values of R/k_s ranging from 15.0 to 126.0, the predictions show excellent agreement with the data. As lower Re_D are approached, the computed results follow the transitionally rough data and eventually show smooth-wall behavior for low roughness Reynolds numbers. Thus the distribution of the sublayer thickness with roughness Reynolds number given by Eqn. (4-64) is a reliable representation of sandgrain roughness. In the fully rough regime where the skin friction coefficient is a function of k_s/R only, the model represented by Eqn. (4-61) also realistically simulates the flow behavior as influenced by roughness.

In Fig. 4-3, Dipprey and Sabersky's (1963) heat transfer data for pipe flows is presented, along with predictions using the mixing-length offset method for $k_s/D = .0448$ and $k_s/D = .0138$. In some cases, small differences exist between the data and calculations. However, agreement is generally good, and the qualitative trends usually exhibited by the data for three different values of the molecular Prandtl number and for a range of Re_D are well represented by the predictions.

Predictions of the Stanford rough-wall turbulent boundary layer $C_f/2$ and St data with and without transpiration are shown in Figs. 4-4 and 4-5 for freestream velocities of 9.75 m/sec, 27.13 m/sec, and 42.37 m/sec. The skin-friction data in Fig. 4-4 and the Stanton number data in Fig. 4-5 for no blowing show excellent agreement with mixing-length offset and slip-velocity predictions. For cases with $F = .002$ and $F = .004$, mixing-length offset predictions are very good, except for the $F = .004$, $U_\infty = 9.75$ m/sec heat transfer run, and except for small differences with $F = .004$, where the boundary layers are thin and just beginning to develop.

Figure 4-6 shows a comparison between mean velocity profiles and predictions for a transitionally rough flow, fully rough flows, and a fully rough flow with $F = .002$ blowing. The agreement between the mixing-length offset predictions and the data in all cases is excellent. Slip-velocity predictions are also shown for the fully rough cases, and, again, excellent agreement between data and prediction exists.

Temperature profile predictions are compared to measurements in Fig. 4-7 for a transitionally rough flow, a fully rough flow, a fully rough flow with $F = .002$ blowing, and a fully rough flow where $\xi > 0$. The temperature-profile predictions, using the mixing-length offset method, are excellent. Also included on Fig. 4-7 is the thermal, fully rough law of the wall, given by Eqn. (4-59). The agreement among predictions, data, and Eqn. (4-59) is important for fully rough flows with $\xi = 0$ and $F = 0$, since this indicates that neglecting molecular effects outside the conduction sublayer is not an unrealistic assumption.

The results shown in Fig. 4-7 for the $\xi > 0$ layer are from a thermal boundary layer which is thinner than the hydrodynamic boundary layer, due to unheated starting length effects. Stanton number predictions for flows with $\xi > 0$ are discussed in Section 3.2.4 and shown in Figs. 3-15 through 3-17 for freestream velocities of 26.8 m/sec, 15.8 m/sec, and 10.1 m/sec. In these figures, agreement between the predictions and St data is very good, except for small differences at 10.1 m/sec.

The computer results for the downstream development of the momentum thickness are also consistent with data for the three freestream velocities tested. Correct prediction of growth rates assures agreement between Stanton number and skin friction data and predictions when plotted versus either downstream distance or integral length scales such as Λ_2 or δ_2.

A comparison is made in Figs. 4-8a and 4-8b between predictions and data for flows over the present roughness with non-zero pressure gradients. In Fig. 4-8a, $K_R = 0.15 \times 10^{-3}$, and in Fig. 4-8b, $K_R = 0.29 \times 10^{-3}$, where $K_R = (r/U_\infty)(dU_\infty/dx)$. In the figures, the correct trends of constant St and $C_f/2$ with downstream distance are shown by the predictions. The St predictions show excellent agreement with the St data; the $C_f/2$ predictions are about 13% higher than C_f/e measurements. Fig. 4-9 shows mean velocity and temperature profile predictions with $K_R = 0.15 \times 10^{-3}$ acceleration. The differences in the predicted and measured profiles are

due to the over-prediction of the skin friction. It should be mentioned that the constants used in the mixing-length equation (4-62), the turbulent Prandtl number equation, and the wall-temperature step equation (4-68) were determined from zero-pressure-gradient data and not modified for these predictions of accelerated flows.

Predictions were also made for boundary layer flow over the present roughness subjected to complicated boundary conditions. Fig. 4-10a shows Stanton numbers measured in a fully rough boundary layer with an arbitrary variation of freestream velocity, steps in blowing, and a variable blowing distribution. In Fig. 4-10b, the fully rough boundary layer data were taken in a flow with the same distribution of freestream velocity and blowing as 4-10a, along with a step in wall temperature in the region of variable blowing. The distributions of freestream velocity and blowing are shown in Fig. 4-10c. In both Figs. 4-10a and 4-10b, agreement between predictions and data is very good, particularly for data from the downstream end of the test section.

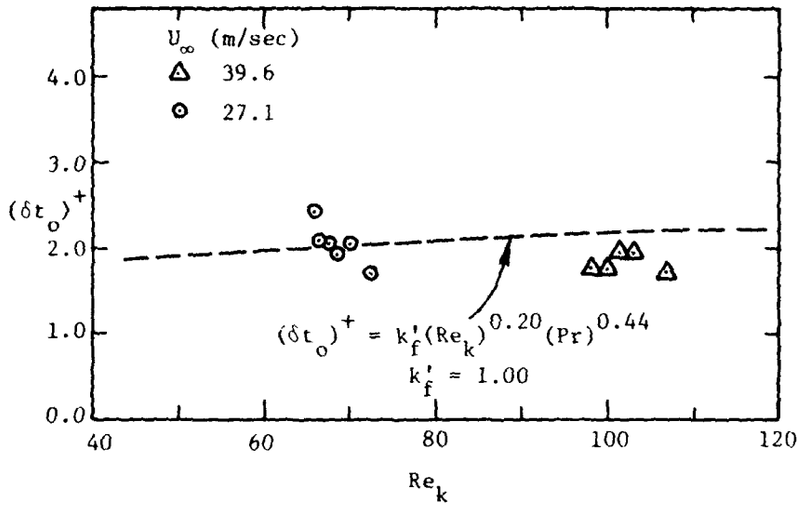

Fig. 4-1. Conduction sublayer temperature drop as a function of roughness Reynolds number.

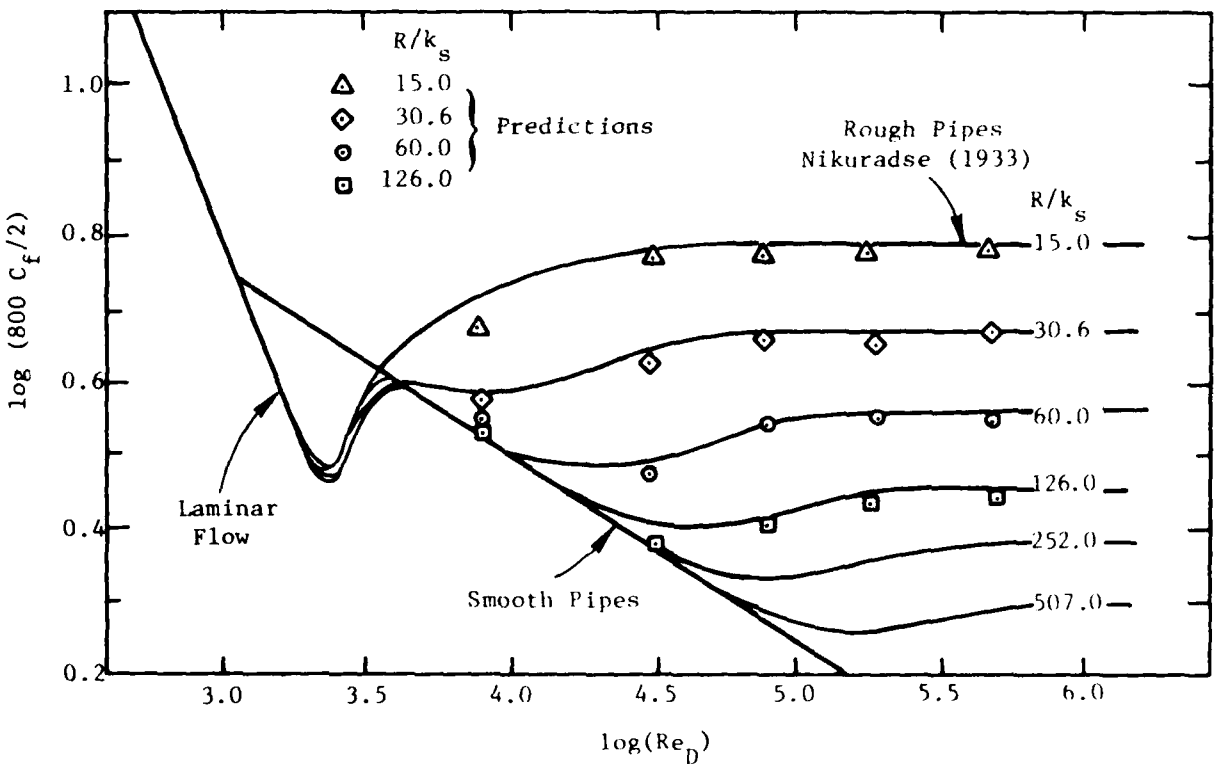

Fig. 4-2. Prediction of Nikuradse's (1933) pipe skin friction coefficient data.

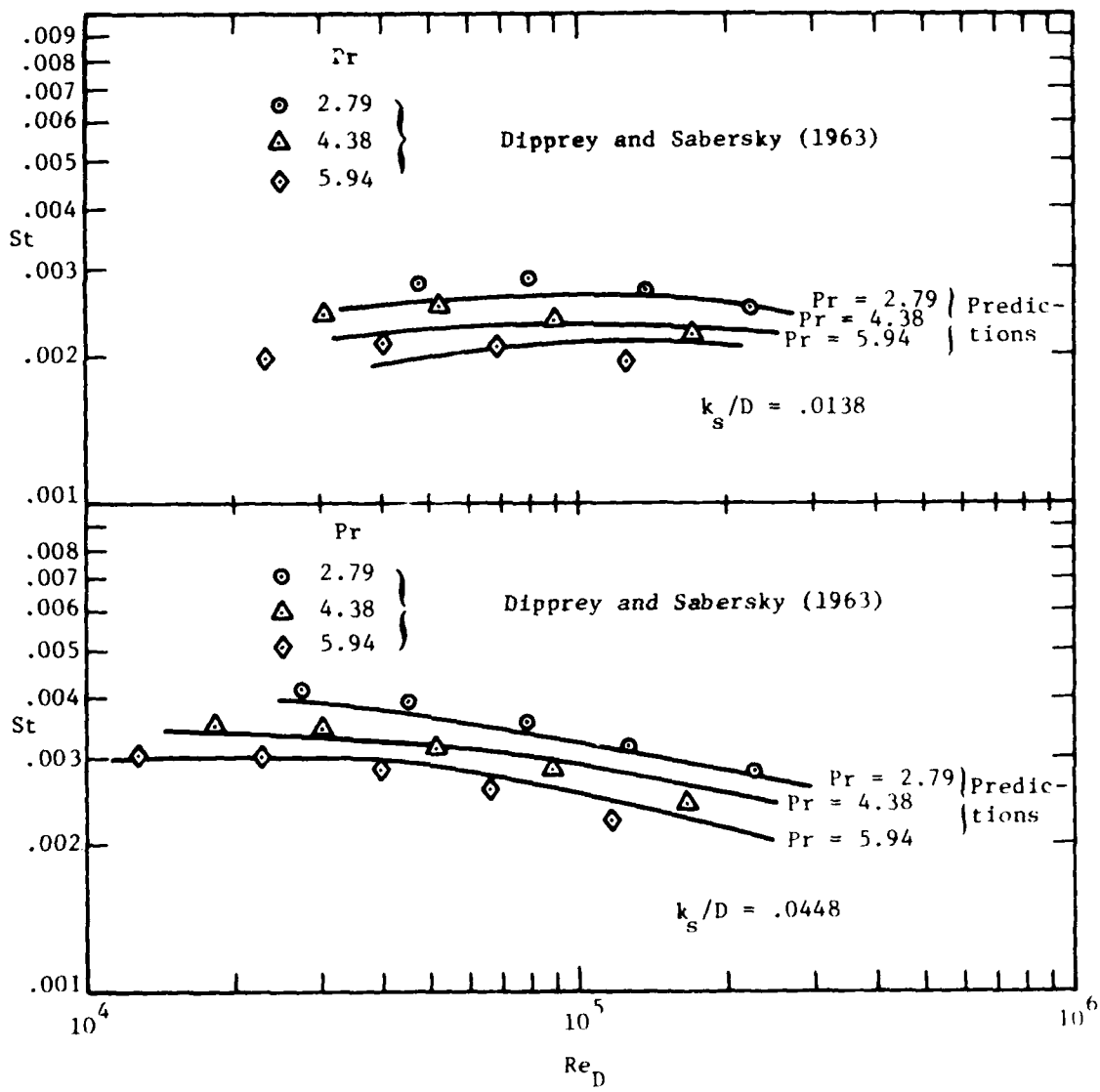

Fig. 4-3. Prediction of Dipprey and Sabersky's (1963) pipe heat transfer data.

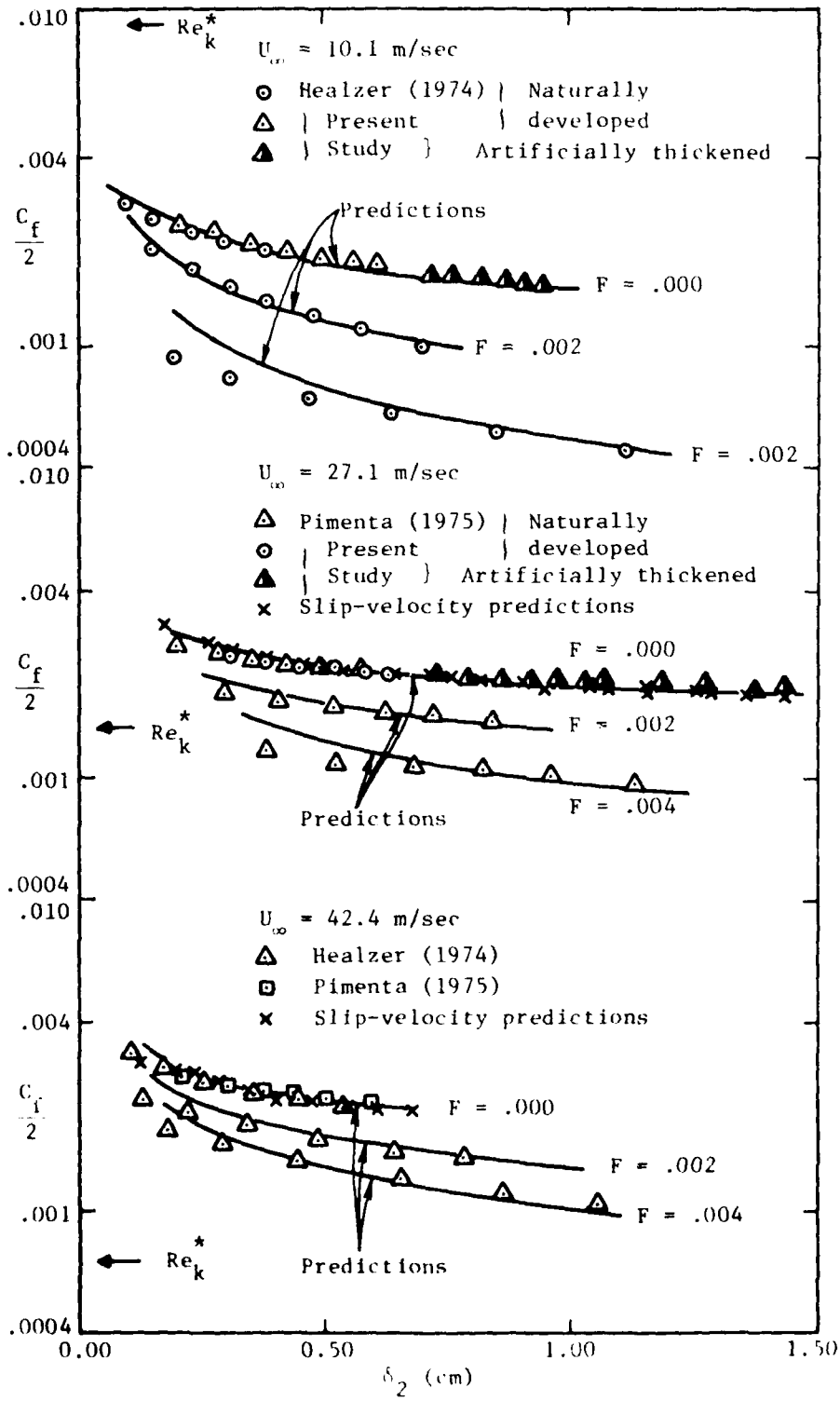

Fir. 4-4. Prediction of skin friction coefficients in naturally developed boundary layers with and without transpiration, and in artificially thickened boundary layers.

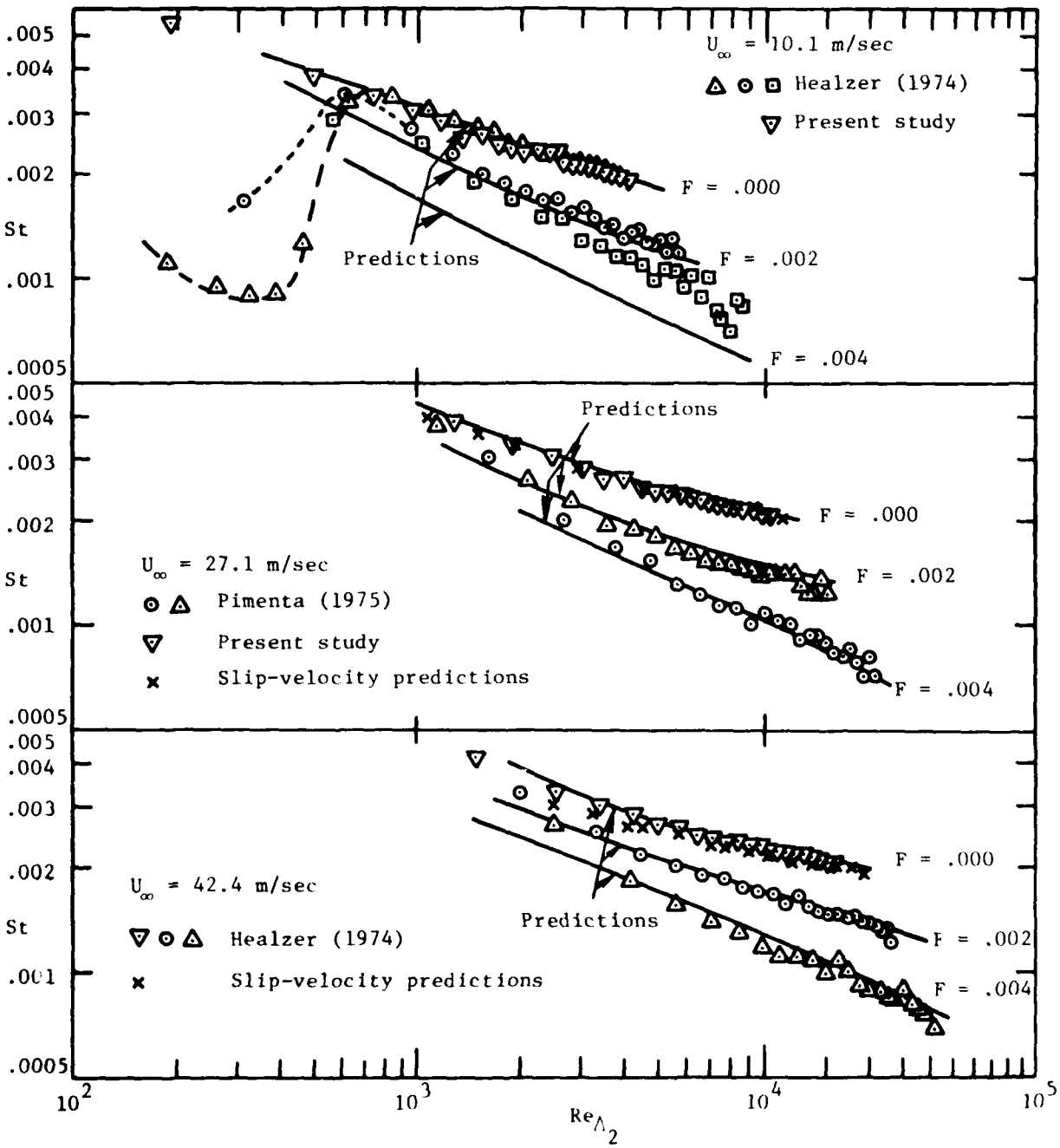

Fig. 4-5. Prediction of Stanton numbers in naturally developed boundary layers with and without transpiration.

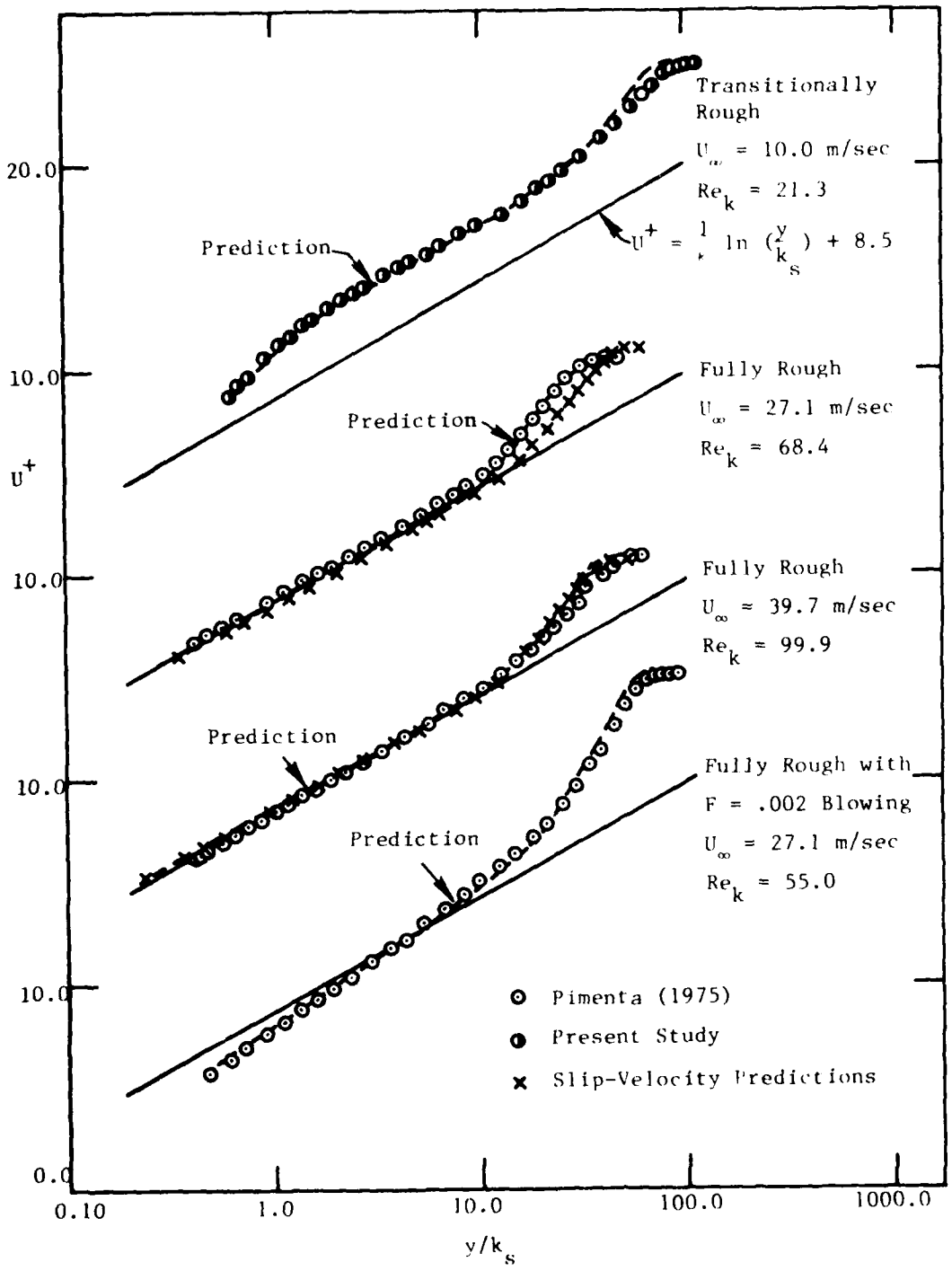

Fig. 4-6. Prediction of mean velocity profiles in a transitionally rough boundary layer, fully rough boundary layers, and a fully rough boundary layer with transpiration.

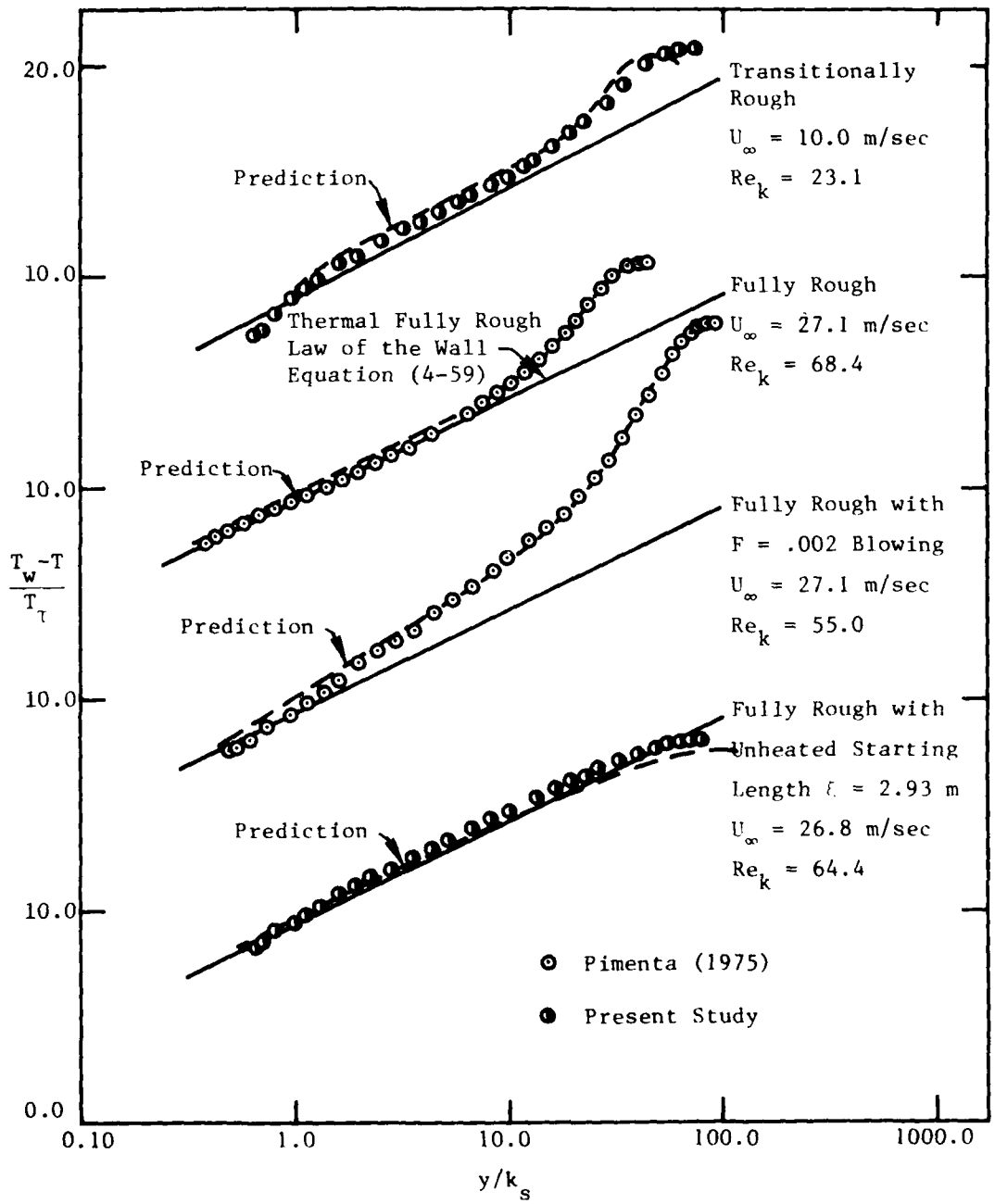

Fig. 4-7. Prediction of mean temperature profiles in a transitionally rough boundary layer, a fully rough boundary layer, a fully rough boundary layer with transpiration, and a fully rough boundary layer with an unheated starting length.

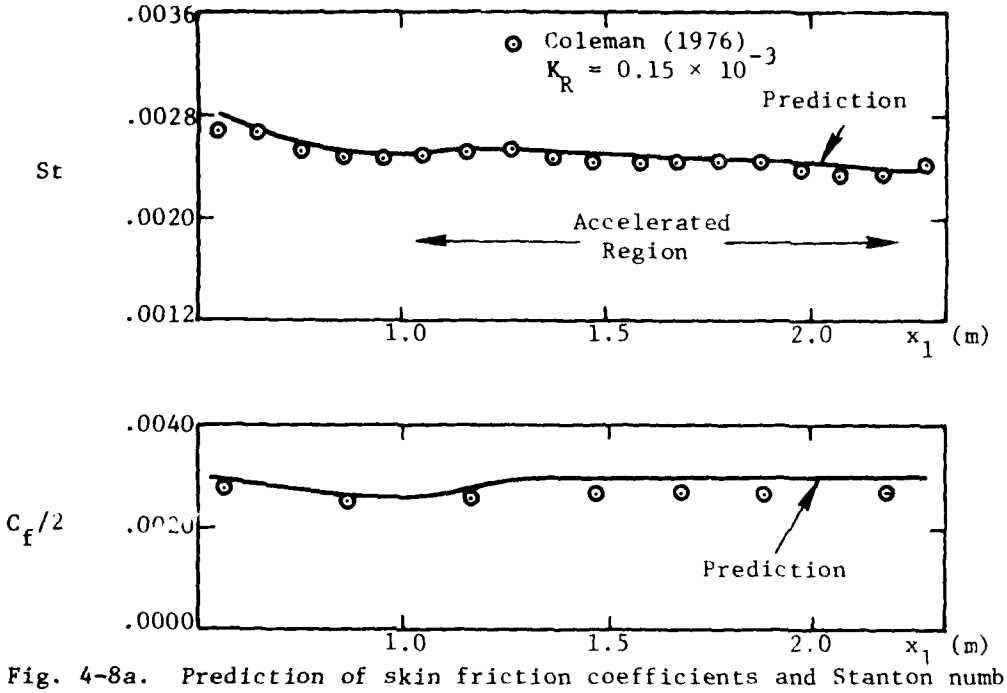

Fig. 4-8a. Prediction of skin friction coefficients and Stanton numbers in an accelerated, fully rough boundary layer, $K_R = .15 \times 10^{-3}$.

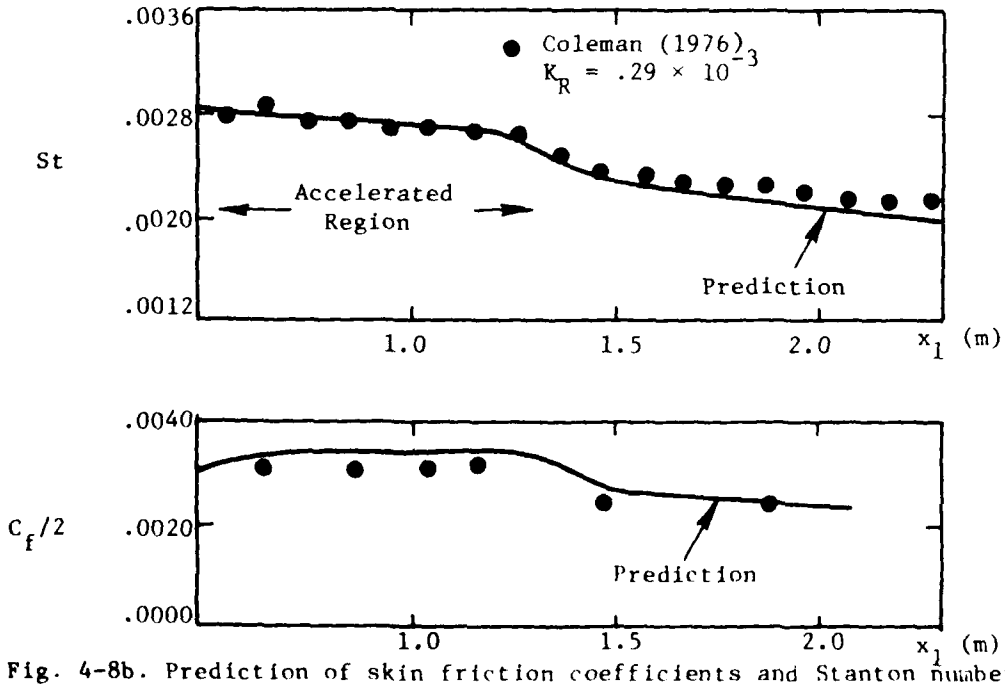

Fig. 4-8b. Prediction of skin friction coefficients and Stanton numbers in an accelerated, fully rough boundary layer, $K_R = .29 \times 10^{-3}$.

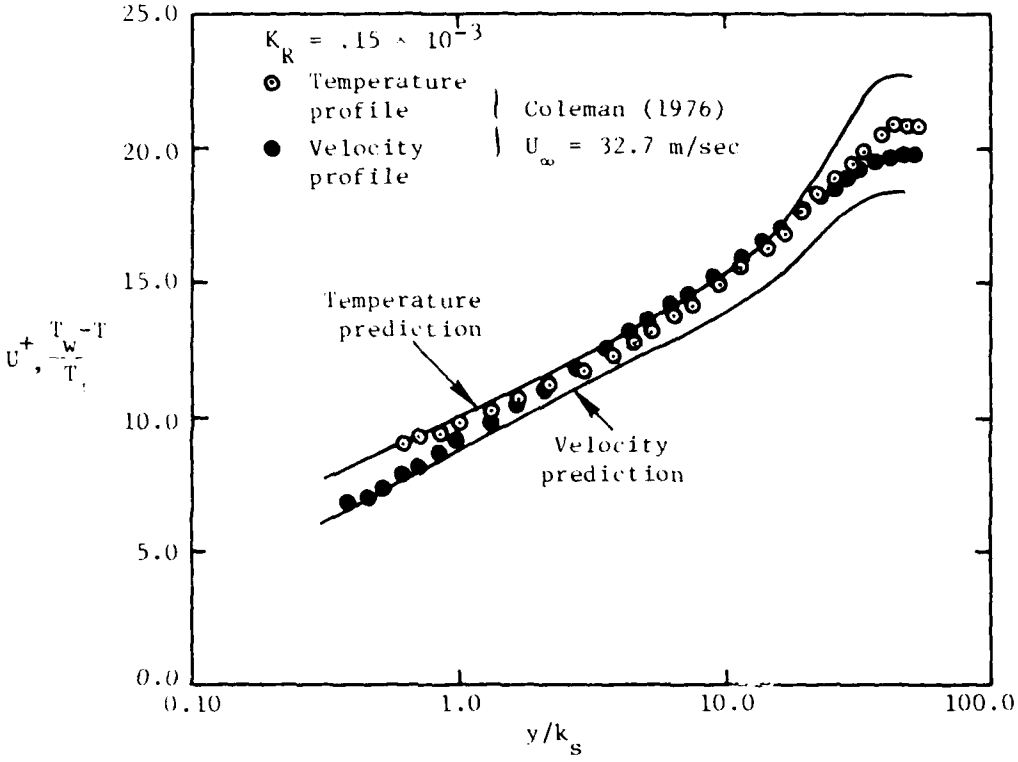

Fig. 4-9. Prediction of mean temperature and mean velocity profiles in an accelerated, fully rough boundary layer, $K_R = .15 \times 10^{-3}$.

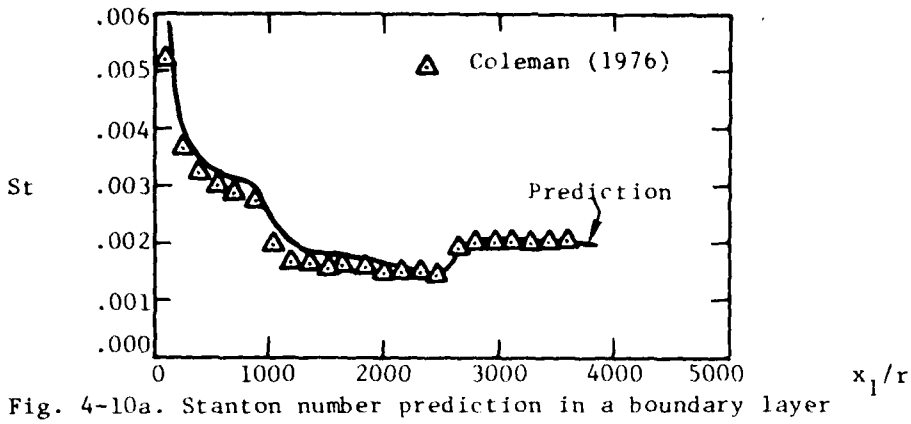

Fig. 4-10a. Stanton number prediction in a boundary layer with acceleration, steps in blowing, and variable blowing.

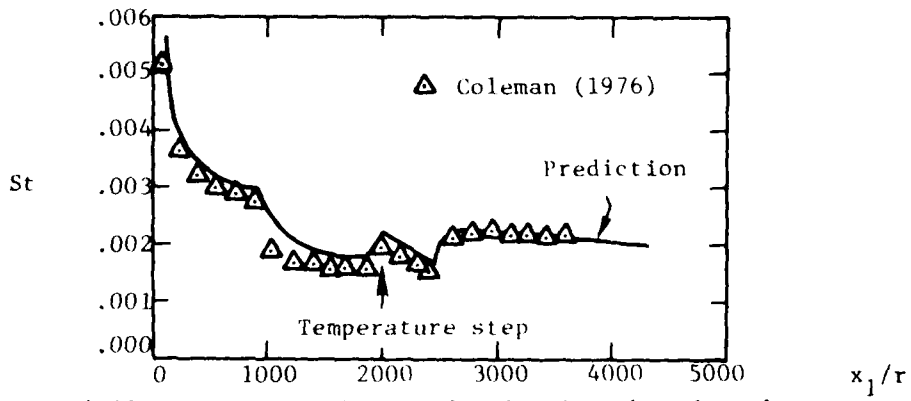

Fig. 4-10b. Stanton number prediction in a boundary layer with acceleration, steps in blowing, variable blowing, and a wall temperature step.

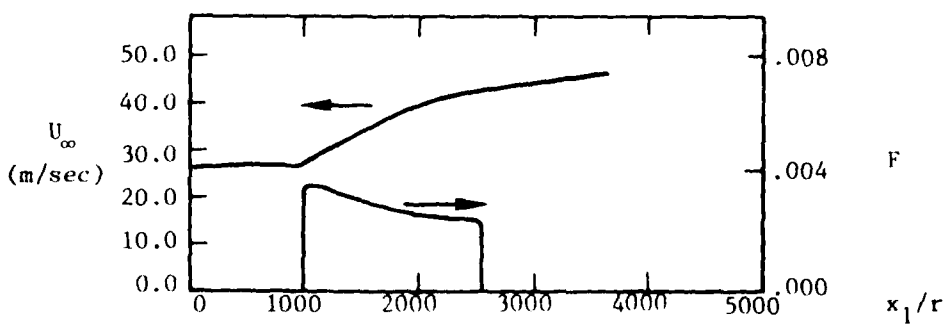

Fig. 4-10c. Free stream velocity and blowing distributions.

Chapter 5

CONCLUSIONS

The thermal and hydrodynamic behavior of thick, rough-wall, turbulent boundary layers has been investigated in naturally developed and artificially thickened boundary layers in zero pressure gradients. The important results and conclusions from this study are as follows.

1) Smooth-wall, artificially thickened, turbulent boundary layers can be produced which are two-dimensional and at equilibrium with properties representative of natural behavior to the level of the cross-correlation coefficient for the turbulent shear stress and the Reynolds shear stress/turbulence kinetic energy ratio.

2) Rough-wall, artificially thickened, turbulent boundary layers can be produced which are two-dimensional and at equilibrium with properties representative of natural behavior to the level of one-dimensional spectra of the longitudinal velocity fluctuations.

3) The distributions of $\overline{u'^2}/U_\tau^2$ in rough-wall boundary layers asymptotically approach behavior where the profiles are nearly invariant with U , both as U_∞ decreases and increases. The invariant $\overline{u'^2}$ profiles at high velocities are fully rough, and the invariant $\overline{u'^2}$ profiles at low velocities are smooth. In between, the flows are transitionally rough, and the distributions of $\overline{u'^2}/U_\tau^2$ change continuously from fully rough behavior to smooth behavior, as the freestream velocity of the flow changes. Fully rough $\overline{u'^2}/U_\tau^2$ profiles can then be distinguished from transitionally rough profiles, since the transitionally rough profiles vary significantly as U_∞ changes, whereas fully rough profiles do not.

4) The normalizing variable U_τ collapses the outer regions of profiles of $\overline{u'^2}$ for boundary layers at different downstream locations and at different freestream velocities. U_τ is considered a more universal normalizing variable for $\overline{u'^2}$ profiles than U_∞. When normalized using U_∞, profiles of $\overline{u'^2}$ seem to show downstream similarity for flows at a given freestream velocity only when the skin friction coefficient, $C_f/2$, is approximately constant with downstream distance.

5) When normalized using U_τ, profiles of $\overline{q^2}$ collapse for boundary layers at different freestream velocities which are approximately the same thickness. Profiles of $\overline{q^2}$ show downstream similarity when normalized using U_∞, for flows at a given freestream velocity. Generally, U_τ is considered a more universal normalizing variable for $\overline{q^2}$ profiles than U_∞.

6) For $U_\infty \geq 15.8$ m/sec, the normalizing variable U_∞ collapses profiles of $\overline{v'^2}$ and $\overline{w'^2}$ for flows at different downstream locations and at different freestream velocities, better than does U_τ.

7) As the freestream velocity decreases below 15.8 m/sec, profiles of $\overline{v'^2}/U_\infty^2$ and $\overline{w'^2}/U_\infty^2$ are different from the universal behavior shown by fully rough and transitionally rough flows with freestream velocities greater than or equal to 15.8 m/sec. These profiles are diverging from the $U_\infty \geq$ 15.8 m/sec behavior to approach smooth-wall behavior.

8) The change from smooth to fully rough behavior in boundary layers over uniform-spheres roughness is more abrupt and occurs over a smaller range of roughness Reynolds numbers than boundary layer flows over sandgrain roughness. A correlation for the velocity distribution constant, B, as a function of Re_k for uniform-spheres roughness can be used in conjunction with law of the wake and law of the wall equations to predict the dependence on Re_k of viscous sublayer thickness, velocity profile shifts, and skin friction coefficients in transitionally rough flows.

9) The shift of transitionally rough velocity profiles between the smooth law of the wall and the fully rough law of the wall, and the near-wall variations in transitionally rough profiles of $\overline{u'^2}$ are a consequence of variations in the thickness of the viscous sublayer, where the thickness decreases as Re_k increases.

10) Stanton numbers in rough-wall thermal boundary layers having unheated starting lengths $(\xi > 0)$ are lower than $\xi = 0$ rough-wall flows when compared at the same enthalpy thickness and when $\Delta_2/r < 3$-4. Temperature profiles in $\xi > 0$ thermal boundary layers are shifted above $\xi = 0$ temperature profiles in $(T_w-T)/(T_2-T_\infty)$ versus U/U_∞ coordinates, yet show a temperature jump similar to the $\xi = 0$ profiles when extrapolated to the wall.

11) Mean profiles, Stanton numbers, and skin friction coefficients can be predicted in fully rough turbulent boundary layers with and without favorable pressure gradients and with and without transpiration, using the following relationship for the near-wall mixing length:

$$\ell = \kappa\left[y + .0307(k_s)\left(1 + 16.0\ e\ \frac{V_o}{U_\tau} - \frac{U'_\tau}{U_\tau}\right)\right] \qquad (5\text{-}1)$$

with a wall temperature step given by

$$(\delta t_o)^+ = gk'_f(\overline{Re_k})^{0.20}\ (Pr)^{0.44} \qquad (5\text{-}2)$$

These can be used in conjunction with smooth-wall, outer-region, mixing-length equations and the smooth-wall, turbulent Prandtl number distribution.

12) Transitionally rough skin friction coefficient data usually show qualitative trends which could be interpreted as being consistent with the Prandtl-Schlichting hypothesis that fully rough flows will eventually become transitionally rough and then smooth if allowed to develop far enough downstream. The fully rough skin friction data at $U_\infty = 26.8$ m/sec decrease only slowly with x, however, and experimental uncertainties do not allow a conclusive proof that the return to transitionally rough and smooth behavior actually occurs.

13) Mean velocity profile data and $\overline{u'^2}$ profiles at a transitionally rough freestream velocity of 10.1 m/sec approach smooth behavior with downstream development. A comparison of profiles of $\overline{u'^2}$ at different downstream locations for higher freestream velocities indicates that fully rough flows do not approach transitionally rough behavior, and transitionally rough flows do not approach smooth behavior for $\delta_2 < 1.45$ cm.

14) The production of turbulence kinetic energy approximately balances the viscous dissipation of turbulence kinetic energy throughout the thickness of fully rough, turbulent boundary layers.

15) One-dimensional spectra of $\overline{u'^2}$ indicate that fully rough turbulent boundary layers have an inertial subrange that extends to higher wave numbers and have more energy at higher wave numbers than smooth-wall boundary layer and channel flows, when compared at the same y/δ.

16) The magnitudes of Kolmogorov length scales of fully rough turbulent boundary layers are approximately half the magnitudes for smooth-wall boundary layer and channel flows, when compared at the same y/δ.

REFERENCES

Adams, J. C., Jr., and Hodge, B. K., "The Calculation of Compressible, Transitional, Turbulent, and Relaminarizational Boundary Layers over Smooth and Rough Surfaces Using an Extended Mixing Length Hypothesis," AIAA 10th Fluid & Plasmadynamics Conference, Report 77-682, June 27-29, 1977.

Anderson, P. S., Kays, W M., and Moffat, R. J., "The Turbulent Boundary Layer on a Porous Plate: An Experimental Study of the Fluid Mechanics for Adverse Free-Stream Pressure Gradients," Report No. HMT-15, Thermosciences Division, Dept. of Mechanical Engineering, Stanford University, 1972.

Antonia, R. A., and Wood, D. H., "Calculation of a Turbulent Boundary Layer Downstream of a Small Step Change in Surface Roughness," Aeronautical Quarterly, Vol. 26, Aug., 1975, pp. 202-210.

Blackwell, B. F., Kays, W. M., and Moffat, R. J., "The Turbulent Boundary Layer on a Porous Plate: An Experimental Study of the Heat Transfer Behavior with Adverse Pressure Gradients," Report No. HMT-16, Thermosciences Div., Dept. of Mechanical Engineering, Stanford University, 1972.

Bradshaw, P., "The Turbulence Structure of Equilibrium Boundary Layers," NPL Aero Report 1184, 1966.

Bradshaw, P., An Introduction to Turbulence and Its Measurement, The Commonwealth and International Library of Science Technology Engineering and Liberal Studies, Pergamon Press, 1971.

Cebeci, T., and Bradshaw, P., Momentum Transfer in Boundary Layers, McGraw-Hill/Hemisphere, Washington, D. C., 1977.

Cebeci, T., and Chang, K. C., "Calculation of Incompressible Rough-Wall Boundary-Layer Flows," AIAA Journal, Vol. 16, No. 7, pp. 730-735, July, 1978.

Cebeci, T., and Chang, K. C., "Reply by Authors to A. F. Mills," AIAA Jour., Vol. 17, No. 2, pp. 221-222, 1979.

Champagne, F. H., "The Fine-Scale Structure of the Turbulent Velocity Field," Jour. of Fluid Mechanics, Vol. 86, Part 1, pp. 67-108, 1978.

Clauser, F. H., "The Turbulent Boundary Layer," Advances in Applied Mechanics, Vol. IV, pp. 1-51, Academic Press, New York, 1956.

Clauser, F. H., "Turbulent Boundary Layers in Adverse Pressure Gradients," Jour. of Aeronautical Science, Vol. 21, p. 91, 1954.

Cockrell, D. J., and Lee, B. E., "Methods and Consequences of Atmospheric Boundary Layer Simulation," Paper 13-AGARD Conference, Proc. No. 48 on Aerodynamics of Atmospheric Shear Flows, Munich, 1969.

Coleman, H. W., Moffat, R. J., and Kays, W. M., "Momentum and Energy Transport in the Accelerated Fully Rough Turbulent Boundary Layer," Report No. HMT-24, Thermosciences Div., Dept. of Mechanical Engineering, Stanford University, 1976.

Coles, D., "The Law of the Wake in the Turbulent Boundary Layers," Jour. of Fluid Mechanics, Vol. 1, pp. 191-226, 1956.

Counihan, J., "An Improved Method of Simulating an Atmospheric Boundary Layer in a Wind Tunnel," Atmospheric Environment, Vol. 3, pp. 197-214, 1969a.

Counihan, J., "A Method of Simulating a Neutral Atmospheric Boundary Layer in a Wind Tunnel," Paper 14-AGARD Conference, Proc. No. 48 on Aerodynamics of Atmospheric Shear Flows, Munich, 1969b.

Counihan, J., "Further Measurements in a Simulated Atmospheric Boundary Layer," Atmospheric Environment, Vol. 4, pp. 259-275, 1970.

Counihan, J., "Simulation of an Adiabatic Urban Boundary Layer in a Wind Tunnel," Atmospheric Environment, Vol. 7, pp. 673-689, 1973.

Counihan, J., Hunt, J.C.R., and Jackson, P. S., "Wakes Behind Two-Dimensional Surface Obstacles in Turbulent Boundary Layers," Jour. of Fluid Mechanics, Vol. 64, pp. 529-563, 1974.

Crawford, M. E., and Kays, W. M., "STAN5--A Program for Numerical Computation of Two-Dimensional Internal/External Boundary Layer Flows," Report No. HMT-23, Thermosc. Div., Dept. of Mechanical Engineering, Stanford University, 1975.

Dipprey, D. F., and Sabersky, R., "Heat and Momentum Transfer in Smooth and Rough Tubes at Various Prandtl Numbers," Int. J. Heat Mass Transfer, Vol. 6, pp. 329-353, 1963.

Donne, M. D., and Meyer, L., "Turbulent Convective Heat Transfer from Rough Surfaces with Two-Dimensional Rectangular Ribs," International Jour. of Heat and Mass Transfer, Vol. 20, pp. 583-620, 1977.

Dvorak, F. A., "Calculation of Turbulent Boundary Layers on Rough Surfaces in Pressure Gradient," AIAA Jour. Vol. 7, No. 9, Sept. 1969, pp. 1752-1758.

Dvorak, F. A., "Calculations of Compressible Turbulent Boundary Layers with Roughness and Heat Transfer," AIAA Jour., Vol. 10, No. 11, Nov. 1972, pp. 1447-1451.

Finson, M. L., "A Reynolds Stress Model for Boundary Layer Transition with Application to Rough Surfaces," AFOSR-TR-76-0322, August, 1975.

Frenkiel, F. N., "Effects of Wire Length in Turbulence Investigations with a Hot-Wire Anemometer," The Aero. Quarterly, Vol. V, pp. 1-24, May, 1954.

Furuya, Y., Miyata, M., and Fuiita, H., "Turbulent Boundary Layer and Flow Resistance on Plates Roughened by Wires," ASME, Fluids Engrg. Division, Gas Turbine and Fluids Engineering Conference, 1976.

Gartshore, I. S., and de Croos, K. A., "Roughness Element Geometry Required for Wind Tunnel Simulations of the Atmospheric Wind," Fluids Engrg. Div., ASME, Winter Annual Meeting, New York, Dec., 1976.

Grass, A. J., "Structural Features of Turbulent Flow over Smooth and Rough Boundaries," Jour. of Fluid Mechanics, Vol. 50, Part 2, pp. 233-255, 1971.

Hama, F. R., "Boundary Layer Characteristics for Smooth and Rough Surfaces," Trans. Soc. Naval Architects Marine Engrs., Vol. 62, pp. 333-358, 1954.

Hatton, A. P., and Walklate, P. J., "A Mixing-Length Method for Predicting Heat Transfer in Rough Pipes," Int. J. Heat and Mass Transfer, Vol. 19, pp. 1425-1431, December, 1976.

Healzer, J. M., Moffat, R. J., and Kays, W. M., "The Turbulent Boundary Layer on a Rough, Porous Plate: Experimental Heat Transfer with Uniform Blowing," Report No. HMT-18, Thermosc. Div., Dept. of Mech. Engrg., Stanford University, 1974.

Hinze, J. O., Turbulence, 2nd edition, McGraw-Hill Book Co., 1975.

Hunt, J.C.R., and Fernholz, H., "Wind-Tunnel Simulation of the Atmospheric Boundary Layer: A Report on Euromech 50," Jour. of Fluid Mechanics, Vol. 70, pp. 543-559, 1975.

Hussain, A.K.M.F., and Reynolds, W. C., "Measurements in Fully Developed Turbulent Channel Flow," ASME Trans., Jour. of Fluids Engineering, Vol. 97, pp. 568-578, 1975.

Ioselevich, V. A., and Pilipenko, V. I., "Logarithmic Velocity Profile for Flow of a Weak Polymer Solution Near a Rough Surface," Sov. Phys. Dokl., Vol. 18, p. 790, 1974.

Jayatilleke, C.L.V., "The Influence of Prandtl Number and Surface Roughness on the Resistance of the Laminar Sub-Layer to Momentum and Heat Transfer," Progress in Heat and Mass Transfer, Vol. 1, pp. 193-329, 1969.

Kader, B. A., and Yaglom, A. M., "Turbulent Heat and Mass Transfer from a Wall with Parallel Roughness Ridges," Int. Jour. of Heat and Mass Transfer, Vol. 20, pp. 345-357, 1977.

Kays, W. M., Convective Heat and Mass Transfer, McGraw-Hill Book Co., New York, 1966.

Keel, A. G., Jr., "Influence of Surface Roughness on Skin Friction and Heat Transfer for Compressible Turbulent Boundary Layers," AIAA 15th Aerospace Sciences Meeting, Los Angeles, 1977.

Kerschen, E. J., private communication, Dept. of Mech. Engrg., Stanford University, 1977.

Kerschen, E. J., and Johnston, J. P., "Modal Content of Noise Generated by a Coaxial Jet in a Pipe," Report No. MD-38, Thermosciences Division, Dept. of Mechanical Engineering, Stanford University, 1978.

Klebanoff, P. S., "Characteristics of Turbulence in a Boundary Layer with Zero Pressure Gradient," NACA Technical Note 3178, 1954.

Klebanoff, P. S., and Diehl, Z. W., "Some Features of Artificially Thickened, Fully Developed, Turbulent Boundary Layers with Zero Pressure Gradient," NACA Report 1110, 1952.

Laufer, J., "The Structure of Turbulence in Fully Developed Pipe Flow," NACA Report 1174, 1954.

Liu, C. K., Kline, S. J., and Johnston, J. P., "An Experimental Study of Turbulent Boundary Layers on Rough Walls," Report MD-15, Thermosc. Div., Dept. of Mechanical Engineering, Stanford University, 1966.

McDonald, H., and Fish, R. W., "Practical Calculations of Transitional Boundary Layers," Int. J. Heat Mass Transfer, Vol. 16, pp. 1729-1744, 1973.

Moffat, R. J., and Kays, W. M., "The Turbulent Boundary Layer on a Porous Plate: Experimental Heat Transfer with Uniform Blowing and Suction," Report No. HMT-1, Thermosc. Div., Dept. of Mechanical Engineering, Stanford University, 1967.

Monin, A. S., and Yaglom, A. M., Statistical Fluid Mechanics, Vol. 1, The MIT Press, 1971.

Moore, W. L., "An Experimental Investigation of Boundary Layer Development Along a Rough Surface," Ph.D. dissertation, State University of Iowa, August, 1951.

Nagib, H. M., Morkovin, M. V., Yung, J. T., and Tan-Atichat, J., "On Modeling of Atmospheric Surface Layers by the Counter-Jet Technique," AIAA Paper No. 74-638, AIAA 8th Aerodynamic Testing Converence, Bethesda, 1974.

Narayana, P.A.A., "An Experimental Investigation of Turbulent Boundary Layers over Smooth and Rough Surfaces," Report LR-235, Dept. of Aerospace Engineering, Delft University of Technology, Delft, 1977.

Nikuradse, J., "Strömungsgesetze in rauhen Rohren," VDI Forschungsschaft, No. 361, 1933, English translation, NACA-TM 1292, 1950.

Orlando, A. F., Moffat, R. J., and Kays, W. M., "Turbulent Transport of Heat and Momentum in a Boundary Layer Subject to Deceleration, Suction, and Variable Wall Temperature," Report No. HMT-17, Thermosc. Div., Dept. of Mechanical Engineering, Stanford University, 1974.

Osaka, M., Shimizu, T., Nakamura, T., and Furuya, Y., "The Spanwise Non-Uniformity of Nominally Two-Dimensional Turbulent Boundary Layers," Bulletin of the Japan Society of Mechanical Engineers, Vol. 20, No. 141, pp. 307-314, 1977.

Otten, L. J., III, and Van Kuren, J. T., "Artificial Thickening of High Subsonic Mach Number Boundary Layers," AIAA Jour., Vol. 14, No. 11, pp. 1528-1533, 1976.

Owen, P. R., and Thomson, W. R., "Heat Transfer across Rough Surfaces," Jour. Fluid Mech., Vol. 15, pp. 321-334, 1963.

Pao, Y. H., "Structure of Turbulent Velocity and Scalar Fields at Large Wavenumbers," Physics of Fluids, Vol. 8, No. 6, pp. 1063-1075, June, 1965.

Perry, A. E., and Abell, C. J., "Asymptotic Similarity of Turbulence Structures in Smooth- and Rough-Walled Pipes," Jour. Fluid Mechanics, Vol. 79, Part 4, pp. 785-799, 1977.

Perry, A. E., and Joubert, P. H., "Rough-Wall Boundary Layers in Adverse Pressure Gradients," Jour. Fluid Mech., Vol. 37, pp. 193-211, 1963.

Peterka, J. A., and Cermak, J. E., "Simulation of Atmospheric Flows in Short Wind Tunnel Test Sections," CER 73-74JAP-JEC32, Fluid Mechanics Program, Colorado State University, 1974.

Pimenta, M. M., Moffat, R. J., and Kays, W. M., "The Turbulent Boundary Layer: An Experimental Study of the Transport of Momentum and Heat with the Effect of Roughness," Report HMT-21, Thermosc. Div., Dept. of Mechanical Engineering, Stanford University, 1975.

Rabiner, L. R., and Gold, B., Theory and Application of Digital Signal Processing, pp. 414-418, Prentice-Hall, Englewood Cliffs, N. J., 1975.

Reynolds, W. C., Kays, W. M., and Kline, S. J., "Heat Transfer in the Turbulent, Incompressible Boundary Layer. II - Step Wall-Temperature Distribution," NASA Memo 12-2-58W, 1958.

Rotta, J. C., "Über die Theorie der turbulenten Grenzschichten," Mitteilungen aus dem Max-Planck-Institüt für Strömungsforschung (Gottingen), No. 1, 1950. English translation, NACA TM-1344, 1953.

Rotta, J. C., "Similar Solutions of Turbulent Boundary Layers," Jour. of Aeronautical Sciences, Vol. 22, pp. 215-216, 1955.

Rotta, J. C., "Turbulent Boundary Layers in Incompressible Flow," Progress in Aerospace Science, Vol. 2, pp. 1-219, 1962.

Rouse, H., and Hassan, M. M., "Cavitation Free Inlets and Contractions," Mechanical Engineering, Vol. 71, Part 3, pp. 213-216, 1949.

Sabot, J., Saleh, I., and Comte-Bellot, G., "Effects of Roughness on the Intermittent Maintenance of Reynolds Shear Stress in Pipe Flow," The Physics of Fluids, Vol. 20, No. 10, Part II, pp. S150-S155, 1977.

Schetz, J. A., Nerney, B., "Turbulent Boundary Layer with Injection and Surface Roughness," AIAA Jour., Vol. 15, No. 9, pp. 1288-1294, 1977.

Schlichting, H., Boundary Layer Theory, 6th edition, McGraw-Hill Book Co., Inc., New York, 1968.

Schultz-Grunow, F., "New Frictional Resistance Law for Smooth Plates," NACA TM 986, 1941.

Seidman, M. H., "Rough Wall Heat Transfer in a Compressible Turbulent Boundary Layer," AIAA 16th Aerospace Sciences Meeting, Huntsville, 1978.

Simpson, R. L., Kays, W. M., and Moffat, R. J., "The Turbulent Boundary Layer on a Porous Plate: An Experimental Study of the Fluid Dynamics with Injection and Suction," Report No. HMT-2, Thermosc. Div., Dept. of Mechanical Engineering, Stanford University, 1967.

Tennekes, H., and Lumley, J. L., A First Course in Turbulence, The MIT Press, 1972.

Townsend, A. A., The Structure of Turbulent Shear Flow, First Edition, Cambridge University Press, 1956a.

Townsend, A. A., The Structure of Turbulent Shear Flow, Second Edition, Cambridge University Press, pp. 150-158, 1976.

Townsend, A. A., "The Properties of Equilibrium Boundary Layers," Jour. of Fluid Mechanics, Vol. 1, pp. 561-573, 1956b.

Uberoi, M. S., and Kovasznay, L.S.G., "On Mapping and Measurement of Random Fields," Quart. Appl. Math., Vol. 10, No. 4, pp. 375-393, 1953.

van Driest, E. R., "On Turbulent Flow Near a Wall," Heat Transfer and Fluid Mechanics Institute, 1955.

Voisinet, R.L.P., "Influence of Surface Roughness and Mass Transfer on Turbulent Boundary Layer Flow," paper submitted for presentation and publication to the Data Exchange Agreement Meeting on Viscous and Interacting Flow Field Effects, U. S. Naval Postgraduate School, 1978.

Voisinet, R.L.P., "Combined Influence of Roughness and Mass Transfer on Turbulent Skin Friction at Mach 2.9," 17th Aerospace Sciences Meeting, New Orleans, 1979.

Wassel, A. T., and Mills, A. F., "Calculation of Variable Property Turbulent Friction and Heat Transfer in Rough Pipes" (to be submitted for publication), 1979.

Willmarth, W. W., and Bogar, T. J., "Survey and New Measurements of Turbulent Structure Near the Wall," The Physics of Fluids, Vol. 20, No. 10, Pt. 11, pp. S9-S21, 1977.

Wyngaard, J. C., "Measurement of Small-Scale Turbulence Structure with Hot Wires," Jour. of Scientific Instruments (Jour. of Physics E), Vol. 1, Series 2, pp. 1105-1108, 1968.

Yaglom, A. M., and Kader, B. A., "Heat and Mass Transfer between a Rough Wall and Turbulent Fluid Flow at High Reynolds and Peclet Number," Jour. Fluid Mechanics, Vol. 62, Part 3, 11, pp. 601-623, 1974.

AD-A094 011 STANFORD UNIV CALIF THERMOSCIENCES DIV F/G 20/4
THE THERMAL AND HYDRODYNAMIC BEHAVIOR OF THICK, ROUGH-WALL, TUR--ETC(U)
AUG 79 P M LIGRANI, R J MOFFAT, W M KAYS N00014-67-A-0112-0072
UNCLASSIFIED HMT-29 NL

3 OF 3
AD A
094011

END
DATE
FILMED
2-81
DTIC

Appendix I

WIND TUNNEL MODIFICATIONS

The wind tunnels used for the present study were the HMT-1 wind tunnel, which is described by Moffat (1967), Anderson (1972), and Blackwell (1972), and the HMT-18 wind tunnel, which is described by Healzer (1974), Pimenta (1975), and Coleman (1976). Both wind tunnels were modified so that an artificial thickening device could be installed to produce thick boundary layers along the test surface.

For the HMT-1 tunnel, the plexiglass section upstream of the test surface was replaced with a new section which allowed installation of the smooth-wall, artificial thickening device. The spires and barrier which comprised the thickening device were mounted on a plexiglass plate for modular insertion into the new plexiglass section. All parts of the spires were made of a fast casting petroleum-based plastic made by REN Plastics, except for the upstream blades, which were made of balsa wood. The barrier was made of plexiglass.

The modifications to the HMT-18 wind tunnel were more extensive. The side walls of the test surface channel were replaced with new walls providing a deeper channel for thicker layers. The channel was deep enough that the turbulence fields $(1.4\ \delta)$ for the top wall boundary layer and the thickest augmented boundary layer did not overlap at the downstream end. The old nozzle and diffuser were also replaced with new components. An additional screen pack was added, and the bottom 12.70 cm of the inlet header box, heat exchanger, filter, and screen packs were blocked off so that no steps existed on the floor of the flow channel upstream of the nozzle. The new nozzle was similar to the one designed by Healzer (1974), with a new area ratio of 7.47 instead of 19.80 for the Healzer design. The design was based on suggestions by Rouse and Hassan (1949), with the new nozzle equations given by

$$y = 4.50 + 9.50\left[\left(\frac{x}{L}\right)^4 \left(15-24\left(\frac{x}{L}\right)+10\left(\frac{x}{L}\right)^2\right)\right] \qquad \text{(I-1)}$$

for the top and bottom walls, and

$$y = 10.0 + 14.0\left[\left(\frac{x}{L}\right)^4 \left(15-24\left(\frac{x}{L}\right) + 10\left(\frac{x}{L}\right)^2\right)\right] \qquad \text{(I-2)}$$

for the side walls, where L is the total streamwise length of the nozzle and $x/L = 0$ at the nozzle exit.

The rough-wall, artificial thickening spires were made of the same fast-casting petroleum-based plastic as was used for the smooth-wall spires. The cross-bar was made of aluminum, and the barrier was made of brass. These components were mounted on a plexiglass plate which allowed adjustment of barrier height using spacers and different brass segments. The plexiglass mounting plate was designed for modular insertion into a rectangular hole on the bottom of the nozzle just upstream of the test surface. The plexiglass plate with the spires could be replaced with a plate without spires to allow a naturally developed boundary layer to exist along the test surface.

After the installation of the new components on the HMT-18 roughness rig, the flow field without an augmented boundary layer was checked for its two-dimensionality. Across the entire exit plane of the nozzle, the total and static pressures were found to vary less than 0.03 cm of water. Spanwise profiles of the mean velocity at the downstream end of the test surface ($z = 0$, $z = -7.62$ cm, and $z = 7.62$ cm) showed a variation of momentum thickness of less than 2.1% about the mean. This variation was about the same as was measured by Healzer (1974) before the recent modifications.

Appendix II

MEASUREMENT TECHNIQUES

II.1 STANTON NUMBERS

Stanton numbers were determined by performing an energy balance on each of the plates of the test surface. The power input to each plate was measured and then losses were subtracted to determine the wall heat flux, $\dot{q}''_w$. The Stanton number was then calculated from the definition

$$St = \frac{\dot{q}''_w}{\rho_\infty U_\infty C_p (T_w - T_{\infty,o})} \qquad \text{(II-1)}$$

A temperature difference, $T_w - T_{\infty,o}$, of approximately 16°C was maintained to limit the effects of variable properties and to provide minimum Stanton number uncertainty.

For the HMT-1 roughness rig, the plate losses considered were the radiative losses from the upper and lower surfaces of the plate, the conduction losses from the plate to the casting, and the conduction loss through the stagnant air below the test plate when there was no transpiration. The data-reduction program used for calculating losses was the same as that used by Healzer (1974), Pimenta (1975), and Coleman (1976). The models for energy losses used by these investigators were confirmed from energy balance tests made at the beginning of the present study. The results of these tests were in excellent agreement with the original tests of Healzer (1974).

The enthalpy thickness variations were determined directly from Stanton measurements using a method verified by Blackwell (1972) to be accurate for two-dimensional flow fields. This relation was determined directly from the energy integral equation, and is given by

$$\Delta_2 \Big|_x = \int_o^x (St + F)\, dx \qquad \text{(II-2)}$$

which is evaluated with respect to downstream distance from the leading edge of the first heated plate. All enthalpy thickness deduced from mean temperature and mean velocity profiles were in excellent agreement with those determined from Stanton numbers with a maximum deviation of approximately 10%.

II.2 MEAN TEMPERATURES

Mean temperature profile measurements were made using a Chromel-constantan thermocouple mounted in a traversing mechanism similar to the ones used for mean velocity profile and $\overline{u'^2}$ measurements. Freestream temperatures were measured using an iron constantan thermocouple probe installed for use in the HMT-18 and HMT-1 wind tunnels. All probes were calibrated in a Rosemount Model 910A Temperature Calibration Oil Bath, using a Hewlett-Packard Model 2801A Quartz Thermometer as a standard.

II.3 SKIN FRICTION

Skin friction coefficients were determined from freestream velocity measurements, and from near-wall measurements of the Reynolds shear stress and mean velocity, using

$$\frac{C_f}{2} = \frac{(-\overline{u'v'})_{y'}}{U_\infty^2} + \frac{\nu}{U_\infty^2}\frac{\partial U}{\partial y'}\bigg|_{y'} + \frac{U(y')}{U_\infty^2}\frac{\partial}{\partial x}\int_o^{y'} U\,dy' - \frac{1}{U_\infty^2}\frac{\partial}{\partial x}\int_o^{y'} U^2\,dy' \qquad \text{(II-3)}$$

For the smooth- and rough-wall boundary layers investigated in the present study, the last three terms in (II-3) were found to be less than 2-4% of the Reynolds shear stress term. This allowed estimation of $C_f/2$ using only the first term in (II-3) for flows where the downstream development of velocity profiles were not measured. The full form of Eqn. (II-3) was used to determine $C_f/2$ for the rough-wall, artificially thickened cases studied at 10.1 m/sec, 15.8 m/sec, and 26.8 m/sec, and for the rough-wall, naturally developed cases studied at 10.1 m/sec and 26.8 m/sec. The skin friction coefficients for all other rough-wall cases studied and the smooth-wall cases studied were estimated using only the Reynolds shear stress term in (II-3).

The value of y' for the measurement of $-\overline{u'v'}$ was 0.330 cm, due to limitations of slant-wire probe size which allowed measurements to be made only for $y' > .318$ cm.

Equation (II-3) is also discussed by Pimenta (1975) and Coleman (1976).

II.4 MEAN VELOCITY

The mean velocity measurements in the smooth-wall boundary layer were made using a 0.508 mm outer diameter total-pressure pitot probe in conjunction with a Combust micromanometer. The probe was mounted on a traversing mechanism with a micrometer to adjust the distance of the probe from the wall.

The mean velocity measurements in the rough-wall boundary layer were made using a 1.25 mm DISA 55F04 platinum-plated, tungsten hot wire, mounted on the same type of traversing mechanism as was used for the pitot probe. The hot-wire probe was connected to a TSI Model 1050 bridge operated in a constant-temperature / constant-resistance mode with a wire overheat ratio of 1.5. The bridge was connected to a TSI Model 1052 linearizer, followed by a Hewlett-Packard Model 2401 C integrating digital voltmeter. The mean voltage signal used to obtain mean velocity was integrated for 10 seconds using the IDVM connected to an external clock.

II.5 REYNOLDS STRESS TENSOR COMPONENTS

The Reynolds stress tensor components were measured using a horizontal hot-wire probe and a rotatable, slanted, hot-wire probe. For both the smooth-wall and rough-wall studies, the horizontal wire was used for $\overline{u'^2}$ measurements. For the smooth-wall study, the slant wire was used (in conjunction with the horizontal wire) to measure $\overline{v'^2}$, $\overline{w'^2}$, and $-\overline{u'v'}$. For the rough-wall study, the slant wire was used (also in conjunction with the horizontal wire) to measure $\overline{v'^2}$, $\overline{w'^2}$, $\overline{v'w'}$, $\overline{u'w'}$, and $-\overline{u'v'}$. The slant-wire probes were mounted on a device which allowed the hot wire to be rotated about the probe axis in 45° increments. The traversing mechanisms were similar to those described earlier. Additional details of these probes are presented by Pimenta (1975) and Coleman (1976).

For the smooth-wall measurements, platinum-plated tungsten sensors were used which had a diameter of 5 microns. Both sensing wires were connected directly to the wire prongs without wire plating of any kind. The horizontal wire had a sensing length of 3 mm; the slant wire was slightly longer. For the measurements, DISA 55M01 anemometers with CTA Standard Bridges were operated in the constant-temperature mode. The anemometer output voltages

were linearized using a TSI Model 1072 fourth-order linearizer. Either a DISA Model 55D15 true rms meter or a TSI Model 1076 true rms meter was used to determine the rms values of the fluctuating voltage. The rms meters were calibrated using a function generator which produced sine waves with known rms values.

For the rough-wall measurements, a DISA 55F04 horizontal wire and a DISA 55F02 slant wire were used. Both wires were made of platinum-plated tungsten with gold plating on the ends. The sensing length of the horizontal wire was 1.25 mm. These wires were chosen for the present study because they had sensing lengths close to those used by Pimenta (1975) and Coleman (1976). The probes would allow the baseline measurements of these authors to be more readily reproduced, and also would allow measurements to be compared with those of Pimenta and Coleman without accounting for wire-length effects. The effect of wire-sensor length on $\overline{u'^2}$ measurement is discussed in Appendix III. The rms meter was the TSI Model 1076 device. The bridge and linearizers used were the same as those used for mean velocity profile measurements in the rough-wall flow.

The integration time used for the rms voltage signals was 33.0 seconds. This value was determined by placing the 55F04 horizontal wire in the inner regions of a fully rough flow. Then sample voltages were taken using different averaging times. The standard deviations of these samples were calculated and it was found that the value of the standard deviation at first decreased very quickly, and then very slowly as the integration time increased. For averaging times of 33.0 seconds and greater, the standard deviation appeared to be almost constant. Between data readings, three rms time constants were allowed to pass before new readings were taken. When rms voltages were measured for the determination of $-\overline{u'v'}$ for $C_f/2$, the average of three consecutive stable rms values was used for the calculations.

The hot-wire probes were calibrated for both mean and fluctuating signals using methods described by Pimenta (1975) and Coleman (1976). The calibrations were made in a constant-temperature jet produced by a 20:1 contraction ASME nozzle. The velocities of the jet were measured using two manometers: a Combust micromanometer for low velocities, and a Mariam inclined manometer for high velocities. The pressure ranges of the manometers always overlapped, and the two manometers were always compared to see if the

same reading was obtained by both devices. The same temperature used for an individual calibration was used for measurements in the HMT-1 and HMT-18 tunnels, where the freestream temperatures in the tunnels were checked before every profile using the freestream temperature probes discussed earlier. The wire cold resistances were also checked at least once per profile in order to maintain the same conditions in the wind tunnels as were used for the calibrations.

The freestream velocities measured by the hot wires were checked by comparing to values obtained using a Kiel-type pressure probe and an inclined manometer. The calibrations were further verified by measuring the Reynolds stress tensor components in a fully developed two-dimensional channel documented by Hussain and Reynolds (1975). These channel measurements, as well as the calibrations, were occasionally repeated to check equipment or to verify probe conditions.

The positions of the probes with respect to the probe wall stops were determined using an optical comparator. This allowed accurate determination of the distance of the probe from the crests of the roughness elements for profile measurements in the HMT-18 wind tunnel. This also allowed determination of probe distance from the smooth wall in the HMT-1 wind tunnel. The experimental procedure for locating the probe stop at the wall for a profile was the same as that used by Pimenta (1975).

The equations used to determine the Reynolds stress tensor components are based on Jorgensen's directional sensitivity equation for hot-wire probes (see Coleman (1976)), given as

$$u_{eff}^2 = u_2^2 + k_1^2 v_2^2 + k_2^2 w_2^2 \qquad \text{(II-4)}$$

where u_2, v_2, and w_2 are the velocity components in a wire coordinate system, and k_1 and k_2 are the directional sensitivity coefficients of the probe. In the wire coordinate system, u_2 and w_2 represent velocities normal to the wire, with u_2 in the plane of the prongs; and v_2 represents velocities tangent to the direction of the wire. In the present study, $k_1 = 0.20$ and $k_2 = 1.02$.

In a laboratory coordinate system, (II-4) may be rewritten as

$$u_{eff}^2 = Au_1^2 + Bv_1^2 + Cw_1^2 + Du_1w_1 + Ev_1w_1 + Fu_1w_1 \qquad \text{(II-5)}$$

where

$$\begin{aligned}
A &= \cos^2\phi + k_1^2 \sin^2\phi, \\
B &= (\sin^2\phi + k_1^2 \cos^2\phi)\cos^2\theta + k_2^2 \sin^2\theta, \\
C &= (\sin^2\phi + k_1^2 \cos^2\phi)\sin^2\theta + k_2^2 \cos^2\theta, \\
D &= (1-k_1^2)\sin 2\phi \cos\theta, \\
E &= (\sin^2\phi + k_1^2 \cos^2\phi - k_2^2)\sin 2\theta, \\
F &= (1-k_1^2)\sin 2\phi \sin\theta.
\end{aligned} \qquad \text{(II-6)}$$

In Eqn. (II-6), θ represents the rotation of the hot wire about the probe axis and ϕ represents the slant of the hot wire measured relative to a normal to the probe axis (see Coleman (1976)). Eqn. (II-5) can then be further rearranged to become

$$\overline{u_{eff}'^2} = A\,\overline{u'^2} + \frac{D^2}{4A}\overline{v'^2} + \frac{F^2}{4A}\overline{w'^2} + D\,\overline{u'v'} + \frac{DF}{2A}\overline{v'w'} + F\,\overline{u'w'} + O(3) \qquad \text{(II-7)}$$

and

$$U_{eff} = \sqrt{A}\,U + O(2) \qquad \text{(II-8)}$$

when

$$\begin{aligned}
u_1 &= U + u' \\
v_1 &= v' \\
w_1 &= w'
\end{aligned} \qquad \text{(II-9)}$$

For the present study, Eqns. (II-7) and (II-8) were used to determine the Reynolds stress tensor components. For the smooth-wall wind tunnel tests, after $\overline{u'^2}$ was measured using the horizontal wire, the rotatable slant-wire was used with three rotations (θ = 45°, 90°, and 135°) to

determine $\overline{w'^2}$, $\overline{v'^2}$, and $-\overline{u'v'}$. For the rough-wall tests, the horizontal wire was first used to determine $\overline{u'^2}$. Then $-\overline{u'v'}$ and $\overline{v'^2}$ were determined using the slant wire with $\theta = 0°$ and $\theta = 180°$, and $\overline{u'w'}$ and $\overline{w'^2}$ were determined using the slant wire with $\theta = 90°$ and $\theta = 270°$. Finally, $\overline{v'w'}$ was determined using the slant-wire probe with $\theta = 45°$.

II.6 SPECTRA OF THE LONGITUDINAL VELOCITY FLUCTUATIONS

Spectra measurements were made using techniques developed by Kerschen (1977) which incorporate the averaged periodogram method described by Rabiner and Gold (1975). A schematic of the apparatus used for the measurements is shown in Fig. II-1.

In Fig. II-1, after leaving the hot-wire anemometer bridge and linearizer, the signal passes through four low-pass Spencer-Kennedy laboratory filters connected in series. All signals above 8000 Hz were removed to avoid the possibility of aliasing in later signal processing. The gain and broad-band frequency characterstics of the filter system were checked using a sine-wave input and were accounted for in data reduction. A Bruel and Kjaer Model 2010 Heterodyne Analyzer was used to remove the DC portion of the signal and to amplify the fluctuating portion above 2 Hz. The continuous signal was then converted to digital samples using a Hewlett-Packard 2440A analog-digital interface, which provides a resolution of 12 bits and a choice of several different sampling rates. For the present measurements, a sampling rate of 20,000 Hz was used. 2048 data samples were taken from the signal, providing a maximum spectral resolution of 9.77 Hz.

The digital samples were processed using a computer program called PIPE (see Kerschen and Johnston (1978)), which was stored on a Hewlett-Packard 2100 minicomputer. The program first operates on the digital samples using a Hamming data window, and then discrete Fourier transforms each sample. Spectra were averaged in ensembles of 64, where the ensemble means were monitored during measurements every two integrations to check convergence. After ensemble averaging, the PIPE program averages the spectra over bandwidths of 31.6 Hz, and then normalizes them to a 1 Hz bandwidth for printout. Since the computer analysis took place in real time, the total length of time for the processing of all samples was 7-8 minutes.

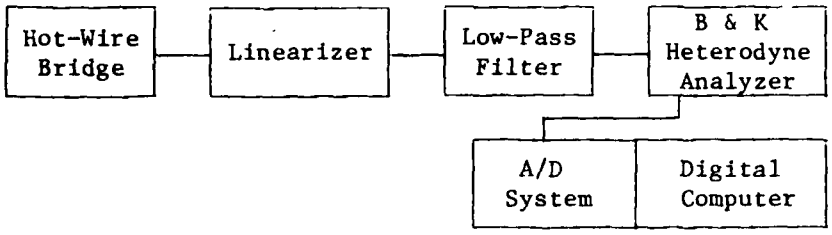

Fig. II-1. Schematic of equipment used for spectra measurements.

For all measurements, root mean squares of the fluctuating signal were determined from the spectra and showed agreement witn analog measurements within a few per cent. The spectra measurement techniques were further checked by comparing measurements with those of Hussain and Reynolds (1975) in a fully developed two-dimensional channel flow for $y/\delta = .0856$, 0.625, and 1.000. The spectra from the present study showed good agreement with the measurements of Hussain and Reynolds, with a few per cent difference in the low wave number regions.

The hot-wire probe used for the rough-wall spectra measurements discussed in Section 3.4 was the 0.45 mm DISA 55A53 probe, which is designated C in Table III-1. The probe used for the smooth-wall channel measurements was the 1.25 mm DISA 55F04 probe, which is designated B in Table III-1. These wire lengths were used to minimize high wave-number error caused by eddy averaging across wires having a finite length.

A discussion of the effects of wire length on spectra measurements is presented in Appendix III.

Appendix III

THE EFFECT OF SENSOR LENGTH OF HOT-WIRE ANEMOMETRY PROBES ON THE MEASUREMENT OF TURBULENCE INTENSITY IN A FULLY ROUGH TURBULENT BOUNDARY LAYER

III.1 INTRODUCTION AND PRIOR WORK

Many investigators, including Pao (1965), Laufer (1954), and Klebanoff (1954), have encountered the problem of a finite hot-wire sensing length in the measurement of small-scale turbulence. The effects are most apparent in high wave-number regions of spectra of turbulence intensity and can be compensated using one of several correction methods discussed in the literature. One of the earliest of these is presented in the form of a wire-length correction formula by Uberoi and Kovasznay (1953). Frenkiel (1954) also discusses the problem and expresses the effect of wire length in terms of the integral length scales of a turbulent field. For large $\ell/\mathcal{L}_y$, where $\mathcal{L}_y$ is the integral length scale for the energy-containing eddies in the y direction, Frenkiel says that the ratio of the measured to actual turbulence intensity, $\overline{u'^2}_m/\overline{u'^2}$, is proportional to the inverse of the length of the wire sensor. Later, Wyngaard (1968) quantified the effects of wire length by relating the one-dimensional wavenumber, k_1, to wire length, ℓ, and Kolmogorov length scale, η. His results are very convenient to use and express measured $f_u(k_1)_m$ to actual $f_u(k_1)$ in figures in which $f_u(k_1)_m/f_u(k_1)$ is plotted versus $k_1\ell$ and parametric in η/ℓ. Wyngaard's method is based on a correction to Pao's (1965) equation for one-dimensional spectra and shows agreement with measurements in a curved mixing layer where $\eta = 6.1 \times 10^{-3}$ cm. His technique is used by many investigators, including Champagne (1978) and Perry and Abell (1977). Willmarth (1977) circumvented the problem of small wire length entirely by developing probes with sensing lengths as small as 100 μm. His measurements using these small hot wires are significant, since they show the existing standards for smooth-wall turbulence intensity in the inner 15% of smooth-wall boundary layers (i.e., Klebanoff (1954)) to be seriously in error.

III.2 PRESENT EXPERIMENT

The purpose of the present experiment was to quantify the effect of wire length on the measurement of turbulence intensity $\overline{u'^2}$ in a fully rough turbulent boundary layer. The magnitudes of errors caused by eddy averaging from the wires were to be separated from any errors resulting from transient thermal effects which might influence $\overline{u'^2}$ measurement. Descriptions of the hot-wire sensing elements used for the experiment are presented in Table III-1

Table III-1

Hot-Wire Sensing Elements

Designation	Wire Type - Sensor Material	Gold-Plated	ℓ(mm)	d(μm)
A	Tungsten (platinum-plated)	No	3.00	5.0
B	DISA 55F04-tungsten (plat.-pltd.)	Yes	1.25	5.0
C	DISA 55A53-tungsten (plat.-pltd.)	No	0.45	5.0
D	Platinum	No	0.45	5.0
E	Platinum	No	0.45	2.0

III.3 EXPERIMENTAL RESULTS

Figures III-1 and III-2 show measurements of $\overline{u'^2}$ in the fully rough turbulent boundary layer and in a fully developed, two-dimensional, smooth channel, respectively. Measurements using all of the hot wires described in Table III-1 are shown in III-1, whereas only measurements using those designated A, B, and C are shown in III-2. Spectra taken in the fully rough turbulent boundary layer using all five sensors are shown in Fig. III-3 for $y'/\delta = .078$ and in Fig. III-4 for $y'/\delta = .600$.

Transient thermal effects are detected by comparing signals from wire sensors having different transient conduction losses from the wire to the support prongs. Different heat transfer boundary conditions are produced by changing the diameter and material of the sensors while the length is held constant. The wires designated C, D, and E in Table III-1 are used for this purpose. Results shown in Figs. III-1, III-3, and III-4 indicate

that transient thermal conduction does not influence the measurement of turbulence intensity, $\overline{u'^2}$, or spectra of $\overline{u'^2}$, since these quantities are the same for wires C, D, and E. Such behavior is not surprising, because any deviations between measurements using these probes caused by transient thermal effects would be the result of a failure of the hot-wire bridge electronics to maintain a constant temperature distribution along the lengths of the wire sensors with time.

The distributions of $\overline{u'^2}$ measured using the hot wires designated A, B, and C are different in the inner 30% of the fully rough turbulent boundary layer, as shown in Fig. III-1. Since transient-conduction effects do not seem to affect these results and since each wire sensor has the same diameter and consists of the same material, the differences observed in Fig. III-1 are related to the varying sensing lengths of the hot-wire probes. Fig. III-3 shows that at $y'/\delta = .078$ these differences occur in the high-frequency end of the spectra. These high-frequency differences are significant, because they account for as much as 10% of the total magnitude of $\overline{u'^2}$ and extend to frequencies low enough to be well inside the inertial subrange. As y'/δ increases, the differences in the measured values of $\overline{u'^2}/U_\infty^2$ versus y/δ and $f_u(n)$ versus n for the three probes diminish, as shown in Figs. III-1 and III-4. Additionally, Fig. III-2 shows that the same three probes produce identical distributions of $\overline{u'^2}$ in the outer 90% of a fully developed, smooth-wall channel flow.

The variations in the differences in the measured spectra and total magnitude of $\overline{u'^2}$ using sensing wires having different lengths are a result of the fact that hot wires measure the average value of $\overline{u'^2}$ along their length. Contributions to measured $\overline{u'^2}$ by eddies with characteristic lengths smaller than the length of the wires are diminished to values less than actually exist. Usually, more eddies are averaged as the sensing length, ℓ, increases, resulting in decreases in the apparent magnitude of $\overline{u'^2}$. According to Wyngaard (1968), the amount of this averaging is dependent on the ratio of wire length to the Kolmogorov length scale, ℓ/η, and the wave number/wire length product, $k_1\ell$, where negligible error occurs when $\ell/\eta \sim 1.0$. Thus, the differences between the measured value of $\overline{u'^2}$ using hot wires A, B, and C are larger at some measuring locations than at others, due to variations in the value of η in the flows. In

the present rough-wall flow, $\eta = 4.10 \times 10^{-3}$ cm at $y'/\delta = .078$ and $\eta = 6.44 \times 10^{-3}$ cm at $y'/\delta = .600$.

Figures III-3 and III-4 also show the spectra corrected to account for the effects of wire length, using the method recommended by Wyngaard (1968). For all of the sensors used in the present experiment, the same corrected spectra resulted at $y'/\delta = .078$ and at $y'/\delta = .600$. The figures show these corrected spectra to be in close agreement for the range of frequency shown, with the measurements made using the wires having the 0.45 mm sensing lengths (even though spectra measured using .45 mm sensing lengths may be in error for $n > 6000$ Hz). Moreover, the $\ell = .045$ mm hot-wire measurements are in agreement with the universal small-scale behavior given by Pao's (1965) equation for $\overline{u'^2}$ spectra, as shown in Fig. 3-29. The Wyngaard (1968) correction method to account for the effects of $\overline{u'^2}$ averaging along the lengths of the hot wires is then consistent with the present measurements, and is recommended for future corrections.

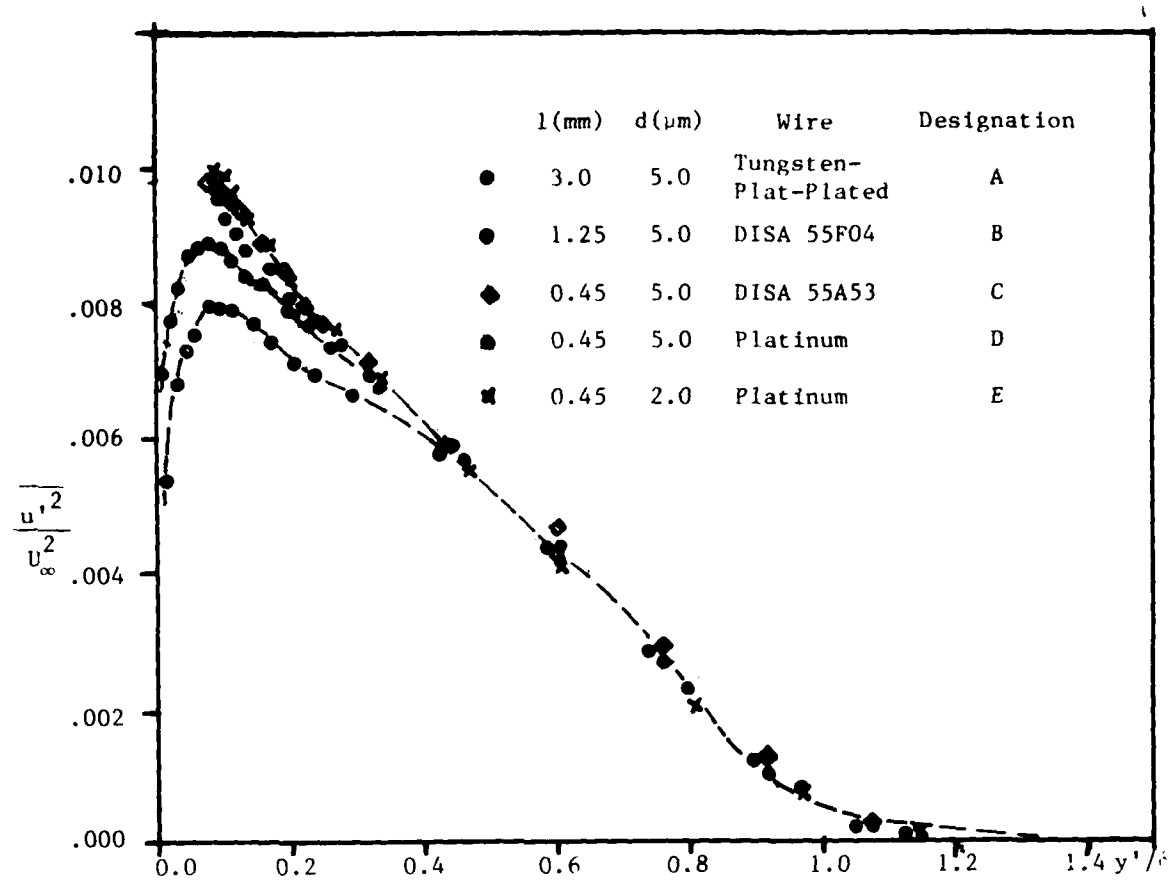

Fig. III-1. Longitudinal turbulence intensity profiles in a fully rough turbulent boundary layer measured using hot wires with different sensing lengths.

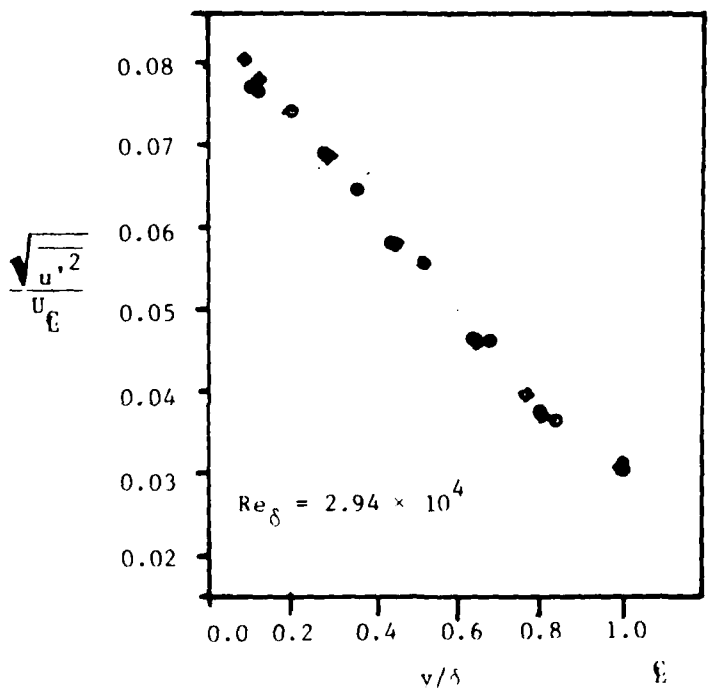

Fig. III-2. Longitudinal turbulence intensity profiles in a fully developed two-dimensional channel flow measured using hot wires with different sensing lengths.

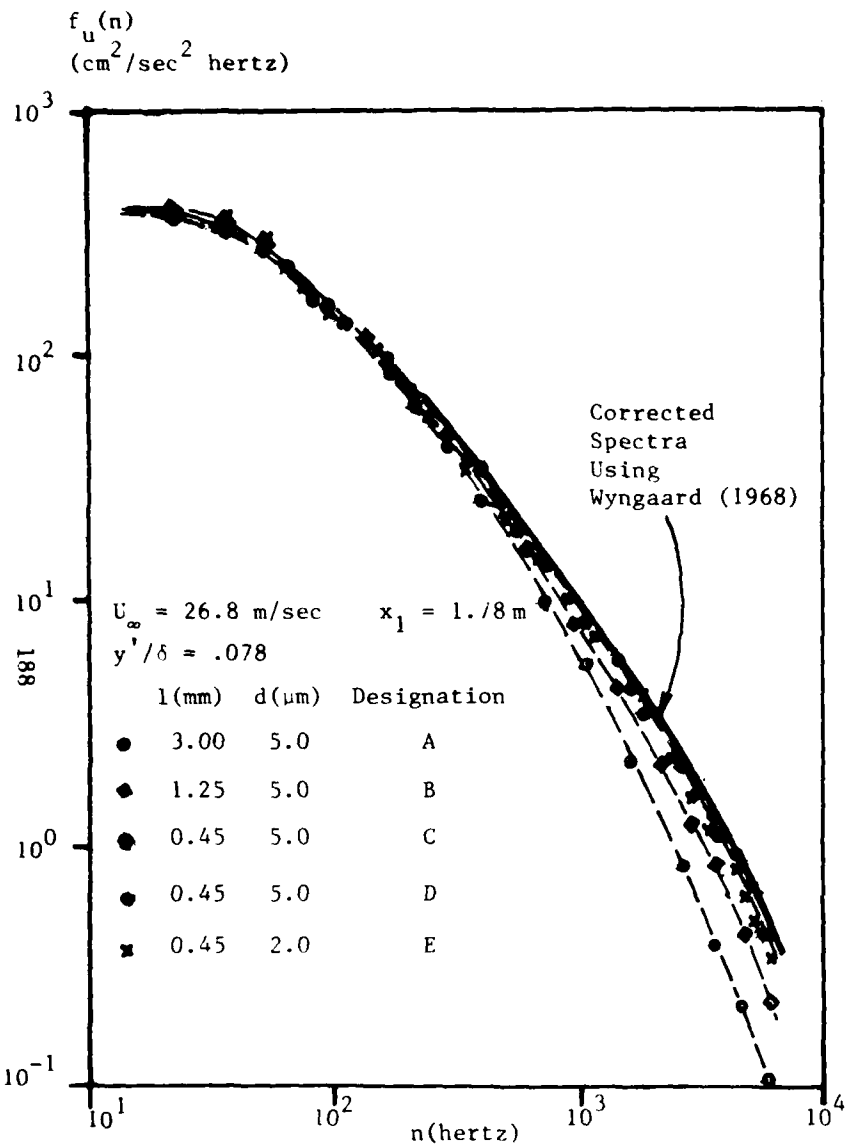

Fig. III-3. Spectra of longitudinal turbulence intensity in a fully rough turbulent boundary layer, y'/δ = .078, measured using hot wires with different sensing lengths.

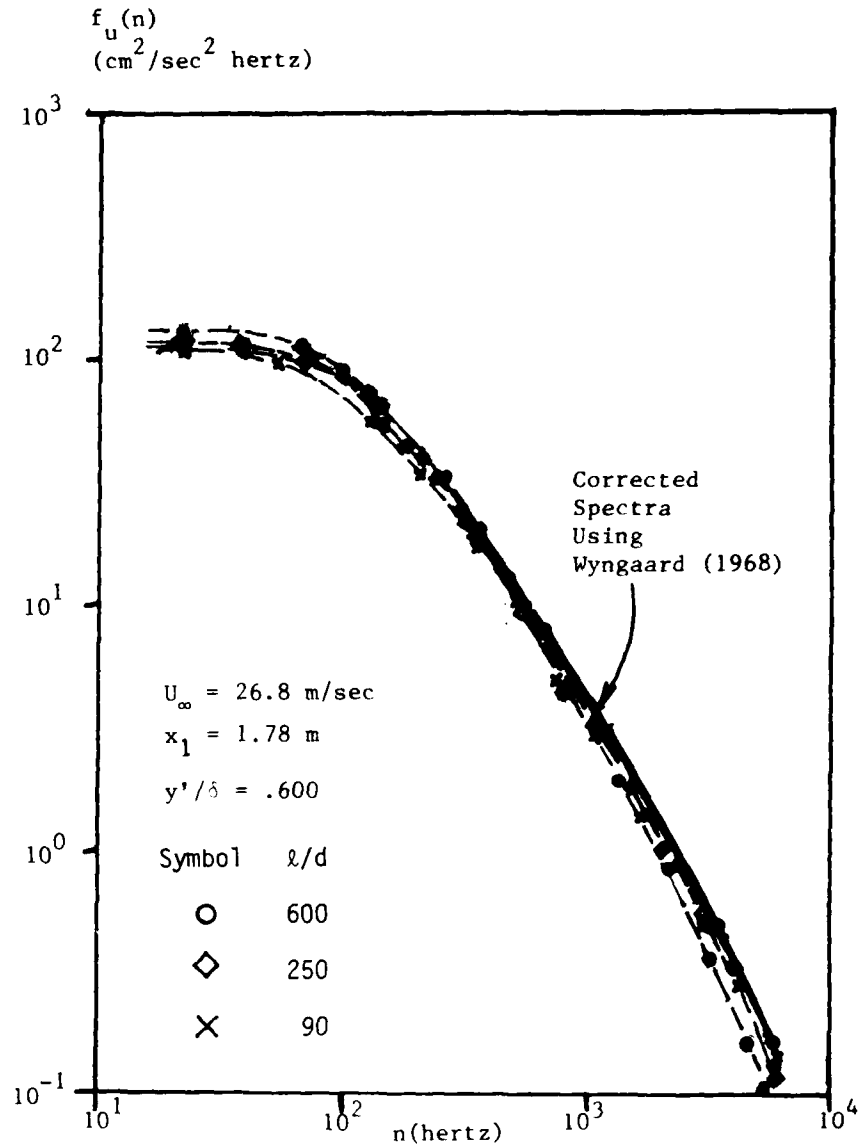

Fig. III-4. Spectra of longitudinal turbulence intensity in a fully rough turbulent boundary layer, y'/δ = .600, measured using hot wires with different sensing lengths.

Appendix IV

TABULATION OF EXPERIMENTAL DATA

This appendix provides tabular listings of the experimental data of this investigation. Smooth-wall data are first presented in the following order: (1) Stanton numbers, (2) mean velocity profiles, and (3) Reynolds stress tensor component profiles. Then rough-wall data are presented in the following order: (1) Stanton numbers, (2) mean temperature profiles, (3) mean velocity profiles, (4) Reynolds stress tensor component profiles, and (5) spectra of longitudinal velocity fluctuations.

Abbreviations used in the listings follow.

CF/2	Skin friction coefficient, $C_f/2$.
DE	Hydrodynamic boundary layer thickness, δ (cm).
DE1	Displacement thickness, δ_1 (cm).
DE2	Momentum thickness, δ_2 (cm).
DEH	Thermal boundary layer thickness, Δ (cm)
DEH2	Enthalpy thickness, Δ_2 (cm).
DELY	Distance between ball crests and velocity virtual origin, Δy (cm).
F	Blowing fraction, $F = \rho_o V_o/\rho_\infty U_\infty$.
FU(K1)	$\overline{u'^2}$ turbulent energy associated with k_1, $f_u(k_1)$ (cm^3/sec^2).
FU(N)	$\overline{u'^2}$ turbulent energy associated witn n, $f_u(n)$ (cm^2/sec^2Hz).
G	Clauser shape factor, G.
H	Karman shape factor, $H = \delta_1/\delta_2$.
K1	One-dimensional wave number, $k_1 = 2\pi n/U$ (cm^{-1}).
L/D	Hot-wire sensor length-to-diameter ratio, ℓ/d.
N	Frequency, n. (Hertz).
PAMB	Ambient pressure, mercury barometer (cm).
PL,PLATE	Plate number (HMT-18 rig).
PORT	Port number (HMT-1 rig).

PT	Point number in profile.
Q2/UINF2	$\overline{q^2}/U_\infty^2$.
REDEH2	Enthalpy thickness Reynolds number, Re_{Δ_2}.
REK	Roughness Reynolds number, $Re_k = U_\tau k_s/\nu$.
REM	Momentum thickness Reynolds number, Re_{δ_2}.
REX2	x_2 Reynolds number, Re_{x_2}.
RH	Relative humidity.
RQ2	$-\overline{u'v'}/\overline{q^2}$.
RUV	$-\overline{u'v'}/\sqrt{\overline{u'^2}\ \overline{v'^2}}$.
RUN	Date (month, day, year).
ST	Stanton number, St.
T	Mean static temperature, T (°C).
T^+	$T^+ = T/T_\tau = T/(\dot{q}_o''/\rho C_p U_\tau)$.
TBAR	$(T_w - T)/(T_w - T_\infty)$.
TDB	Dry bulb temperature (°C).
TINF	Freestream static temperature, T_∞ (°C).
TINFO	Freestream total temperature, $T_{\infty,o}$ (°C).
TW	Wall temperature, T_w (°C).
TWB	Wet bulb temperature (°C).
U	Mean velocity, U (m/sec).
U+	U/U_τ.
UINF	Freestream velocity, U_∞ (m/sec).
UTAU	Friction velocity, U_τ (m/sec).
U/UINF	U/U_∞.
-U'V'/UINF2	$-\overline{u'v'}/U_\infty^2$.
U'2	$\overline{u'^2}$ (m^2/sec^2).
U'2/UINF2	$\overline{u'^2}/U_\infty^2$.

V'2/UINF2	$\overline{v'^2}/U_\infty^2$.
W'2/UINF2	$\overline{w'^2}/U_\infty^2$.
X1	Distance along test surface, x_1 (m).
X2	Distance from hydrodynamic virtual origin, x_2 (m).
XI	Unheated starting length, ξ (m).
Y	Distance normal to test surface measured from velocity virtual origin, $y = y' + \Delta y$ (cm).
Y'	Distance normal to test surface measured from ball crests, y' (cm).
Y+	$y^+ = yU_\tau/\nu$.
Y/DE	y/δ.
Y'/DE	y'/δ.
Y/DEH2	y/Δ_2.

SMOOTH WALL STANTON NO. RUN UINF=10.1M/SEC
ARTIFICIALLY THICKENED XI= 3.82M

RUN = 90976 TINFO = 18.04 TINF = 17.99
UINF = 10.00 RH = 0.47 PAMB = 75.77

PL	X1	X2	ST	DEH2	REDEH2	REX2	TW
1	0.05	2.65	0.00000	0.000	0.	0.18E 07	
2	0.15	2.76	0.00000	0.000	0.	0.18E 07	
3	0.25	2.86	0.00000	0.000	0.	0.19E 07	
4	0.36	2.96	0.00000	0.000	0.	0.20E 07	
5	0.46	3.06	0.00000	0.000	0.	0.20E 07	
6	0.56	3.16	0.00000	0.000	0.	0.21E 07	
7	0.66	3.26	0.00000	0.000	0.	0.22E 07	
8	0.76	3.37	0.00000	0.000	0.	0.22E 07	
9	0.86	3.47	0.00000	0.000	0.	0.23E 07	
10	0.97	3.57	0.00000	0.000	0.	0.24E 07	
11	1.07	3.67	0.00000	0.000	0.	0.24E 07	
12	1.17	3.77	0.00000	0.000	0.	0.25E 07	
13	1.27	3.87	0.00362	0.033	223.	0.26E 07	34.60
14	1.37	3.97	0.00264	0.065	434.	0.27E 07	34.69
15	1.47	4.08	0.00255	0.091	608.	0.27E 07	34.76
16	1.57	4.18	0.00244	0.117	778.	0.28E 07	34.73
17	1.68	4.28	0.00236	0.141	938.	0.29E 07	34.79
18	1.78	4.38	0.00231	0.165	1097.	0.29E 07	34.77
19	1.88	4.48	0.00226	0.187	1248.	0.30E 07	34.82
20	1.98	4.58	0.00221	0.211	1405.	0.31E 07	34.75
21	2.08	4.69	0.00217	0.234	1555.	0.31E 07	34.72
22	2.18	4.79	0.00216	0.255	1699.	0.32E 07	34.75
23	2.29	4.89	0.00214	0.277	1840.	0.33E 07	34.79
24	2.39	4.99	0.00209	0.295	1987.	0.33E 07	34.75

SMOOTH WALL STANTON NO. RUN UINF=10.1M/SEC
ARTIFICIALLY THICKENED W/F=.004 PLTS 1-4 XI=2.96M

RUN = 100976 TINFO = 17.42 TINF = 17.37
UINF = 10.13 RH = 0.69 PAMB = 75.69

PL	X1	X2	ST	DEH2	REDEH2	REX2	TW
1	0.05	3.01	0.00321	0.046	308.	0.20E 07	34.33
2	0.15	3.12	0.00181	0.112	747.	0.21E 07	34.58
3	0.25	3.22	0.00149	0.167	1130.	0.22E 07	34.63
4	0.36	3.32	0.00125	0.222	1506.	0.23E 07	34.51
5	0.46	3.42	0.00194	0.259	1755.	0.23E 07	34.49
6	0.56	3.52	0.00221	0.279	1892.	0.24E 07	34.54
7	0.66	3.62	0.00213	0.303	2049.	0.25E 07	34.48
8	0.76	3.72	0.00211	0.323	2184.	0.25E 07	34.56
9	0.86	3.83	0.00204	0.346	2340.	0.26E 07	34.46
10	0.97	3.93	0.00204	0.365	2467.	0.27E 07	34.55
11	1.07	4.03	0.00202	0.387	2608.	0.27E 07	34.54
12	1.17	4.13	0.00201	0.407	2746.	0.28E 07	34.54
13	1.27	4.23	0.00201	0.432	2917.	0.29E 07	34.34
14	1.37	4.33	0.00198	0.450	3036.	0.29E 07	34.44
15	1.47	4.44	0.00199	0.470	3177.	0.30E 07	34.41
16	1.57	4.54	0.00198	0.488	3299.	0.31E 07	34.49
17	1.68	4.64	0.00198	0.509	3445.	0.31E 07	34.44
18	1.78	4.74	0.00194	0.526	3559.	0.32E 07	34.54
19	1.88	4.84	0.00194	0.547	3710.	0.33E 07	34.46
20	1.98	4.94	0.00195	0.564	3824.	0.33E 07	34.56
21	2.08	5.05	0.00192	0.587	3972.	0.34E 07	34.49
22	2.18	5.15	0.00194	0.608	4106.	0.35E 07	34.48
23	2.29	5.25	0.00195	0.626	4216.	0.35E 07	34.58
24	2.39	5.35	0.00191	0.648	4368.	0.36E 07	34.50

SMOOTH WALL STANTCN NC. RUN UINF=10.1M/SEC
ARTIFICIALLY THICKENED XI= 2.60M

RUN = 82076 TINFO = 16.78 TINF = 16.73
UINF = 10.05 RH = 0.72 PAMB = 75.59

PL	X1	X2	ST	DFH2	REDEH2	REX2	TW
1	0.05	2.65	0.00533	0.040	271.	0.18E 07	35.25
2	0.15	2.76	0.00323	0.084	559.	0.18E 07	35.42
3	0.25	2.86	0.00285	0.115	768.	0.19E 07	35.38
4	0.36	2.96	0.00262	0.142	956.	0.20E 07	35.34
5	0.46	3.06	0.00247	0.168	1127.	0.21E 07	35.40
6	0.56	3.16	0.00242	0.193	1296.	0.21E 07	35.36
7	0.66	3.26	0.00232	0.217	1458.	0.22E 07	35.36
8	0.76	3.37	0.00227	0.240	1615.	0.23E 07	35.36
9	0.86	3.47	0.00220	0.262	1765.	0.23E 07	35.39
10	0.97	3.57	0.00218	0.285	1916.	0.24E 07	35.38
11	1.07	3.67	0.00216	0.306	2059.	0.25E 07	35.43
12	1.17	3.77	0.00212	0.329	2209.	0.25E 07	35.38
13	1.27	3.87	0.00212	0.351	2364.	0.26E 07	35.31
14	1.37	3.97	0.00207	0.370	2495.	0.27E 07	35.40
15	1.47	4.08	0.00207	0.392	2639.	0.27E 07	35.38
16	1.57	4.18	0.00202	0.415	2787.	0.28E 07	35.33
17	1.68	4.28	0.00200	0.435	2926.	0.29E 07	35.31
18	1.78	4.38	0.00197	0.454	3049.	0.29E 07	35.39
19	1.88	4.48	0.00199	0.476	3199.	0.30E 07	35.31
20	1.98	4.58	0.00198	0.496	3332.	0.31E 07	35.32
21	2.08	4.69	0.00194	0.515	3465.	0.32E 07	35.32
22	2.18	4.79	0.00196	0.536	3600.	0.32E 07	35.31
23	2.29	4.89	0.00198	0.554	3718.	0.33E 07	35.39
24	2.39	4.99	0.00195	0.576	3868.	0.34E 07	35.32

SMOOTH WALL STANTON NO. RUN UINF=10.1M/SEC
ARTIFICIALLY THICKENED XI= 3.21M

RUN = 82176 TINFO = 19.10 TINF = 19.06
UINF = 10.10 RH = 0.72 PAMB = 75.59

PL	X1	X2	ST	DFH2	REDEH2	REX2	TW
1	0.05	2.65	0.00000	0.000	0.	0.18E 07	
2	0.15	2.76	0.00000	0.000	0.	0.18E 07	
3	0.25	2.86	0.00000	0.000	0.	0.19E 07	
4	0.36	2.96	0.00000	0.000	0.	0.20E 07	
5	0.46	3.06	0.00000	0.000	0.	0.20E 07	
6	0.56	3.16	0.00000	0.000	0.	0.21E 07	
7	0.66	3.26	0.00381	0.023	151.	0.22E 07	36.73
8	0.76	3.37	0.00276	0.055	368.	0.22E 07	37.03
9	0.86	3.47	0.00259	0.082	547.	0.23E 07	37.09
10	0.97	3.57	0.00249	0.108	720.	0.24E 07	37.09
11	1.07	3.67	0.00240	0.133	887.	0.24E 07	37.04
12	1.17	3.77	0.00236	0.158	1048.	0.25E 07	37.04
13	1.27	3.87	0.00233	0.181	1206.	0.26E 07	37.06
14	1.37	3.97	0.00225	0.204	1358.	0.27E 07	37.09
15	1.47	4.08	0.00227	0.227	1511.	0.27E 07	37.10
16	1.57	4.18	0.00222	0.251	1669.	0.28E 07	37.02
17	1.68	4.28	0.00220	0.273	1814.	0.28E 07	37.07
18	1.78	4.38	0.00217	0.295	1962.	0.29E 07	37.07
19	1.88	4.48	0.00216	0.316	2106.	0.30E 07	37.09
20	1.98	4.58	0.00211	0.339	2253.	0.30E 07	37.07
21	2.08	4.69	0.00208	0.360	2397.	0.31E 07	37.05
22	2.18	4.79	0.00209	0.380	2525.	0.32E 07	37.14
23	2.29	4.89	0.00209	0.402	2672.	0.32E 07	37.11
24	2.39	4.99	0.00207	0.424	2821.	0.33E 07	37.05

SMOOTH WALL MEAN VELOCITY PROFILE
ARTIFICIALLY THICKENED UINF=10.1 M/SEC

RUN	=	81676	DE	=	4.455
PORT	=	7	DE1	=	0.869
X1	=	0.36	DE2	=	0.626
X2	=	2.96	H	=	1.39
UINF	=	10.12	G	=	6.92
CF/2	=	0.00163	REX2	=	0.20E 07
UTAU	=	0.409	REH	=	4160.2

PT	Y	Y/DE	Y+	U	U/UINF	U+
1	0.025	0.00570	6.81	2.86	0.283	7.00
2	0.028	0.00627	7.49	3.13	0.310	7.67
3	0.030	0.00684	8.17	3.21	0.317	7.85
4	0.033	0.00741	8.85	3.30	0.326	8.07
5	0.036	0.00798	9.53	3.37	0.333	8.25
6	0.038	0.00855	10.22	3.42	0.338	8.37
7	0.041	0.00912	10.90	3.55	0.351	8.70
8	0.046	0.01026	12.26	3.85	0.380	9.42
9	0.051	0.01140	13.62	4.08	0.403	9.99
10	0.058	0.01311	15.66	4.43	0.438	10.84
11	0.066	0.01482	17.71	4.57	0.452	11.20
12	0.079	0.01767	21.11	4.96	0.490	12.13
13	0.091	0.02053	24.52	5.19	0.513	12.72
14	0.117	0.02623	31.33	5.47	0.540	13.38
15	0.168	0.03763	44.95	5.79	0.572	14.17
16	0.218	0.04903	58.57	6.09	0.602	14.90
17	0.282	0.06329	75.59	6.21	0.614	15.20
18	0.345	0.07754	92.62	6.43	0.635	15.73
19	0.409	0.09179	109.64	6.50	0.642	15.91
20	0.472	0.10605	126.67	6.62	0.654	16.20
21	0.599	0.13455	160.72	6.79	0.672	16.63
22	0.726	0.16306	194.77	6.97	0.689	17.06
23	0.853	0.19157	228.82	7.12	0.704	17.44
24	0.980	0.22007	262.88	7.28	0.720	17.83
25	1.234	0.27709	330.98	7.49	0.741	18.34
26	1.488	0.33410	399.08	7.69	0.760	18.83
27	1.996	0.44813	535.28	8.19	0.810	20.06
28	2.504	0.56216	671.49	8.56	0.846	20.96
29	3.139	0.70469	841.74	8.99	0.889	22.02
30	3.774	0.84723	1012.00	9.41	0.930	23.04
31	4.409	0.98976	1182.26	9.99	0.987	24.45
32	5.044	1.13230	1352.51	10.11	1.000	24.76
33	5.806	1.30334	1556.82	10.12	1.000	24.77
34	6.314	1.41737	1693.02	10.12	1.000	24.77

SMOOTH WALL MEAN VELOCITY PROFILE
ARTIFICIALLY THICKENED UINF=10.1 M/SEC

RUN	=	81676	DE	=	4.969
PORT	=	15	DE1	=	0.955
X1	=	0.76	DE2	=	0.691
X2	=	3.36	H	=	1.38
UINF	=	10.06	G	=	6.98
CF/2	=	0.00157	REX2	=	0.22E 07
UTAU	=	0.399	REH	=	4571.1

PT	Y	Y/DE	Y+	U	U/UINF	U+
1	0.026	0.00511	6.66	3.00	0.298	7.53
2	0.028	0.00562	7.33	3.09	0.307	7.74
3	0.030	0.00613	7.99	3.20	0.318	8.03
4	0.033	0.00665	8.66	3.33	0.331	8.35
5	0.036	0.00716	9.32	3.46	0.344	8.68
6	0.041	0.00818	10.66	3.74	0.372	9.39
7	0.048	0.00971	12.65	4.01	0.399	10.06
8	0.061	0.01227	15.98	4.42	0.440	11.10
9	0.086	0.01738	22.64	4.98	0.495	12.50
10	0.112	0.02249	29.30	5.25	0.522	13.17
11	0.137	0.02760	35.96	5.45	0.541	13.66
12	0.201	0.04038	52.61	5.79	0.575	14.52
13	0.264	0.05316	69.26	5.97	0.594	14.99
14	0.328	0.06594	85.91	6.13	0.609	15.38
15	0.391	0.07872	102.56	6.32	0.628	15.86
16	0.456	0.09150	119.21	6.46	0.642	16.20
17	0.518	0.10428	135.86	6.55	0.651	16.43
18	0.645	0.12984	169.15	6.83	0.679	17.13
19	0.772	0.15539	202.45	6.93	0.689	17.39
20	0.899	0.18095	235.75	7.08	0.704	17.77
21	1.026	0.20651	269.05	7.21	0.716	18.08
22	1.280	0.25763	335.64	7.42	0.738	18.62
23	1.534	0.30874	402.24	7.67	0.762	19.23
24	2.042	0.41098	535.43	8.05	0.800	20.19
25	2.550	0.51321	668.62	8.33	0.828	20.89
26	3.185	0.64100	835.11	8.71	0.865	21.84
27	3.820	0.76880	1001.60	9.18	0.912	23.02
28	4.455	0.89659	1168.09	9.67	0.961	24.27
29	5.090	1.02438	1334.58	10.01	0.995	25.11
30	6.360	1.27996	1667.55	10.05	0.999	25.20
31	6.955	1.40775	1834.04	10.05	0.999	25.22
32	7.376	1.48443	1933.94	10.06	1.000	25.24
33	7.630	1.53555	2000.53	10.06	1.000	25.24

SMOOTH WALL MEAN VELOCITY PROFILE
ARTIFICIALLY THICKENED UINF=10.1 M/SEC

RUN	=	81676	DE	=	5.717
PORT	=	23	DE1	=	0.957
X1	=	1.17	DE2	=	0.707
X2	=	3.77	H	=	1.35
UINF	=	10.14	G	=	6.74
CF/2	=	0.00150	REX2	=	0.25E 07
UTAU	=	0.393	REM	=	4668.4

PT	Y	Y/DE	Y+	U	U/UINF	U+
1	0.025	0.00444	6.50	3.01	0.297	7.68
2	0.028	0.00489	7.15	3.05	0.301	7.77
3	0.030	0.00533	7.80	3.26	0.322	8.31
4	0.033	0.00578	8.45	3.42	0.337	8.70
5	0.036	0.00622	9.09	3.56	0.351	9.08
6	0.046	0.00800	11.69	4.04	0.398	10.28
7	0.058	0.01022	14.94	4.53	0.447	11.54
8	0.084	0.01466	21.44	5.09	0.502	12.97
9	0.147	0.02577	37.68	5.58	0.551	14.23
10	0.211	0.03688	53.92	5.94	0.586	15.13
11	0.274	0.04799	70.16	6.27	0.619	15.98
12	0.338	0.05909	86.40	6.40	0.631	16.30
13	0.401	0.07020	102.64	6.49	0.640	16.53
14	0.465	0.08131	118.88	6.67	0.658	17.00
15	0.592	0.10353	151.36	6.86	0.676	17.46
16	0.719	0.12574	183.84	7.09	0.699	18.05
17	0.846	0.14796	216.32	7.20	0.710	18.33
18	0.973	0.17017	248.80	7.35	0.725	18.72
19	1.227	0.21461	313.77	7.60	0.750	19.37
20	1.481	0.25904	378.73	7.80	0.770	19.87
21	1.989	0.34790	508.65	8.10	0.800	20.65
22	2.497	0.43677	638.57	8.48	0.836	21.59
23	3.132	0.54785	800.98	8.77	0.866	22.35
24	3.767	0.65893	963.38	9.14	0.902	23.29
25	4.402	0.77001	1125.79	9.51	0.939	24.24
26	5.037	0.88109	1288.19	9.83	0.970	25.04
27	5.672	0.99217	1450.60	10.03	0.989	25.54
28	6.307	1.10325	1613.00	10.14	1.000	25.82
29	6.942	1.21433	1775.41	10.14	1.000	25.82

SMOOTH WALL MEAN VELOCITY PROFILE
ARTIFICIALLY THICKENED UINF=10.1 M/SEC

RUN	=	81676	DE	=	6.555
PORT	=	31	DE1	=	1.045
X1	=	1.57	DE2	=	0.771
X2	=	4.17	H	=	1.36
UINF	=	10.22	G	=	6.82
CF/2	=	0.00148	REX2	=	0.28E 07
UTAU	=	0.393	REM	=	5106.6

PT	Y	Y/DE	Y+	U	U/UINF	U+
1	0.025	0.00388	6.48	2.76	0.270	7.01
2	0.028	0.00426	7.12	2.80	0.273	7.11
3	0.030	0.00465	7.77	2.82	0.276	7.17
4	0.033	0.00504	8.42	2.98	0.292	7.58
5	0.036	0.00543	9.07	3.13	0.306	7.95
6	0.041	0.00620	10.36	3.46	0.339	8.80
7	0.046	0.00698	11.66	3.70	0.362	9.41
8	0.053	0.00814	13.60	3.98	0.389	10.12
9	0.066	0.01008	16.84	4.49	0.439	11.42
10	0.079	0.01201	20.07	4.84	0.473	12.30
11	0.091	0.01395	23.31	5.09	0.498	12.96
12	0.117	0.01783	29.79	5.35	0.524	13.61
13	0.180	0.02751	45.97	5.72	0.560	14.56
14	0.244	0.03720	62.16	5.95	0.583	15.14
15	0.371	0.05658	94.54	6.35	0.622	16.16
16	0.498	0.07595	126.92	6.66	0.652	16.95
17	0.625	0.09533	159.29	6.79	0.664	17.27
18	0.752	0.11470	191.67	6.99	0.684	17.77
19	0.879	0.13408	224.05	7.16	0.701	18.21
20	1.133	0.17283	288.80	7.40	0.724	18.83
21	1.387	0.21158	353.55	7.75	0.759	19.72
22	1.641	0.25033	418.30	7.83	0.766	19.91
23	2.149	0.32784	547.81	8.24	0.806	20.95
24	2.657	0.40534	677.32	8.53	0.835	21.70
25	3.292	0.50222	839.20	8.94	0.875	22.74
26	3.927	0.59910	1001.08	9.21	0.901	23.43
27	4.562	0.69599	1162.97	9.56	0.935	24.30
28	5.197	0.79285	1324.85	9.79	0.958	24.89
29	6.467	0.98661	1649.61	10.11	0.989	25.70
30	7.737	1.18037	1972.38	10.19	0.997	25.92
31	8.372	1.27725	2134.26	10.20	0.998	25.95
32	9.007	1.37412	2296.15	10.22	1.000	25.99
33	9.261	1.41288	2360.90	10.22	1.000	25.99

SMOOTH WALL MEAN VELOCITY PROFILE
ARTIFICIALLY THICKENED UINF=10.1 M/SEC

RUN	=	81676	DE	=	6.774
PORT	=	39	DE1	=	1.104
X1	=	1.98	DE2	=	0.813
X2	=	4.58	H	=	1.36
UINF	=	10.16	G	=	6.90
CF/2	=	0.00146	REX2	=	0.30E 07
UTAU	=	0.388	REM	=	5407.7

PT	Y	Y/DE	Y+	U	U/UINF	U+
1	0.025	0.00375	6.45	2.94	0.289	7.56
2	0.028	0.00412	7.10	2.92	0.288	7.53
3	0.030	0.00450	7.74	3.09	0.303	7.94
4	0.033	0.00487	8.39	3.25	0.319	8.36
5	0.036	0.00525	9.03	3.42	0.337	8.81
6	0.043	0.00637	10.97	3.77	0.371	9.70
7	0.056	0.00825	14.20	4.21	0.414	10.83
8	0.074	0.01087	18.71	4.68	0.460	12.05
9	0.099	0.01462	25.17	5.10	0.502	13.13
10	0.163	0.02400	41.30	5.62	0.553	14.46
11	0.226	0.03337	57.43	5.86	0.577	15.09
12	0.353	0.05212	89.70	6.17	0.607	15.88
13	0.490	0.07037	121.96	6.42	0.631	16.53
14	0.607	0.08962	154.23	6.68	0.657	17.19
15	0.734	0.10837	186.50	6.87	0.676	17.70
16	0.988	0.14587	251.03	7.16	0.704	18.43
17	1.242	0.18337	315.56	7.42	0.730	19.10
18	1.496	0.22087	380.09	7.62	0.750	19.62
19	2.004	0.29587	509.15	7.98	0.786	20.56
20	2.512	0.37086	638.22	8.30	0.817	21.38
21	3.147	0.46461	799.54	8.68	0.854	22.35
22	3.782	0.55836	960.87	8.99	0.885	23.16
23	4.417	0.65211	1122.20	9.29	0.914	23.92
24	5.052	0.74585	1283.53	9.55	0.940	24.60
25	5.687	0.83960	1444.86	9.78	0.962	25.19
26	6.322	0.93335	1606.19	9.98	0.982	25.69
27	6.957	1.02710	1767.52	10.08	0.992	25.97
28	7.592	1.12084	1928.84	10.14	0.998	26.12
29	8.227	1.21459	2090.17	10.16	1.000	26.17
30	8.862	1.30834	2251.50	10.16	1.000	26.17

SMOOTH WALL MEAN VELOCITY PROFILE
ARTIFICIALLY THICKENED UINF=10.1 M/SEC

RUN	=	81676	DE	=	7.238
PORT	=	45	DE1	=	1.165
X1	=	2.29	DE2	=	0.863
X2	=	4.89	H	=	1.35
UINF	=	10.03	G	=	6.82
CF/2	=	0.00144	REX2	=	0.32E 07
UTAU	=	0.381	REM	=	5671.8

PT	Y	Y/DE	Y+	U	U/UINF	U+
1	0.025	0.00351	6.33	2.87	0.286	7.53
2	0.028	0.00386	6.96	2.90	0.299	7.63
3	0.030	0.00421	7.60	3.16	0.315	8.29
4	0.033	0.00456	8.23	3.25	0.324	8.54
5	0.036	0.00491	8.86	3.38	0.337	8.88
6	0.041	0.00561	10.13	3.70	0.369	9.73
7	0.049	0.00667	12.03	4.01	0.399	10.52
8	0.074	0.01018	18.36	4.67	0.465	12.26
9	0.099	0.01369	24.69	5.07	0.505	13.31
10	0.124	0.01720	31.02	5.35	0.533	14.05
11	0.150	0.02070	37.35	5.55	0.553	14.56
12	0.201	0.02772	50.02	5.73	0.571	15.05
13	0.264	0.03650	65.84	5.90	0.588	15.49
14	0.328	0.04527	81.67	6.12	0.610	16.07
15	0.391	0.05404	97.50	6.21	0.618	16.30
16	0.455	0.06282	113.33	6.36	0.634	16.70
17	0.582	0.08036	144.98	6.62	0.660	17.38
18	0.709	0.09791	176.64	6.69	0.667	17.58
19	0.836	0.11545	208.30	6.88	0.686	18.08
20	0.963	0.13300	239.95	7.01	0.699	18.41
21	1.217	0.16809	303.26	7.19	0.717	18.89
22	1.471	0.20319	366.58	7.44	0.741	19.54
23	1.979	0.27337	493.20	7.81	0.778	20.51
24	2.487	0.34356	619.82	8.14	0.811	21.38
25	3.122	0.43129	778.10	8.47	0.844	22.23
26	3.757	0.51902	936.38	8.75	0.872	22.97
27	4.392	0.60675	1094.66	9.03	0.900	23.72
28	5.027	0.69448	1252.94	9.32	0.928	24.47
29	6.297	0.86995	1569.50	9.73	0.970	25.56
30	7.567	1.04541	1886.06	9.98	0.995	26.22
31	8.202	1.13314	2044.34	10.01	0.997	26.29
32	8.837	1.22087	2202.62	10.03	1.000	26.35
33	9.472	1.30860	2360.90	10.03	1.000	26.35

SMOOTH WALL REYNOLDS STRESS TENSOR COMPONENTS
ARTIFICIALLY THICKENED UINF=10.1M/SEC

RUN = 72976 CF/2 = 0.00150 DE = 5.717
PORT = 23 X1 = 1.17 DE1 = 0.957
UINF = 10.21 X2 = 3.77 DE2 = 0.707

Y	Y/DE	U'2/UINF2	V'2/UINF2	W'2/UINF2	Q2/UINF2	-U'V'/UINF2	RUV	RQ2
0.330	0.058	0.00540	0.00123	0.00241	0.00903	0.00150	0.582	0.166
0.635	0.111	0.00478	0.00133	0.00176	0.00788	0.00146	0.578	0.185
1.270	0.222	0.00359	0.00157	0.00154	0.00670	0.00108	0.456	0.162
2.540	0.444	0.00239	0.00117	0.00142	0.00498	0.00083	0.497	0.167
3.810	0.666	0.00176	0.00131	0.00142	0.00449	0.00074	0.490	0.166
5.080	0.889	0.00083	0.00070	0.00036	0.00239	0.00033	0.435	0.139

SMOOTH WALL REYNOLDS STRESS TENSOR COMPONENTS
ARTIFICIALLY THICKENED UINF=10.1M/SEC

RUN = 72976 CF/2 = 0.00148 DE = 6.555
PORT = 31 X1 = 1.57 DE1 = 1.045
UINF = 10.21 X2 = 4.18 DE2 = 0.771

Y	Y/DE	U'2/UINF2	V'2/UINF2	W'2/UINF2	Q2/UINF2	-U'V'/UINF2	RUV	RQ2
0.330	0.050	0.00546	0.00129	0.00320	0.00994	0.00148	0.559	0.149
0.635	0.097	0.00498	0.00142	0.00270	0.00911	0.00139	0.524	0.153
1.270	0.194	0.00420	0.00159	0.00205	0.00784	0.00118	0.455	0.150
2.540	0.387	0.00289	0.00128	0.00171	0.00588	0.00087	0.450	0.147
3.810	0.581	0.00216	0.00111	0.00151	0.00477	0.00076	0.492	0.159
5.080	0.775	0.00140	0.00111	0.00102	0.00353	0.00052	0.418	0.147
6.350	0.969	0.00034	0.00035	0.00023	0.00093	0.00009	0.266	0.099

SMOOTH WALL REYNOIDS STRESS TENSOR COMPONENTS
ARTIFICIALLY THICKENED UINF=10.1M/SEC

RUN = 90676 CF/2 = 0.00146 DE = 6.774
PORT = 39 X1 = 1.98 DE1 = 1.104
UINF = 10.18 X2 = 4.58 DE2 = 0.813

Y	Y/DE	U'2/UINF2	V'2/UINF2	W'2/UINF2	Q2/UINF2	-U'V'/UINF2	RUV	RQ2
0.330	0.049	0.00535	0.00187	0.00319	0.01041	0.00146	0.463	0.141
0.508	0.075	0.00516	0.00178	0.00344	0.01038	0.00147	0.484	0.141
1.016	0.150	0.00474	0.00233	0.00321	0.01028	0.00149	0.449	0.145
1.778	0.262	0.00408	0.00216	0.00314	0.00938	0.00136	0.459	0.146
2.540	0.375	0.00327	0.00217	0.00326	0.00870	0.00131	0.491	0.150
3.810	0.562	0.00267	0.00105	0.00217	0.00589	0.00092	0.550	0.156
5.080	0.750	0.00183	0.00073	0.00104	0.00361	0.00058	0.501	0.161
6.350	0.937	0.00075	0.00013	0.00031	0.00119	0.00016	0.506	0.134
7.620	1.125	0.00012	0.00004	0.00002	0.00018	0.00002	0.317	0.117

SMOOTH WALL REYNOLDS STRESS TENSOR COMPONENTS
ARTIFICIALLY THICKENED UINF=10.1M/SEC

RUN = 90276 CF/2 = 0.00144 DE = 7.238
PORT = 45 X1 = 2.29 DE1 = 1.165
UINF = 10.18 X2 = 4.89 DE2 = 0.863

Y	Y/DE	U'2/UINF2	V'2/UINF2	W'2/UINF2	Q2/UINF2	-U'V'/UINF2	RUV	RQ2
0.330	0.046	0.00508	0.00262	0.00339	0.01109	0.00144	0.396	0.130
0.508	0.070	0.00490	0.00200	0.00340	0.01030	0.00134	0.429	0.130
1.016	0.140	0.00454	0.00225	0.00337	0.01016	0.00132	0.414	0.130
1.778	0.246	0.00418	0.00231	0.00320	0.00969	0.00137	0.439	0.141
2.540	0.351	0.00372	0.00241	0.00276	0.00889	0.00125	0.418	0.141
3.810	0.526	0.00282	0.00161	0.00224	0.00667	0.00101	0.474	0.151
5.080	0.702	0.00189	0.00096	0.00153	0.00437	0.00067	0.497	0.153
6.350	0.877	0.00085	0.00023	0.00050	0.00158	0.00027	0.619	0.174
7.620	1.053	0.00020	0.00007	0.00000	0.00028	0.00004	0.375	0.161
8.890	1.228	0.00005	0.00010	0.00008	0.00022	0.00000	0.052	0.015

ROUGH WALL STANTON NO. RUN UINF = 10.1 M/SEC.
NATURALLY DEVELOPED XI = 0.0M.

RUN = 82878 TINFO = 19.59 TINF = 19.54 PAMB = 75.90
UINF = 9.97 TDB = 25.56 TWB = 20.56

PL	X1	X2	ST	DEH2	REDEH2	REX2	TW
1	0.05	0.05	0.00545	0.028	183.	0.34E 05	37.84
2	0.15	0.15	0.00382	0.075	496.	0.10E 06	37.80
3	0.25	0.25	0.00335	0.111	737.	0.17E 06	37.80
4	0.36	0.35	0.00309	0.144	953.	0.24E 06	37.82
5	0.46	0.45	0.00298	0.173	1148.	0.30E 06	37.92
6	0.56	0.55	0.00253	0.201	1332.	0.37E 06	37.90
7	0.66	0.65	0.00261	0.227	1507.	0.44E 06	37.88
8	0.76	0.75	0.00244	0.253	1675.	0.50E 06	37.90
9	0.86	0.85	0.00238	0.278	1841.	0.57E 06	37.86
10	0.97	0.97	0.00236	0.302	1998.	0.64E 06	37.88
11	1.07	1.07	0.00239	0.324	2143.	0.71E 06	38.01
12	1.17	1.17	0.00230	0.349	2310.	0.77E 06	37.94
13	1.27	1.27	0.00225	0.369	2443.	0.84E 06	38.09
14	1.37	1.37	0.00216	0.392	2594.	0.91E 06	38.07
15	1.47	1.47	0.00215	0.415	2747.	0.98E 06	38.01
16	1.57	1.57	0.00214	0.436	2889.	0.10E 07	38.03
17	1.68	1.68	0.00217	0.459	3037.	0.11E 07	38.01
18	1.78	1.78	0.00212	0.481	3188.	0.12E 07	37.97
19	1.88	1.88	0.00209	0.503	3329.	0.12E 07	37.97
20	1.98	1.98	0.00203	0.524	3471.	0.13E 07	37.96
21	2.08	2.08	0.00200	0.545	3611.	0.14E 07	37.94
22	2.18	2.18	0.00200	0.567	3753.	0.14E 07	37.90
23	2.29	2.29	0.00201	0.587	3888.	0.15E 07	37.90
24	2.39	2.39	0.00193	0.606	4016.	0.16E 07	37.92

ROUGH WALL STANTON NO. RUN UINF = 10.1 M/SEC.
ARTIFICIALLY THICKENED XI = 2.96 M.

RUN = 82378 TINFO = 18.41 TINF = 18.36 PAMB = 76.00
UINF = 9.94 TDB = 23.05 TWB = 17.78

PL	X1	X2	ST	DEH2	REDEH2	REX2	TW
1	0.05	2.40	0.00000	0.000	0.	0.16E 07	19.24
2	0.15	2.50	0.00000	0.000	0.	0.17E 07	19.15
3	0.25	2.60	0.00000	0.000	0.	0.17E 07	19.19
4	0.36	2.71	0.00000	0.000	0.	0.18E 07	19.24
5	0.46	2.81	0.00000	0.000	0.	0.19E 07	19.56
6	0.56	2.91	0.00000	0.000	0.	0.19E 07	21.35
7	0.66	3.01	0.00409	0.021	138.	0.20E 07	39.08
8	0.76	3.11	0.00274	0.056	370.	0.21E 07	39.04
9	0.86	3.21	0.00267	0.083	553.	0.21E 07	39.06
10	0.97	3.32	0.00260	0.110	731.	0.22E 07	39.08
11	1.07	3.42	0.00253	0.136	907.	0.23E 07	39.10
12	1.17	3.52	0.00264	0.163	1086.	0.23E 07	39.10
13	1.27	3.62	0.00252	0.189	1259.	0.24E 07	39.12
14	1.37	3.72	0.00239	0.214	1427.	0.25E 07	39.10
15	1.47	3.82	0.00239	0.238	1587.	0.25E 07	39.12
16	1.57	3.92	0.00238	0.253	1750.	0.26E 07	39.10
17	1.68	4.03	0.00242	0.287	1913.	0.27E 07	39.10
18	1.78	4.13	0.00236	0.312	2077.	0.28E 07	39.08
19	1.88	4.23	0.00235	0.336	2236.	0.28E 07	39.08
20	1.98	4.33	0.00227	0.358	2384.	0.29E 07	39.16
21	2.08	4.43	0.00223	0.382	2545.	0.30E 07	39.08
22	2.18	4.53	0.00224	0.404	2694.	0.30E 07	39.10
23	2.29	4.64	0.00226	0.427	2844.	0.31E 07	39.12
24	2.39	4.74	0.00218	0.449	2994.	0.32E 07	39.12

ROUGH WALL STANTON NO. RUN UINF = 10.1 M/SEC.
ARTIFICIALLY THICKENED XI = 3.57 M.

RUN = 82278 TINFO = 18.60 TINF = 18.56 PAMB = 75.87
UINF = 9.95 TDB = 24.72 TWB = 16.94

PL	X1	X2	ST	DEH2	REDEH2	REX2	TW
1	0.05	2.40	0.00000	0.000	0.	0.16E 07	19.52
2	0.15	2.50	0.00000	0.000	0.	0.17E 07	19.40
3	0.25	2.60	0.00000	0.000	0.	0.17E 07	19.40
4	0.36	2.71	0.00000	0.000	0.	0.18E 07	19.40
5	0.46	2.81	0.00000	0.000	0.	0.19E 07	19.48
6	0.56	2.91	0.00000	0.000	0.	0.19E 07	19.46
7	0.66	3.01	0.00000	0.000	0.	0.20E 07	19.52
8	0.76	3.11	0.00000	0.000	0.	0.21E 07	19.48
9	0.86	3.21	0.00000	0.000	0.	0.21E 07	19.46
10	0.97	3.32	0.00000	0.000	0.	0.22E 07	19.56
11	1.07	3.42	0.00000	0.000	0.	0.23E 07	19.81
12	1.17	3.52	0.00000	0.000	0.	0.23E 07	21.23
13	1.27	3.62	0.00406	0.021	137.	0.24E 07	38.53
14	1.37	3.72	0.00272	0.055	368.	0.25E 07	38.37
15	1.47	3.82	0.00269	0.082	549.	0.25E 07	38.49
16	1.57	3.92	0.00262	0.109	727.	0.26E 07	38.51
17	1.68	4.03	0.00262	0.136	904.	0.27E 07	38.51
18	1.78	4.13	0.00254	0.162	1077.	0.27E 07	38.54
19	1.88	4.23	0.00251	0.187	1246.	0.28E 07	38.56
20	1.98	4.33	0.00240	0.212	1413.	0.29E 07	38.56
21	2.08	4.43	0.00236	0.237	1575.	0.29E 07	38.54
22	2.18	4.53	0.00234	0.261	1736.	0.30E 07	38.53
23	2.29	4.64	0.00235	0.285	1896.	0.31E 07	38.51
24	2.39	4.74	0.00226	0.309	2055.	0.32E 07	38.47

ROUGH WALL STANTON NO. RUN UINF = 15.8 M/SEC.
ARTIFICIALLY THICKENED XI = 3.07 M.

RUN = 80278 TINFO = 17.10 TINF = 16.97 PAMB = 75.74
UINF = 15.84 TDB = 25.56 TWB = 20.00

PL	X1	X2	ST	DEH2	REDEH2	REX2	TW
1	0.05	2.51	0.00000	0.000	0.	0.27E 07	17.99
2	0.15	2.61	0.00000	0.000	0.	0.28E 07	17.76
3	0.25	2.71	0.00000	0.000	0.	0.29E 07	17.76
4	0.36	2.82	0.00000	0.000	0.	0.30E 07	17.76
5	0.46	2.92	0.00000	0.000	0.	0.31E 07	17.97
6	0.56	3.02	0.00000	0.000	0.	0.32E 07	19.15
7	0.66	3.12	0.00403	0.020	218.	0.33E 07	36.36
8	0.76	3.22	0.00291	0.056	593.	0.34E 07	36.40
9	0.86	3.32	0.00279	0.085	905.	0.35E 07	36.33
10	0.97	3.43	0.00269	0.113	1201.	0.37E 07	36.34
11	1.07	3.53	0.00266	0.140	1494.	0.38E 07	36.31
12	1.17	3.63	0.00264	0.166	1766.	0.39E 07	36.48
13	1.27	3.73	0.00257	0.193	2054.	0.40E 07	36.42
14	1.37	3.83	0.00249	0.218	2321.	0.41E 07	36.48
15	1.47	3.93	0.00244	0.243	2593.	0.42E 07	36.44
16	1.57	4.03	0.00243	0.269	2868.	0.43E 07	36.36
17	1.68	4.14	0.00240	0.295	3144.	0.44E 07	36.27
18	1.78	4.24	0.00241	0.319	3399.	0.45E 07	36.31
19	1.88	4.34	0.00238	0.343	3662.	0.46E 07	36.29
20	1.98	4.44	0.00230	0.367	3915.	0.47E 07	36.29
21	2.08	4.54	0.00227	0.390	4158.	0.48E 07	36.31
22	2.18	4.64	0.00225	0.414	4412.	0.50E 07	36.27
23	2.29	4.75	0.00225	0.436	465[illegible].	0.51E 07	36.29
24	2.39	4.85	0.00216	0.458	4891.	0.52E 07	36.33

ROUGH WALL STANTON NO. RUN UINF = 15.8 M/SEC.
ARTIFICIALLY THICKENED XI = 3.68 M.

RUN = 80478 TINFO = 17.60 TINF = 17.48 PAMB = 75.82
UINF = 15.91 TDB = 25.56 TWB = 20.00

PL	XI	X2	ST	DEH2	REDEH2	REX2	TW
1	0.05	2.51	0.00000	0.000	0.	0.27E 07	18.52
2	0.15	2.61	0.00000	0.000	0.	0.28E 07	18.29
3	0.25	2.71	0.00000	0.000	0.	0.29E 07	18.25
4	0.36	2.82	0.00000	0.000	0.	0.30E 07	18.21
5	0.46	2.92	0.00000	0.000	0.	0.31E 07	18.36
6	0.56	3.02	0.00000	0.000	0.	0.32E 07	18.36
7	0.66	3.12	0.00000	0.000	0.	0.33E 07	18.32
8	0.76	3.22	0.00000	0.000	0.	0.34E 07	18.29
9	0.86	3.32	0.00000	0.000	0.	0.36E 07	18.25
10	0.97	3.43	0.00000	0.000	0.	0.37E 07	18.31
11	1.07	3.53	0.00000	0.000	0.	0.38E 07	18.50
12	1.17	3.63	0.00000	0.000	0.	0.39E 07	19.34
13	1.27	3.73	0.00392	0.020	213.	0.40E 07	35.83
14	1.37	3.83	0.00286	0.055	583.	0.41E 07	35.73
15	1.47	3.93	0.00275	0.083	891.	0.42E 07	35.66
16	1.57	4.03	0.00268	0.111	1185.	0.43E 07	35.66
17	1.68	4.14	0.00266	0.138	1474.	0.44E 07	35.68
18	1.78	4.24	0.00259	0.165	1760.	0.45E 07	35.66
19	1.88	4.34	0.00256	0.190	2034.	0.46E 07	35.71
20	1.98	4.44	0.00245	0.216	2304.	0.47E 07	35.73
21	2.08	4.54	0.00241	0.239	2558.	0.49E 07	35.81
22	2.18	4.64	0.00240	0.264	2819.	0.50E 07	35.81
23	2.29	4.75	0.00237	0.288	3081.	0.51E 07	35.79
24	2.39	4.85	0.00227	0.312	3337.	0.52E 07	35.77

ROUGH WALL STANTON NO. RUN UINF = 26.8 M/SEC.
NATURALLY DEVELOPED XI= 0.04.

RUN = 62077 TINFO = 22.85 TINF = 22.49 PAMB = 75.77
UINF = 27.06 TDB = 25.00 TWB = 18.06

PL	XI	X2	ST	DEH2	REDEH2	REX2	TW
1	0.05	0.05	0.00527	0.027	473.	0.90E 05	40.33
2	0.15	0.15	0.00383	0.073	1287.	0.27E 06	40.36
3	0.25	0.25	0.00335	0.109	1932.	0.45E 06	40.34
4	0.36	0.36	0.00308	0.142	2508.	0.63E 06	40.34
5	0.46	0.46	0.00284	0.172	3039.	0.81E 06	40.34
6	0.56	0.56	0.00265	0.200	3528.	0.99E 06	40.36
7	0.66	0.65	0.00264	0.226	3995.	0.12E 07	40.40
8	0.76	0.75	0.00250	0.252	4451.	0.13E 07	40.42
9	0.86	0.86	0.00244	0.278	4910.	0.15E 07	40.36
10	0.97	0.97	0.00241	0.302	5334.	0.17E 07	40.40
11	1.07	1.07	0.00236	0.327	5768.	0.19E 07	40.38
12	1.17	1.17	0.00235	0.350	6171.	0.21E 07	40.44
13	1.27	1.27	0.00230	0.374	6603.	0.22E 07	40.40
14	1.37	1.37	0.00225	0.397	7011.	0.24E 07	40.40
15	1.47	1.47	0.00223	0.420	7405.	0.26E 07	40.42
16	1.57	1.57	0.00219	0.444	7834.	0.28E 07	40.34
17	1.68	1.68	0.00218	0.456	8218.	0.30E 07	40.36
18	1.78	1.78	0.00218	0.498	8609.	0.31E 07	40.36
19	1.88	1.89	0.00214	0.508	8959.	0.33E 07	40.44
20	1.98	1.98	0.00211	0.529	9331.	0.35E 07	40.46
21	2.08	2.09	0.00206	0.553	9757.	0.37E 07	40.36
22	2.18	2.18	0.00207	0.570	10053.	0.39E 07	40.50
23	2.29	2.29	0.00205	0.594	10479.	0.40E 07	40.40
24	2.39	2.39	0.00197	0.614	10840.	0.42E 07	40.40

ROUGH WALL STANTON NO. RUN UINF = 26.8 M/SEC.
ARTIFICIALLY THICKENED XI = 2.934.

RUN = 71778 TINFD = 21.22 TINF = 20.87 PAMB = 75.51
UINF = 26.94 TDB = 26.11 TWB = 21.67

PL	X1	X2	ST	DEH2	REDEH2	REX2	TW
1	0.05	2.37	0.00000	0.000	0.	0.42E 07	21.37
2	0.15	2.47	0.00000	0.000	0.	0.44E 07	21.21
3	0.25	2.57	0.00000	0.000	0.	0.45E 07	21.25
4	0.36	2.68	0.00000	0.000	0.	0.47E 07	21.27
5	0.46	2.78	0.00000	0.000	0.	0.49E 07	21.35
6	0.56	2.88	0.00000	0.000	0.	0.51E 07	21.85
7	0.66	2.98	0.00407	0.021	365.	0.53E 07	33.07
8	0.76	3.08	0.00307	0.057	1002.	0.54E 07	33.10
9	0.86	3.18	0.00291	0.087	1541.	0.56E 07	33.08
10	0.97	3.29	0.00278	0.116	2049.	0.58E 07	33.10
11	1.07	3.39	0.00273	0.145	2558.	0.60E 07	33.03
12	1.17	3.49	0.00270	0.171	3013.	0.62E 07	33.16
13	1.27	3.59	0.00266	0.199	3510.	0.63E 07	33.10
14	1.37	3.69	0.00256	0.225	3978.	0.65E 07	33.10
15	1.47	3.79	0.00249	0.252	4452.	0.67E 07	33.05
16	1.57	3.89	0.00250	0.278	4900.	0.69E 07	33.05
17	1.68	4.00	0.00246	0.303	5345.	0.71E 07	33.05
18	1.78	4.10	0.00248	0.328	5797.	0.72E 07	33.03
19	1.88	4.20	0.00245	0.353	6238.	0.74E 07	33.03
20	1.98	4.30	0.00238	0.378	6671.	0.76E 07	33.03
21	2.08	4.40	0.00236	0.399	7052.	0.78E 07	33.10
22	2.18	4.50	0.00234	0.424	7485.	0.80E 07	33.08
23	2.29	4.61	0.00231	0.448	7903.	0.81E 07	33.08
24	2.39	4.71	0.00222	0.471	8309.	0.83E 07	33.08

ROUGH WALL STANTON NO. RUN UINF = 26.8 M/SEC.
ARTIFICIALLY THICKENED XI = 3.54 M

RUN = 71878 TINFD = 21.38 TINF = 21.02 PAMB = 75.41
UINF = 26.88 TDB = 28.33 TWB = 21.67

PL	X1	X2	ST	DEH2	REDEH2	REX2	TW
1	0.05	2.37	0.00000	0.000	0.	0.42E 07	21.77
2	0.15	2.47	0.00000	0.000	0.	0.43E 07	21.50
3	0.25	2.57	0.00000	0.000	0.	0.45E 07	21.46
4	0.36	2.68	0.00000	0.000	0.	0.47E 07	21.44
5	0.46	2.78	0.00000	0.000	0.	0.49E 07	21.64
6	0.56	2.88	0.00000	0.000	0.	0.51E 07	21.60
7	0.66	2.98	0.00000	0.000	0.	0.52E 07	21.56
8	0.76	3.08	0.00000	0.000	0.	0.54E 07	21.52
9	0.86	3.18	0.00000	0.000	0.	0.56E 07	21.48
10	0.97	3.29	0.00000	0.000	0.	0.58E 07	21.50
11	1.07	3.39	0.00000	0.000	0.	0.60E 07	21.67
12	1.17	3.49	0.00000	0.000	0.	0.61E 07	22.11
13	1.27	3.59	0.00392	0.020	350.	0.63E 07	37.46
14	1.37	3.69	0.00301	0.055	969.	0.65E 07	37.46
15	1.47	3.79	0.00286	0.095	1497.	0.67E 07	37.42
16	1.57	3.89	0.00277	0.114	2005.	0.68E 07	37.38
17	1.68	4.00	0.00270	0.141	2485.	0.70E 07	37.44
18	1.78	4.10	0.00268	0.168	2962.	0.72E 07	37.46
19	1.88	4.20	0.00261	0.195	3427.	0.74E 07	37.49
20	1.98	4.30	0.00252	0.221	3889.	0.76E 07	37.48
21	2.08	4.40	0.00248	0.246	4331.	0.77E 07	37.49
22	2.18	4.50	0.00245	0.272	4777.	0.79E 07	37.48
23	2.29	4.61	0.00246	0.297	5217.	0.81E 07	37.48
24	2.39	4.71	0.00233	0.322	5658.	0.83E 07	37.44

ROUGH WALL STANTON NO. RUN UINF = 26.8 M/SEC.
ARTIFICIALLY THICKENED WITH E =.008 PLATES E-6. XI = 4.52 M.

RUN = 72178 TINFO = 21.57 TINF = 21.21 PAMB = 75.51
UINF = 27.05 TOR = 27.78 TWB = 21.67

PL	X1	X2	ST	DEH2	REDEH2	REX2	TW
1	0.05	3.35	0.00000	0.000	0.	0.59E 07	22.11
2	0.15	3.45	0.00000	0.000	0.	0.61E 07	21.88
3	0.25	3.55	0.00000	0.000	0.	0.63E 07	21.81
4	0.36	3.65	0.00000	0.000	0.	0.65E 07	21.71
5	0.46	3.75	0.00000	0.000	0.	0.67E 07	21.81
6	0.56	3.85	0.00000	0.000	0.	0.68E 07	21.94
7	0.66	3.95	0.00000	0.000	0.	0.70E 07	21.79
8	0.76	4.05	0.00000	0.000	0.	0.72E 07	21.75
9	0.86	4.16	0.00000	0.000	0.	0.74E 07	21.73
10	0.97	4.27	0.00000	0.000	0.	0.76E 07	21.75
11	1.07	4.37	0.00000	0.000	0.	0.77E 07	21.85
12	1.17	4.47	0.00000	0.000	0.	0.79E 07	22.36
13	1.27	4.57	0.00371	0.019	334.	0.81E 07	37.69
14	1.37	4.67	0.00287	0.052	927.	0.83E 07	37.69
15	1.47	4.77	0.00274	0.081	1434.	0.85E 07	37.65
16	1.57	4.87	0.00267	0.108	1913.	0.86E 07	37.72
17	1.68	4.98	0.00254	0.136	2406.	0.88E 07	37.61
18	1.78	5.08	0.00263	0.162	2870.	0.90E 07	37.67
19	1.88	5.18	0.00257	0.188	3338.	0.92E 07	37.67
20	1.98	5.28	0.00247	0.213	3779.	0.94E 07	37.72
21	2.08	5.38	0.00244	0.237	4206.	0.95E 07	37.78
22	2.18	5.48	0.00241	0.263	4653.	0.97E 07	37.74
23	2.29	5.59	0.00244	0.289	5119.	0.99E 07	37.65
24	2.39	5.69	0.00233	0.311	5510.	0.10E 08	37.76

ROUGH WALL MEAN TEMPERATURE PROFILE
NATURALLY DEVELOPED UINF= 10.1M/SEC

RUN	=	82878	DEH	=	2.970
PLATE	=	12	DEH2	=	0.361
X1	=	1.17	DE	=	2.830
X2	=	1.17	DE2	=	0.359
DELY	=	0.023	TINF	=	19.37
UINF	=	9.96	TW	=	37.54
CF/2	=	0.00209	ST	=	0.00230

PT	Y	Y/DEH2	T	TBAR	T+
1	0.048	0.134	31.99	0.320	6.36
2	0.053	0.148	31.45	0.343	6.94
3	0.061	0.169	30.93	0.378	7.51
4	0.069	0.190	30.48	0.402	7.98
5	0.076	0.211	29.97	0.429	8.53
6	0.086	0.239	29.39	0.460	9.15
7	0.099	0.275	28.90	0.487	9.68
8	0.112	0.310	28.45	0.511	10.16
9	0.124	0.345	28.12	0.529	10.51
10	0.150	0.416	27.61	0.556	11.06
11	0.201	0.556	27.00	0.589	11.72
12	0.251	0.697	26.42	0.621	12.34
13	0.302	0.838	26.10	0.638	12.67
14	0.378	1.049	25.57	0.666	13.24
15	0.455	1.261	25.17	0.688	13.67
16	0.531	1.472	24.83	0.706	14.04
17	0.632	1.754	24.48	0.725	14.41
18	0.734	2.035	24.08	0.746	14.84
19	0.836	2.317	23.77	0.763	15.17
20	0.937	2.599	23.44	0.781	15.52
21	1.039	2.880	23.17	0.795	15.81
22	1.166	3.233	22.83	0.814	16.18
23	1.293	3.585	22.48	0.832	16.55
24	1.801	4.993	21.35	0.893	17.76
25	2.309	6.402	20.42	0.943	18.75
26	2.817	7.810	19.71	0.982	19.51
27	3.325	9.219	19.40	0.998	19.84
28	3.833	10.627	19.37	1.000	19.88
29	4.341	12.036	19.37	1.000	19.88

ROUGH WALL MEAN TEMPERATURE PROFILE
NATURALLY DEVELOPED UINF= 10.1M/SEC

RUN	=	82878	DEH	=	4.123
PLATE	=	18	DEH2	=	0.503
X1	=	1.78	DE	=	3.940
X2	=	1.78	DE2	=	0.502
DELY	=	0.023	TINF	=	19.36
UINF	=	9.96	TW	=	37.98
CF/2	=	0.00192	ST	=	0.00212

PT	Y	Y/DEH2	T	TBAR	T+
1	0.048	0.096	31.52	0.347	7.17
2	0.053	0.106	31.26	0.361	7.46
3	0.061	0.121	30.58	0.397	8.21
4	0.074	0.147	29.99	0.429	8.87
5	0.086	0.172	29.54	0.453	9.36
6	0.099	0.197	29.10	0.477	9.86
7	0.124	0.248	28.40	0.514	10.63
8	0.150	0.298	28.04	0.534	11.03
9	0.201	0.399	27.44	0.566	11.69
10	0.251	0.500	26.91	0.594	12.28
11	0.302	0.601	26.63	0.609	12.59
12	0.378	0.753	26.20	0.632	13.07
13	0.455	0.904	25.82	0.653	13.49
14	0.531	1.056	25.55	0.667	13.79
15	0.658	1.309	25.12	0.690	14.27
16	0.785	1.561	24.76	0.710	14.67
17	0.912	1.814	24.40	0.729	15.07
18	1.039	2.066	24.08	0.746	15.42
19	1.166	2.319	23.78	0.762	15.75
20	1.293	2.572	23.49	0.778	16.08
21	1.547	3.077	22.98	0.806	16.65
22	1.801	3.582	22.51	0.830	17.16
23	2.309	4.593	21.69	0.874	18.07
24	2.817	5.603	20.93	0.916	18.93
25	3.579	7.119	19.97	0.967	19.99
26	4.341	8.634	19.45	0.995	20.56
27	5.103	10.150	19.36	1.000	20.67
28	6.119	12.171	19.36	1.000	20.67

ROUGH WALL MEAN TEMPERATURE PROFILE
NATURALLY DEVELOPED UINF= 10.1M/SEC

RUN	=	82878	DEH	=	4.714
PLATE	=	21	DEH2	=	0.597
X1	=	2.08	DE	=	4.415
X2	=	2.08	DE2	=	0.569
DELY	=	0.023	TINF	=	19.37
UINF	=	9.96	TW	=	37.94
CF/2	=	0.00185	ST	=	0.00200

PT	Y	Y/DEH2	T	TBAR	T+
1	0.048	0.082	32.31	0.303	6.52
2	0.053	0.091	31.85	0.328	7.06
3	0.061	0.104	31.52	0.346	7.44
4	0.074	0.125	30.66	0.392	8.43
5	0.086	0.147	30.04	0.426	9.15
6	0.099	0.169	29.63	0.448	9.63
7	0.124	0.212	28.88	0.488	10.49
8	0.150	0.255	28.40	0.514	11.05
9	0.201	0.342	27.72	0.550	11.83
10	0.251	0.428	27.36	0.570	12.25
11	0.302	0.515	26.96	0.591	12.71
12	0.378	0.645	26.61	0.610	13.12
13	0.455	0.775	26.18	0.633	13.62
14	0.531	0.904	25.85	0.651	14.00
15	0.658	1.121	25.42	0.674	14.50
16	0.785	1.337	25.16	0.688	14.81
17	0.912	1.553	24.91	0.707	15.21
18	1.039	1.770	24.46	0.726	15.61
19	1.293	2.203	23.93	0.754	16.22
20	1.801	3.068	23.01	0.804	17.29
21	2.436	4.150	21.97	0.860	18.49
22	3.071	5.232	21.12	0.906	19.48
23	3.833	6.530	20.26	0.952	20.48
24	4.595	7.828	19.63	0.986	21.21
25	5.357	9.126	19.40	0.998	21.47
26	6.119	10.424	19.39	0.999	21.49
27	6.881	11.722	19.37	1.000	21.51

ROUGH WALL MEAN TEMPERATURE PROFILE
ARTIFICIALLY THICKENED UINF= 10.1M/SEC

RUN	=	82378	DEH	=	3.027
PLATE	=	12	DEH2	=	0.159
X1	=	1.17	DE	=	6.539
X2	=	3.52	DE2	=	0.779
DELY	=	0.023	TINF	=	18.57
UINF	=	9.94	TW	=	39.11
CF/2	=	0.00165	ST	=	0.00264

PT	Y	Y/DEH2	T	TBAR	T+
1	0.048	0.303	29.48	0.469	7.21
2	0.053	0.334	28.75	0.504	7.76
3	0.061	0.382	27.83	0.549	8.45
4	0.074	0.462	26.95	0.592	9.11
5	0.086	0.541	26.27	0.625	9.62
6	0.099	0.621	26.01	0.638	9.82
7	0.112	0.701	25.59	0.658	10.13
8	0.124	0.780	25.43	0.666	10.25
9	0.150	0.940	24.83	0.695	10.70
10	0.175	1.099	24.40	0.716	11.02
11	0.201	1.258	23.79	0.746	11.48
12	0.226	1.417	23.53	0.759	11.67
13	0.277	1.736	23.10	0.780	11.99
14	0.328	2.054	22.62	0.803	12.35
15	0.378	2.373	22.23	0.822	12.65
16	0.455	2.851	21.92	0.837	12.88
17	0.531	3.329	21.54	0.855	13.16
18	0.658	4.125	21.09	0.874	13.50
19	0.785	4.921	20.76	0.893	13.75
20	1.039	6.514	20.19	0.921	14.17
21	1.293	8.106	19.82	0.939	14.45
22	1.547	9.699	19.59	0.950	14.62
23	1.801	11.292	19.35	0.962	14.80
24	2.055	12.884	19.11	0.974	14.98
25	2.563	16.070	18.90	0.984	15.14
26	3.198	20.051	18.76	0.991	15.25
27	3.833	24.033	18.68	0.995	15.31
28	4.468	28.014	18.64	0.997	15.34
29	5.103	31.996	18.62	0.998	15.35
30	12.723	79.774	18.57	1.000	15.39

ROUGH WALL MEAN TEMPERATURE PROFILE
ARTIFICIALLY THICKENED UINF= 10.1M/SEC

RUN	=	82378	DEH	=	4.119
PLATE	=	15	DEH2	=	0.219
X1	=	1.47	DE	=	7.137
X2	=	3.83	DE2	=	0.824
DELY	=	0.023	TINF	=	18.51
UINF	=	9.94	TW	=	39.13
CF/2	=	0.00163	ST	=	0.00239

PT	Y	Y/DEH2	T	TBAR	T+
1	0.048	0.220	29.91	0.452	7.63
2	0.053	0.244	29.33	0.475	8.03
3	0.061	0.278	28.65	0.509	8.58
4	0.074	0.336	27.74	0.552	9.33
5	0.086	0.394	27.15	0.581	9.81
6	0.099	0.453	26.64	0.606	10.23
7	0.112	0.511	26.27	0.624	10.53
8	0.124	0.569	25.87	0.643	10.86
9	0.150	0.685	25.28	0.672	11.35
10	0.175	0.801	24.93	0.689	11.63
11	0.201	0.917	24.47	0.711	12.01
12	0.226	1.033	24.24	0.722	12.20
13	0.277	1.265	23.69	0.749	12.65
14	0.328	1.497	23.21	0.772	13.04
15	0.378	1.729	22.92	0.786	13.28
16	0.455	2.077	22.54	0.804	13.59
17	0.531	2.425	22.21	0.820	13.86
18	0.658	3.005	21.70	0.845	14.27
19	0.785	3.585	21.44	0.858	14.49
20	1.039	4.745	20.81	0.889	15.01
21	1.293	5.906	20.42	0.907	15.33
22	1.547	7.066	20.00	0.928	15.67
23	1.801	8.226	19.63	0.946	15.98
24	2.055	9.387	19.40	0.957	16.16
25	2.563	11.707	19.14	0.969	16.37
26	3.198	14.608	18.93	0.979	16.55
27	3.833	17.508	18.77	0.987	16.68
28	4.468	20.409	18.67	0.992	16.76
29	5.103	23.310	18.62	0.994	16.80
30	12.723	58.118	18.51	1.000	16.89

ROUGH WALL MEAN TEMPERATURE PROFILE
ARTIFICIALLY THICKENED UINF= 10.1M/SEC

RUN	=	82378	DEH	=	5.110
PLATE	=	18	DEH2	=	0.294
X1	=	1.78	DE	=	7.628
X2	=	4.13	DE2	=	0.870
DELY	=	0.023	TINF	=	18.49
UINF	=	9.94	TW	=	39.09
CF/2	=	0.00160	ST	=	0.00236

PT	Y	Y/DEH2	T	TBAR	T+
1	0.048	0.164	30.35	0.424	7.19
2	0.053	0.182	30.11	0.436	7.39
3	0.061	0.208	29.02	0.489	8.29
4	0.074	0.251	28.42	0.518	8.78
5	0.086	0.294	27.73	0.552	9.35
6	0.099	0.337	27.18	0.578	9.80
7	0.124	0.424	26.29	0.622	10.54
8	0.150	0.510	25.74	0.648	10.98
9	0.175	0.597	25.24	0.672	11.39
10	0.213	0.727	24.75	0.696	11.80
11	0.277	0.943	24.06	0.730	12.37
12	0.340	1.159	23.64	0.750	12.71
13	0.404	1.376	23.35	0.764	12.96
14	0.467	1.592	22.92	0.785	13.31
15	0.531	1.808	22.77	0.792	13.43
16	0.658	2.241	22.28	0.816	13.84
17	0.785	2.673	21.90	0.835	14.15
18	1.039	3.538	21.29	0.865	14.66
19	1.293	4.403	20.77	0.889	15.07
20	1.547	5.269	20.47	0.904	15.33
21	1.801	6.134	20.00	0.927	15.71
22	2.055	6.999	19.77	0.938	15.90
23	2.563	8.729	19.40	0.956	16.20
24	3.198	10.892	19.14	0.969	16.42
25	3.833	13.055	18.93	0.979	16.59
26	4.468	15.217	18.79	0.986	16.71
27	5.103	17.380	18.71	0.990	16.78
28	5.738	19.543	18.64	0.993	16.83
29	6.373	21.706	18.61	0.994	16.86
30	12.723	43.334	18.49	1.000	16.95

ROUGH WALL MEAN TEMPERATURE PROFILE
ARTIFICIALLY THICKENED UINF= 10.1M/SEC

RUN	=	82278	DEH	=	2.892
PLATE	=	18	DEH2	=	0.169
X1	=	1.78	DE	=	7.628
X2	=	4.13	DE2	=	0.870
DELY	=	0.023	TINF	=	18.81
UINF	=	9.95	TW	=	38.55
CF/2	=	0.00160	ST	=	0.00254

PT	Y	Y/DEH2	T	TBAR	T+
1	0.048	0.285	29.69	0.450	7.04
2	0.053	0.315	28.94	0.487	7.67
3	0.061	0.360	28.18	0.526	8.28
4	0.074	0.435	27.43	0.563	8.87
5	0.086	0.510	26.87	0.592	9.32
6	0.099	0.585	26.34	0.619	9.74
7	0.124	0.735	25.38	0.667	10.51
8	0.150	0.886	24.82	0.696	10.96
9	0.175	1.036	24.35	0.719	11.33
10	0.213	1.261	23.89	0.743	11.70
11	0.277	1.636	23.12	0.782	12.31
12	0.340	2.011	22.67	0.804	12.67
13	0.404	2.386	22.33	0.822	12.94
14	0.467	2.762	21.98	0.839	13.22
15	0.531	3.137	21.66	0.856	13.48
16	0.658	3.887	21.38	0.870	13.70
17	0.785	4.638	20.94	0.892	14.05
18	1.039	6.139	20.42	0.919	14.47
19	1.293	7.640	20.05	0.937	14.76
20	1.547	9.141	19.76	0.952	15.00
21	1.801	10.642	19.35	0.973	15.32
22	2.055	12.142	19.24	0.978	15.41
23	2.563	15.144	19.08	0.986	15.54
24	3.198	18.857	18.98	0.991	15.61
25	3.833	22.649	18.92	0.995	15.67
26	4.468	26.401	18.88	0.996	15.69
27	5.103	30.154	18.88	0.997	15.69
28	5.738	33.906	18.86	0.997	15.71
29	6.373	37.658	18.86	0.997	15.71
30	12.723	75.181	18.81	1.000	15.75

ROUGH WALL MEAN TEMPERATURE PROFILE
ARTIFICIALLY THICKENED UINF= 10.1M/SEC

RUN	=	82278	DEH	=	3.921
PLATE	=	21	DEH2	=	0.225
X1	=	2.08	DE	=	8.354
X2	=	4.44	DE2	=	0.922
DELY	=	0.023	TINF	=	18.78
UINF	=	9.95	TW	=	38.55
CF/2	=	0.00157	ST	=	0.00236

PT	Y	Y/DEH2	T	TBAR	T+
1	0.048	0.215	29.74	0.445	7.48
2	0.053	0.237	29.46	0.460	7.72
3	0.061	0.271	28.70	0.498	8.36
4	0.074	0.328	27.98	0.535	8.98
5	0.086	0.384	27.28	0.570	9.57
6	0.099	0.441	26.80	0.594	9.98
7	0.124	0.554	25.96	0.637	10.70
8	0.150	0.667	25.49	0.660	11.09
9	0.175	0.780	25.01	0.685	11.50
10	0.213	0.949	24.37	0.717	12.04
11	0.277	1.231	23.74	0.749	12.58
12	0.340	1.514	23.30	0.772	12.95
13	0.404	1.796	22.97	0.788	13.23
14	0.467	2.079	22.62	0.806	13.53
15	0.531	2.361	22.28	0.823	13.82
16	0.658	2.926	21.98	0.843	14.15
17	0.785	3.491	21.46	0.864	14.51
18	1.039	4.621	21.02	0.887	14.89
19	1.293	5.750	20.50	0.913	15.33
20	1.547	6.880	20.17	0.929	15.61
21	1.801	8.010	19.79	0.949	15.93
22	2.055	9.140	19.55	0.961	16.14
23	2.563	11.399	19.35	0.971	16.30
24	3.198	14.223	19.12	0.983	16.50
25	3.833	17.048	19.00	0.989	16.61
26	4.468	19.872	18.91	0.993	16.68
27	5.103	22.696	18.87	0.996	16.72
28	5.738	25.521	18.81	0.997	16.75
29	6.373	28.345	18.83	0.997	16.75
30	12.723	56.588	18.78	1.000	16.79

ROUGH WALL MEAN TEMPERATURE PROFILE
ARTIFICIALLY THICKENED UINF= 10.1M/SEC

RUN	=	82278	DEH	=	4.798
PLATE	=	23	DEH2	=	0.271
X1	=	2.29	DE	=	8.568
X2	=	4.64	DE2	=	0.950
DELY	=	0.023	TINF	=	18.73
UINF	=	9.95	TW	=	38.51
CF/2	=	0.00154	ST	=	0.00235

PT	Y	Y/DEH2	T	TBAR	T+
1	0.048	0.178	30.86	0.387	6.46
2	0.053	0.197	30.14	0.423	7.07
3	0.061	0.225	29.35	0.463	7.74
4	0.074	0.272	28.42	0.519	8.52
5	0.086	0.319	27.81	0.541	9.04
6	0.099	0.366	27.41	0.561	9.37
7	0.124	0.460	26.47	0.609	10.17
8	0.150	0.554	25.72	0.647	10.80
9	0.175	0.647	25.34	0.666	11.12
10	0.213	0.788	24.77	0.695	11.61
11	0.277	1.023	24.09	0.729	12.19
12	0.340	1.257	23.66	0.751	12.54
13	0.404	1.492	23.38	0.765	12.78
14	0.467	1.727	23.05	0.782	13.05
15	0.531	1.961	22.61	0.804	13.43
16	0.658	2.430	22.24	0.822	13.73
17	0.785	2.900	21.87	0.842	14.05
18	1.039	3.838	21.26	0.872	14.56
19	1.293	4.776	20.87	0.892	14.89
20	1.547	5.715	20.51	0.910	15.19
21	1.801	6.653	20.01	0.935	15.62
22	2.055	7.591	19.88	0.942	15.73
23	2.563	9.468	19.56	0.958	16.00
24	3.198	11.814	19.29	0.972	16.23
25	3.833	14.160	19.09	0.982	16.40
26	4.468	16.506	18.98	0.988	16.49
27	5.103	18.852	18.90	0.992	16.56
28	5.738	21.198	18.85	0.994	16.60
29	6.373	23.544	18.82	0.996	16.63
30	12.723	47.003	18.73	1.000	16.70

ROUGH WALL MEAN TEMPERATURE PROFILE
ARTIFICIALLY THICKENED UINF= 15.8M/SEC

RUN	=	80278	DEH	=	3.199
PLATE	=	12	DEH2	=	0.159
X1	=	1.17	DE	=	6.693
X2	=	3.63	DE2	=	0.830
DELY	=	0.023	TINF	=	17.10
UINF	=	16.01	TW	=	36.48
CF/2	=	0.00187	ST	=	0.00264

PT	Y	Y/DEH2	T	TBAR	T+
1	0.048	0.303	26.24	0.529	8.66
2	0.053	0.335	25.84	0.549	9.00
3	0.061	0.383	25.46	0.569	9.32
4	0.074	0.463	24.73	0.606	9.93
5	0.086	0.543	24.30	0.629	10.30
6	0.099	0.623	23.87	0.651	10.68
7	0.112	0.703	23.57	0.666	10.91
8	0.124	0.783	23.32	0.679	11.12
9	0.150	0.942	22.91	0.700	11.47
10	0.175	1.102	22.45	0.724	11.86
11	0.201	1.282	22.27	0.733	12.01
12	0.226	1.421	21.91	0.752	12.32
13	0.277	1.741	21.55	0.771	12.62
14	0.328	2.060	21.06	0.796	13.04
15	0.378	2.380	20.73	0.813	13.31
16	0.455	2.859	20.36	0.832	13.63
17	0.531	3.338	20.05	0.848	13.89
18	0.658	4.137	19.58	0.872	14.29
19	0.785	4.935	19.35	0.884	14.48
20	1.039	6.532	19.77	0.914	14.97
21	1.293	8.130	18.36	0.935	15.32
22	1.547	9.727	18.09	0.943	15.55
23	1.801	11.324	17.88	0.960	15.73
24	2.055	12.921	17.70	0.969	15.87
25	2.563	16.116	17.46	0.981	16.08
26	3.198	20.109	17.33	0.990	16.21
27	3.833	24.101	17.23	0.998	16.27
28	4.468	28.094	17.18	0.996	16.32
29	5.103	32.087	17.16	0.997	16.33
30	12.723	80.003	17.10	1.000	16.38

ROUGH WALL MEAN TEMPERATURE PROFILE
ARTIFICIALLY THICKENED UINF= 15.8M/SEC

RUN	=	80278	DEH	=	4.402
PLATE	=	15	DEH2	=	0.239
X1	=	1.47	DE	=	7.425
X2	=	3.93	DE2	=	0.894
DELY	=	0.023	TINF	=	17.09
UINF	=	16.01	TW	=	36.44
CF/2	=	0.00184	ST	=	0.00244

PT	Y	Y/DEH2	T	TBAR	T+
1	0.048	0.202	27.13	0.481	8.46
2	0.053	0.223	26.62	0.508	8.93
3	0.061	0.255	26.17	0.531	9.33
4	0.074	0.308	25.47	0.567	9.96
5	0.086	0.361	24.99	0.592	10.40
6	0.099	0.414	24.61	0.611	10.75
7	0.112	0.468	24.40	0.622	10.94
8	0.124	0.521	24.03	0.641	11.27
9	0.150	0.627	23.57	0.665	11.69
10	0.175	0.733	23.19	0.685	12.04
11	0.201	0.839	22.93	0.698	12.28
12	0.226	0.946	22.61	0.714	12.56
13	0.277	1.158	22.14	0.739	12.99
14	0.328	1.371	21.77	0.758	13.32
15	0.378	1.583	21.54	0.770	13.53
16	0.455	1.902	21.12	0.792	13.92
17	0.531	2.221	20.74	0.811	14.26
18	0.658	2.752	20.30	0.834	14.66
19	0.785	3.283	20.04	0.847	14.89
20	1.039	4.346	19.44	0.878	15.44
21	1.293	5.409	18.99	0.901	15.85
22	1.547	6.471	18.61	0.921	16.20
23	1.801	7.534	18.37	0.934	16.42
24	2.055	8.596	18.16	0.945	16.61
25	2.563	10.722	17.87	0.960	16.87
26	3.198	13.378	17.57	0.975	17.14
27	3.833	16.034	17.39	0.984	17.31
28	4.468	18.691	17.27	0.990	17.41
29	5.103	21.347	17.22	0.993	17.46
30	5.738	24.004	17.19	0.995	17.49
31	12.723	53.225	17.04	1.000	17.58

ROUGH WALL MEAN TEMPERATURE PROFILE
ARTIFICIALLY THICKENED UINF= 15.8M/SEC

RUN	=	80278	DEH	=	5.267
PLATE	=	18	DEH2	=	0.307
X1	=	1.78	DE	=	7.920
X2	=	4.24	DE2	=	0.935
DELY	=	0.023	TINF	=	17.29
UINF	=	16.01	TW	=	36.31
CF/2	=	0.00183	ST	=	0.00241

PT	Y	Y/DEH2	T	TBAR	T+
1	0.048	0.157	27.13	0.483	8.57
2	0.053	0.174	26.78	0.501	8.89
3	0.061	0.199	26.30	0.526	9.34
4	0.074	0.240	25.74	0.556	9.87
5	0.086	0.282	25.47	0.570	10.11
6	0.099	0.323	24.96	0.597	10.59
7	0.124	0.406	24.44	0.624	11.07
8	0.150	0.489	24.06	0.644	11.43
9	0.175	0.571	23.69	0.664	11.78
10	0.213	0.696	23.32	0.683	12.12
11	0.277	0.903	22.74	0.713	12.66
12	0.340	1.110	22.31	0.736	13.06
13	0.404	1.317	22.00	0.752	13.35
14	0.467	1.524	21.54	0.776	13.78
15	0.531	1.731	21.36	0.786	13.95
16	0.658	2.145	20.92	0.809	14.36
17	0.785	2.559	20.58	0.827	14.68
18	1.039	3.387	19.99	0.858	15.23
19	1.293	4.215	19.59	0.878	15.61
20	1.547	5.043	19.28	0.895	15.89
21	1.801	5.871	18.97	0.911	16.18
22	2.055	6.699	18.72	0.925	16.42
23	2.563	8.355	18.36	0.944	16.75
24	3.198	10.425	18.01	0.962	17.08
25	3.833	12.495	17.75	0.976	17.32
26	4.468	14.565	17.62	0.983	17.44
27	5.103	16.635	17.51	0.989	17.55
28	5.738	18.705	17.44	0.992	17.61
29	6.373	20.776	17.33	0.995	17.66
30	7.008	22.846	17.37	0.996	17.67
31	12.723	41.477	17.29	1.000	17.75

ROUGH WALL MEAN TEMPERATURE PROFILE
ARTIFICIALLY THICKENED UINF= 15.8M/SEC

RUN	=	80478	DEH	=	3.295
PLATE	=	18	DEH2	=	0.167
X1	=	1.78	DE	=	7.920
X2	=	4.24	DE2	=	0.935
DELY	=	0.023	TINF	=	17.68
UINF	=	16.01	TW	=	35.66
CF/2	=	0.00183	ST	=	0.00259

PT	Y	Y/DEH2	T	TBAR	T+
1	0.048	0.298	26.48	0.510	8.43
2	0.053	0.319	26.10	0.531	8.78
3	0.061	0.364	25.67	0.555	9.17
4	0.074	0.440	25.03	0.591	9.77
5	0.086	0.516	24.56	0.617	10.19
6	0.099	0.592	24.13	0.641	10.59
7	0.124	0.743	23.74	0.663	10.95
8	0.150	0.895	23.34	0.685	11.32
9	0.175	1.047	22.80	0.716	11.82
10	0.213	1.274	22.38	0.738	12.20
11	0.277	1.653	21.86	0.768	12.68
12	0.340	2.032	21.45	0.790	13.06
13	0.404	2.412	21.02	0.814	13.45
14	0.467	2.791	20.78	0.828	13.67
15	0.531	3.170	20.47	0.845	13.96
16	0.658	3.928	20.03	0.869	14.36
17	0.785	4.687	19.67	0.889	14.69
18	1.039	6.204	19.24	0.913	15.09
19	1.293	7.720	18.87	0.934	15.43
20	1.547	9.237	18.62	0.948	15.65
21	1.801	10.754	18.42	0.959	15.84
22	2.055	12.271	18.25	0.968	15.99
23	2.563	15.304	18.04	0.980	16.18
24	3.198	19.096	17.88	0.989	16.33
25	3.833	22.888	17.81	0.993	16.40
26	4.468	26.680	17.76	0.996	16.44
27	5.103	30.472	17.74	0.997	16.46
28	5.738	34.264	17.72	0.998	16.48
29	6.373	38.056	17.72	0.998	16.48
30	12.723	75.975	17.68	1.000	16.52

ROUGH WALL MEAN TEMPERATURE PROFILE
ARTIFICIALLY THICKENED UINF= 15.8M/SEC

RUN	=	80478	DEH	=	4.417
PLATE	=	21	DEH2	=	0.236
X1	=	2.08	DE	=	8.433
X2	=	4.54	DE2	=	0.996
DELY	=	0.023	TINF	=	17.68
UINF	=	16.01	TW	=	35.81
CF/2	=	0.00182	ST	=	0.00241

PT	Y	Y/DEH2	T	TBAR	T+
1	0.048	0.205	26.86	0.493	8.74
2	0.053	0.226	26.55	0.511	9.04
3	0.061	0.258	26.17	0.532	9.42
4	0.074	0.312	25.51	0.568	10.06
5	0.086	0.366	25.17	0.587	10.39
6	0.099	0.420	24.81	0.607	10.74
7	0.124	0.527	24.25	0.638	11.29
8	0.150	0.635	23.73	0.666	11.79
9	0.175	0.743	23.47	0.681	12.05
10	0.213	0.904	23.09	0.702	12.42
11	0.277	1.173	22.53	0.733	12.97
12	0.340	1.442	21.97	0.763	13.51
13	0.404	1.712	21.71	0.778	13.77
14	0.467	1.991	21.33	0.799	14.14
15	0.531	2.250	21.18	0.807	14.28
16	0.658	2.788	20.63	0.837	14.82
17	0.785	3.326	20.32	0.855	15.13
18	1.039	4.403	19.80	0.883	15.63
19	1.293	5.479	19.38	0.906	16.05
20	1.547	6.556	19.14	0.920	16.28
21	1.801	7.632	18.89	0.933	16.52
22	2.055	8.709	18.70	0.944	16.71
23	2.563	10.861	18.38	0.962	17.02
24	3.198	13.553	18.10	0.977	17.29
25	3.833	16.244	17.97	0.984	17.42
26	4.468	18.935	17.86	0.990	17.53
27	5.103	21.626	17.81	0.993	17.58
28	5.738	24.317	17.77	0.995	17.61
29	6.373	27.008	17.75	0.996	17.63
30	12.723	53.920	17.68	1.000	17.70

ROUGH WALL MEAN TEMPERATURE PROFILE
ARTIFICIALLY THICKENED UINF= 15.8M/SEC

RUN	=	80478	DEH	=	5.136
PLATE	=	23	DEH2	=	0.288
X1	=	2.29	DE	=	8.750
X2	=	4.75	DE2	=	1.033
DELY	=	0.023	TINF	=	17.79
UINF	=	16.01	TW	=	35.79
CF/2	=	0.00183	ST	=	0.00237

PT	Y	Y/DEH2	T	TBAR	T+
1	0.048	0.168	27.59	0.455	8.22
2	0.053	0.185	27.33	0.470	8.49
3	0.061	0.212	26.78	0.501	9.04
4	0.074	0.256	26.22	0.532	9.60
5	0.086	0.300	25.72	0.560	10.10
6	0.099	0.344	25.24	0.586	10.58
7	0.124	0.433	24.72	0.615	11.10
8	0.150	0.521	24.21	0.643	11.61
9	0.175	0.609	23.93	0.659	11.89
10	0.213	0.742	23.55	0.680	12.28
11	0.277	0.963	22.99	0.711	12.84
12	0.340	1.183	22.61	0.732	13.22
13	0.404	1.404	22.18	0.756	13.65
14	0.467	1.625	21.87	0.773	13.96
15	0.531	1.846	21.61	0.788	14.22
16	0.658	2.287	21.21	0.810	14.62
17	0.785	2.729	20.94	0.831	15.00
18	1.039	3.612	20.28	0.862	15.55
19	1.293	4.495	19.89	0.883	15.94
20	1.547	5.379	19.57	0.901	16.27
21	1.801	6.262	19.33	0.915	16.51
22	2.055	7.145	19.08	0.928	16.76
23	2.563	8.911	18.71	0.949	17.13
24	3.198	11.119	18.42	0.965	17.42
25	3.833	13.327	18.20	0.978	17.65
26	4.468	15.535	18.06	0.985	17.78
27	5.103	17.743	17.98	0.989	17.86
28	5.738	19.951	17.93	0.992	17.91
29	6.373	22.159	17.90	0.994	17.95
30	12.723	44.238	17.79	1.000	18.05

ROUGH WALL PEAK TEMPERATURE PROFILE
ARTIFICIALLY THICKENED UINF= 26.8M/SEC

RUN	=	71778	DEH	=	3.647
PLATE	=	12	DEH2	=	0.179
X1	=	1.17	DP	=	6.713
X2	=	3.49	DP2	=	0.864
DELY	=	0.023	TINF	=	21.07
UINF	=	26.94	TW	=	33.16
CF/2	=	0.00202	ST	=	0.00270

PT	Y	Y/DEH2	T	TBAR	T+
1	0.048	0.270	27.13	0.499	8.31
2	0.053	0.298	26.94	0.514	8.56
3	0.061	0.341	26.68	0.536	8.93
4	0.074	0.412	26.24	0.572	9.52
5	0.086	0.483	25.93	0.598	9.96
6	0.099	0.554	25.71	0.617	10.26
7	0.112	0.625	25.56	0.629	10.47
8	0.124	0.696	25.31	0.650	10.81
9	0.150	0.838	25.02	0.673	11.21
10	0.175	0.980	24.76	0.695	11.57
11	0.201	1.122	24.55	0.712	11.85
12	0.226	1.264	24.35	0.729	12.13
13	0.277	1.548	24.07	0.752	12.52
14	0.328	1.831	23.82	0.773	12.87
15	0.378	2.115	23.63	0.788	13.12
16	0.455	2.541	23.34	0.812	13.52
17	0.531	2.967	23.13	0.830	13.82
18	0.658	3.677	22.86	0.852	14.19
19	0.785	4.387	22.60	0.873	14.53
20	1.039	5.807	22.25	0.903	15.02
21	1.293	7.226	22.00	0.923	15.37
22	1.547	8.646	21.79	0.940	15.65
23	1.801	10.066	21.64	0.953	15.87
24	2.055	11.486	21.52	0.963	16.03
25	2.563	14.325	21.34	0.978	16.28
26	3.198	17.874	21.22	0.987	16.44
27	3.833	21.424	21.19	0.990	16.48
28	4.468	24.973	21.17	0.991	16.50
29	12.723	71.114	21.07	1.000	16.65

ROUGH WALL MEAN TEMPERATURE PROFILE
ARTIFICIALLY THICKENED UINF= 26.8M/SEC

RUN	=	71778	DEH	=	5.420
PLATE	=	15	DEH2	=	0.254
X1	=	1.47	DP	=	7.191
X2	=	3.79	DP2	=	0.916
DELY	=	0.023	TINF	=	21.30
UINF	=	26.90	TW	=	33.05
CF/2	=	0.00202	ST	=	0.00249

PT	Y	Y/DEH2	T	TBAR	T+
1	0.048	0.190	27.48	0.474	8.56
2	0.053	0.210	27.32	0.487	8.79
3	0.061	0.240	27.12	0.504	9.10
4	0.074	0.290	26.72	0.538	9.72
5	0.086	0.341	26.46	0.561	10.13
6	0.099	0.391	26.29	0.575	10.39
7	0.112	0.441	26.12	0.590	10.64
8	0.124	0.491	25.92	0.607	10.95
9	0.150	0.591	25.58	0.635	11.47
10	0.175	0.691	25.38	0.652	11.78
11	0.201	0.791	25.20	0.668	12.06
12	0.226	0.891	25.03	0.683	12.32
13	0.277	1.092	24.69	0.711	12.84
14	0.328	1.292	24.46	0.731	13.20
15	0.378	1.492	24.26	0.748	13.51
16	0.455	1.793	23.95	0.774	13.97
17	0.531	2.093	23.82	0.786	14.18
18	0.658	2.594	23.53	0.810	14.62
19	0.785	3.095	23.29	0.830	14.99
20	1.039	4.096	22.90	0.863	15.58
21	1.293	5.098	22.62	0.888	16.02
22	1.547	6.099	22.40	0.907	16.36
23	1.801	7.101	22.21	0.922	16.65
24	2.055	8.103	22.06	0.936	16.89
25	2.563	10.106	21.83	0.955	17.23
26	3.198	12.609	21.62	0.973	17.56
27	3.833	15.113	21.52	0.981	17.71
28	4.468	17.617	21.46	0.986	17.80
29	5.103	20.121	21.43	0.989	17.85
30	12.723	50.168	21.30	1.000	18.05

ROUGH WALL MEAN TEMPERATURE PROFILE
ARTIFICIALLY THICKENED UINF= 26.8M/SEC

RUN	=	71778	DEH	=	6.457
PLATE	=	18	DEH2	=	0.325
X1	=	1.78	DP	=	7.709
X2	=	4.10	DP2	=	0.978
DELY	=	0.023	TINF	=	21.28
UINF	=	26.90	TW	=	33.03
CF/2	=	0.00204	ST	=	0.00248

PT	Y	Y/DEH2	T	TBAR	T+
1	0.048	0.147	27.69	0.454	8.28
2	0.053	0.162	27.51	0.470	8.56
3	0.061	0.185	27.19	0.497	9.05
4	0.074	0.224	26.89	0.523	9.52
5	0.086	0.263	26.66	0.543	9.88
6	0.099	0.301	26.47	0.559	10.17
7	0.124	0.378	26.10	0.590	10.74
8	0.150	0.456	25.85	0.611	11.13
9	0.175	0.533	25.60	0.633	11.52
10	0.213	0.649	25.34	0.654	11.92
11	0.277	0.842	24.96	0.687	12.51
12	0.340	1.035	24.65	0.713	12.99
13	0.404	1.228	24.40	0.734	13.38
14	0.467	1.421	24.22	0.750	13.66
15	0.531	1.614	24.08	0.762	13.87
16	0.658	2.000	23.76	0.789	14.37
17	0.785	2.386	23.52	0.809	14.74
18	1.039	3.158	23.17	0.839	15.29
19	1.293	3.930	22.88	0.864	15.73
20	1.547	4.702	22.65	0.884	16.10
21	1.801	5.474	22.44	0.901	16.42
22	2.055	6.246	22.29	0.914	16.65
23	2.563	7.790	22.03	0.937	17.06
24	3.198	9.721	21.79	0.957	17.43
25	3.833	11.651	21.61	0.972	17.71
26	4.469	13.581	21.50	0.982	17.88
27	5.103	15.511	21.44	0.987	17.97
28	5.738	17.441	21.41	0.989	18.01
29	6.373	19.372	21.40	0.990	18.03
30	12.723	38.674	21.29	1.000	18.21

ROUGH WALL MEAN TEMPERATURE PROFILE
ARTIFICIALLY THICKENED UINF= 26.8M/SEC

RUN	=	71878	DEH	=	3.530
PLATE	=	18	DEH2	=	0.169
X1	=	1.78	DE	=	7.709
X2	=	4.10	DE2	=	0.978
DELY	=	0.023	TINF	=	20.70
UINF	=	26.82	TW	=	37.46
CF/2	=	0.00204	ST	=	0.00268

PT	Y	Y/DEH2	T	TBAR	T+
1	0.048	0.285	28.67	0.525	8.84
2	0.053	0.315	28.42	0.540	9.09
3	0.061	0.360	28.10	0.558	9.41
4	0.074	0.435	27.55	0.591	9.96
5	0.086	0.510	27.22	0.611	10.30
6	0.099	0.585	26.90	0.630	10.62
7	0.124	0.735	26.43	0.658	11.09
8	0.150	0.885	26.00	0.684	11.52
9	0.175	1.035	25.66	0.704	11.86
10	0.213	1.260	25.30	0.726	12.23
11	0.277	1.635	24.70	0.762	12.83
12	0.340	2.010	24.32	0.784	13.21
13	0.404	2.385	23.97	0.805	13.56
14	0.467	2.760	23.77	0.817	13.76
15	0.531	3.136	23.47	0.835	14.06
16	0.658	3.886	23.07	0.859	14.47
17	0.785	4.636	22.77	0.876	14.77
18	1.039	6.136	22.30	0.904	15.24
19	1.293	7.636	21.97	0.924	15.58
20	1.547	9.137	21.70	0.940	15.85
21	1.801	10.637	21.48	0.954	16.07
22	2.055	12.137	21.32	0.963	16.22
23	2.563	15.138	21.10	0.976	16.45
24	3.198	16.888	20.92	0.987	16.63
25	3.833	22.639	20.84	0.991	16.71
26	4.468	26.390	20.81	0.993	16.74
27	5.103	30.140	20.80	0.994	16.75
28	12.723	75.148	20.70	1.000	16.85

ROUGH WALL MEAN TEMPERATURE PROFILE
ARTIFICIALLY THICKENED UINF= 26.8M/SEC

RUN	=	71878	DEH	=	4.793
PLATE	=	21	DEH2	=	0.242
X1	=	2.08	DE	=	9.573
X2	=	4.40	DE2	=	1.038
DELY	=	0.023	TINF	=	20.93
UINF	=	26.82	TW	=	37.50
CF/2	=	0.00202	ST	=	0.00248

PT	Y	Y/DEH2	T	TBAR	T+
1	0.048	0.199	29.18	0.499	9.05
2	0.053	0.220	28.95	0.513	9.30
3	0.061	0.252	28.58	0.535	9.70
4	0.074	0.304	28.15	0.561	10.17
5	0.086	0.357	27.78	0.583	10.57
6	0.099	0.409	27.48	0.601	10.83
7	0.124	0.514	26.98	0.631	11.44
8	0.150	0.619	26.54	0.657	11.91
9	0.175	0.724	26.31	0.671	12.16
10	0.213	0.881	25.88	0.697	12.64
11	0.277	1.143	25.39	0.726	13.17
12	0.340	1.406	25.00	0.750	13.59
13	0.404	1.668	24.68	0.769	13.93
14	0.467	1.930	24.38	0.787	14.26
15	0.531	2.192	24.13	0.802	14.53
16	0.658	2.717	23.71	0.827	14.99
17	0.785	3.241	23.38	0.847	15.35
18	1.039	4.290	22.89	0.876	15.88
19	1.293	5.339	22.56	0.896	16.24
20	1.547	6.388	22.29	0.913	16.54
21	1.801	7.437	22.03	0.928	16.81
22	2.055	8.486	21.85	0.939	17.02
23	2.563	10.584	21.58	0.955	17.31
24	3.198	13.206	21.29	0.973	17.63
25	3.833	15.828	21.13	0.982	17.80
26	4.468	18.451	21.03	0.988	17.90
27	5.103	21.073	20.97	0.991	17.97
28	5.738	23.695	20.94	0.993	18.00
29	6.373	26.318	20.94	0.994	18.01
30	12.723	52.541	20.83	1.000	18.12

ROUGH WALL MEAN TEMPERATURE PROFILE
ARTIFICIALLY THICKENED UINF= 26.8M/SEC

RUN	=	71878	DEH	=	6.159
PLATE	=	23	DEH2	=	0.290
X1	=	2.29	DE	=	8.938
X2	=	4.61	DE2	=	1.078
DELY	=	0.023	TINF	=	20.86
UINF	=	26.82	TW	=	37.48
CF/2	=	0.00202	ST	=	0.00246

PT	Y	Y/DEH2	T	TBAR	T+
1	0.048	0.166	29.34	0.490	8.94
2	0.053	0.184	29.14	0.502	9.16
3	0.061	0.210	28.88	0.518	9.46
4	0.074	0.254	28.46	0.543	9.92
5	0.086	0.298	28.11	0.564	10.30
6	0.099	0.342	27.79	0.583	10.65
7	0.124	0.429	27.34	0.610	11.14
8	0.150	0.517	26.93	0.635	11.60
9	0.175	0.605	26.62	0.653	11.93
10	0.213	0.736	26.26	0.675	12.34
11	0.277	0.955	25.72	0.709	12.93
12	0.340	1.174	25.30	0.733	13.39
13	0.404	1.393	25.01	0.750	13.70
14	0.467	1.612	24.80	0.763	13.94
15	0.531	1.831	24.46	0.783	14.31
16	0.658	2.269	24.08	0.807	14.74
17	0.785	2.708	23.77	0.825	15.07
18	1.039	3.584	23.27	0.855	15.62
19	1.293	4.460	22.90	0.877	16.03
20	1.547	5.336	22.55	0.898	16.42
21	1.801	6.213	22.36	0.910	16.62
22	2.055	7.089	22.14	0.923	16.86
23	2.563	8.841	21.82	0.942	17.21
24	3.198	11.032	21.52	0.961	17.55
25	3.833	13.223	21.32	0.972	17.76
26	4.468	15.413	21.18	0.981	17.92
27	5.103	17.604	21.10	0.985	18.00
28	5.738	19.794	21.06	0.988	18.05
29	6.373	21.985	21.02	0.990	18.09
30	12.723	43.891	20.86	1.000	18.27

ROUGH WALL MEAN TEMPERATURE PROFILE
ARTIFICIALLY THICKENED (W/F=.008 PLTS 1-6)

RUN	=	72178	DEH	=	2.342
PLATE	=	15	DEH2	=	0.077
X1	=	1.47	DE	=	8.153
X2	=	4.77	DE2	=	1.110
DELY	=	0.023	TINF	=	21.25
UINF	=	26.94	TW	=	37.65
CF/2	=	0.00198	ST	=	0.00274

PT	Y	Y/DEH2	T	TBAR	T+
1	0.048	0.624	28.43	0.562	9.13
2	0.053	0.689	28.07	0.584	9.49
3	0.061	0.788	27.75	0.603	9.80
4	0.074	0.952	27.24	0.635	10.31
5	0.086	1.116	26.85	0.658	10.69
6	0.099	1.280	26.44	0.684	11.10
7	0.112	1.444	26.14	0.702	11.40
8	0.124	1.609	25.92	0.715	11.61
9	0.150	1.937	25.49	0.742	12.04
10	0.175	2.265	25.10	0.765	12.42
11	0.201	2.593	24.82	0.782	12.70
12	0.226	2.922	24.59	0.797	12.94
13	0.277	3.578	24.15	0.823	13.37
14	0.328	4.235	23.75	0.847	13.76
15	0.378	4.891	23.52	0.862	13.99
16	0.455	5.876	23.22	0.880	14.23
17	0.531	6.861	22.93	0.897	14.57
18	0.658	8.502	22.57	0.920	14.94
19	0.785	10.144	22.35	0.933	15.15
20	1.039	13.426	22.00	0.954	15.50
21	1.293	16.709	21.76	0.969	15.73
22	1.547	19.992	21.66	0.975	15.94
23	1.801	23.274	21.55	0.982	15.94
24	2.055	26.557	21.47	0.987	16.03
25	2.563	33.122	21.41	0.990	16.08
26	3.198	41.329	21.39	0.992	16.11
27	3.833	49.536	21.36	0.993	16.13
28	15.263	197.257	21.25	1.000	16.24

ROUGH WALL MEAN TEMPERATURE PROFILE
ARTIFICIALLY THICKENED (W/F=.008 PLTS 1-6)

RUN	=	72178	DEH	=	4.501
PLATE	=	19	DEH2	=	0.191
X1	=	1.88	DE	=	9.515
X2	=	5.18	DE2	=	1.184
DELY	=	0.023	TINF	=	21.28
UINF	=	26.94	TW	=	37.67
CF/2	=	0.00198	ST	=	0.00257

PT	Y	Y/DEH2	T	TBAR	T+
1	0.048	0.252	29.00	0.529	9.16
2	0.053	0.279	28.73	0.546	9.45
3	0.061	0.319	28.46	0.562	9.73
4	0.074	0.385	28.03	0.588	10.18
5	0.086	0.452	27.68	0.610	10.55
6	0.099	0.518	27.41	0.626	10.84
7	0.124	0.651	26.90	0.657	11.38
8	0.150	0.784	26.51	0.681	11.79
9	0.175	0.917	26.24	0.697	12.07
10	0.213	1.116	25.84	0.722	12.50
11	0.277	1.448	25.34	0.752	13.03
12	0.340	1.780	25.09	0.768	13.29
13	0.404	2.113	24.54	0.801	13.88
14	0.467	2.445	24.27	0.818	14.16
15	0.531	2.777	24.10	0.828	14.34
16	0.658	3.441	23.67	0.855	14.80
17	0.785	4.106	23.40	0.871	15.08
18	1.039	5.434	22.96	0.898	15.54
19	1.293	6.763	22.64	0.917	15.88
20	1.547	8.092	22.39	0.932	16.14
21	1.801	9.420	22.17	0.946	16.38
22	2.055	10.749	22.05	0.953	16.50
23	2.563	13.406	21.83	0.967	16.74
24	3.198	16.728	21.62	0.979	16.96
25	3.833	20.050	21.53	0.985	17.05
26	4.468	23.371	21.45	0.990	17.14
27	5.103	26.693	21.41	0.992	17.18
28	5.738	30.015	21.40	0.993	17.19
29	15.263	79.840	21.28	1.000	17.31

ROUGH WALL MEAN TEMPERATURE PROFILE
ARTIFICIALLY THICKENED (W/F=.008 PLTS 1-6)

RUN	=	72178	DEH	=	6.831
PLATE	=	23	DEH2	=	0.286
X1	=	2.29	DE	=	10.239
X2	=	5.59	DE2	=	1.272
DELY	=	0.023	TINF	=	21.27
UINF	=	26.98	TW	=	37.65
CF/2	=	0.00199	ST	=	0.00244

PT	Y	Y/DEH2	T	TBAR	T+
1	0.048	0.169	29.69	0.486	8.89
2	0.053	0.187	29.44	0.501	9.16
3	0.061	0.213	29.11	0.521	9.53
4	0.074	0.258	28.66	0.549	10.03
5	0.086	0.302	28.29	0.571	10.44
6	0.099	0.347	28.01	0.588	10.76
7	0.112	0.391	27.74	0.605	11.06
8	0.124	0.436	27.52	0.618	11.30
9	0.150	0.524	27.12	0.643	11.75
10	0.175	0.613	26.84	0.660	12.06
11	0.201	0.702	26.57	0.676	12.36
12	0.226	0.791	26.30	0.693	12.66
13	0.277	0.969	26.00	0.711	13.00
14	0.328	1.147	25.67	0.731	13.37
15	0.378	1.325	25.30	0.754	13.78
16	0.455	1.591	24.93	0.776	14.19
17	0.531	1.858	24.71	0.790	14.44
18	0.658	2.302	24.36	0.811	14.83
19	0.785	2.747	24.00	0.833	15.23
20	1.039	3.636	23.57	0.859	15.71
21	1.293	4.525	23.20	0.882	16.13
22	1.547	5.414	22.95	0.897	16.41
23	1.801	6.303	22.69	0.913	16.69
24	2.055	7.192	22.52	0.923	16.88
25	2.563	8.970	22.24	0.941	17.20
26	3.198	11.192	21.95	0.958	17.52
27	3.833	13.415	21.79	0.968	17.70
28	4.468	15.637	21.67	0.976	17.84
29	5.103	17.860	21.56	0.982	17.96
30	5.738	20.082	21.50	0.986	18.02
31	6.373	22.305	21.46	0.989	18.07
32	15.263	53.419	21.27	1.000	18.28

ROUGH WALL MEAN VELOCITY PROFILE
NATURALLY DEVELOPED UINF=10.1 M/SEC

RUN	=	82678	DE	=	1.739
PLATE	=	6	DE1	=	0.313
X1	=	0.56	DE2	=	0.219
X2	=	0.56	H	=	1.43
DELY	=	0.023	G	=	6.03
UINF	=	10.04	REX2	=	0.37E 06
CF/2	=	0.00243	REM	=	1446.5
UTAU	=	0.495	REK	=	25.64

PT	Y	Y/DE	U	U/UINF	U+
1	0.048	0.027	4.27	0.425	8.63
2	0.053	0.030	4.52	0.450	9.13
3	0.061	0.035	4.74	0.472	9.57
4	0.069	0.039	4.94	0.492	9.98
5	0.076	0.043	5.14	0.512	10.38
6	0.086	0.049	5.34	0.532	10.80
7	0.099	0.056	5.50	0.548	11.11
8	0.112	0.063	5.66	0.564	11.45
9	0.124	0.071	5.79	0.577	11.71
10	0.150	0.085	6.02	0.600	12.17
11	0.201	0.114	6.35	0.633	12.84
12	0.251	0.143	6.62	0.660	13.38
13	0.302	0.172	6.84	0.681	13.82
14	0.378	0.215	7.12	0.709	14.39
15	0.455	0.258	7.37	0.734	14.90
16	0.531	0.301	7.61	0.758	15.38
17	0.632	0.359	7.91	0.788	15.98
18	0.734	0.417	8.17	0.814	16.51
19	0.836	0.474	8.43	0.840	17.03
20	0.937	0.532	8.67	0.863	17.51
21	1.039	0.590	8.89	0.885	17.96
22	1.166	0.662	9.16	0.912	18.50
23	1.293	0.734	9.40	0.936	18.99
24	1.547	0.878	9.76	0.973	19.73
25	1.801	1.022	9.95	0.992	20.11
26	2.055	1.166	10.01	0.997	20.23
27	2.309	1.310	10.04	1.000	20.29
28	2.563	1.455	10.04	1.000	20.29
29	2.817	1.599	10.04	1.000	20.29

ROUGH WALL MEAN VELOCITY PROFILE
NATURALLY DEVELOPED UINF=10.1 M/SEC

RUN	=	82678	DE	=	2.315
PLATE	=	9	DE1	=	0.412
X1	=	0.86	DE2	=	0.291
X2	=	0.86	H	=	1.41
DELY	=	0.023	G	=	6.14
UINF	=	10.01	REX2	=	0.57E 06
CF/2	=	0.00228	REM	=	1917.0
UTAU	=	0.478	REK	=	24.77

PT	Y	Y/DE	U	U/UINF	U+
1	0.048	0.021	4.06	0.406	8.50
2	0.053	0.023	4.29	0.428	8.97
3	0.061	0.026	4.52	0.452	9.46
4	0.069	0.029	4.71	0.470	9.84
5	0.076	0.033	4.90	0.489	10.25
6	0.086	0.037	5.04	0.503	10.54
7	0.099	0.042	5.25	0.525	10.99
8	0.112	0.048	5.43	0.542	11.35
9	0.124	0.053	5.58	0.557	11.66
10	0.150	0.064	5.92	0.581	12.17
11	0.201	0.086	6.11	0.610	12.77
12	0.251	0.108	6.35	0.634	13.28
13	0.302	0.129	6.56	0.655	13.71
14	0.378	0.162	6.78	0.677	14.18
15	0.455	0.194	7.02	0.701	14.68
16	0.531	0.227	7.23	0.722	15.12
17	0.632	0.270	7.48	0.747	15.64
18	0.734	0.314	7.70	0.769	16.10
19	0.836	0.357	7.89	0.788	16.50
20	0.937	0.401	8.09	0.808	16.93
21	1.039	0.444	8.30	0.829	17.36
22	1.166	0.499	8.53	0.852	17.84
23	1.293	0.553	8.73	0.872	18.26
24	1.547	0.662	9.11	0.910	19.06
25	1.801	0.770	9.45	0.944	19.77
26	2.055	0.879	9.73	0.972	20.36
27	2.309	0.987	9.91	0.990	20.72
28	2.563	1.096	9.99	0.998	20.90
29	2.817	1.205	10.00	0.999	20.92
30	3.071	1.313	10.01	1.000	20.94
31	4.087	1.748	10.01	1.000	20.94

ROUGH WALL MEAN VELOCITY PROFILE
NATURALLY DEVELOPED UINF=10.1 M/SEC

RUN	=	82678	DE	=	2.830
PLATE	=	12	DE1	=	0.505
X1	=	1.17	DE2	=	0.359
X2	=	1.17	H	=	1.41
DELY	=	0.023	G	=	6.33
UINF	=	10.03	REX2	=	0.77E 06
CF/2	=	0.00209	REM	=	2370.5
UTAU	=	0.459	REK	=	23.76

PT	Y	Y/DE	U	U/UINF	U+
1	0.048	0.017	3.96	0.395	8.42
2	0.053	0.019	4.11	0.410	8.96
3	0.061	0.021	4.36	0.435	9.52
4	0.069	0.024	4.53	0.452	9.89
5	0.076	0.027	4.71	0.470	10.28
6	0.086	0.030	4.94	0.493	10.78
7	0.099	0.035	5.15	0.513	11.23
8	0.112	0.039	5.28	0.527	11.53
9	0.124	0.044	5.37	0.535	11.71
10	0.150	0.053	5.66	0.565	12.35
11	0.201	0.070	5.94	0.593	12.96
12	0.251	0.088	6.22	0.620	13.56
13	0.302	0.106	6.36	0.634	13.86
14	0.378	0.133	6.63	0.661	14.45
15	0.455	0.159	6.82	0.680	14.88
16	0.531	0.186	7.00	0.698	15.26
17	0.632	0.222	7.21	0.718	15.71
18	0.734	0.257	7.42	0.740	16.18
19	0.836	0.293	7.60	0.758	16.58
20	0.937	0.329	7.77	0.775	16.95
21	1.039	0.364	7.97	0.795	17.38
22	1.166	0.409	8.17	0.814	17.81
23	1.293	0.453	8.33	0.831	18.17
24	1.801	0.631	9.00	0.897	19.63
25	2.309	0.809	9.56	0.953	20.85
26	2.817	0.987	9.91	0.988	21.62
27	3.325	1.166	10.02	0.999	21.86
28	3.833	1.344	10.03	1.000	21.87
29	4.341	1.522	10.03	1.000	21.87

ROUGH WALL MEAN VELOCITY PROFILE
NATURALLY DEVELOPED UINF=10.1 M/SEC

RUN	=	82678	DF	=	3.399
PLATE	=	15	DE1	=	0.609
X1	=	1.47	DE2	=	0.433
X2	=	1.47	H	=	1.41
DELY	=	0.023	G	=	6.46
UINF	=	10.04	REX2	=	0.97E 06
CF/2	=	0.00200	REM	=	2858.9
UTAU	=	0.449	REK	=	23.25

PT	Y	Y/DE	U	U/UINF	U+
1	0.048	0.014	3.75	0.374	8.36
2	0.053	0.016	3.91	0.390	8.71
3	0.061	0.018	4.22	0.420	9.40
4	0.074	0.022	4.51	0.449	10.05
5	0.086	0.025	4.74	0.472	10.56
6	0.099	0.029	4.96	0.495	11.06
7	0.124	0.036	5.27	0.525	11.73
8	0.150	0.044	5.46	0.544	12.17
9	0.201	0.059	5.75	0.573	12.80
10	0.251	0.073	6.00	0.597	13.36
11	0.302	0.088	6.18	0.615	13.76
12	0.378	0.111	6.38	0.636	14.22
13	0.455	0.133	6.57	0.655	14.64
14	0.531	0.155	6.75	0.672	15.03
15	0.658	0.192	7.02	0.699	15.63
16	0.785	0.229	7.26	0.723	16.18
17	0.912	0.266	7.48	0.745	16.66
18	1.039	0.304	7.64	0.761	17.02
19	1.166	0.341	7.81	0.779	17.41
20	1.293	0.378	8.01	0.798	17.84
21	1.547	0.452	8.[illegible]3	0.830	18.55
22	1.801	0.526	8.63	0.860	19.24
23	2.309	0.675	9.15	0.912	20.39
24	2.817	0.823	9.61	0.957	21.41
25	3.579	1.046	9.98	0.995	22.24
26	4.341	1.269	10.04	1.000	22.36
27	5.103	1.491	10.04	1.000	22.36
28	6.119	1.788	10.04	1.000	22.36

ROUGH WALL MEAN VELOCITY PROFILE
NATURALLY DEVELOPED UINF=10.1 M/SEC

RUN	=	82578	DE	=	3.940
PLATE	=	18	DE1	=	0.705
X1	=	1.78	DE2	=	0.502
X2	=	1.78	H	=	1.40
DELY	=	0.023	G	=	6.57
UINF	=	10.03	REX2	=	0.12E 07
CF/2	=	0.00192	REM	=	3311.0
UTAU	=	0.439	REK	=	22.76

PT	Y	Y/DE	U	U/UINF	U+
1	0.048	0.012	3.42	0.341	7.79
2	0.053	0.013	3.66	0.365	8.34
3	0.061	0.015	3.92	0.391	8.93
4	0.074	0.019	4.31	0.430	9.81
5	0.086	0.022	4.57	0.456	10.40
6	0.099	0.025	4.79	0.474	10.90
7	0.124	0.031	5.12	0.511	11.66
8	0.150	0.038	5.31	0.529	12.08
9	0.201	0.051	5.63	0.562	12.82
10	0.251	0.063	5.86	0.584	13.33
11	0.302	0.076	6.06	0.604	13.79
12	0.378	0.096	6.26	0.624	14.24
13	0.455	0.115	6.44	0.642	14.65
14	0.531	0.134	6.61	0.660	15.05
15	0.658	0.166	6.86	0.684	15.61
16	0.785	0.198	7.09	0.706	16.11
17	0.912	0.230	7.23	0.721	16.46
18	1.039	0.262	7.42	0.739	16.88
19	1.166	0.294	7.60	0.758	17.30
20	1.293	0.326	7.75	0.773	17.64
21	1.547	0.390	8.07	0.805	18.36
22	1.801	0.454	8.34	0.831	18.97
23	2.309	0.583	8.82	0.880	20.08
24	2.817	0.711	9.27	0.925	2[illegible]10
25	3.579	0.903	9.78	0.975	22.25
26	4.341	1.095	10.01	0.998	22.77
27	5.103	1.288	10.03	1.000	22.82
28	6.119	1.544	10.03	1.000	22.82
29	6.373	1.608	10.03	1.000	22.82

ROUGH WALL MEAN VELOCITY PROFILE
NATURALLY DEVELOPED UINF=10.1 M/SEC

RUN	=	82578	DE	=	4.415
PLATE	=	21	DE1	=	0.796
X1	=	2.08	DE2	=	0.569
X2	=	2.08	H	=	1.40
DELY	=	0.023	G	=	6.61
UINF	=	10.05	REX2	=	0.14E 07
CF/2	=	0.00185	REM	=	3760.5
UTAU	=	0.432	REK	=	22.38

PT	Y	Y/DE	U	U/UINF	U+
1	0.048	0.011	3.47	0.346	8.04
2	0.053	0.012	3.70	0.369	8.57
3	0.061	0.014	4.01	0.399	9.29
4	0.074	0.017	4.31	0.429	9.98
5	0.086	0.019	4.58	0.456	10.59
6	0.099	0.022	4.78	0.476	11.07
7	0.124	0.028	5.09	0.506	11.77
8	0.150	0.034	5.30	0.528	12.27
9	0.201	0.045	5.55	0.553	12.85
10	0.251	0.057	5.83	0.580	13.48
11	0.302	0.068	5.95	0.592	13.77
12	0.378	0.085	6.20	0.617	14.35
13	0.455	0.102	6.35	0.632	14.69
14	0.531	0.120	6.50	0.647	15.05
15	0.658	0.148	6.73	0.669	15.56
16	0.785	0.177	6.93	0.690	16.04
17	0.912	0.205	7.11	0.707	16.45
18	1.039	0.234	7.30	0.727	16.89
19	1.293	0.291	7.59	0.756	17.57
20	1.801	0.406	8.12	0.808	18.79
21	2.436	0.549	8.67	0.863	20.07
22	3.071	0.692	9.20	0.916	21.29
23	3.833	0.864	9.70	0.965	22.44
24	4.595	1.035	9.99	0.994	23.12
25	5.357	1.207	10.03	0.998	23.22
26	6.119	1.379	10.04	1.000	23.24
27	6.[illegible]81	1.551	10.05	1.000	23.25

ROUGH WALL MEAN VELOCITY PROFILE
NATURALLY DEVELOPED UINF=10.1 M/SEC

RUN	=	82578	DE	=	4.739
PLATE	=	23	DE1	=	0.856
X1	=	2.29	DE2	=	0.612
X2	=	2.29	H	=	1.40
DELY	=	0.023	G	=	6.67
UINF	=	10.05	REX2	=	0.15E 07
CF/2	=	0.00182	REM	=	4050.1
UTAU	=	0.429	REK	=	22.22

PT	Y	Y/DE	U	U/UINF	U+
1	0.048	0.010	3.39	0.337	7.90
2	0.053	0.011	3.55	0.353	8.27
3	0.061	0.013	3.91	0.389	9.11
4	0.074	0.015	4.20	0.417	9.79
5	0.086	0.018	4.47	0.445	10.42
6	0.099	0.021	4.70	0.467	10.95
7	0.124	0.026	5.02	0.499	11.70
8	0.150	0.031	5.22	0.519	12.18
9	0.201	0.042	5.49	0.546	12.80
10	0.251	0.053	5.75	0.572	13.40
11	0.302	0.063	5.92	0.589	13.80
12	0.378	0.079	6.09	0.605	14.19
13	0.455	0.095	6.33	0.629	14.75
14	0.531	0.111	6.42	0.639	14.98
15	0.658	0.138	6.68	0.664	15.56
16	0.785	0.165	6.83	0.680	15.93
17	0.912	0.191	7.07	0.703	16.48
18	1.039	0.218	7.18	0.714	16.74
19	1.293	0.272	7.53	0.749	17.55
20	1.801	0.378	8.01	0.797	18.68
21	2.436	0.512	8.55	0.850	19.93
22	3.071	0.645	9.02	0.897	21.04
23	3.833	0.805	9.53	0.948	22.22
24	4.555	0.965	9.91	0.985	23.09
25	5.357	1.125	10.04	0.998	23.40
26	6.119	1.285	10.05	1.000	23.44
27	6.881	1.445	10.05	1.000	23.44

ROUGH WALL MEAN VELOCITY PROFILE
ARTIFICIALLY THICKENED UINF=10.1 M/SEC

RUN	=	81678	DE	=	4.887
PLATE	=	6	DE1	=	0.967
X1	=	0.56	DE2	=	0.689
X2	=	2.91	H	=	1.40
DELY	=	0.023	G	=	7.14
UINF	=	10.09	REX2	=	0.19E 07
CF/2	=	0.00162	REM	=	4560.1
UTAU	=	0.406	REK	=	20.98

PT	Y	Y/DE	U	U/UINF	U+
1	0.048	0.010	3.43	0.340	8.46
2	0.053	0.011	3.63	0.360	8.94
3	0.061	0.012	3.91	0.388	9.63
4	0.074	0.015	4.22	0.419	10.39
5	0.086	0.018	4.52	0.448	11.14
6	0.099	0.020	4.70	0.466	11.59
7	0.112	0.023	4.86	0.482	11.97
8	0.124	0.025	5.03	0.499	12.39
9	0.150	0.031	5.18	0.513	12.76
10	0.175	0.036	5.44	0.539	13.40
11	0.201	0.041	5.48	0.544	13.51
12	0.226	0.046	5.66	0.561	13.95
13	0.277	0.056	5.87	0.582	14.47
14	0.328	0.067	6.03	0.597	14.84
15	0.378	0.077	6.12	0.607	15.08
16	0.455	0.093	6.32	0.626	15.56
17	0.531	0.108	6.45	0.639	15.89
18	0.658	0.134	6.65	0.659	16.38
19	0.785	0.160	6.78	0.672	16.70
20	0.912	0.186	6.97	0.691	17.16
21	1.039	0.212	7.09	0.703	17.46
22	1.293	0.263	7.28	0.722	17.93
23	1.547	0.315	7.50	0.744	18.48
24	1.801	0.367	7.69	0.763	18.95
25	2.055	0.418	7.92	0.785	19.49
26	2.563	0.522	8.30	0.822	20.43
27	3.198	0.651	8.78	0.870	21.61
28	3.833	0.781	9.30	0.922	22.91
29	4.468	0.910	9.77	0.969	24.06
30	5.103	1.039	10.05	0.996	24.74
31	5.738	1.169	10.09	1.000	24.84
32	6.373	1.298	10.09	1.000	24.85
33	7.008	1.427	10.09	1.000	24.85

ROUGH WALL MEAN VELOCITY PROFILE
ARTIFICIALLY THICKENED UINF=10.1 M/SEC

RUN	=	81678	DE	=	5.690
PLATE	=	9	DE1	=	1.013
X1	=	0.86	DE2	=	0.782
X2	=	3.22	H	=	1.18
DELY	=	0.023	G	=	6.74
UINF	=	10.03	REX2	=	0.21E 07
CF/2	=	0.00169	REM	=	4817.2
UTAU	=	0.412	REK	=	21.30

PT	Y	Y/DE	U	U/UINF	U+
1	0.048	0.009	3.45	0.344	8.33
2	0.053	0.009	3.50	0.349	8.50
3	0.061	0.011	3.83	0.382	9.28
4	0.074	0.013	4.15	0.414	10.07
5	0.086	0.015	4.45	0.444	10.81
6	0.099	0.017	4.64	0.463	11.26
7	0.112	0.020	4.83	0.482	11.72
8	0.124	0.022	5.03	0.502	12.20
9	0.150	0.026	5.21	0.519	12.63
10	0.175	0.031	5.38	0.537	13.06
11	0.201	0.035	5.52	0.550	13.39
12	0.226	0.040	5.64	0.562	13.68
13	0.277	0.048	5.84	0.582	14.16
14	0.328	0.057	5.96	0.594	14.45
15	0.378	0.066	6.05	0.604	14.68
16	0.455	0.080	6.22	0.620	15.08
17	0.531	0.093	6.38	0.636	15.47
18	0.658	0.115	6.58	0.656	15.96
19	0.785	0.137	6.80	0.673	16.49
20	1.039	0.182	7.11	0.709	17.26
21	1.293	0.226	7.27	0.725	17.64
22	1.547	0.271	7.53	0.751	18.27
23	1.801	0.315	7.67	0.765	18.62
24	2.055	0.360	7.88	0.786	19.11
25	2.563	0.449	8.23	0.821	19.98
26	3.198	0.560	8.66	0.864	21.01
27	3.833	0.671	9.10	0.903	22.08
28	4.468	0.782	9.48	0.945	23.00
29	5.103	0.893	9.75	0.972	23.64
30	5.738	1.004	9.93	0.990	24.09
31	6.373	1.115	10.01	0.998	24.29
32	7.008	1.227	10.04	1.001	24.35
33	7.643	1.338	10.03	1.000	24.33
34	8.913	1.560	10.03	1.000	24.33

ROUGH WALL MEAN VELOCITY PROFILE
ARTIFICIALLY THICKENED UINF=10.1 M/SEC

RUN	=	81678	DE	=	6.538
PLATE	=	12	DE1	=	1.061
X1	=	1.17	DE2	=	0.778
X2	=	3.52	H	=	1.36
DELY	=	0.023	G	=	6.56
UINF	=	10.00	REX2	=	0.23E 07
CF/2	=	0.00165	REM	=	5109.8
UTAU	=	0.406	REK	=	21.00

PT	Y	Y/DE	U	U/UINF	U+
1	0.048	0.007	3.37	0.337	8.30
2	0.053	0.008	3.55	0.355	8.74
3	0.061	0.009	3.79	0.379	9.32
4	0.074	0.011	4.13	0.413	10.18
5	0.086	0.013	4.46	0.446	10.98
6	0.099	0.015	4.71	0.471	11.59
7	0.112	0.017	4.86	0.486	11.96
8	0.124	0.019	4.95	0.495	12.18
9	0.150	0.023	5.17	0.517	12.73
10	0.175	0.027	5.34	0.534	13.15
11	0.201	0.031	5.52	0.552	13.58
12	0.226	0.034	5.64	0.563	13.87
13	0.277	0.042	5.83	0.583	14.36
14	0.329	0.050	5.92	0.592	14.58
15	0.378	0.058	6.12	0.612	15.07
16	0.455	0.069	6.31	0.630	15.52
17	0.531	0.081	6.46	0.646	15.91
18	0.658	0.100	6.60	0.659	16.23
19	0.785	0.120	6.82	0.682	16.79
20	1.039	0.158	7.02	0.702	17.27
21	1.293	0.197	7.29	0.729	17.94
22	1.547	0.236	7.50	0.749	18.45
23	1.801	0.274	7.71	0.771	18.97
24	2.055	0.313	7.91	0.791	19.46
25	2.563	0.391	8.24	0.824	20.28
26	3.198	0.487	8.59	0.859	21.14
27	3.833	0.584	8.95	0.894	22.02
28	4.469	0.681	9.27	0.927	22.82
29	5.103	0.778	9.55	0.955	23.51
30	5.738	0.875	9.76	0.975	24.01
31	6.373	0.971	9.88	0.987	24.31
32	7.008	1.068	9.96	0.996	24.51
33	7.643	1.165	9.98	0.998	24.57
34	8.278	1.262	10.00	1.000	24.62
35	8.913	1.358	10.00	1.000	24.62

ROUGH WALL MEAN VELOCITY PROFILE
ARTIFICIALLY THICKENED UINF=10.1 M/SEC

RUN	=	81678	DE	=	7.137
PLATE	=	15	DE1	=	1.105
X1	=	1.47	DE2	=	0.824
X2	=	3.83	H	=	1.34
DELY	=	0.023	G	=	6.30
UINF	=	9.98	REX2	=	0.25E 07
CF/2	=	0.00163	REM	=	5397.3
UTAU	=	0.403	REK	=	20.92

PT	Y	Y/DE	U	U/UINF	U+
1	0.048	0.007	3.53	0.353	8.75
2	0.053	0.007	3.80	0.380	9.42
3	0.061	0.009	3.93	0.394	9.76
4	0.074	0.010	4.30	0.431	10.68
5	0.086	0.012	4.54	0.455	11.26
6	0.099	0.014	4.70	0.471	11.67
7	0.112	0.016	4.91	0.492	12.19
8	0.124	0.017	5.04	0.505	12.51
9	0.150	0.021	5.24	0.526	13.02
10	0.175	0.024	5.44	0.545	13.51
11	0.201	0.028	5.54	0.555	13.74
12	0.226	0.032	5.64	0.565	13.99
13	0.277	0.039	5.91	0.593	14.68
14	0.328	0.046	6.03	0.604	14.97
15	0.378	0.053	6.18	0.619	15.34
16	0.455	0.064	6.27	0.628	15.56
17	0.531	0.074	6.47	0.648	16.05
18	0.658	0.092	6.71	0.672	16.65
19	0.785	0.110	6.85	0.686	17.00
20	1.039	0.145	7.06	0.708	17.53
21	1.293	0.181	7.37	0.738	18.29
22	1.547	0.216	7.58	0.760	18.82
23	1.801	0.252	7.70	0.772	19.11
24	2.055	0.287	7.90	0.792	19.61
25	2.563	0.358	8.16	0.817	20.25
26	3.198	0.447	8.51	0.853	21.13
27	3.833	0.535	8.82	0.883	21.88
28	4.468	0.624	9.14	0.916	22.68
29	5.103	0.713	9.36	0.938	23.24
30	5.738	0.801	9.57	0.959	23.76
31	6.373	0.890	9.76	0.979	24.24
32	7.008	0.979	9.86	0.988	24.48
33	7.643	1.067	9.92	0.994	24.62
34	8.278	1.156	9.97	0.999	24.75
35	8.913	1.245	9.97	0.999	24.75
36	9.421	1.316	9.97	0.999	24.75
37	12.723	1.777	9.98	1.000	24.77
38	12.977	1.812	9.98	1.000	24.77

ROUGH WALL MEAN VELOCITY PROFILE
ARTIFICIALLY THICKENED UINF=10.1 M/SEC

RUN	=	81678	DE	=	7.623
PLATE	=	18	DE1	=	1.161
X1	=	1.78	DE2	=	0.870
X2	=	4.13	H	=	1.34
DELY	=	0.023	G	=	6.23
UINF	=	9.98	REX2	=	0.27E 07
CF/2	=	0.00160	REM	=	5696.6
UTAU	=	0.399	REK	=	20.61

PT	Y	Y/DE	U	U/UINF	U+
1	0.048	0.006	3.35	0.335	8.39
2	0.053	0.007	3.43	0.344	8.59
3	0.061	0.008	3.74	0.374	9.36
4	0.074	0.010	4.06	0.406	10.16
5	0.086	0.011	4.37	0.438	10.95
6	0.099	0.013	4.64	0.465	11.62
7	0.124	0.016	4.93	0.494	12.35
8	0.150	0.020	5.16	0.517	12.92
9	0.175	0.023	5.42	0.543	13.57
10	0.233	0.028	5.59	0.560	13.99
11	0.277	0.036	5.84	0.585	14.64
12	0.340	0.044	6.06	0.607	15.18
13	0.404	0.053	6.22	0.623	15.57
14	0.467	0.061	6.33	0.634	15.85
15	0.531	0.069	6.52	0.653	16.32
16	0.658	0.086	6.67	0.668	16.71
17	0.785	0.103	6.83	0.684	17.10
18	1.039	0.136	7.06	0.708	17.70
19	1.293	0.169	7.34	0.736	18.39
20	1.547	0.202	7.52	0.754	18.84
21	1.801	0.235	7.73	0.775	19.37
22	2.055	0.269	7.88	0.789	19.73
23	2.563	0.335	8.11	0.813	20.32
24	3.198	0.418	8.50	0.851	21.29
25	3.833	0.501	8.75	0.877	21.91
26	4.468	0.584	9.02	0.904	22.60
27	5.103	0.667	9.24	0.926	23.15
28	5.738	0.750	9.45	0.946	23.66
29	6.373	0.833	9.64	0.966	24.14
30	7.008	0.916	9.77	0.979	24.46
31	7.643	0.999	9.89	0.990	24.75
32	8.278	1.082	9.93	0.995	24.88
33	8.913	1.165	9.98	1.000	24.99
34	9.421	1.231	9.98	1.000	24.99
35	12.723	1.663	9.98	1.000	25.00
36	12.977	1.696	9.98	1.000	25.00

ROUGH WALL MEAN VELOCITY PROFILE
ARTIFICIALLY THICKENED UINF=10.1 M/SEC

RUN	=	81678	DE	=	8.354
PLATE	=	21	DE1	=	1.227
X1	=	2.08	DE2	=	0.922
X2	=	4.44	H	=	1.33
DELY	=	0.023	G	=	6.27
UINF	=	10.23	REX2	=	0.30E 07
CF/2	=	0.00157	REM	=	6190.1
UTAU	=	0.405	REK	=	20.35

PT	Y	Y/DE	U	U/UINF	U+
1	0.048	0.006	3.49	0.341	8.60
2	0.053	0.006	3.56	0.348	8.78
3	0.061	0.007	3.85	0.376	9.49
4	0.074	0.009	4.24	0.414	10.45
5	0.086	0.010	4.53	0.443	11.18
6	0.099	0.012	4.80	0.469	11.84
7	0.124	0.015	5.10	0.498	12.58
8	0.150	0.018	5.28	0.516	13.03
9	0.175	0.021	5.42	0.529	13.36
10	0.213	0.025	5.71	0.558	14.09
11	0.277	0.033	5.93	0.579	14.62
12	0.340	0.041	6.09	0.595	15.03
13	0.404	0.048	6.38	0.624	15.75
14	0.467	0.056	6.47	0.632	15.96
15	0.531	0.063	6.62	0.648	16.34
16	0.658	0.079	6.82	0.667	16.83
17	0.785	0.094	7.02	0.686	17.31
18	1.039	0.124	7.27	0.711	17.94
19	1.293	0.154	7.47	0.730	18.43
20	1.547	0.185	7.67	0.749	18.91
21	1.801	0.215	7.85	0.767	19.36
22	2.055	0.245	7.95	0.777	19.61
23	2.563	0.306	8.30	0.811	20.47
24	3.198	0.382	8.61	0.842	21.24
25	3.833	0.458	8.85	0.865	21.82
26	4.468	0.533	9.16	0.896	22.60
27	5.103	0.609	9.36	0.915	23.08
28	5.738	0.685	9.57	0.936	23.61
29	6.373	0.761	9.75	0.953	24.05
30	7.008	0.837	9.92	0.970	24.48
31	7.643	0.912	10.03	0.981	24.75
32	8.278	0.988	10.12	0.989	24.96
33	8.913	1.064	10.18	0.995	25.12
34	9.421	1.125	10.22	0.999	25.21
35	12.723	1.519	10.23	1.000	25.24
36	12.977	1.549	10.23	1.000	25.24

ROUGH WALL MEAN VELOCITY PROFILE
ARTIFICIALLY THICKENED UINF=10.1 M/SEC

RUN	=	81678	DE	=	8.567
PLATE	=	23	DE1	=	1.260
X1	=	2.29	DE2	=	0.951
X2	=	4.64	H	=	1.33
DELY	=	0.023	G	=	6.26
UINF	=	10.11	REX2	=	0.31E 07
CF/2	=	0.00154	REM	=	6306.5
UTAU	=	0.397	REK	=	20.50

PT	Y	Y/DE	U	U/UINF	U+
1	0.048	0.006	3.44	0.340	8.67
2	0.053	0.006	3.49	0.345	8.79
3	0.061	0.007	3.86	0.382	9.73
4	0.074	0.009	4.21	0.417	10.62
5	0.086	0.010	4.46	0.441	11.25
6	0.099	0.012	4.71	0.466	11.86
7	0.124	0.014	5.04	0.499	12.71
8	0.150	0.017	5.23	0.517	13.19
9	0.175	0.020	5.41	0.535	13.64
10	0.213	0.025	5.64	0.557	14.20
11	0.277	0.032	5.86	0.580	14.78
12	0.340	0.040	6.07	0.600	15.30
13	0.404	0.047	6.29	0.622	15.85
14	0.467	0.054	6.40	0.633	16.13
15	0.531	0.062	6.54	0.647	16.48
16	0.658	0.077	6.76	0.668	17.03
17	0.785	0.091	6.88	0.681	17.34
18	1.039	0.121	7.19	0.712	18.13
19	1.293	0.151	7.40	0.732	18.66
20	1.547	0.180	7.60	0.751	19.15
21	1.801	0.210	7.72	0.764	19.47
22	2.055	0.239	7.88	0.780	19.87
23	2.563	0.298	8.19	0.810	20.64
24	3.198	0.372	8.45	0.836	21.30
25	3.833	0.446	8.71	0.862	21.96
26	4.468	0.520	9.00	0.890	22.67
27	5.103	0.594	9.19	0.909	23.17
28	5.738	0.668	9.38	0.928	23.65
29	6.373	0.742	9.57	0.947	24.13
30	7.008	0.816	9.72	0.961	24.49
31	7.643	0.890	9.88	0.977	24.90
32	8.278	0.964	9.97	0.986	25.13
33	8.913	1.038	10.05	0.994	25.32
34	9.421	1.097	10.09	0.998	25.42
35	12.977	1.511	10.11	1.000	25.48
36	13.231	1.540	10.11	1.000	25.48

ROUGH WALL MEAN VELOCITY PROFILE
NATURALLY DEVELOPED UINF =15.8 M/SEC

RUN	=	83078	DE	=	3.919
PLATE	=	18	DE1	=	0.765
X1	=	1.78	DE2	=	0.526
X2	=	1.78	H	=	1.45
DELY	=	0.023	G	=	6.93
UINF	=	16.05	REX2	=	0.18E 07
CF/2	=	0.00203	REM	=	5441.1
UTAU	=	0.723	REK	=	36.69

PT	Y	Y/DE	U	U/UINF	U+
1	0.048	0.012	5.47	0.341	7.56
2	0.053	0.014	5.70	0.355	7.88
3	0.058	0.015	5.94	0.370	8.22
4	0.066	0.017	6.22	0.387	8.60
5	0.074	0.019	6.46	0.402	8.93
6	0.086	0.022	6.79	0.423	9.39
7	0.099	0.025	7.05	0.439	9.75
8	0.150	0.038	7.79	0.485	10.77
9	0.188	0.048	8.09	0.504	11.19
10	0.251	0.064	8.66	0.539	11.97
11	0.315	0.080	9.06	0.565	12.53
12	0.378	0.096	9.40	0.585	12.99
13	0.455	0.115	9.78	0.609	13.53
14	0.531	0.135	10.08	0.628	13.93
15	0.658	0.167	10.44	0.651	14.44
16	0.785	0.199	10.89	0.677	15.04
17	0.912	0.231	11.20	0.698	15.48
18	1.039	0.264	11.45	0.713	15.83
19	1.293	0.328	12.09	0.753	16.71
20	1.801	0.457	13.09	0.816	18.10
21	2.309	0.586	13.96	0.870	19.30
22	2.817	0.715	14.77	0.920	20.42
23	3.579	0.908	15.65	0.975	21.64
24	4.341	1.101	16.02	0.998	22.15
25	5.103	1.295	16.05	1.000	22.19
26	5.865	1.488	16.05	1.000	22.19

ROUGH WALL MEAN VELOCITY PROFILE
ARTIFICIALLY THICKENED UINF=15.8 M/SEC

RUN	=	73078	DF	=	5.017
PLATE	=	6	DE1	=	1.020
X1	=	0.56	DE2	=	0.717
X2	=	3.02	H	=	1.42
DELY	=	0.023	G	=	6.81
UINF	=	15.98	REX2	=	0.31E 07
CF/2	=	0.00189	REM	=	7369.4
UTAU	=	0.695	REK	=	35.16

PT	Y	Y/DF	U	U/UINF	U+
1	0.048	0.010	5.68	0.356	8.18
2	0.053	0.011	5.77	0.361	8.31
3	0.061	0.012	6.13	0.383	8.82
4	0.074	0.015	6.51	0.407	9.37
5	0.086	0.017	6.90	0.432	9.93
6	0.099	0.020	7.08	0.443	10.20
7	0.112	0.022	7.30	0.457	10.51
8	0.124	0.025	7.50	0.470	10.80
9	0.150	0.030	7.81	0.489	11.25
10	0.175	0.035	8.06	0.505	11.61
11	0.201	0.040	8.32	0.521	11.98
12	0.226	0.045	8.52	0.533	12.26
13	0.277	0.055	8.83	0.553	12.71
14	0.328	0.065	9.07	0.568	13.06
15	0.378	0.075	9.35	0.585	13.46
16	0.455	0.090	9.65	0.604	13.89
17	0.531	0.105	9.95	0.623	14.33
18	0.658	0.131	10.26	0.642	14.77
19	0.785	0.156	10.53	0.659	15.16
20	0.912	0.181	10.82	0.677	15.58
21	1.039	0.206	11.02	0.690	15.87
22	1.293	0.257	11.41	0.714	16.42
23	1.547	0.307	11.75	0.736	16.92
24	1.801	0.357	12.06	0.755	17.36
25	2.055	0.408	12.45	0.779	17.92
26	2.563	0.509	12.99	0.813	18.71
27	3.198	0.635	13.77	0.862	19.83
28	3.833	0.761	14.59	0.913	21.00
29	4.468	0.887	15.36	0.961	22.10
30	5.103	1.013	15.85	0.992	22.82
31	5.738	1.139	15.95	0.998	22.96
32	6.373	1.265	15.98	1.000	23.00
33	7.008	1.391	15.98	1.000	23.00
34	8.913	1.769	15.98	1.000	23.00
35	9.421	1.869	15.98	1.000	23.00

ROUGH WALL MEAN VELOCITY PROFILE
ARTIFICIALLY THICKENED UINF=15.8 M/SEC

RUN	=	73078	DF	=	5.844
PLATE	=	9	DE1	=	1.036
X1	=	0.86	DE2	=	0.772
X2	=	3.32	H	=	1.41
DELY	=	0.023	G	=	6.72
UINF	=	15.90	REX2	=	0.34E 07
CF/2	=	0.00185	REM	=	7850.7
UTAU	=	0.684	REK	=	34.62

PT	Y	Y/DF	U	U/UINF	U+
1	0.048	0.008	5.56	0.349	8.13
2	0.053	0.009	5.72	0.360	8.36
3	0.061	0.010	6.06	0.381	8.86
4	0.074	0.013	6.39	0.402	9.34
5	0.086	0.015	6.74	0.424	9.85
6	0.099	0.017	7.01	0.441	10.25
7	0.112	0.019	7.22	0.454	10.55
8	0.124	0.021	7.39	0.464	10.80
9	0.150	0.026	7.67	0.483	11.22
10	0.175	0.030	8.02	0.504	11.73
11	0.201	0.034	8.20	0.516	11.99
12	0.226	0.039	8.36	0.526	12.22
13	0.277	0.047	8.67	0.545	12.67
14	0.328	0.056	9.00	0.566	13.16
15	0.378	0.065	9.23	0.580	13.49
16	0.455	0.077	9.53	0.599	13.93
17	0.531	0.090	9.83	0.617	14.34
18	0.658	0.112	10.13	0.637	14.82
19	0.785	0.134	10.40	0.654	15.20
20	1.039	0.177	10.90	0.685	15.94
21	1.293	0.220	11.33	0.713	16.57
22	1.547	0.264	11.68	0.734	17.07
23	1.801	0.307	11.98	0.754	17.52
24	2.055	0.350	12.29	0.773	17.96
25	2.563	0.437	12.89	0.811	18.85
26	3.198	0.545	13.63	0.857	19.92
27	3.833	0.653	14.28	0.898	20.88
28	4.468	0.762	14.92	0.938	21.82
29	5.103	0.870	15.44	0.971	22.57
30	5.738	0.978	15.71	0.988	22.96
31	6.373	1.086	15.83	0.995	23.14
32	7.008	1.195	15.87	0.998	23.21
33	7.643	1.303	15.88	0.999	23.22
34	8.913	1.519	15.89	0.999	23.23
35	9.421	1.606	15.89	0.999	23.23
36	12.723	2.169	15.90	1.000	23.25
37	12.977	2.212	15.90	1.000	23.25

ROUGH WALL MEAN VELOCITY PROFILE
ARTIFICIALLY THICKENED UINF=15.8 M/SEC

RUN	=	73078	DF	=	6.692
PLATE	=	12	DE1	=	1.151
X1	=	1.17	DE2	=	0.830
X2	=	3.63	H	=	1.39
DELY	=	0.023	G	=	6.44
UINF	=	15.88	REX2	=	0.37E 07
CF/2	=	0.00187	REM	=	8475.2
UTAU	=	0.687	REK	=	34.76

PT	Y	Y/DF	U	U/UINF	U+
1	0.048	0.007	5.53	0.348	8.05
2	0.053	0.008	5.73	0.364	8.42
3	0.061	0.009	6.04	0.380	8.79
4	0.074	0.011	6.51	0.410	9.48
5	0.086	0.013	6.78	0.427	9.87
6	0.099	0.015	7.07	0.445	10.30
7	0.112	0.017	7.24	0.456	10.54
8	0.124	0.019	7.38	0.465	10.75
9	0.150	0.022	7.72	0.486	11.23
10	0.175	0.026	8.02	0.505	11.67
11	0.201	0.030	8.13	0.512	11.84
12	0.226	0.034	8.36	0.526	12.17
13	0.277	0.041	8.70	0.548	12.66
14	0.328	0.049	8.83	0.556	12.86
15	0.378	0.056	9.19	0.578	13.38
16	0.455	0.068	9.49	0.597	13.91
17	0.531	0.079	9.69	0.610	14.11
18	0.658	0.098	10.18	0.641	14.82
19	0.785	0.117	10.42	0.656	15.17
20	1.039	0.155	10.85	0.683	15.79
21	1.293	0.193	11.35	0.715	16.53
22	1.547	0.230	11.66	0.734	16.98
23	1.801	0.268	11.99	0.755	17.45
24	2.055	0.306	12.30	0.774	17.90
25	2.563	0.382	12.80	0.806	18.63
26	3.198	0.476	13.45	0.847	19.58
27	3.833	0.571	14.11	0.888	20.54
28	4.468	0.665	14.63	0.921	21.31
29	5.103	0.760	15.11	0.952	22.00
30	5.738	0.854	15.41	0.970	22.44
31	6.373	0.949	15.65	0.985	22.78
32	7.008	1.044	15.76	0.992	22.95
33	7.643	1.138	15.81	0.995	23.01
34	8.278	1.233	15.83	0.997	23.05
35	8.913	1.327	15.84	0.998	23.07
36	9.421	1.403	15.85	0.998	23.08
37	12.723	1.895	15.88	1.000	23.12
38	12.977	1.932	15.88	1.000	23.12

ROUGH WALL MEAN VELOCITY PROFILE
ARTIFICIALLY THICKENED UINF=15.8 M/SEC

RUN	=	73078	DE	=	7.424
PLATE	=	15	DE1	=	1.218
X1	=	1.47	DE2	=	0.884
X2	=	3.93	H	=	1.38
DELY	=	0.023	G	=	6.40
UINF	=	15.93	REX2	=	0.40E 07
CF/2	=	0.00184	REM	=	9085.6
UTAU	=	0.683	REK	=	34.73

PT	Y	Y/DE	U	U/UINF	U+
1	0.048	0.006	5.51	0.346	8.06
2	0.053	0.007	5.73	0.360	8.39
3	0.061	0.008	6.07	0.381	8.88
4	0.074	0.010	6.46	0.406	9.45
5	0.086	0.012	6.68	0.419	9.78
6	0.099	0.013	6.90	0.433	10.10
7	0.112	0.015	7.16	0.449	10.47
8	0.124	0.017	7.33	0.460	10.73
9	0.150	0.020	7.63	0.479	11.16
10	0.175	0.024	7.90	0.496	11.55
11	0.201	0.027	8.16	0.512	11.94
12	0.226	0.030	8.26	0.518	12.08
13	0.277	0.037	8.65	0.543	12.65
14	0.328	0.044	8.90	0.559	13.02
15	0.378	0.051	9.13	0.573	13.37
16	0.455	0.061	9.38	0.589	13.73
17	0.531	0.071	9.74	0.611	14.25
18	0.658	0.088	10.04	0.630	14.69
19	0.785	0.105	10.42	0.654	15.24
20	1.039	0.140	10.97	0.689	16.05
21	1.293	0.174	11.35	0.713	16.61
22	1.547	0.208	11.57	0.726	16.93
23	1.801	0.242	11.95	0.750	17.49
24	2.055	0.276	12.23	0.768	17.90
25	2.563	0.344	12.76	0.801	18.68
26	3.198	0.429	13.38	0.840	19.58
27	3.833	0.515	13.95	0.875	20.41
28	4.468	0.600	14.44	0.906	21.12
29	5.103	0.685	14.90	0.935	21.80
30	5.738	0.770	15.26	0.958	22.33
31	6.373	0.856	15.52	0.974	22.72
32	7.008	0.941	15.69	0.985	22.96
33	7.643	1.026	15.80	0.992	23.12
34	8.278	1.112	15.85	0.995	23.20
35	8.913	1.197	15.88	0.997	23.23
36	9.421	1.265	15.89	0.998	23.26
37	12.723	1.708	15.93	1.000	23.31
38	12.977	1.743	15.93	1.000	23.31

ROUGH WALL MEAN VELOCITY PROFILE
ARTIFICIALLY THICKENED UINF=15.8 M/SEC

RUN	=	73178	DE	=	7.921
PLATE	=	18	DE1	=	1.285
X1	=	1.78	DE2	=	0.935
X2	=	4.24	H	=	1.37
DELY	=	0.023	G	=	6.36
UINF	=	15.97	REX2	=	0.44E 07
CF/2	=	0.00183	REM	=	9628.2
UTAU	=	0.683	REK	=	34.67

PT	Y	Y/DE	U	U/UINF	U+
1	0.048	0.006	5.36	0.335	7.84
2	0.053	0.007	5.51	0.345	8.06
3	0.061	0.008	5.87	0.368	8.59
4	0.074	0.009	6.33	0.397	9.27
5	0.086	0.011	6.62	0.414	9.68
6	0.099	0.012	6.85	0.429	10.02
7	0.124	0.016	7.31	0.457	10.69
8	0.150	0.019	7.67	0.480	11.22
9	0.175	0.022	7.86	0.492	11.50
10	0.213	0.027	8.12	0.509	11.89
11	0.277	0.035	8.63	0.540	12.63
12	0.340	0.043	8.96	0.561	13.12
13	0.404	0.051	9.26	0.580	13.56
14	0.467	0.059	9.54	0.598	13.97
15	0.531	0.067	9.69	0.607	14.18
16	0.658	0.083	10.10	0.632	14.78
17	0.785	0.099	10.44	0.653	15.27
18	1.039	0.131	10.86	0.680	15.89
19	1.293	0.163	11.24	0.704	16.45
20	1.547	0.195	11.60	0.726	16.98
21	1.801	0.227	11.92	0.746	17.44
22	2.055	0.259	12.23	0.765	17.89
23	2.563	0.323	12.67	0.793	18.54
24	3.198	0.403	13.23	0.829	19.37
25	3.833	0.482	13.83	0.866	20.24
26	4.468	0.562	14.25	0.892	20.86
27	5.103	0.642	14.72	0.922	21.55
28	5.738	0.722	15.07	0.944	22.06
29	6.373	0.802	15.41	0.965	22.56
30	7.008	0.882	15.60	0.976	22.82
31	7.643	0.962	15.74	0.985	23.03
32	8.278	1.042	15.86	0.993	23.21
33	8.913	1.122	15.91	0.996	23.28
34	9.421	1.186	15.94	0.998	23.33
35	12.723	1.602	15.97	1.000	23.38
36	12.977	1.634	15.97	1.000	23.38

ROUGH WALL MEAN VELOCITY PROFILE
ARTIFICIALLY THICKENED UINF=15.8 M/SEC

RUN	=	73178	DE	=	8.434
PLATE	=	21	DE1	=	1.354
X1	=	2.08	DE2	=	0.996
X2	=	4.54	H	=	1.36
DELY	=	0.023	G	=	6.20
UINF	=	15.87	REX2	=	0.47E 07
CF/2	=	0.00182	REM	=	10203.2
UTAU	=	0.677	REK	=	34.41

PT	Y	Y/DE	U	U/UINF	U+
1	0.048	0.006	5.35	0.337	7.93
2	0.053	0.006	5.66	0.356	8.35
3	0.061	0.007	5.96	0.375	8.80
4	0.074	0.009	6.30	0.397	9.30
5	0.086	0.010	6.66	0.420	9.84
6	0.099	0.012	6.88	0.433	10.16
7	0.124	0.015	7.27	0.458	10.73
8	0.150	0.018	7.52	0.474	11.11
9	0.175	0.021	7.91	0.498	11.68
10	0.213	0.025	8.20	0.516	12.10
11	0.277	0.033	8.55	0.539	12.62
12	0.340	0.040	8.96	0.565	13.23
13	0.404	0.048	9.16	0.577	13.53
14	0.467	0.055	9.52	0.600	14.06
15	0.531	0.063	9.71	0.611	14.33
16	0.658	0.078	9.85	0.621	14.55
17	0.785	0.093	10.39	0.654	15.34
18	1.039	0.123	10.74	0.677	15.86
19	1.293	0.153	11.23	0.708	16.59
20	1.547	0.183	11.46	0.722	16.93
21	1.801	0.213	11.85	0.746	17.50
22	2.055	0.243	12.14	0.765	17.93
23	2.563	0.303	12.54	0.790	18.51
24	3.198	0.378	13.11	0.826	19.36
25	3.833	0.453	13.56	0.854	20.02
26	4.468	0.528	14.01	0.882	20.68
27	5.103	0.603	14.39	0.907	21.25
28	5.738	0.678	14.74	0.929	21.77
29	6.373	0.754	15.06	0.949	22.24
30	7.008	0.829	15.31	0.965	22.61
31	7.643	0.904	15.52	0.978	22.92
32	8.278	0.979	15.66	0.987	23.13
33	8.913	1.054	15.74	0.992	23.24
34	9.421	1.114	15.79	0.995	23.32
35	12.723	1.504	15.87	1.000	23.44
36	12.977	1.534	15.87	1.000	23.44

ROUGH WALL MEAN VELOCITY PROFILE
ARTIFICIALLY THICKENED UINF=15.8 M/SEC

RUN	=	73178	DF	=	8.750
PLATE	=	23	DEI	=	1.400
X1	=	2.29	DF2	=	1.033
X2	=	4.74	H	=	1.36
DELY	=	0.023	G	=	6.15
UINF	=	16.00	REX2	=	0.49E 07
CF/2	=	0.00182	REM	=	10647.2
UTAU	=	0.683	RPK	=	34.64

PT	Y	Y/DF	U	U/UINF	U+
1	0.048	0.006	5.31	0.332	7.78
2	0.053	0.006	5.68	0.355	8.32
3	0.061	0.007	5.92	0.370	8.67
4	0.074	0.008	6.34	0.396	9.29
5	0.086	0.010	6.66	0.416	9.76
6	0.099	0.011	6.90	0.431	10.11
7	0.124	0.014	7.31	0.457	10.71
8	0.150	0.017	7.56	0.472	11.07
9	0.175	0.020	7.81	0.488	11.44
10	0.213	0.024	8.15	0.510	11.94
11	0.277	0.032	8.55	0.534	12.52
12	0.340	0.039	8.98	0.561	13.15
13	0.404	0.046	9.26	0.579	13.57
14	0.467	0.053	9.47	0.592	13.87
15	0.531	0.061	9.72	0.607	14.23
16	0.658	0.075	10.10	0.631	14.80
17	0.785	0.089	10.40	0.650	15.23
18	1.039	0.118	10.92	0.682	15.99
19	1.293	0.147	11.34	0.708	16.61
20	1.547	0.176	11.55	0.722	16.92
21	1.801	0.205	11.87	0.742	17.39
22	2.055	0.234	12.13	0.758	17.76
23	2.563	0.292	12.65	0.790	18.52
24	3.198	0.365	13.16	0.822	19.28
25	3.833	0.437	13.55	0.847	19.84
26	4.469	0.509	14.05	0.878	20.59
27	5.103	0.582	14.40	0.900	21.09
28	5.738	0.654	14.74	0.921	21.59
29	6.373	0.726	15.06	0.941	22.06
30	7.008	0.799	15.34	0.958	22.47
31	7.643	0.871	15.52	0.970	22.74
32	8.278	0.944	15.69	0.980	22.98
33	8.913	1.016	15.80	0.987	23.14
34	9.421	1.074	15.88	0.992	23.26
35	12.977	1.479	16.00	1.000	23.44
36	13.231	1.508	16.00	1.000	23.44

ROUGH WALL MEAN VELOCITY PROFILE
NATURALLY DEVELOPED UINF =20.4 M/SEC

RUN	=	82778	DF	=	3.862
PLATE	=	19	DEI	=	0.755
X1	=	1.78	DF2	=	0.518
X2	=	1.78	H	=	1.46
DELY	=	0.023	G	=	6.84
UINF	=	20.07	REX2	=	0.23E 07
CF/2	=	0.00210	REM	=	6707.3
UTAU	=	0.920	RPK	=	46.69

PT	Y	Y/DF	U	U/UINF	U+
1	0.048	0.012	7.03	0.350	7.64
2	0.053	0.014	7.29	0.363	7.93
3	0.058	0.015	7.55	0.376	8.21
4	0.066	0.017	7.90	0.394	8.59
5	0.074	0.019	8.08	0.403	8.78
6	0.086	0.022	8.47	0.422	9.21
7	0.099	0.026	8.73	0.435	9.49
8	0.150	0.039	9.65	0.481	10.49
9	0.188	0.048	10.20	0.508	11.09
10	0.251	0.065	10.75	0.536	11.69
11	0.315	0.081	11.33	0.564	12.32
12	0.378	0.097	11.81	0.589	12.84
13	0.455	0.117	12.22	0.609	13.28
14	0.531	0.137	12.58	0.627	13.68
15	0.658	0.169	13.06	0.651	14.20
6	0.785	0.202	13.66	0.681	14.85
7	0.912	0.235	14.00	0.697	15.22
8	1.039	0.267	14.40	0.717	15.65
9	1.293	0.333	15.11	0.753	16.42
0	1.801	0.464	16.43	0.819	17.86
1	2.309	0.594	17.57	0.875	19.10
2	2.817	0.725	18.51	0.922	20.13
3	3.579	0.921	19.60	0.977	21.31
4	4.341	1.117	20.07	1.000	21.82
5	5.103	1.314	20.07	1.000	21.82

ROUGH WALL MEAN VELOCITY PROFILE
ARTIFICIALLY THICKENED UINF = 20.4 M/SEC

RUN	=	82978	DF	=	8.597
PLATE	=	23	DEI	=	1.413
X1	=	2.29	DF2	=	1.033
X2	=	4.66	H	=	1.37
DELY	=	0.023	G	=	6.26
UINF	=	20.39	REX2	=	0.61E 07
CF/2	=	0.00184	REM	=	13594.7
UTAU	=	0.875	RPK	=	44.41

PT	Y	Y/DF	U	U/UINF	U+
1	0.048	0.006	7.06	0.346	8.07
2	0.053	0.006	7.27	0.356	8.31
3	0.061	0.007	7.59	0.372	8.68
4	0.074	0.009	7.93	0.389	9.07
5	0.086	0.010	8.30	0.407	9.49
6	0.099	0.011	8.58	0.421	9.81
7	0.124	0.014	9.04	0.443	10.34
8	0.150	0.017	9.50	0.466	10.86
9	0.175	0.020	9.72	0.477	11.12
10	0.213	0.025	10.13	0.497	11.59
11	0.277	0.032	10.75	0.527	12.29
12	0.340	0.039	11.21	0.550	12.82
13	0.404	0.047	11.55	0.567	13.21
14	0.467	0.054	11.91	0.584	13.62
15	0.531	0.062	12.22	0.599	13.97
16	0.658	0.076	12.61	0.619	14.42
17	0.785	0.091	13.02	0.639	14.99
18	1.039	0.121	13.81	0.678	15.79
19	1.293	0.150	14.18	0.696	16.22
20	1.547	0.179	14.62	0.717	16.72
21	1.801	0.209	15.09	0.740	17.26
22	2.055	0.238	15.43	0.757	17.65
23	2.563	0.297	16.00	0.785	18.30
24	3.198	0.371	16.68	0.818	19.08
25	3.833	0.445	17.35	0.851	19.84
26	4.468	0.518	17.85	0.875	20.41
27	5.103	0.592	18.35	0.900	20.96
28	5.738	0.666	18.81	0.922	21.51
29	6.373	0.739	19.19	0.941	21.94
30	7.008	0.813	19.59	0.961	22.40
31	7.643	0.887	19.83	0.973	22.67
32	8.278	0.960	20.04	0.983	22.91
33	8.913	1.034	20.19	0.990	23.08
34	9.421	1.093	20.25	0.993	23.16
35	12.977	1.505	20.39	1.000	23.31
36	13.231	1.535	20.39	1.000	23.31

ROUGH WALL MEAN VELOCITY PROFILE
NATURALLY DEVELOPED UINF =26.8 M/SEC

RUN	=	62177	DF	=	4.034
PLATE	=	18	DF1	=	0.821
X1	=	1.78	DF2	=	0.558
X2	=	1.78	H	=	1.47
DELY	=	0.023	G	=	6.89
UINF	=	26.75	REX2	=	0.31E 07
CF/2	=	0.00217	REM	=	9570.9
UTAU	=	1.246	REK	=	62.96

PT	Y	Y/DF	U	U/UINF	U+
1	0.049	0.012	9.12	0.341	7.32
2	0.056	0.014	9.53	0.356	7.65
3	0.069	0.017	10.17	0.380	8.16
4	0.081	0.020	10.58	0.396	8.49
5	0.094	0.023	10.98	0.411	8.81
6	0.107	0.026	11.37	0.425	9.12
7	0.119	0.029	11.69	0.437	9.38
8	0.132	0.033	12.06	0.451	9.68
9	0.157	0.039	12.51	0.468	10.04
10	0.208	0.051	13.37	0.500	10.73
11	0.272	0.067	14.13	0.523	11.34
12	0.335	0.083	14.90	0.557	11.96
13	0.462	0.114	15.72	0.588	12.62
14	0.589	0.145	16.61	0.621	13.33
15	0.716	0.177	17.27	0.646	13.86
16	0.843	0.208	17.88	0.669	14.35
17	1.097	0.270	18.91	0.707	15.17
18	1.605	0.396	20.83	0.779	16.71
19	2.240	0.552	22.77	0.851	18.28
20	2.875	0.709	24.37	0.911	19.56
21	3.510	0.865	25.61	0.958	20.56
22	4.145	1.022	26.60	0.994	21.35
23	4.780	1.178	26.76	1.000	21.47
24	5.415	1.335	26.75	1.000	21.47

ROUGH WALL MEAN VELOCITY PROFILE
ARTIFICIALLY THICKENED UINF=26.8 M/SEC

RUN	=	62778	DF	=	5.090
PLATE	=	6	DF1	=	1.057
X1	=	0.56	DF2	=	0.731
X2	=	2.89	H	=	1.44
DELY	=	0.023	G	=	6.66
UINF	=	26.80	REX2	=	0.50E 07
CF/2	=	0.00211	REM	=	12704.4
UTAU	=	1.231	REK	=	62.66

PT	Y	Y/DF	U	U/UINF	U+
1	0.048	0.009	9.22	0.344	7.49
2	0.053	0.010	9.60	0.358	7.80
3	0.061	0.012	9.97	0.372	8.10
4	0.074	0.014	10.53	0.393	8.56
5	0.086	0.017	11.01	0.411	8.94
6	0.099	0.019	11.23	0.419	9.13
7	0.112	0.022	11.69	0.436	9.50
8	0.124	0.024	11.95	0.446	9.71
9	0.150	0.029	12.51	0.467	10.17
10	0.175	0.034	12.96	0.484	10.53
11	0.201	0.039	13.35	0.498	10.85
12	0.226	0.044	13.65	0.510	11.09
13	0.277	0.054	14.28	0.533	11.60
14	0.328	0.064	14.84	0.554	12.05
15	0.378	0.074	15.14	0.565	12.30
16	0.455	0.089	15.73	0.587	12.78
17	0.531	0.104	16.18	0.604	13.14
18	0.658	0.129	16.81	0.627	13.66
19	0.785	0.154	17.36	0.648	14.11
20	0.912	0.178	17.80	0.664	14.46
21	1.039	0.203	18.17	0.678	14.76
22	1.293	0.253	18.88	0.705	15.34
23	1.547	0.303	19.50	0.728	15.84
24	1.801	0.352	20.08	0.749	16.32
25	2.055	0.402	20.65	0.771	16.77
26	2.563	0.501	21.68	0.803	17.61
27	3.198	0.626	22.97	0.857	18.66
28	3.833	0.750	24.35	0.909	19.78
29	4.468	0.874	25.70	0.959	20.88
30	5.103	0.998	26.52	0.990	21.55
31	5.738	1.122	26.77	0.999	21.75
32	6.373	1.247	26.80	1.000	21.77
33	7.008	1.371	26.80	1.000	21.77
34	8.913	1.743	26.80	1.000	21.77
35	9.421	1.843	26.80	1.000	21.77

ROUGH WALL MEAN VELOCITY PROFILE
ARTIFICIALLY THICKENED UINF=26.8 M/SEC

RUN	=	277800	DF	=	5.775
PLATE	=	9	DF1	=	1.144
X1	=	0.86	DF2	=	0.796
X2	=	3.18	H	=	1.44
DELY	=	0.023	G	=	6.72
UINF	=	26.86	REX2	=	0.55E 07
CF/2	=	0.00205	REM	=	13753.8
UTAU	=	1.207	REK	=	61.58

PT	Y	Y/DF	U	U/UINF	U+
1	0.048	0.008	8.96	0.336	7.42
2	0.053	0.009	9.33	0.350	7.73
3	0.061	0.011	9.69	0.364	8.03
4	0.074	0.013	10.25	0.384	8.49
5	0.086	0.015	10.75	0.403	8.90
6	0.099	0.017	11.04	0.414	9.15
7	0.112	0.019	11.34	0.425	9.40
8	0.124	0.021	11.63	0.436	9.63
9	0.150	0.026	12.19	0.457	10.10
10	0.175	0.030	12.62	0.473	10.46
11	0.201	0.035	12.99	0.487	10.76
12	0.226	0.039	13.38	0.502	11.08
13	0.277	0.048	11.86	0.520	11.48
14	0.328	0.057	14.42	0.541	11.95
15	0.378	0.065	14.76	0.554	12.23
16	0.455	0.078	15.40	0.577	12.75
17	0.531	0.092	15.77	0.591	13.06
18	0.658	0.113	16.49	0.618	13.66
19	0.785	0.135	16.89	0.634	13.98
20	1.039	0.179	17.75	0.666	14.70
21	1.293	0.223	18.56	0.696	15.37
22	1.547	0.267	19.06	0.715	15.79
23	1.801	0.311	19.71	0.739	16.33
24	2.055	0.354	20.30	0.761	16.81
25	2.563	0.442	21.31	0.799	17.65
26	3.198	0.552	22.54	0.845	18.67
27	3.833	0.661	23.82	0.893	19.73
28	4.468	0.771	24.96	0.936	20.68
29	5.103	0.880	25.83	0.969	21.39
30	5.738	0.990	26.36	0.989	21.84
31	6.373	1.099	26.56	0.996	22.00
32	7.008	1.209	26.63	0.999	22.06
33	7.643	1.318	26.63	0.999	22.06
34	8.913	1.537	26.65	0.999	22.07
35	9.421	1.625	26.65	1.000	22.08
36	12.469	2.151	26.66	1.000	22.09

ROUGH WALL MEAN VELOCITY PROFILE
ARTIFICIALLY THICKENED UINF=26.8 M/SEC

RUN	=	277800	DE	=	6.714
PLATE	=	12	DE1	=	1.223
X1	=	1.17	DE2	=	0.864
X2	=	3.49	H	=	1.42
DELY	=	0.023	G	=	6.53
UINF	=	26.86	REX2	=	0.61E 07
CF/2	=	0.00202	REM	=	14993.5
UTAU	=	1.207	REK	=	61.46

PT	Y	Y/DE	U	U/UINF	U+
1	0.048	0.007	9.09	0.339	7.53
2	0.053	0.008	9.43	0.351	7.81
3	0.061	0.009	9.86	0.367	8.17
4	0.074	0.011	10.26	0.382	8.50
5	0.086	0.013	10.74	0.400	8.90
6	0.099	0.015	11.20	0.417	9.28
7	0.112	0.017	11.39	0.424	9.44
8	0.124	0.018	11.76	0.438	9.74
9	0.150	0.022	12.24	0.456	10.14
10	0.175	0.026	12.62	0.470	10.46
11	0.201	0.030	13.07	0.487	10.83
12	0.226	0.034	13.39	0.499	11.10
13	0.277	0.041	13.97	0.520	11.57
14	0.328	0.049	14.39	0.536	11.92
15	0.378	0.056	14.89	0.555	12.34
16	0.455	0.067	15.41	0.574	12.77
17	0.531	0.079	15.86	0.590	13.14
18	0.658	0.098	16.51	0.615	13.68
19	0.785	0.117	17.03	0.634	14.11
20	1.039	0.154	17.94	0.668	14.86
21	1.293	0.192	18.59	0.692	15.39
22	1.547	0.230	19.26	0.717	15.96
23	1.801	0.267	19.80	0.737	16.40
24	2.055	0.305	20.32	0.757	16.84
25	2.563	0.380	21.37	0.796	17.70
26	3.198	0.475	22.53	0.839	18.66
27	3.833	0.569	23.58	0.878	19.53
28	4.468	0.663	24.61	0.916	20.39
29	5.103	0.757	25.43	0.947	21.06
30	5.738	0.852	26.09	0.971	21.61
31	6.373	0.946	26.47	0.985	21.92
32	7.008	1.040	26.64	0.992	22.07
33	7.643	1.135	26.72	0.995	22.14
34	8.278	1.229	26.76	0.996	22.16
35	8.913	1.323	26.78	0.997	22.19
36	9.421	1.398	26.79	0.997	22.19
37	12.723	1.889	26.86	1.000	22.25

ROUGH WALL MEAN VELOCITY PROFILE
ARTIFICIALLY THICKENED UINF=26.8 M/SEC

RUN	=	277800	DE	=	7.150
PLATE	=	15	DE1	=	1.292
X1	=	1.47	DE2	=	0.921
X2	=	3.79	H	=	1.40
DELY	=	0.023	G	=	6.39
UINF	=	26.80	REX2	=	0.66E 07
CF/2	=	0.00202	REM	=	15988.8
UTAU	=	1.205	REK	=	61.45

PT	Y	Y/DE	U	U/UINF	U+
1	0.048	0.007	9.11	0.340	7.56
2	0.053	0.007	9.33	0.348	7.75
3	0.061	0.008	9.67	0.361	8.02
4	0.074	0.010	10.26	0.383	8.52
5	0.086	0.012	10.65	0.397	8.84
6	0.099	0.014	11.03	0.411	9.16
7	0.112	0.016	11.32	0.422	9.40
8	0.124	0.017	11.56	0.431	9.60
9	0.150	0.021	12.16	0.454	10.09
10	0.175	0.024	12.68	0.473	10.52
11	0.201	0.028	12.97	0.484	10.77
12	0.226	0.032	13.35	0.498	11.08
13	0.277	0.039	13.96	0.521	11.59
14	0.328	0.046	14.41	0.538	11.96
15	0.378	0.053	14.86	0.554	12.34
16	0.455	0.063	15.43	0.576	12.81
17	0.531	0.074	15.83	0.591	13.14
18	0.658	0.092	16.56	0.618	13.74
19	0.785	0.109	17.01	0.635	14.12
20	1.039	0.145	18.04	0.673	14.98
21	1.293	0.180	18.52	0.691	15.37
22	1.547	0.216	19.21	0.717	15.95
23	1.801	0.251	19.70	0.735	16.35
24	2.055	0.286	20.26	0.756	16.82
25	2.563	0.357	21.15	0.789	17.55
26	3.198	0.446	22.18	0.828	18.41
27	3.833	0.534	23.18	0.865	19.24
28	4.468	0.623	24.01	0.896	19.93
29	5.103	0.711	24.82	0.926	20.61
30	5.738	0.800	25.48	0.951	21.15
31	6.373	0.888	26.02	0.971	21.60
32	7.008	0.977	26.43	0.986	21.94
33	7.643	1.066	26.61	0.993	22.09
34	8.278	1.154	26.71	0.997	22.17
35	8.913	1.243	26.75	0.998	22.21
36	9.421	1.313	26.76	0.998	22.21
37	12.723	1.774	26.80	1.000	22.25
38	12.977	1.809	26.80	1.000	22.25

ROUGH WALL MEAN VELOCITY PROFILE
ARTIFICIALLY THICKENED UINF=26.8 M/SEC

RUN	=	62878	DE	=	7.708
PLATE	=	18	DE1	=	1.361
X1	=	1.78	DE2	=	0.978
X2	=	4.10	H	=	1.39
DELY	=	0.023	G	=	6.24
UINF	=	26.87	REX2	=	0.71E 07
CF/2	=	0.00204	REM	=	17020.7
UTAU	=	1.214	REK	=	61.91

PT	Y	Y/DE	U	U/UINF	U+
1	0.048	0.006	8.91	0.332	7.34
2	0.053	0.007	9.26	0.345	7.63
3	0.061	0.008	9.59	0.357	7.91
4	0.074	0.010	10.11	0.376	8.33
5	0.086	0.011	10.58	0.394	8.72
6	0.099	0.013	10.95	0.407	9.02
7	0.124	0.016	11.72	0.436	9.66
8	0.150	0.019	12.12	0.451	9.99
9	0.175	0.023	12.66	0.471	10.43
10	0.213	0.028	13.27	0.494	10.94
11	0.277	0.036	13.84	0.515	11.41
12	0.340	0.044	14.64	0.545	12.06
13	0.404	0.052	15.08	0.561	12.43
14	0.467	0.060	15.46	0.575	12.74
15	0.531	0.069	15.89	0.591	13.09
16	0.658	0.085	16.57	0.617	13.65
17	0.785	0.102	17.05	0.635	14.05
18	1.039	0.134	17.91	0.667	14.76
19	1.293	0.167	18.52	0.689	15.26
20	1.547	0.200	19.14	0.712	15.77
21	1.801	0.233	19.72	0.734	16.25
22	2.055	0.266	20.13	0.749	16.59
23	2.563	0.331	21.06	0.784	17.36
24	3.198	0.414	22.07	0.821	18.18
25	3.833	0.496	23.05	0.858	18.99
26	4.468	0.578	23.85	0.888	19.65
27	5.103	0.660	24.45	0.910	20.15
28	5.738	0.742	25.14	0.936	20.72
29	6.373	0.824	25.65	0.955	21.14
30	7.008	0.906	26.13	0.973	21.53
31	7.643	0.989	26.49	0.986	21.83
32	8.278	1.071	26.70	0.994	22.00
33	8.913	1.153	26.78	0.997	22.06
34	9.421	1.219	26.80	0.997	22.08
35	12.723	1.646	26.87	1.000	22.14
36	12.577	1.679	26.87	1.000	22.14

ROUGH WALL MEAN VELOCITY PROFILE
ARTIFICIALLY THICKENED UINF=26.8 M/SEC

RUN	=	62878	DE	=	8.574
PLATE	=	21	DE1	=	1.439
X1	=	2.08	DE2	=	1.039
X2	=	4.40	H	=	1.39
DELY	=	0.023	G	=	6.19
UINF	=	26.79	REX2	=	0.76E 07
CF/2	=	0.00202	REM	=	18016.4
UTAU	=	1.204	RTK	=	61.42

PT	Y	Y/DE	U	U/UINF	U+
1	0.048	0.006	8.83	0.330	7.34
2	0.053	0.006	9.19	0.343	7.63
3	0.061	0.007	9.45	0.353	7.85
4	0.074	0.009	9.92	0.370	8.24
5	0.086	0.010	10.54	0.393	8.75
6	0.099	0.012	11.00	0.411	9.14
7	0.124	0.014	11.62	0.434	9.65
8	0.150	0.017	12.06	0.450	10.02
9	0.175	0.020	12.49	0.466	10.37
10	0.213	0.025	13.02	0.486	10.81
11	0.277	0.032	13.85	0.517	11.50
12	0.340	0.040	14.53	0.543	12.07
13	0.404	0.047	15.04	0.561	12.49
14	0.467	0.054	15.37	0.574	12.76
15	0.531	0.062	15.80	0.590	13.12
16	0.658	0.077	16.41	0.613	13.63
17	0.785	0.091	16.94	0.633	14.07
18	1.039	0.121	17.80	0.665	14.79
19	1.293	0.150	18.34	0.685	15.23
20	1.547	0.180	18.98	0.708	15.76
21	1.801	0.209	19.48	0.727	16.18
22	2.055	0.239	20.02	0.747	16.63
23	2.563	0.298	20.79	0.776	17.27
24	3.198	0.372	21.68	0.809	18.01
25	3.833	0.446	22.61	0.844	18.78
26	4.468	0.520	23.41	0.874	19.44
27	5.103	0.594	24.13	0.901	20.04
28	5.738	0.667	24.74	0.924	20.55
29	6.373	0.741	25.33	0.945	21.04
30	7.008	0.815	25.77	0.962	21.41
31	7.643	0.889	26.18	0.977	21.75
32	8.278	0.963	26.39	0.985	21.92
33	8.913	1.037	26.56	0.991	22.06
34	9.421	1.096	26.65	0.995	22.13
35	12.723	1.480	26.79	1.000	22.25
36	12.977	1.510	26.79	1.000	22.25

ROUGH WALL MEAN VELOCITY PROFILE
ARTIFICIALLY THICKENED UINF=26.8 M/SEC

RUN	=	62878	DE	=	8.939
PLATE	=	23	DE1	=	1.489
X1	=	2.29	DE2	=	1.078
X2	=	4.61	H	=	1.38
DELY	=	0.023	G	=	6.15
UINF	=	26.77	REX2	=	0.90E 07
CF/2	=	0.00202	REM	=	18703.2
UTAU	=	1.203	RTK	=	61.40

PT	Y	Y/DE	U	U/UINF	U+
1	0.048	0.005	8.83	0.330	7.34
2	0.053	0.006	9.19	0.343	7.64
3	0.061	0.007	9.52	0.356	7.91
4	0.074	0.008	10.14	0.379	8.43
5	0.086	0.010	10.52	0.393	8.75
6	0.099	0.011	10.87	0.406	9.04
7	0.124	0.014	11.44	0.427	9.51
8	0.150	0.017	12.00	0.448	9.97
9	0.175	0.020	12.49	0.466	10.38
10	0.213	0.024	13.04	0.487	10.84
11	0.277	0.031	13.71	0.512	11.40
12	0.340	0.038	14.31	0.534	11.89
13	0.404	0.045	14.93	0.558	12.41
14	0.467	0.052	15.42	0.576	12.81
15	0.531	0.059	15.75	0.588	13.09
16	0.658	0.073	16.37	0.612	13.61
17	0.785	0.088	16.82	0.628	13.98
18	1.039	0.116	17.68	0.661	14.70
19	1.293	0.144	18.48	0.690	15.36
20	1.547	0.173	19.02	0.710	15.81
21	1.801	0.201	19.38	0.724	16.11
22	2.055	0.229	19.78	0.739	16.44
23	2.563	0.286	20.64	0.771	17.15
24	3.198	0.357	21.53	0.804	17.89
25	3.833	0.428	22.40	0.837	18.62
26	4.468	0.499	23.24	0.868	19.31
27	5.103	0.569	23.94	0.894	19.90
28	5.738	0.640	24.51	0.916	20.37
29	6.373	0.711	25.03	0.935	20.81
30	7.008	0.782	25.56	0.955	21.24
31	7.643	0.853	25.96	0.970	21.57
32	8.278	0.924	26.25	0.981	21.82
33	8.913	0.995	26.45	0.988	21.98
34	9.421	1.051	26.59	0.993	22.09
35	12.977	1.448	26.77	1.000	22.25
36	13.231	1.476	26.77	1.000	22.25

ROUGH WALL MEAN VELOCITY PROFILE
ARTIFICIALLY THICKENED UINF=26.8 M/SEC
WITH P=.0080 BLOWING PLATES 1-6

RUN	=	72078	DF	=	8.154
PLATE	=	15	DF1	=	1.574
X1	=	1.47	DF2	=	1.110
X2	=	4.77	H	=	1.42
DELY	=	0.023	G	=	6.63
UINF	=	26.71	REX2	=	0.82E 07
CF/2	=	0.00198	REM	=	19120.8
UTAU	=	1.189	REK	=	60.16

PT	Y	Y/DF	U	U/UINF	U+
1	0.048	0.006	8.93	0.334	7.52
2	0.053	0.007	9.15	0.343	7.70
3	0.061	0.007	9.51	0.356	8.00
4	0.074	0.009	9.97	0.373	8.39
5	0.086	0.011	10.33	0.387	8.69
6	0.099	0.012	10.79	0.404	9.08
7	0.112	0.014	11.11	0.416	9.35
8	0.124	0.015	11.38	0.426	9.57
9	0.150	0.018	11.82	0.443	9.95
10	0.175	0.021	12.36	0.463	10.40
11	0.201	0.025	12.63	0.473	10.63
12	0.226	0.028	12.95	0.485	10.89
13	0.277	0.034	13.58	0.508	11.42
14	0.328	0.040	14.01	0.525	11.79
15	0.378	0.046	14.45	0.541	12.16
16	0.455	0.056	14.85	0.556	12.49
17	0.531	0.065	15.30	0.573	12.87
18	0.658	0.080	15.92	0.596	13.39
19	0.785	0.096	16.42	0.615	13.81
20	1.039	0.127	17.09	0.640	14.38
21	1.293	0.158	17.66	0.661	14.86
22	1.547	0.189	18.12	0.678	15.24
23	1.801	0.220	18.70	0.700	15.74
24	2.055	0.251	19.04	0.713	16.02
25	2.563	0.313	19.83	0.742	16.68
26	3.198	0.391	20.85	0.781	17.54
27	3.833	0.469	21.83	0.817	18.37
28	4.468	0.546	22.73	0.851	19.12
29	5.103	0.624	23.53	0.881	19.80
30	5.738	0.702	24.41	0.914	20.54
31	6.373	0.779	25.16	0.942	21.17
32	7.008	0.857	25.78	0.965	21.69
33	7.643	0.935	26.20	0.981	22.05
34	8.278	1.012	26.42	0.989	22.23
35	8.913	1.090	26.57	0.995	22.36
36	9.421	1.152	26.60	0.996	22.38
37	15.263	1.867	26.71	1.000	22.47
38	15.517	1.898	26.71	1.000	22.47

ROUGH WALL MEAN VELOCITY PROFILE
ARTIFICIALLY THICKENED UINF=26.8 M/SEC
WITH P=.0080 BLOWING PLATES 1-6

RUN	=	72078	DF	=	9.515
PLATE	=	19	DF1	=	1.645
X1	=	1.88	DF2	=	1.184
X2	=	5.18	H	=	1.39
DELY	=	0.023	G	=	6.30
UINF	=	26.80	REX2	=	0.90E 07
CF/2	=	0.00198	REM	=	20461.6
UTAU	=	1.192	REK	=	60.57

PT	Y	Y/DF	U	U/UINF	U+
1	0.048	0.005	8.91	0.333	7.47
2	0.053	0.006	9.19	0.343	7.71
3	0.061	0.006	9.62	0.359	8.06
4	0.074	0.008	10.15	0.379	8.51
5	0.086	0.009	10.56	0.394	8.85
6	0.099	0.010	10.95	0.409	9.19
7	0.124	0.013	11.55	0.431	9.69
8	0.150	0.016	12.05	0.450	10.11
9	0.175	0.018	12.51	0.467	10.49
10	0.213	0.022	13.02	0.486	10.92
11	0.277	0.029	13.80	0.515	11.57
12	0.340	0.036	14.29	0.533	11.98
13	0.404	0.042	14.74	0.550	12.36
14	0.467	0.049	15.19	0.567	12.74
15	0.531	0.056	15.56	0.581	13.05
16	0.658	0.069	16.17	0.603	13.56
17	0.785	0.082	16.77	0.626	14.07
18	1.039	0.109	17.42	0.650	14.61
19	1.293	0.136	18.02	0.672	15.11
20	1.547	0.162	18.49	0.690	15.50
21	1.801	0.189	19.11	0.713	16.03
22	2.055	0.215	19.31	0.721	16.20
23	2.563	0.269	20.05	0.748	16.82
24	3.198	0.335	20.96	0.782	17.58
25	3.833	0.402	21.74	0.811	18.23
26	4.468	0.468	22.50	0.839	18.87
27	5.103	0.535	23.25	0.868	19.50
28	5.738	0.602	23.90	0.892	20.05
29	6.373	0.668	24.58	0.917	20.61
30	7.008	0.735	25.17	0.939	21.11
31	7.643	0.801	25.70	0.959	21.55
32	8.278	0.868	26.07	0.973	21.87
33	8.913	0.935	26.34	0.983	22.09
34	9.421	0.988	26.50	0.989	22.22
35	15.263	1.600	26.80	1.000	22.47
36	15.517	1.627	26.90	1.000	22.47

ROUGH WALL MEAN VELOCITY PROFILE
ARTIFICIALLY THICKENED UINF=26.8 M/SEC
WITH P=.0080 BLOWING PLATES 1-6

RUN	=	72078	DF	=	10.239
PLATE	=	23	DF1	=	1.743
X1	=	2.29	DF2	=	1.272
X2	=	5.59	H	=	1.37
DELY	=	0.023	G	=	6.06
UINF	=	26.79	REX2	=	0.97E 07
CF/2	=	0.00199	REM	=	21972.6
UTAU	=	1.195	REK	=	60.69

PT	Y	Y/DF	U	U/UINF	U+
1	0.048	0.005	8.96	0.334	7.50
2	0.053	0.005	9.19	0.343	7.69
3	0.061	0.006	9.71	0.363	8.13
4	0.074	0.007	10.15	0.379	8.49
5	0.086	0.008	10.47	0.391	8.77
6	0.099	0.010	10.85	0.405	9.08
7	0.112	0.011	11.19	0.418	9.37
8	0.124	0.012	11.47	0.428	9.60
9	0.150	0.015	12.08	0.451	10.11
10	0.175	0.017	12.40	0.463	10.38
11	0.201	0.020	12.73	0.475	10.66
12	0.226	0.022	13.14	0.491	11.00
13	0.277	0.027	13.77	0.514	11.52
14	0.328	0.032	14.16	0.528	11.85
15	0.378	0.037	14.56	0.543	12.18
16	0.455	0.044	15.16	0.566	12.69
17	0.531	0.052	15.60	0.583	13.06
18	0.658	0.064	16.20	0.605	13.56
19	0.785	0.076	16.75	0.625	14.02
20	1.039	0.101	17.42	0.651	14.58
21	1.293	0.126	18.11	0.676	15.16
22	1.547	0.151	18.57	0.693	15.54
23	1.801	0.175	18.98	0.709	15.89
24	2.055	0.200	19.46	0.726	16.28
25	2.563	0.250	20.12	0.751	16.84
26	3.198	0.312	20.82	0.777	17.43
27	3.833	0.374	21.55	0.805	18.04
28	4.468	0.435	22.29	0.832	18.65
29	5.103	0.497	22.94	0.856	19.20
30	5.738	0.559	23.50	0.877	19.67
31	6.373	0.621	24.07	0.899	20.14
32	7.008	0.683	24.66	0.921	20.64
33	7.643	0.745	25.13	0.938	21.04
34	8.278	0.807	25.56	0.954	21.40
35	8.913	0.869	25.92	0.968	21.69
36	9.421	0.918	26.17	0.977	21.90
37	15.263	1.487	26.78	1.000	22.42
38	15.517	1.512	26.78	1.000	22.42

ROUGH WALL MEAN VELOCITY PROFILE
ARTIFICIALLY THICKENED UINF=26.8 M/SEC
WITH F=.0086 BLOWING PLATES 1-9

RUN	=	72578	DF	=	11.466
PLATE	=	23	DE1	=	1.007
X1	=	2.29	DE2	=	1.434
X2	=	6.41	H	=	1.33
DELY	=	0.023	G	=	6.44
UINF	=	26.98	REX2	=	0.11E 08
CF/2	=	0.00192	REM	=	25018.0
UTAU	=	1.182	REK	=	60.20

PT	Y	Y/DF	U	U/UINF	U+
1	0.048	0.004	8.55	0.317	7.24
2	0.053	0.005	8.74	0.324	7.40
3	0.061	0.005	8.88	0.329	7.52
4	0.074	0.006	9.77	0.362	8.27
5	0.086	0.008	10.26	0.380	8.68
6	0.099	0.009	10.48	0.389	8.87
7	0.112	0.010	10.63	0.394	9.00
8	0.124	0.011	10.83	0.401	9.16
9	0.150	0.013	11.42	0.423	9.66
10	0.175	0.015	11.85	0.439	10.03
11	0.201	0.017	12.21	0.453	10.33
12	0.226	0.020	12.56	0.466	10.63
13	0.277	0.024	13.31	0.493	11.26
14	0.328	0.029	13.89	0.515	11.75
15	0.378	0.033	14.09	0.522	11.92
16	0.455	0.040	14.71	0.545	12.45
17	0.531	0.046	15.13	0.561	12.80
18	0.658	0.057	15.80	0.586	13.36
19	0.785	0.068	16.13	0.598	13.65
20	1.039	0.090	17.05	0.632	14.42
21	1.293	0.113	17.56	0.651	14.86
22	1.547	0.135	18.05	0.669	15.27
23	1.801	0.157	18.51	0.686	15.66
24	2.055	0.179	18.84	0.698	15.94
25	2.563	0.223	19.44	0.721	16.45
26	3.199	0.278	20.25	0.751	17.13
27	3.833	0.334	20.99	0.778	17.76
28	4.468	0.389	21.70	0.804	18.36
29	5.103	0.444	22.31	0.827	18.88
30	5.739	0.499	23.04	0.854	19.49
31	6.373	0.555	23.58	0.874	19.95
32	7.008	0.610	24.20	0.897	20.47
33	7.643	0.665	24.76	0.918	20.95
34	8.278	0.721	25.32	0.938	21.42
35	8.913	0.776	25.77	0.955	21.80
36	9.421	0.820	26.09	0.967	22.06
37	10.056	0.875	26.39	0.978	22.32
38	11.326	0.986	26.69	0.990	22.58
39	12.596	1.096	26.86	0.996	22.72
40	13.866	1.207	26.98	0.996	22.74
41	15.263	1.328	26.98	1.000	22.82
42	15.517	1.351	26.98	1.000	22.82

ROUGH WALL MEAN VELOCITY PROFILE
ARTIFICIALLY THICKENED UINF=26.8 M/SEC
WITH F=.0086 BLOWING PLATES 1-9

RUN	=	72578	DF	=	10.484
PLATE	=	20	DE1	=	1.933
X1	=	1.98	DE2	=	1.374
X2	=	6.11	H	=	1.41
DELY	=	0.023	G	=	6.75
UINF	=	27.00	REX2	=	0.11E 08
CF/2	=	0.00186	REM	=	23992.7
UTAU	=	1.164	REK	=	59.30

PT	Y	Y/DF	U	U/UINF	U+
1	0.048	0.005	8.62	0.319	7.40
2	0.053	0.005	8.87	0.323	7.62
3	0.061	0.006	9.32	0.345	8.00
4	0.074	0.007	9.76	0.362	8.38
5	0.086	0.008	10.16	0.376	8.73
6	0.099	0.009	10.58	0.392	9.09
7	0.112	0.011	10.90	0.404	9.36
8	0.124	0.012	11.15	0.413	9.57
9	0.150	0.014	11.65	0.431	10.00
10	0.175	0.017	12.14	0.450	10.42
11	0.201	0.019	12.58	0.466	10.80
12	0.226	0.022	12.87	0.477	11.05
13	0.277	0.026	13.34	0.494	11.46
14	0.328	0.031	13.77	0.510	11.82
15	0.378	0.036	14.22	0.527	12.21
16	0.455	0.043	14.75	0.546	12.67
17	0.531	0.051	15.11	0.560	12.98
18	0.658	0.063	15.64	0.579	13.43
19	0.785	0.075	16.15	0.598	13.87
20	1.039	0.099	16.82	0.623	14.44
21	1.293	0.123	17.21	0.638	14.78
22	1.547	0.147	17.80	0.660	15.29
23	1.801	0.171	18.15	0.672	15.59
24	2.055	0.196	18.73	0.694	16.09
25	2.563	0.244	19.38	0.718	16.64
26	3.198	0.304	20.15	0.747	17.31
27	3.833	0.365	20.99	0.777	18.03
28	4.468	0.425	21.72	0.804	18.65
29	5.103	0.486	22.57	0.836	19.38
30	5.738	0.546	23.27	0.862	19.99
31	6.373	0.607	24.02	0.890	20.63
32	7.008	0.667	24.66	0.914	21.18
33	7.643	0.727	25.24	0.935	21.68
34	8.278	0.788	25.76	0.954	22.13
35	8.913	0.848	26.24	0.972	22.54
36	9.421	0.897	26.47	0.980	22.73
37	10.056	0.957	26.64	0.987	22.88
38	11.326	1.078	26.80	0.993	23.02
39	12.596	1.199	26.84	0.994	23.05
40	13.866	1.320	26.85	0.995	23.06
41	15.263	1.453	27.00	1.000	23.19
42	15.517	1.477	27.00	1.000	23.19

ROUGH WALL REYNOLDS STRESS TENSOR COMPONENT PROFILE
NATURALLY DEVELOPED UINF=10.1 M/SEC

RUN = 90879 X1 = 1.78 DE = 3.651 UTAU = 0.425
PLATE = 18 X2 = 1.79 DE1 = 0.699 CF/2 = 0.00192
UINF = 9.69 DELY = 0.023 DE2 = 0.455 REK = 21.92

Y'	Y'/DE	Y/DE	U'2/UINF2	V'2/UINF2	W'2/UINF2	-U'V'/UINF2	Q2/UINF2	RUV	RQ2
0.025	0.007	0.012	0.01149						
0.038	0.010	0.016	0.01125						
0.051	0.013	0.019	0.01082						
0.076	0.020	0.026	0.00984						
0.127	0.033	0.035	0.00809						
0.190	0.049	0.055	0.00714						
0.254	0.066	0.071	0.00669						
0.330	0.086	0.091	0.00644	0.00274	0.00434	0.00182	0.01352	0.433	0.135
0.509	0.132	0.137	0.00603	0.00268	0.00413	0.00182	0.01284	0.454	0.142
1.270	0.330	0.334	0.00480	0.00225	0.00334	0.00156	0.01039	0.475	0.150
2.032	0.528	0.532	0.00342	0.00193	0.00260	0.00123	0.00795	0.478	0.154
2.794	0.726	0.727	0.00211	0.00109	0.00145	0.00071	0.00464	0.471	0.154
3.556	0.923	0.924	0.00078	0.00052	0.00054	0.00025	0.00184	0.396	0.137
4.318	1.121	1.121	0.00009						

ROUGH WALL REYNOLDS STRESS TENSOR COMPONENT PROFILE
ARTIFICIALLY THICKENED UINF=10.1 M/SEC

RUN = 91778 X1 = 1.17 DE = 6.538 UTAU = 0.406
PLATE = 12 X2 = 3.52 DE1 = 1.062 CF/2 = 0.00165
UINF = 10.00 DELY = 0.023 DE2 = 0.779 REK = 20.94

Y'	Y'/DE	Y/DE	U'2/UINF2	V'2/UINF2	W'2/UINF2	-U'V'/UINF2	Q2/UINF2	RUV	RQ2
0.025	0.004	0.007	0.01277						
0.038	0.006	0.009	0.01188						
0.051	0.008	0.011	0.01130						
0.076	0.012	0.015	0.00927						
0.127	0.019	0.023	0.00802						
0.190	0.029	0.033	0.00720						
0.254	0.039	0.042	0.00676						
0.330	0.051	0.054	0.00650	0.00261	0.00466	0.00163	0.01377	0.396	0.118
0.508	0.078	0.081	0.00625	0.00272	0.00467	0.00162	0.01364	0.392	0.118
0.762	0.117	0.120	0.00618	0.00264	0.00434	0.00164	0.01316	0.407	0.125
1.270	0.194	0.197	0.00563	0.00301	0.00434	0.00172	0.01298	0.418	0.132
2.032	0.311	0.313	0.00520	0.00299	0.00439	0.00169	0.01258	0.428	0.134
2.794	0.427	0.429	0.00473	0.00297	0.00421	0.00164	0.01191	0.438	0.138
3.556	0.544	0.545	0.00411	0.00264	0.00365	0.00144	0.01040	0.439	0.139
4.318	0.660	0.662	0.00335	0.00213	0.00276	0.00108	0.00824	0.406	0.132
5.334	0.816	0.816	0.00192	0.00151	0.00160	0.00060	0.00503	0.355	0.120
6.350	0.971	0.971	0.00071						

ROUGH WALL REYNOLDS STRESS TENSOR COMPONENT PROFILE
ARTIFICIALLY THICKENED UINF=10.1 M/SEC

RUN = 91779 X1 = 1.78 DE = 7.628 UTAU = 0.401
PLATE = 18 X2 = 4.13 DE1 = 1.161 CF/2 = 0.00160
UINF = 10.01 DELY = 0.023 DE2 = 0.870 REK = 20.66

Y'	Y'/DE	Y/DE	U'2/UINF2	V'2/UINF2	W'2/UINF2	-U'V'/UINF2	Q2/UINF2	RUV	RQ2
0.025	0.003	0.006	0.01283						
0.038	0.005	0.009	0.01209						
0.051	0.007	0.010	0.01122						
0.076	0.010	0.013	0.00958						
0.127	0.017	0.020	0.00816						
0.190	0.025	0.028	0.00719						
0.254	0.033	0.036	0.00692						
0.330	0.043	0.046	0.00677	0.00251	0.00469	0.00156	0.01397	0.379	0.112
0.508	0.067	0.069	0.00670	0.00253	0.00457	0.00157	0.01380	0.381	0.114
0.762	0.100	0.103	0.00652	0.00255	0.00424	0.00158	0.01330	0.389	0.119
1.270	0.167	0.169	0.00578	0.00293	0.00428	0.00161	0.01299	0.390	0.124
2.032	0.266	0.269	0.00522	0.00284	0.00424	0.00161	0.01231	0.417	0.131
2.794	0.366	0.368	0.00466	0.00275	0.00391	0.00153	0.01131	0.429	0.136
3.556	0.466	0.468	0.00404	0.00236	0.00360	0.00131	0.01000	0.425	0.131
4.318	0.566	0.567	0.00339	0.00224	0.00308	0.00114	0.00871	0.413	0.131
5.334	0.699	0.700	0.00252	0.00154	0.00209	0.00083	0.00625	0.408	0.133
6.350	0.833	0.833	0.00157	0.00124	0.00130	0.00050	0.00392	0.380	0.127
7.874	1.032	1.032	0.00039						

ROUGH WALL REYNOLDS STRESS TENSOR COMPONENT PROFILE
ARTIFICIALLY THICKENED UINF=10.1 M/SEC

RUN = 81778 X1 = 2.29 DF = 8.568 UTAU = 0.393
PLATE = 23 X2 = 4.64 DE1 = 1.260 CF/2 = 0.00154
UINF = 10.01 DELY = 0.023 DE2 = 0.950 REK = 20.22

Y'	Y'/DF	Y/DF	U'2/UINF2	V'2/UINF2	W'2/UINF2	-U'V'/UINF2	Q2/UINF2	RUV	RQ2
0.025	0.003	0.006	0.01283						
0.038	0.004	0.007	0.01194						
0.051	0.006	0.009	0.01099						
0.076	0.009	0.012	0.00972						
0.127	0.015	0.017	0.00788						
0.190	0.022	0.025	0.00714						
0.254	0.030	0.032	0.00698						
0.330	0.039	0.041	0.00666	0.00281	0.00495	0.00153	0.01443	0.354	0.106
0.508	0.059	0.062	0.00648	0.00292	0.00490	0.00156	0.01430	0.358	0.109
0.762	0.089	0.091	0.00637	0.00274	0.00451	0.00160	0.01363	0.382	0.117
1.270	0.148	0.151	0.00585	0.00297	0.00403	0.00160	0.01275	0.390	0.125
2.032	0.237	0.239	0.00512	0.00270	0.00375	0.00144	0.01157	0.387	0.125
2.794	0.326	0.328	0.00445	0.00253	0.00356	0.00136	0.01058	0.402	0.129
3.556	0.415	0.417	0.00387	0.00236	0.00340	0.00125	0.00964	0.414	0.130
4.318	0.504	0.505	0.00336	0.00219	0.00297	0.00114	0.00852	0.419	0.133
5.334	0.623	0.624	0.00256	0.00171	0.00241	0.00087	0.00668	0.418	0.131
6.350	0.741	0.742	0.00193	0.00129	0.00152	0.00065	0.00473	0.410	0.137
7.620	0.889	0.890	0.00099	0.00067	0.00084	0.00029	0.00230	0.356	0.126
8.890	1.038	1.039	0.00030						

ROUGH WALL REYNOLDS STRESS TENSOR COMPONENT PROFILE
NATURALLY DEVELOPED UINF=15.8 M/SEC

RUN = 83079 X1 = 1.79 DF = 3.919 UTAU = 0.722
PLATE = 18 X2 = 1.78 DE1 = 0.765 CF/2 = 0.00203
UINF = 16.02 DELY = 0.023 DE2 = 0.526 REK = 36.60

Y'	Y'/DF	Y/DF	U'2/UINF2	V'2/UINF2	W'2/UINF2	-U'V'/UINF2	Q2/UINF2	RUV	RQ2
0.025	0.006	0.012	0.00870						
0.038	0.010	0.015	0.00846						
0.051	0.013	0.019	0.00816						
0.076	0.019	0.025	0.00773						
0.127	0.032	0.038	0.00741						
0.190	0.049	0.054	0.00751						
0.254	0.065	0.070	0.00738						
0.330	0.084	0.090	0.00741	0.00301	0.00472	0.00198	0.01514	0.420	0.131
0.508	0.130	0.135	0.00713	0.00295	0.00432	0.00190	0.01440	0.415	0.132
1.270	0.324	0.328	0.00565	0.00294	0.00392	0.00177	0.01251	0.434	0.142
2.032	0.518	0.521	0.00416	0.00236	0.00322	0.00142	0.00974	0.452	0.145
2.794	0.713	0.715	0.00258	0.00155	0.00194	0.00089	0.00607	0.447	0.147
3.556	0.907	0.908	0.00097	0.00073	0.00073	0.00034	0.00243	0.398	0.138
4.318	1.102	1.101	0.00012						

ROUGH WALL REYNOLDS STRESS TENSOR COMPONENT PROFILE
ARTIFICIALLY THICKENED UINF=15.8 M/SEC

RUN = 80178 X1 = 1.17 DF = 6.693 UTAU = 0.690
PLATE = 12 X2 = 3.63 DE1 = 1.151 CF/2 = 0.00187
UINF = 15.95 DELY = 0.023 DE2 = 0.830 REK = 35.03

Y'	Y'/DF	Y/DF	U'2/UINF2	V'2/UINF2	W'2/UINF2	-U'V'/UINF2	Q2/UINF2	RUV	RQ2
0.025	0.004	0.007	0.00879						
0.038	0.006	0.009	0.00848						
0.051	0.008	0.011	0.00813						
0.127	0.019	0.022	0.00777						
0.254	0.038	0.041	0.00767						
0.330	0.049	0.053	0.00770	0.00256	0.00470	0.00181	0.01497	0.408	0.121
0.508	0.076	0.079	0.00773	0.00253	0.00466	0.00181	0.01492	0.410	0.121
0.762	0.114	0.117	0.00737	0.00287	0.00470	0.00181	0.01494	0.393	0.121
1.016	0.152	0.155	0.00702	0.00299	0.00462	0.00185	0.01462	0.405	0.127
1.778	0.266	0.268	0.00629	0.00308	0.00451	0.00190	0.01387	0.432	0.137
2.540	0.380	0.382	0.00559	0.00327	0.00457	0.00186	0.01344	0.436	0.139
3.175	0.474	0.476	0.00499	0.00312	0.00429	0.00176	0.01241	0.446	0.142
3.810	0.569	0.571	0.00430	0.00292	0.00369	0.00155	0.01081	0.445	0.143
4.445	0.664	0.665	0.00355	0.00229	0.00283	0.00126	0.00867	0.440	0.145
5.080	0.759	0.760	0.00254	0.00181	0.00192	0.00089	0.00627	0.418	0.143
5.715	0.854	0.854	0.00156	0.00135	0.00117	0.00057	0.00408	0.390	0.139
6.350	0.949	0.949	0.00076						

ROUGH WALL REYNOLDS STRESS TENSOR COMPONENT PROFILE
ARTIFICIALLY THICKENED UINF=15.8 M/SEC

RUN = 80178 X1 = 1.78 DE = 7.920 UTAU = 0.679
PLATE = 18 X2 = 4.24 DE1 = 1.295 CF/2 = 0.00183
UINF = 15.88 DELY = 0.023 DE2 = 0.935 REK = 34.25

Y'	Y'/DE	Y/DE	U'2/UINF2	V'2/UINF2	W'2/UINF2	-U'V'/UINF2	Q2/UINF2	RUV	RQ2
0.025	0.003	0.006	0.00901						
0.038	0.005	0.008	0.00865						
0.051	0.006	0.009	0.00827						
0.127	0.016	0.019	0.00800						
0.254	0.032	0.035	0.00797						
0.330	0.042	0.044	0.00817	0.00232	0.00466	0.00178	0.01515	0.408	0.117
0.508	0.064	0.067	0.00814	0.00263	0.00470	0.00184	0.01546	0.397	0.119
0.762	0.096	0.099	0.00793	0.00270	0.00434	0.00184	0.01497	0.398	0.123
1.206	0.152	0.155	0.00744	0.00282	0.00436	0.00190	0.01461	0.414	0.130
1.905	0.241	0.243	0.00649	0.00313	0.00435	0.00191	0.01397	0.423	0.137
2.540	0.321	0.323	0.00581	0.00320	0.00451	0.00187	0.01353	0.434	0.139
3.302	0.417	0.419	0.00517	0.00281	0.00401	0.00166	0.01199	0.434	0.138
4.064	0.513	0.515	0.00429	0.00260	0.00331	0.00147	0.01019	0.441	0.144
5.080	0.641	0.642	0.00333	0.00199	0.00240	0.00114	0.00773	0.441	0.147
6.096	0.770	0.770	0.00205	0.00148	0.00158	0.00070	0.00511	0.402	0.137
6.858	0.866	0.866	0.00125	0.00103	0.00094	0.00043	0.00321	0.379	0.134
7.874	0.994	0.994	0.00048						

ROUGH WALL REYNOLDS STRESS TENSOR COMPONENT PROFILE
ARTIFICIALLY THICKENED UINF=15.8 M/SEC

RUN = 80178 X1 = 2.29 DE = 8.750 UTAU = 0.680
PLATE = 23 X2 = 4.75 DE1 = 1.400 CF/2 = 0.00182
UINF = 15.95 DELY = 0.023 DE2 = 1.033 REK = 34.56

Y'	Y'/DE	Y/DE	U'2/UINF2	V'2/UINF2	W'2/UINF2	-U'V'/UINF2	Q2/UINF2	RUV	RQ2
0.025	0.003	0.006	0.00908						
0.038	0.004	0.007	0.00863						
0.051	0.006	0.008	0.00844						
0.127	0.015	0.017	0.00787						
0.254	0.029	0.032	0.00800						
0.330	0.038	0.040	0.00803	0.00271	0.00529	0.00177	0.01603	0.379	0.110
0.508	0.058	0.061	0.00817	0.00275	0.00491	0.00181	0.01583	0.382	0.114
0.762	0.087	0.089	0.00793	0.00281	0.00475	0.00180	0.01550	0.380	0.116
1.270	0.145	0.147	0.00731	0.00303	0.00462	0.00188	0.01496	0.399	0.125
2.032	0.232	0.234	0.00641	0.00296	0.00426	0.00182	0.01363	0.419	0.134
2.794	0.319	0.321	0.00568	0.00282	0.00403	0.00176	0.01252	0.439	0.140
3.556	0.406	0.408	0.00494	0.00268	0.00368	0.00156	0.01130	0.428	0.138
4.319	0.493	0.495	0.00425	0.00208	0.00294	0.00129	0.00923	0.433	0.139
5.334	0.610	0.611	0.00326	0.00191	0.00251	0.00110	0.00768	0.443	0.144
6.350	0.726	0.726	0.00224	0.00142	0.00178	0.00072	0.00544	0.405	0.133
7.874	0.900	0.900	0.00095	0.00077	0.00076	0.00031	0.00248	0.368	0.127
9.398	1.074	1.074	0.00020						

ROUGH WALL REYNOLDS STRESS TENSOR COMPONENT PROFILE
NATURALLY DEVELOPED UINF=20.4 M/SEC

RUN = 82678 X1 = 1.78 DE = 3.861 UTAU = 0.940
PLATE = 18 X2 = 1.78 DE1 = 0.754 CF/2 = 0.00210
UINF = 20.52 DELY = 0.023 DE2 = 0.518 REK = 47.73

Y'	Y'/DE	Y/DE	U'2/UINF2	V'2/UINF2	W'2/UINF2	-U'V'/UINF2	Q2/UINF2	RUV	RQ2
0.025	0.007	0.012	0.00779						
0.038	0.010	0.016	0.00774						
0.051	0.013	0.019	0.00776						
0.076	0.020	0.026	0.00776						
0.127	0.033	0.039	0.00802						
0.190	0.049	0.055	0.00825						
0.254	0.066	0.071	0.00833						
0.330	0.086	0.091	0.00849	0.00272	0.00447	0.00206	0.01568	0.428	0.131
0.508	0.132	0.137	0.00820	0.00272	0.00441	0.00209	0.01533	0.442	0.136
1.270	0.329	0.333	0.00629	0.00264	0.00388	0.00181	0.01281	0.444	0.141
2.032	0.526	0.529	0.00465	0.00218	0.00311	0.00146	0.00995	0.457	0.146
2.794	0.724	0.725	0.00296	0.00133	0.00192	0.00088	0.00606	0.444	0.146
3.556	0.921	0.922	0.00108	0.00068	0.00064	0.00035	0.00240	0.409	0.146
4.319	1.118	1.119	0.00015						

ROUGH WALL REYNOLDS STRESS TENSOR COMPONENT PROFILE
ARTIFICIALLY THICKENED UINF=20.4 M/SEC

RUN = 82978 X1 = 2.29 DE = 8.598 UTAU = 0.879
PLATE = 23 X2 = 4.66 DE1 = 1.412 CF/2 = 0.00184
UINF = 20.49 DELY = 0.023 DE2 = 1.032 REK = 44.71

Y'	Y'/DE	Y/DE	U'2/UINF2	V'2/UINF2	W'2/UINF2	-U'V'/UINF2	Q2/UINF2	RUV	RQ2
0.025	0.003	0.006	0.00770						
0.038	0.004	0.007	0.00770						
0.051	0.006	0.009	0.00767						
0.076	0.009	0.011	0.00765						
0.127	0.015	0.017	0.00804						
0.254	0.030	0.032	0.00849						
0.330	0.039	0.041	0.00876	0.00310	0.00534	0.00184	0.01720	0.353	0.107
0.508	0.059	0.062	0.00890	0.00279	0.00488	0.00193	0.01657	0.387	0.116
0.762	0.089	0.091	0.00849						
1.270	0.148	0.150	0.00760	0.00293	0.00453	0.00187	0.01506	0.397	0.124
2.032	0.236	0.238	0.00661	0.00270	0.00424	0.00177	0.01355	0.418	0.130
2.794	0.325	0.327	0.00580	0.00287	0.00409	0.00176	0.01276	0.431	0.138
3.556	0.414	0.415	0.00497	0.00235	0.00347	0.00150	0.01079	0.440	0.139
4.318	0.502	0.504	0.00439	0.00197	0.00279	0.00133	0.00915	0.451	0.145
5.334	0.620	0.621	0.00349	0.00175	0.00224	0.00109	0.00748	0.441	0.146
6.350	0.739	0.739	0.00247	0.00119	0.00150	0.00072	0.00517	0.419	0.139
7.874	0.916	0.916	0.00109	0.00051	0.00049	0.00029	0.00209	0.391	0.139
9.398	1.093	1.093	0.00027						

ROUGH WALL REYNOLDS STRESS TENSOR COMPONENT PROFILE
NATURALLY DEVELOPED UINF=26.8 M/SEC

RUN = 71078 X1 = 1.78 DE = 4.034 UTAU = 1.247
PLATE = 18 X2 = 1.78 DE1 = 0.820 CF/2 = 0.00217
UINF = 26.76 DELY = 0.023 DE2 = 0.558 REK = 63.40

Y'	Y'/DE	Y/DE	U'2/UINF2	V'2/UINF2	W'2/UINF2	-U'V'/UINF2	Q2/UINF2	RUV	RQ2
0.025	0.006	0.012	0.00688						
0.086	0.021	0.027	0.00773						
0.137	0.034	0.039	0.00816						
0.213	0.053	0.058	0.00861						
0.264	0.065	0.071	0.00871						
0.315	0.078	0.083	0.00882						
0.391	0.097	0.102	0.00873	0.00264	0.00449	0.00222	0.01587	0.461	0.140
0.518	0.128	0.133	0.00832	0.00313	0.00448	0.00211	0.01593	0.414	0.133
0.772	0.191	0.196	0.00773	0.00322	0.00443	0.00212	0.01537	0.426	0.138
0.899	0.223	0.227	0.00744	0.00285	0.00436	0.00194	0.01466	0.421	0.132
1.290	0.317	0.321	0.00661	0.00314	0.00401	0.00195	0.01376	0.428	0.142
1.788	0.443	0.446	0.00547	0.00245	0.00363	0.00162	0.01154	0.444	0.141
2.423	0.601	0.603	0.00400	0.00189	0.00268	0.00124	0.00856	0.453	0.145
3.058	0.758	0.760	0.00249	0.00107	0.00137	0.00074	0.00493	0.454	0.150
3.693	0.916	0.916	0.00104	0.00034	0.00047	0.00026	0.00185	0.433	0.139
4.328	1.073	1.073	0.00019	0.00014	0.00009	0.00005	0.00042	0.328	0.128

ROUGH WALL REYNOLDS STRESS TENSOR COMPONENT PROFILE
ARTIFICIALLY THICKENED UINF=26.8 M/SEC

RUN = 60878 X1 = 1.17 DE = 6.713 UTAU = 1.207
PLATE = 12 X2 = 3.49 DE1 = 1.222 CF/2 = 0.00202
UINF = 26.86 DELY = 0.023 DE2 = 0.864 REK = 61.60

Y'	Y'/DE	Y/DE	U'2/UINF2	V'2/UINF2	W'2/UINF2	-U'V'/UINF2	Q2/UINF2	RUV	RQ2
0.025	0.004	0.007	0.00689						
0.127	0.019	0.022	0.00836						
0.254	0.038	0.041	0.00904						
0.305	0.045	0.049	0.00921						
0.356	0.053	0.056	0.00914	0.00270	0.00518	0.00199	0.01702	0.400	0.117
0.432	0.064	0.067	0.00902	0.00290	0.00503	0.00199	0.01696	0.388	0.117
0.508	0.076	0.079	0.00898						
0.635	0.095	0.098	0.00863	0.00309	0.00516	0.00200	0.01688	0.388	0.119
1.016	0.151	0.154	0.00809	0.00303	0.00467	0.00207	0.01580	0.417	0.131
1.778	0.265	0.267	0.00698	0.00324	0.00480	0.00203	0.01503	0.426	0.135
2.540	0.378	0.380	0.00620	0.00327	0.00455	0.00199	0.01402	0.442	0.142
3.175	0.473	0.475	0.00562	0.00291	0.00425	0.00190	0.01277	0.469	0.149
3.810	0.566	0.569	0.00487	0.00238	0.00334	0.00159	0.01059	0.467	0.150
4.318	0.643	0.644	0.00403	0.00229	0.00287	0.00137	0.00918	0.452	0.149
5.080	0.757	0.758	0.00290	0.00162	0.00179	0.00095	0.00631	0.438	0.151
5.715	0.851	0.852	0.00181	0.00113	0.00111	0.00057	0.00404	0.399	0.141
6.350	0.946	0.946	0.00089						

ROUGH WALL REYNOLDS STRESS TENSOR COMPONENT PROFILE
ARTIFICIALLY THICKENED UINF=26.9 M/SEC

RUN = 60979 X1 = 1.78 DE = 7.709 UTAU = 1.217
PLATE = 18 X2 = 4.10 DE1 = 1.361 CF/2 = 0.00204
UINF = 26.94 DELY = 0.023 DE2 = 0.978 REK = 62.22

Y'	Y'/DE	Y/DE	U'2/UINF2	V'2/UINF2	W'2/UINF2	-U'V'/UINF2	Q2/UINF2	BUV	BQ2
0.025	0.003	0.006	0.00696						
0.127	0.016	0.019	0.00844						
0.254	0.033	0.036	0.00937						
0.330	0.043	0.046	0.00951	0.00270	0.00496	0.00200	0.01717	0.394	0.116
0.368	0.048	0.051	0.00958	0.00272	0.00492	0.00200	0.01721	0.392	0.116
0.508	0.066	0.069	0.00960						
0.711	0.092	0.095	0.00939	0.00278	0.00498	0.00204	0.01715	0.400	0.119
1.206	0.157	0.159	0.00829	0.00306	0.00496	0.00206	0.01631	0.408	0.126
1.905	0.247	0.249	0.00728	0.00339	0.00467	0.00209	0.01534	0.421	0.136
2.540	0.329	0.331	0.00655	0.00328	0.00468	0.00200	0.01451	0.432	0.138
3.302	0.428	0.430	0.00587	0.00277	0.00388	0.00179	0.01252	0.443	0.143
4.064	0.527	0.529	0.00496	0.00246	0.00343	0.00158	0.01085	0.451	0.145
5.080	0.659	0.660	0.00372	0.00202	0.00261	0.00120	0.00835	0.437	0.144
6.096	0.791	0.791	0.00233	0.00144	0.00162	0.00075	0.00538	0.409	0.139
6.858	0.890	0.890	0.00137	0.00100	0.00098	0.00045	0.00335	0.383	0.134
7.874	1.021	1.021	0.00053						

ROUGH WALL REYNOLDS STRESS TENSOR COMPONENT PROFILE
ARTIFICIALLY THICKENED UINF=26.8 M/SEC

RUN = 60979 X1 = 2.29 DE = 8.938 UTAU = 1.206
PLATE = 23 X2 = 4.61 DE1 = 1.488 CF/2 = 0.00202
UINF = 26.82 DELY = 0.023 DE2 = 1.078 REK = 61.52

Y'	Y'/DE	Y/DE	U'2/UINF2	V'2/UINF2	W'2/UINF2	-U'V'/UINF2	Q2/UINF2	BUV	BQ2
0.025	0.003	0.005	0.00704						
0.127	0.014	0.017	0.00971						
0.254	0.028	0.031	0.00954						
0.330	0.037	0.039	0.00949	0.00253	0.00520	0.00197	0.01722	0.403	0.115
0.381	0.043	0.045	0.00968						
0.508	0.057	0.059	0.00962	0.00260	0.00477	0.00199	0.01693	0.398	0.117
0.762	0.085	0.088	0.00927	0.00265	0.00476	0.00202	0.01668	0.408	0.121
1.270	0.142	0.144	0.00827	0.00300	0.00463	0.00201	0.01590	0.404	0.126
2.032	0.227	0.229	0.00720	0.00305	0.00438	0.00198	0.01462	0.423	0.135
2.794	0.313	0.314	0.00638	0.00277	0.00412	0.00184	0.01327	0.438	0.139
3.556	0.398	0.399	0.00554	0.00270	0.00379	0.00172	0.01203	0.445	0.143
4.318	0.483	0.484	0.00484	0.00235	0.00329	0.00151	0.01048	0.447	0.144
5.334	0.597	0.598	0.00378	0.00195	0.00265	0.00118	0.00833	0.436	0.141
6.350	0.710	0.711	0.00267	0.00148	0.00192	0.00086	0.00608	0.431	0.141
7.874	0.881	0.881	0.00115	0.00078	0.00076	0.00035	0.00269	0.371	0.131
9.398	1.051	1.051	0.00027						

ROUGH WALL REYNOLDS STRESS TENSOR COMPONENT PROFILE
ARTIFICIALLY THICKENED WITH F=.008 PLATES 1-6 UINF=26.8 M/SEC

RUN = 72078 X1 = 2.29 DE = 10.239 UTAU = 1.195
PLATE = 23 X2 = 5.59 DE1 = 1.742 CF/2 = 0.00199
UINF = 26.78 DELY = 0.023 DE2 = 1.272 REK = 60.63

Y'	Y'/DE	Y/DE	U'2/UINF2	V'2/UINF2	W'2/UINF2	-U'V'/UINF2	Q2/UINF2	BUV	BQ2
0.025	0.002	0.005	0.00684						
0.127	0.012	0.015	0.00948						
0.254	0.025	0.027	0.00918						
0.330	0.032	0.034	0.00941	0.00285	0.00543	0.00195	0.01769	0.377	0.110
0.564	0.055	0.057	0.00941						
0.762	0.074	0.076	0.00926	0.00272	0.00494	0.00193	0.01692	0.386	0.114
2.032	0.198	0.200	0.00725	0.00333	0.00508	0.00197	0.01566	0.402	0.126
3.556	0.347	0.349	0.00622	0.00316	0.00464	0.00193	0.01402	0.436	0.133
5.334	0.521	0.522	0.00500	0.00261	0.00383	0.00159	0.01145	0.440	0.139
6.350	0.620	0.621	0.00420	0.00232	0.00297	0.00136	0.00949	0.437	0.144
7.874	0.769	0.770	0.00260	0.00154	0.00170	0.00083	0.00585	0.415	0.142
9.398	0.918	0.918	0.00105	0.00082	0.00070	0.00033	0.00257	0.359	0.130

ROUGH WALL U'2 SPECTRA
DISA WIRE 55A53 SENS. LENGTH=0.45MM L/D=90
NATURALLY DEVELOPED

RUN = 81977 DE = 4.034
PLATE = 18 DE2 = 0.558
U'2 = 6.894 U = 15.36
Y'/DE = 0.078 UINF= 26.70
Y/DE = 0.083

N	K1	EU(N)	EJ(K1)
22.5	0.092	0.3995E 03	0.9767E 05
37.5	0.153	0.3217E 03	0.7866E 05
52.5	0.215	0.2682E 03	0.6558E 05
67.5	0.276	0.2503E 03	0.6120E 05
82.5	0.337	0.2058E 03	0.5032E 05
97.5	0.399	0.1547E 03	0.3782E 05
112.5	0.460	0.1332E 03	0.3257E 05
127.5	0.521	0.1272E 03	0.3110E 05
142.5	0.583	0.1136E 03	0.2778E 05
157.5	0.644	0.9806E 02	0.2397E 05
172.5	0.705	0.8954E 02	0.2192E 05
187.5	0.767	0.8820E 02	0.2157E 05
213.0	0.871	0.7219E 02	0.1765E 05
267.0	1.092	0.5476E 02	0.1339E 05
320.0	1.309	0.4770E 02	0.1166E 05
373.0	1.526	0.3455E 02	0.8448E 04
427.0	1.746	0.3009E 02	0.7358E 04
480.0	1.963	0.2446E 02	0.5981E 04
533.0	2.180	0.2035E 02	0.4975E 04
587.0	2.401	0.2082E 02	0.5090E 04
640.0	2.618	0.1856E 02	0.4537E 04
693.0	2.834	0.1654E 02	0.4043E 04
747.0	3.055	0.1376E 02	0.3363E 04
800.0	3.272	0.1171E 02	0.2863E 04
853.0	3.489	0.1198E 02	0.2929E 04
907.0	3.710	0.8679E 01	0.2122E 04
933.0	3.816	0.9517E 01	0.2327E 04
960.0	3.926	0.9965E 01	0.2436E 04
1013.0	4.143	0.8679E 01	0.2122E 04
1067.0	4.364	0.8679E 01	0.2122E 04
1120.0	4.581	0.8482E 01	0.2074E 04
1173.0	4.798	0.7219E 01	0.1765E 04
1227.0	5.019	0.7559E 01	0.1848E 04
1280.0	5.235	0.5352E 01	0.1308E 04
1333.0	5.452	0.5476E 01	0.1339E 04
1387.0	5.673	0.5734E 01	0.1402E 04
1440.0	5.890	0.5230E 01	0.1279E 04
1493.0	6.107	0.5476E 01	0.1339E 04
1547.0	6.327	0.5476E 01	0.1339E 04
1600.0	6.544	0.4994E 01	0.1221E 04
1653.0	6.761	0.4350E 01	0.1064E 04
1813.0	7.415	0.4060E 01	0.9926E 03
2000.0	8.180	0.2874E 01	0.7027E 03
2213.0	9.051	0.2621E 01	0.6408E 03
2400.0	9.815	0.2283E 01	0.5582E 03
2613.0	10.687	0.2180E 01	0.5330E 03
2800.0	11.452	0.1813E 01	0.4434E 03
3013.0	12.323	0.1543E 01	0.3774E 03
3200.0	13.088	0.1474E 01	0.3604E 03
3413.0	13.960	0.1198E 01	0.2929E 03
3600.0	14.724	0.1093E 01	0.2671E 03
3813.0	15.596	0.9517E 00	0.2327E 03
4000.0	16.360	0.8882E 00	0.2171E 03
4213.0	17.232	0.9088E 00	0.2222E 03
4400.0	17.996	0.9300E 00	0.2274E 03
4613.0	18.868	0.5894E 00	0.1686E 03
4800.0	19.632	0.7055E 00	0.1725E 03
5013.0	20.504	0.6584E 00	0.1610E 03
5200.0	21.269	0.6584E 00	0.1610E 03
5413.0	22.140	0.5604E 00	0.1370E 03
5573.0	22.794	0.4451E 00	0.1088E 03
5600.0	22.905	0.4251E 00	0.1039E 03
5797.0	23.669	0.3877E 00	0.9479E 02
5947.0	24.324	0.3789E 00	0.9263E 02
6000.0	24.541	0.3300E 00	0.8068E 02

ROUGH WALL U'2 SPECTRA
DISA WIRE 55A53 SENS. LENGTH=0.45MM L/D=90
NATURALLY DEVELOPED

RUN = 81977 DE = 4.034
PLATE = 18 DE2 = 0.558
U'2 = 6.145 U = 17.43
Y'/DE = 0.150 UINF= 26.70
Y/DE = 0.155

N	K1	EU(N)	EJ(K1)
22.5	0.081	0.3330E 03	0.9241E 05
37.5	0.135	0.3016E 03	0.8370E 05
52.5	0.189	0.2603E 03	0.7223E 05
67.5	0.243	0.2044E 03	0.5672E 05
82.5	0.297	0.1724E 03	0.4783E 05
97.5	0.351	0.1665E 03	0.4621E 05
112.5	0.405	0.1299E 03	0.3603E 05
127.5	0.459	0.1050E 03	0.2943E 05
142.5	0.514	0.1024E 03	0.2843E 05
157.5	0.568	0.9517E 02	0.2641E 05
172.5	0.622	0.8882E 02	0.2464E 05
187.5	0.676	0.8175E 02	0.2268E 05
213.0	0.768	0.7387E 02	0.2050E 05
267.0	0.962	0.5868E 02	0.1628E 05
320.0	1.153	0.4154E 02	0.1153E 05
373.0	1.344	0.3536E 02	0.9811E 04
427.0	1.539	0.2682E 02	0.7443E 04
480.0	1.730	0.2446E 02	0.6788E 04
533.0	1.921	0.2035E 02	0.5646E 04
587.0	2.115	0.1732E 02	0.4805E 04
640.0	2.306	0.1408E 02	0.3906E 04
693.0	2.497	0.1144E 02	0.3175E 04
747.0	2.692	0.1408E 02	0.3906E 04
800.0	2.883	0.1226E 02	0.3402E 04
853.0	3.074	0.9965E 01	0.2765E 04
907.0	3.269	0.7916E 01	0.2196E 04
960.0	3.460	0.8679E 01	0.2408E 04
1013.0	3.651	0.8289E 01	0.2300E 04
1067.0	3.845	0.7219E 01	0.2003E 04
1120.0	4.036	0.5868E 01	0.1628E 04
1173.0	4.227	0.5476E 01	0.1520E 04
1227.0	4.422	0.6434E 01	0.1785E 04
1280.0	4.613	0.5604E 01	0.1555E 04
1333.0	4.804	0.4770E 01	0.1323E 04
1387.0	4.999	0.4555E 01	0.1264E 04
1440.0	5.190	0.3789E 01	0.1051E 04
1493.0	5.381	0.3702E 01	0.1027E 04
1547.0	5.575	0.3455E 01	0.9588E 03
1573.0	5.669	0.3967E 01	0.1101E 04
1600.0	5.766	0.3536E 01	0.9811E 03
1653.0	5.957	0.3618E 01	0.1004E 04
1813.0	6.534	0.2390E 01	0.6633E 03
2000.0	7.208	0.2621E 01	0.7273E 03
2213.0	7.975	0.2082E 01	0.5777E 03
2400.0	8.649	0.1813E 01	0.5032E 03
2613.0	9.417	0.1654E 01	0.4589E 03
2800.0	10.091	0.1440E 01	0.3997E 03
3013.0	10.858	0.1198E 01	0.3324E 03
3200.0	11.532	0.1068E 01	0.2963E 03
3413.0	12.300	0.1093E 01	0.3032E 03
3600.0	12.974	0.9965E 00	0.2765E 03
3813.0	13.742	0.9088E 00	0.2522E 03
4000.0	14.415	0.8482E 00	0.2354E 03
4213.0	15.183	0.7387E 00	0.2050E 03
4400.0	15.857	0.5604E 00	0.1555E 03
4427.0	15.954	0.6005E 00	0.1666E 03
4613.0	16.625	0.5868E 00	0.1628E 03
4800.0	17.299	0.5604E 00	0.1555E 03
4987.0	17.972	0.5352E 00	0.1485E 03
5013.0	18.066	0.4661E 00	0.1293E 03
5200.0	18.740	0.4451E 00	0.1235E 03
5413.0	19.508	0.4060E 00	0.1126E 03
5467.0	19.702	0.3877E 00	0.1076E 03
5600.0	20.182	0.3789E 00	0.1051E 03
5707.0	20.567	0.3080E 00	0.8545E 02
5813.0	20.949	0.2874E 00	0.7975E 02
5947.0	21.432	0.2745E 00	0.7616E 02
6000.0	21.623	0.2390E 00	0.6633E 02

ROUGH WALL U*2 SPECTRA
DTSA WIRE 55853 SENS. LENGTH=0.45MM L/D=90
NATURALLY DEVELOPED

RUN	=	81977	DE	=	4.034
PLATE	=	18	DE2	=	0.558
U*2	=	2.941	U	=	23.94
Y*/DE	=	0.600	UINF	=	26.70
Y/DE	=	0.602			

N	K1	EU(N)	EJ(K1)
22.5	0.059	0.1123E 03	0.4290E 05
37.5	0.099	0.1022E 03	0.3894E 05
52.5	0.139	0.1022E 03	0.3894E 05
67.5	0.177	0.8760E 02	0.3337E 05
82.5	0.217	0.7971E 02	0.3037E 05
97.5	0.256	0.8482E 02	0.3232E 05
112.5	0.295	0.8232E 02	0.3136E 05
127.5	0.335	0.6676E 02	0.2543E 05
142.5	0.374	0.5439E 02	0.2072E 05
157.5	0.413	0.4390E 02	0.1673E 05
172.5	0.453	0.4290E 02	0.1635E 05
187.5	0.492	0.4261E 02	0.1623E 05
213.0	0.559	0.3618E 02	0.1379E 05
267.0	0.701	0.3377E 02	0.1287E 05
320.0	0.840	0.2231E 02	0.8500E 04
373.0	0.979	0.1732E 02	0.6598E 04
427.0	1.121	0.1408E 02	0.5363E 04
480.0	1.260	0.1344E 02	0.5122E 04
533.3	1.400	0.1144E 02	0.4359E 04
587.0	1.541	0.9517E 01	0.3626E 04
640.0	1.680	0.9088E 01	0.3463E 04
693.0	1.819	0.8289E 01	0.3158E 04
747.0	1.961	0.6288E 01	0.2396E 04
800.0	2.100	0.5604E 01	0.2135E 04
853.0	2.239	0.4881E 01	0.1860E 04
907.0	2.381	0.4555E 01	0.1735E 04
960.0	2.520	0.3967E 01	0.1512E 04
1013.0	2.659	0.3967E 01	0.1512E 04
1067.0	2.801	0.3300E 01	0.1257E 04
1120.0	2.940	0.2745E 01	0.1046E 04
1173.0	3.079	0.3009E 01	0.1147E 04
1227.0	3.220	0.2745E 01	0.1046E 04
1280.0	3.360	0.2621E 01	0.9986E 03
1333.0	3.499	0.2621E 01	0.9986E 03
1387.0	3.640	0.2131E 01	0.8117E 03
1440.0	3.780	0.2336E 01	0.8900E 03
1467.0	3.850	0.2035E 01	0.7752E 03
1493.0	3.919	0.2131E 01	0.8117E 03
1547.0	4.060	0.2035E 01	0.7752E 03
1600.0	4.199	0.1732E 01	0.6598E 03
1653.0	4.339	0.1508E 01	0.5747E 03
1813.0	4.759	0.1692E 01	0.6448E 03
2000.0	5.249	0.1144E 01	0.4359E 03
2213.0	5.808	0.1068E 01	0.4068E 03
2400.0	6.299	0.8482E 00	0.3232E 03
2613.0	6.858	0.7219E 00	0.2751E 03
2800.0	7.349	0.7055E 00	0.2688E 03
3013.0	7.908	0.6584E 00	0.2508E 03
3200.0	8.399	0.5734E 00	0.2185E 03
3413.0	8.958	0.4994E 00	0.1903E 03
3600.0	9.449	0.5111E 00	0.1947E 03
3813.0	10.008	0.4060E 00	0.1547E 03
4000.0	10.499	0.3300E 00	0.1257E 03
4213.0	11.058	0.3877E 00	0.1477E 03
4400.0	11.549	0.3009E 00	0.1147E 03
4613.0	12.108	0.2682E 00	0.1022E 03
4800.0	12.598	0.2561E 00	0.9759E 02
5013.0	13.157	0.2180E 00	0.8306E 02
5200.0	13.648	0.2390E 00	0.9108E 02
5413.0	14.207	0.1899E 00	0.7235E 02
5600.0	14.698	0.1543E 00	0.5880E 02
5813.0	15.257	0.1408E 00	0.5363E 02
6000.0	15.748	0.1344E 00	0.5122E 02

ROUGH WALL U*2 SPECTRA
DTSA WIRE 55853 SENS. LENGTH=0.45MM L/D=90
NATURALLY DEVELOPED

RUN	=	81977	DE	=	4.034
PLATE	=	18	DE2	=	0.558
U*2	=	0.722	U	=	26.21
Y*/DE	=	1.000	UINF	=	26.70
Y/DE	=	1.000			

N	K1	EU(N)	EJ(K1)
22.5	0.054	0.7153E 02	0.2983E 05
37.5	0.090	0.1601E 02	0.6679E 04
52.5	0.126	0.1464E 02	0.6105E 04
67.5	0.162	0.1326E 02	0.5530E 04
82.5	0.198	0.1240E 02	0.5173E 04
97.5	0.234	0.1209E 02	0.5043E 04
112.5	0.270	0.1078E 02	0.4495E 04
127.5	0.306	0.9694E 01	0.4043E 04
142.5	0.342	0.9109E 01	0.3799E 04
157.5	0.378	0.7647E 01	0.3189E 04
172.5	0.414	0.7169E 01	0.2990E 04
187.5	0.450	0.7525E 01	0.3138E 04
213.0	0.511	0.7219E 01	0.3011E 04
267.0	0.640	0.6005E 01	0.2504E 04
320.0	0.767	0.4451E 01	0.1857E 04
373.0	0.894	0.3877E 01	0.1617E 04
427.0	1.024	0.3618E 01	0.1509E 04
480.0	1.151	0.2682E 01	0.1119E 04
533.0	1.278	0.2503E 01	0.1044E 04
587.0	1.407	0.1579E 01	0.6587E 03
640.0	1.534	0.1616E 01	0.6741E 03
693.0	1.661	0.1474E 01	0.6148E 03
747.0	1.791	0.1344E 01	0.5607E 03
800.0	1.918	0.1226E 01	0.5114E 03
853.0	2.045	0.9517E 00	0.3969E 03
907.0	2.175	0.8679E 00	0.3620E 03
960.0	2.302	0.1020E 01	0.4253E 03
1013.0	2.429	0.8482E 00	0.3538E 03
1067.0	2.558	0.7735E 00	0.3226E 03
1120.0	2.685	0.8100E 00	0.3378E 03
1173.0	2.812	0.6584E 00	0.2746E 03
1227.0	2.942	0.6584E 00	0.2746E 03
1280.0	3.069	0.5604E 00	0.2337E 03
1333.0	3.196	0.5868E 00	0.2447E 03
1387.0	3.325	0.4555E 00	0.1900E 03
1440.0	3.452	0.4154E 00	0.1733E 03
1493.0	3.580	0.4251E 00	0.1773E 03
1547.0	3.709	0.3789E 00	0.1580E 03
1600.0	3.836	0.4154E 00	0.1733E 03
1653.0	3.963	0.3702E 00	0.1544E 03
1813.0	4.347	0.2809E 00	0.1171E 03
2000.0	4.795	0.2621E 00	0.1093E 03
2213.0	5.306	0.1616E 00	0.6741E 02
2400.0	5.754	0.1579E 00	0.6587E 02
2613.0	6.265	0.1344E 00	0.5607E 02
2800.0	6.713	0.1344E 00	0.5607E 02
3013.0	7.224	0.1020E 00	0.4253E 02
3200.0	7.672	0.1020E 00	0.4253E 02
3413.0	8.183	0.9517E-01	0.3969E 02
3600.0	8.631	0.8882E-01	0.3704E 02
3813.0	9.142	0.8482E-01	0.3538E 02
4000.0	9.590	0.7219E-01	0.3011E 02
4213.0	10.101	0.5604E-01	0.2337E 02
4400.0	10.549	0.5604E-01	0.2337E 02
4613.0	11.060	0.5868E-01	0.2447E 02
4800.0	11.508	0.5476E-01	0.2284E 02
5013.0	12.019	0.4060E-01	0.1693E 02
5200.0	12.467	0.4451E-01	0.1857E 02
5413.0	12.978	0.3455E-01	0.1441E 02
5600.0	13.426	0.3702E-01	0.1544E 02
5813.0	13.937	0.3225E-01	0.1345E 02
6000.0	14.385	0.2561E-01	0.1068E 02

SMOOTH WALL HEAT SPECTRA
DATA TYPE 55A53 SENS. LENGTH=0.45MM L/D=30
ARTIFICIALLY THICKENED L= 2.32 M.

RHO	=	71.978	DF	=	7.703
PLATE	=	13	RRD	=	0.978
HRD	=	7.797	U	=	16.76
Y+/DF	=	0.078	HTUF	=	26.92
Y/DF	=	0.081			

N	K1	EU(N)	EU(K1)
22.5	0.084	0.6896E 03	0.1839E 06
37.5	0.141	0.4904E 03	0.1332E 06
52.5	0.197	0.3232E 03	0.8623E 05
67.5	0.253	0.2585E 03	0.6897E 05
82.5	0.309	0.2236E 03	0.5965E 05
97.5	0.365	0.1952E 03	0.4515E 05
112.5	0.422	0.1281E 03	0.3417E 05
127.5	0.478	0.1034E 03	0.2758E 05
142.5	0.534	0.8595E 02	0.2294E 05
157.5	0.590	0.7218E 02	0.1926E 05
172.5	0.647	0.7594E 02	0.2026E 05
187.5	0.703	0.7489E 02	0.1998E 05
202.5	0.759	0.6404E 02	0.1709E 05
217.5	0.815	0.5949E 02	0.1587E 05
232.5	0.871	0.5241E 02	0.1398E 05
247.0	1.001	0.4360E 02	0.1163E 05
322.0	1.196	0.3232E 02	0.8623E 04
372.0	1.398	0.2751E 02	0.7339E 04
427.0	1.600	0.2135E 02	0.5697E 04
480.0	1.799	0.1903E 02	0.5077E 04
533.0	1.998	0.1512E 02	0.4033E 04
587.0	2.200	0.1444E 02	0.3852E 04
640.0	2.399	0.1201E 02	0.3204E 04
667.0	2.500	0.1229E 02	0.3278E 04
720.0	2.699	0.1095E 02	0.2922E 04
773.0	2.897	0.8699E 01	0.2321E 04
827.0	3.100	0.8118E 01	0.2166E 04
880.0	3.298	0.6593E 01	0.1761E 04
933.0	3.497	0.7235E 01	0.1930E 04
987.0	3.699	0.6594E 01	0.1761E 04
1013.0	3.797	0.6301E 01	0.1681E 04
1040.0	3.898	0.6018E 01	0.1606E 04
1067.0	3.999	0.5363E 01	0.1431E 04
1120.0	4.198	0.5747E 01	0.1533E 04
1173.0	4.396	0.5005E 01	0.1335E 04
1227.0	4.599	0.4780E 01	0.1275E 04
1280.0	4.797	0.4566E 01	0.1218E 04
1360.0	5.097	0.3797E 01	0.1013E 04
1413.0	5.296	0.3711E 01	0.9900E 03
1493.0	5.596	0.3463E 01	0.9239E 03
1547.0	5.798	0.3797E 01	0.1013E 04
1600.0	5.997	0.2627E 01	0.7009E 03
1627.0	6.098	0.2947E 01	0.7864E 03
1680.0	6.297	0.3158E 01	0.8426E 03
1813.0	6.795	0.2588E 01	0.7172E 03
2000.0	7.496	0.2452E 01	0.6541E 03
2240.0	8.396	0.1862E 01	0.4962E 03
2400.0	8.995	0.1444E 01	0.3852E 03
2613.0	9.794	0.1229E 01	0.3278E 03
2827.0	10.596	0.1147E 01	0.3059E 03
3013.0	11.293	0.1022E 01	0.2727E 03
3093.0	11.593	0.9538E 00	0.2545E 03
3227.0	12.095	0.8698E 00	0.2321E 03
3413.0	12.792	0.7235E 00	0.1930E 03
3653.0	13.792	0.6598E 00	0.1761E 03
3813.0	14.291	0.7270E 00	0.1896E 03
4000.0	14.992	0.6153E 00	0.1643E 03
4213.0	15.790	0.5488E 00	0.1464E 03
4400.0	16.491	0.4555E 00	0.1215E 03
4613.0	17.290	0.4565E 00	0.1218E 03
4800.0	17.990	0.3797E 00	0.1013E 03
5013.0	18.789	0.3711E 00	0.9900E 02
5200.0	19.490	0.3232E 00	0.8623E 02
5413.0	20.289	0.3095E 00	0.8235E 02
5600.0	20.989	0.2627E 00	0.7009E 02
5813.0	21.787	0.2567E 00	0.6849E 02
5960.0	22.888	0.2567E 00	0.6849E 02
6200.0	23.488	0.2288E 00	0.6104E 02

SMOOTH WALL HEAT SPECTRA
DATA TYPE 55A53 SENS. LENGTH=0.45MM L/D=30
ARTIFICIALLY THICKENED L= 2.32 M.

RHO	=	71.978	DF	=	7.703
PLATE	=	13	RRD	=	0.978
HRD	=	6.719	U	=	18.56
Y+/DF	=	0.150	HTUF	=	26.32
Y/DF	=	0.153			

N	K1	EU(N)	EU(K1)
22.5	0.076	0.6925E 03	0.1455E 06
37.5	0.127	0.4200E 03	0.1267E 06
52.5	0.178	0.3358E 03	0.9526E 05
67.5	0.228	0.2379E 03	0.7029E 05
82.5	0.279	0.1797E 03	0.5309E 05
97.5	0.330	0.1505E 03	0.4445E 05
112.5	0.381	0.1299E 03	0.3836E 05
127.5	0.432	0.1078E 03	0.3183E 05
142.5	0.482	0.8403E 02	0.2612E 05
157.5	0.533	0.7806E 02	0.2306E 05
172.5	0.584	0.7252E 02	0.2142E 05
187.5	0.635	0.7152E 02	0.2113E 05
202.5	0.685	0.7066E 02	0.2087E 05
217.5	0.736	0.5800E 02	0.1714E 05
232.5	0.787	0.4576E 02	0.1352E 05
247.0	0.917	0.4451E 02	0.1315E 05
292.0	0.992	0.3463E 02	0.1023E 05
347.0	1.175	0.2452E 02	0.7243E 04
400.0	1.354	0.1903E 02	0.5887E 04
453.0	1.533	0.1776E 02	0.5247E 04
507.0	1.716	0.1317E 02	0.3890E 04
560.0	1.896	0.1317E 02	0.3890E 04
613.0	2.075	0.9760E 01	0.2883E 04
667.0	2.258	0.9538E 01	0.2818E 04
720.0	2.437	0.9538E 01	0.2818E 04
773.0	2.617	0.8698E 01	0.2570E 04
827.0	2.799	0.5122E 01	0.1513E 04
880.0	2.979	0.5881E 01	0.1737E 04
933.0	3.158	0.5881E 01	0.1737E 04
987.0	3.341	0.4892E 01	0.1445E 04
1040.0	3.520	0.4367E 01	0.1288E 04
1093.0	3.700	0.4451E 01	0.1313E 04
1147.0	3.882	0.4163E 01	0.1230E 04
1200.0	4.062	0.3711E 01	0.1096E 04
1253.0	4.241	0.3544E 01	0.1047E 04
1307.0	4.424	0.2880E 01	0.8509E 03
1360.0	4.603	0.2688E 01	0.7941E 03
1413.0	4.783	0.2567E 01	0.7584E 03
1467.0	4.966	0.2751E 01	0.8126E 03
1520.0	5.145	0.2751E 01	0.8126E 03
1547.0	5.236	0.2880E 01	0.8509E 03
1573.0	5.324	0.2688E 01	0.7941E 03
1627.0	5.507	0.2452E 01	0.7243E 03
1680.0	5.687	0.2452E 01	0.7243E 03
1733.0	5.866	0.2239E 01	0.6324E 03
1787.0	6.049	0.1776E 01	0.5247E 03
1840.0	6.228	0.1776E 01	0.5247E 03
1933.0	6.499	0.1557E 01	0.4597E 03
2000.0	6.770	0.1696E 01	0.5011E 03
2213.0	7.491	0.1379E 01	0.4073E 03
2400.0	8.124	0.1173E 01	0.3467E 03
2613.0	8.845	0.1147E 01	0.3388E 03
2800.0	9.478	0.1022E 01	0.3019E 03
2987.0	10.111	0.8901E 00	0.2630E 03
3213.0	10.879	0.7753E 00	0.2290E 03
3400.0	10.832	0.7404E 00	0.2187E 03
3613.0	11.553	0.6018E 00	0.1778E 03
3800.0	12.186	0.5005E 00	0.1479E 03
3813.0	12.907	0.4780E 00	0.1412E 03
4000.0	13.540	0.5122E 00	0.1513E 03
4213.0	14.261	0.4163E 00	0.1230E 03
4400.0	14.894	0.4260E 00	0.1259E 03
4613.0	15.615	0.3463E 00	0.1023E 03
4800.0	16.248	0.3095E 00	0.9144E 02
5013.0	16.969	0.2751E 00	0.8126E 02
5200.0	17.602	0.3015E-09	0.8910E-07
5413.0	18.323	0.2688E 00	0.7941E 02
5600.0	18.956	0.2087E 00	0.6164E 02
5813.0	19.676	0.2530E 00	0.7411E 02
6000.0	20.309	0.1947E 00	0.5753E 02

ROUGH WALL U*2 SPECTRA
DISA WIRE 55A53 SENS. LENGTH=0.45MM L/D=90
ARTIFICIALLY THICKENED L= 2.32 M.

RUN	=	71078	DE	=	7.709
PLATE	=	19	DE2	=	0.978
U*2	=	3.058	U	=	24.27
Y*/DE	=	0.600	UINF=		26.92
Y/DE	=	0.601			

N	K1	EU(N)	EU(K1)
22.5	0.059	0.2289E 03	0.8839E 05
37.5	0.097	0.2101E 03	0.8117E 05
52.5	0.136	0.1587E 03	0.5129E 05
67.5	0.175	0.1287E 03	0.4971E 05
82.5	0.214	0.1083E 03	0.4182E 05
97.5	0.252	0.9214E 02	0.3560E 05
112.5	0.291	0.7576E 02	0.2927E 05
127.5	0.330	0.6316E 02	0.2440E 05
142.5	0.369	0.5840E 02	0.2256E 05
157.5	0.408	0.5134E 02	0.1983E 05
172.5	0.447	0.4078E 02	0.1575E 05
187.5	0.485	0.3122E 02	0.1206E 05
202.5	0.524	0.2947E 02	0.1139E 05
217.5	0.563	0.2880E 02	0.1113E 05
232.5	0.602	0.2446E 02	0.9450E 04
240.0	0.621	0.2452E 02	0.9471E 04
293.0	0.759	0.2135E 02	0.8249E 04
347.0	0.899	0.1347E 02	0.5205E 04
400.0	1.035	0.1317E 02	0.5086E 04
453.0	1.173	0.3500E 01	0.3284E 04
507.0	1.312	0.7070E 01	0.2732E 04
560.0	1.450	0.5881E 01	0.2272E 04
613.0	1.587	0.5488E 01	0.2120E 04
667.0	1.726	0.5005E 01	0.1934E 04
720.0	1.864	0.4260E 01	0.1646E 04
773.0	2.001	0.4069E 01	0.1572E 04
827.0	2.141	0.3086E 01	0.1192E 04
880.0	2.278	0.3086E 01	0.1192E 04
933.0	2.415	0.3544E 01	0.1369E 04
987.0	2.555	0.2567E 01	0.9919E 03
1040.0	2.692	0.2341E 01	0.9045E 03
1093.0	2.829	0.2341E 01	0.9045E 03
1147.0	2.969	0.2087E 01	0.8061E 03
1200.0	3.106	0.1903E 01	0.7352E 03
1253.0	3.243	0.1512E 01	0.5840E 03
1307.0	3.383	0.1411E 01	0.5450E 03
1360.0	3.520	0.1379E 01	0.5326E 03
1413.0	3.657	0.1347E 01	0.52[illegible]5E 03
1467.0	3.797	0.1411E 01	0.5450E 03
1520.0	3.934	0.1257E 01	0.4857E 03
1573.0	4.072	0.1287E 01	0.4971E 03
1627.0	4.211	0.1046E 01	0.4040E 03
1680.0	4.349	0.9997E 00	0.3858E 03
1733.0	4.486	0.9321E 00	0.3601E 03
1787.0	4.625	0.8307E 00	0.3209E 03
1840.0	4.763	0.8901E 00	0.3439E 03
2000.0	5.177	0.8307E 00	0.3209E 03
2213.0	5.728	0.6018E 00	0.2325E 03
2400.0	6.212	0.5747E 00	0.2220E 03
2613.0	6.764	0.4780E 00	0.1847E 03
2800.0	7.248	0.4780E 00	0.1847E 03
3013.0	7.799	0.3463E 00	0.1338E 03
3200.0	8.283	0.3626E 00	0.1401E 03
3413.0	8.834	0.2947E 00	0.1139E 03
3600.0	9.318	0.2341E 00	0.9045E 02
3813.0	9.870	0.2288E 00	0.8839E 02
4000.0	10.354	0.2039E 00	0.7878E 02
4213.0	10.905	0.1903E 00	0.7352E 02
4400.0	11.389	0.1657E 00	0.6403E 02
4613.0	11.940	0.1547E 00	0.5976E 02
4800.0	12.424	0.1657E 00	0.6403E 02
5013.0	12.976	0.1378E 00	0.5326E 02
5200.0	13.460	0.1229E 00	0.4747E 02
5413.0	14.011	0.1201E 00	0.4639E 02
5600.0	14.495	0.1170E 00	0.4134E 02
5813.0	15.046	0.9987E-01	0.3858E 02
6000.0	15.530	0.1046E 00	0.4040E 02

ROUGH WALL U*2 SPECTRA
DISA WIRE 55A53 SENS. LENGTH=0.45MM L/D=90
ARTIFICIALLY THICKENED L= 2.32 M.

RUN	=	71078	DE	=	7.709
PLATE	=	19	DE2	=	0.978
U*2	=	0.446	U	=	26.55
Y*/DE	=	1.000	UINF=		26.92
Y/DE	=	1.000			

N	K1	EU(N)	EU(K1)
22.5	0.053	0.2347E 02	0.9915E 04
37.5	0.089	0.2200E 02	0.9296E 04
52.5	0.124	0.1860E 02	0.7859E 04
67.5	0.160	0.1873E 02	0.7912E 04
82.5	0.195	0.1736E 02	0.7333E 04
97.5	0.231	0.1301E 02	0.5499E 04
112.5	0.266	0.1043E 02	0.4409E 04
127.5	0.302	0.1121E 02	0.4735E 04
142.5	0.337	0.1029E 02	0.4348E 04
157.5	0.373	0.8326E 01	0.3518E 04
172.5	0.408	0.7472E 01	0.3157E 04
187.5	0.444	0.6598E 01	0.2788E 04
202.5	0.479	0.5594E 01	0.2406E 04
217.5	0.515	0.5351E 01	0.2261E 04
232.5	0.550	0.4639E 01	0.1960E 04
240.0	0.568	0.4260E 01	0.1800E 04
293.0	0.693	0.3885E 01	0.1642E 04
347.0	0.821	0.2452E 01	0.1036E 04
400.0	0.947	0.1947E 01	0.8228E 03
453.0	1.072	0.1657E 01	0.7003E 03
507.0	1.200	0.1583E 01	0.6688E 03
560.0	1.325	0.1347E 01	0.5692E 03
613.0	1.451	0.9760E 00	0.4124E 03
667.0	1.579	0.8307E 00	0.3510E 03
720.0	1.704	0.7753E 00	0.3276E 03
773.0	1.829	0.6448E 00	0.2725E 03
827.0	1.957	0.5488E 00	0.2319E 03
880.0	2.083	0.5747E 00	0.2428E 03
933.0	2.208	0.5005E 00	0.2115E 03
987.0	2.336	0.4892E 00	0.2067E 03
1040.0	2.461	0.4461E 00	0.1885E 03
1093.0	2.587	0.4260E 00	0.1800E 03
1147.0	2.715	0.3307E 00	0.1397E 03
1200.0	2.840	0.2880E 00	0.1217E 03
1253.0	2.965	0.2341E 00	0.9892E 02
1307.0	3.093	0.3086E 00	0.1304E 03
1360.0	3.219	0.2751E 00	0.1162E 03
1413.0	3.344	0.2396E 00	0.1012E 03
1467.0	3.472	0.2396E 00	0.1012E 03
1520.0	3.597	0.2039E 00	0.8616E 02
1573.0	3.723	0.2087E 00	0.8816E 02
1627.0	3.851	0.1947E 00	0.8228E 02
1680.0	3.976	0.1411E 00	0.5361E 02
1707.0	4.040	0.1547E 00	0.6536E 02
1760.0	4.165	0.1512E 00	0.6387E 02
1813.0	4.291	0.1620E 00	0.6844E 02
2000.0	4.733	0.1444E 00	0.6100E 02
2213.0	5.238	0.1121E 00	0.4735E 02
2400.0	5.680	0.1095E 00	0.4627E 02
2613.0	6.184	0.7576E-01	0.3201E 02
2800.0	6.627	0.6158E-01	0.2602E 02
3013.0	7.131	0.6301E-01	0.2663E 02
3200.0	7.573	0.5122E-01	0.2164E 02
3413.0	8.078	0.4360E-01	0.1842E 02
3600.0	8.520	0.4260E-01	0.1800E 02
3813.0	9.024	0.3976E-01	0.1680E 02
4000.0	9.467	0.3384E-01	0.1430E 02
4213.0	9.971	0.2880E-01	0.1217E 02
4400.0	10.414	0.2751E-01	0.1162E 02
4613.0	10.918	0.2627E-01	0.1110E 02
4800.0	11.360	0.2185E-01	0.9232E 01
5013.0	11.864	0.2688E-01	0.1136E 02
5200.0	12.307	0.2396E-01	0.1012E 02
5413.0	12.811	0.1903E-01	0.8041E 01
5600.0	13.254	0.1860E-01	0.7858E 01
5813.0	13.758	0.1477E-01	0.6242E 01
6000.0	14.200	0.1547E-01	0.6536E 01